UV tracing of the recent star formation activity in galaxy disks within the S^{4}G sample: from strangulation to XUV emission

Formación estelar en el UV en discos de galaxias de la exploración S^{4}G: estrangulamiento y emisión UV extensa

PhD dissertation presentation

Friday, June 1, 2018

by PhD candidate:
Alexandre Yuichiro Kléber Bouquin

supervised by:
Dr. Armando Gil de Paz

Universidad Complutense de Madrid (UCM)

Departamento de Física de la Tierra y Astrofísica

Table of Contents

Table of Contents

1. Introduction

The Big Picture

Planck's Cosmic Microwave Background map at z=1089

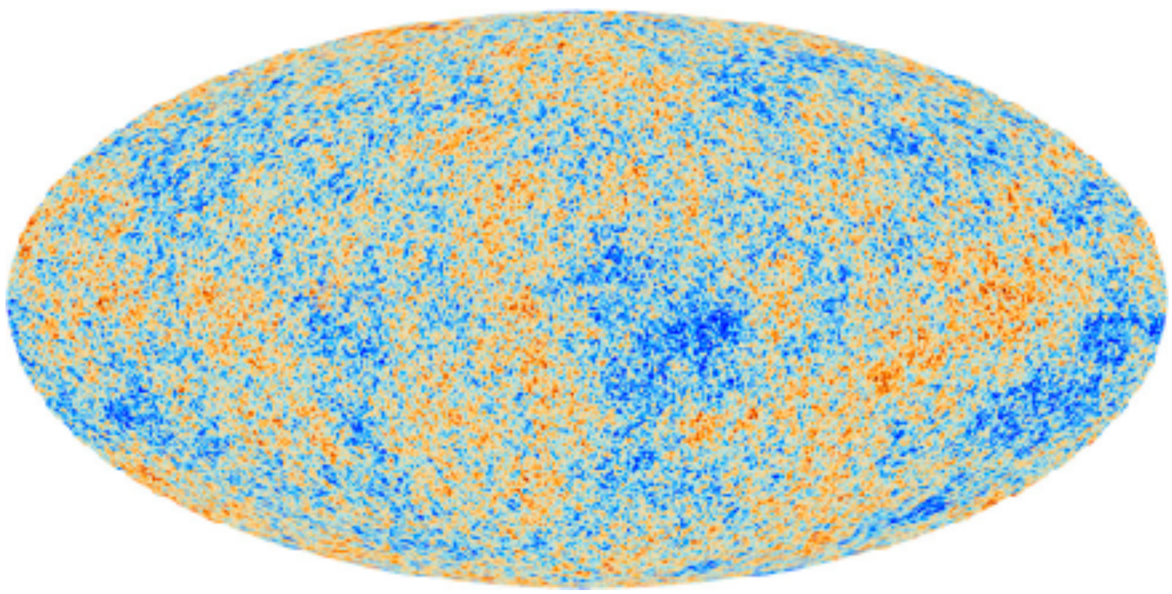

ESA & the Planck Collaboration (2013)

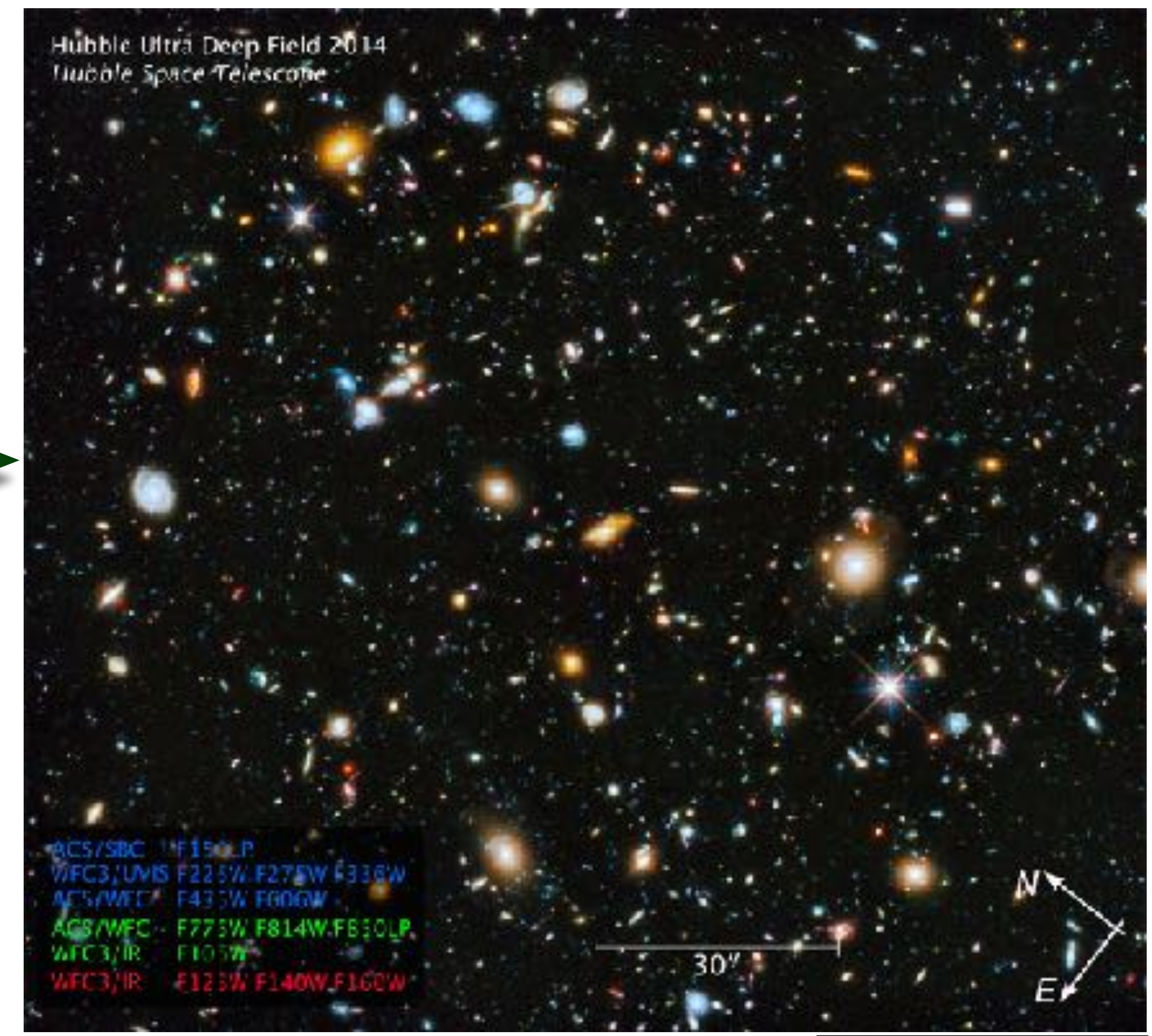

HUDF 2014 HST **NASA/STScI**

The Big questions:
How do galaxies form and evolve?

1. Introduction

The Big Picture

Planck's Cosmic Microwave Background map
at z=1089

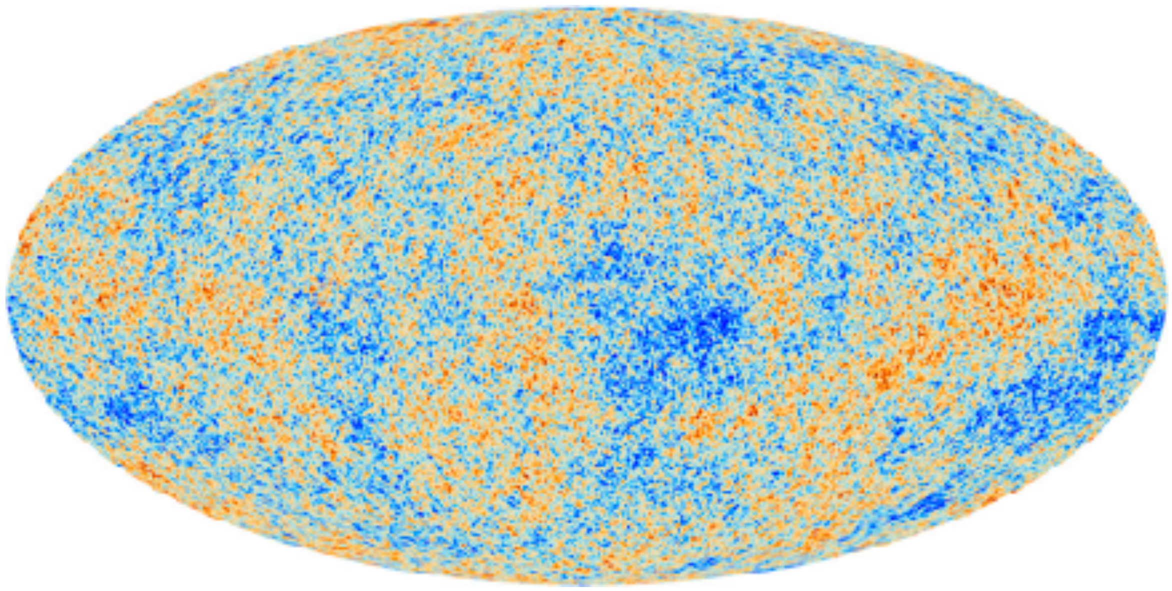

ESA & the Planck Collaboration (2013)

?

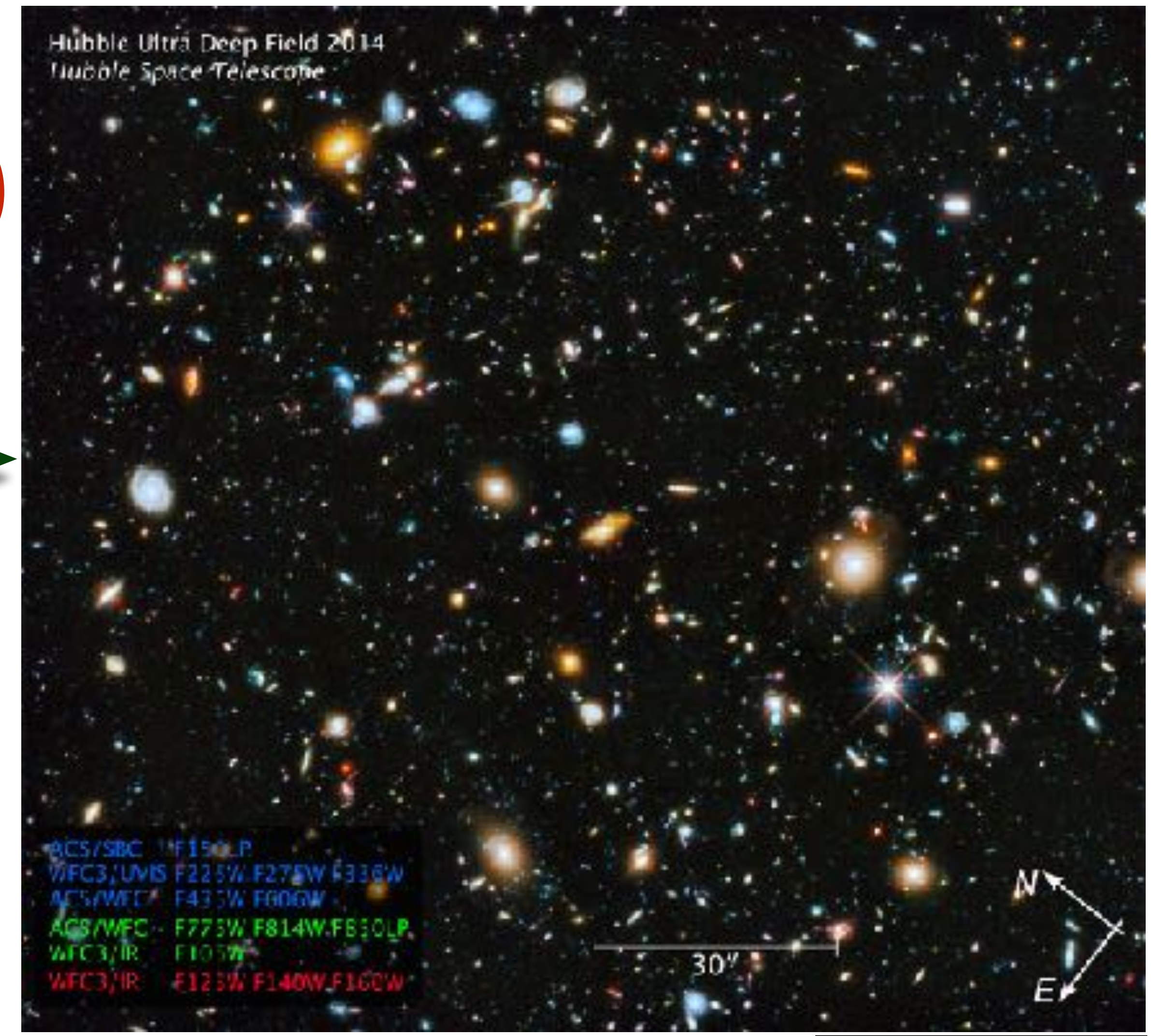

HUDF 2014 HST

NASA/STScI

The Big questions:
How do galaxies form and evolve?

1. Introduction

NASA/WMAP Science Team (2012)

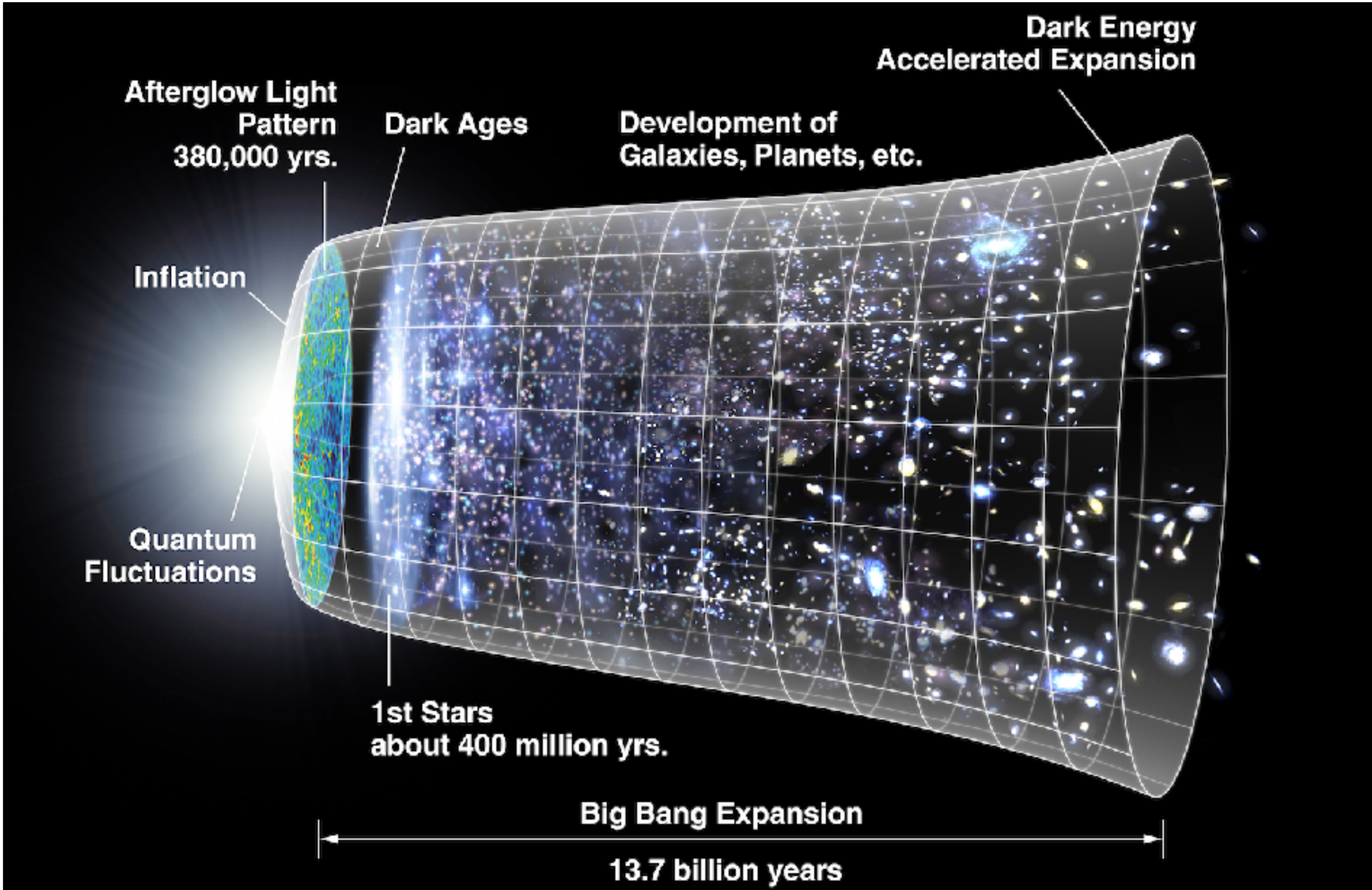

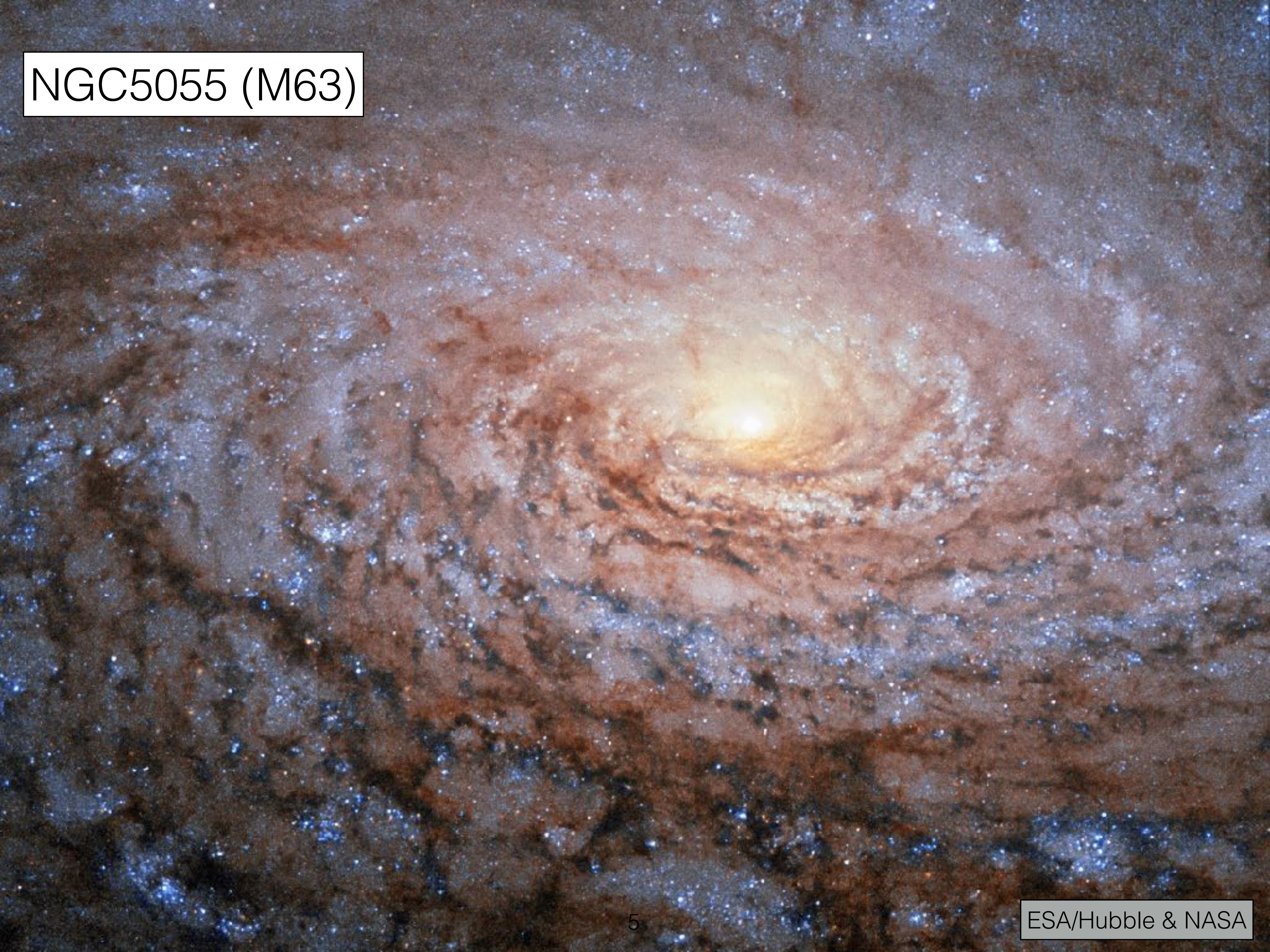
NGC5055 (M63)
ESA/Hubble & NASA

1. Introduction

A simplistic picture of galaxy formation and evolution

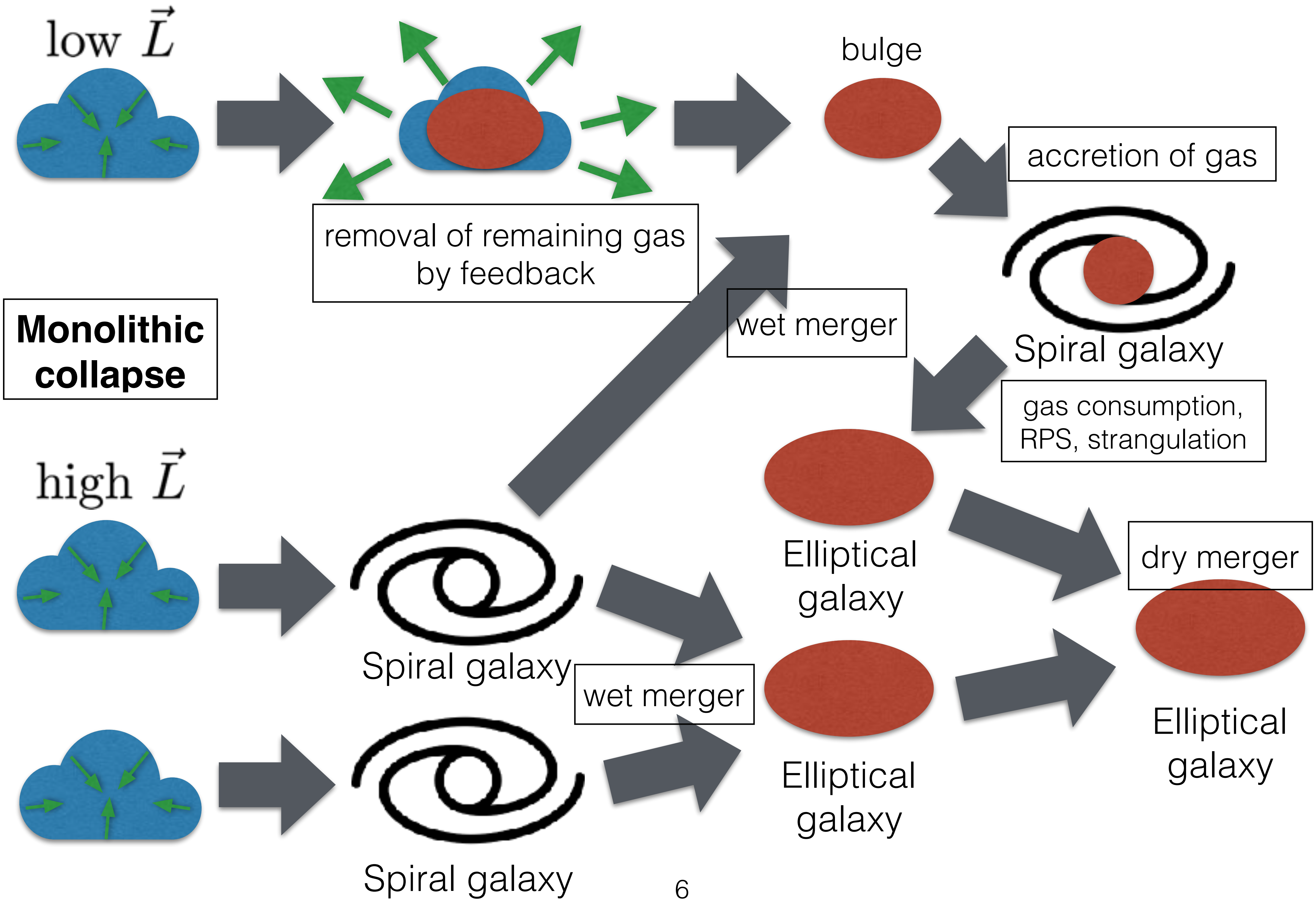

1. Introduction

Morphological classifications and star formation

quiescent

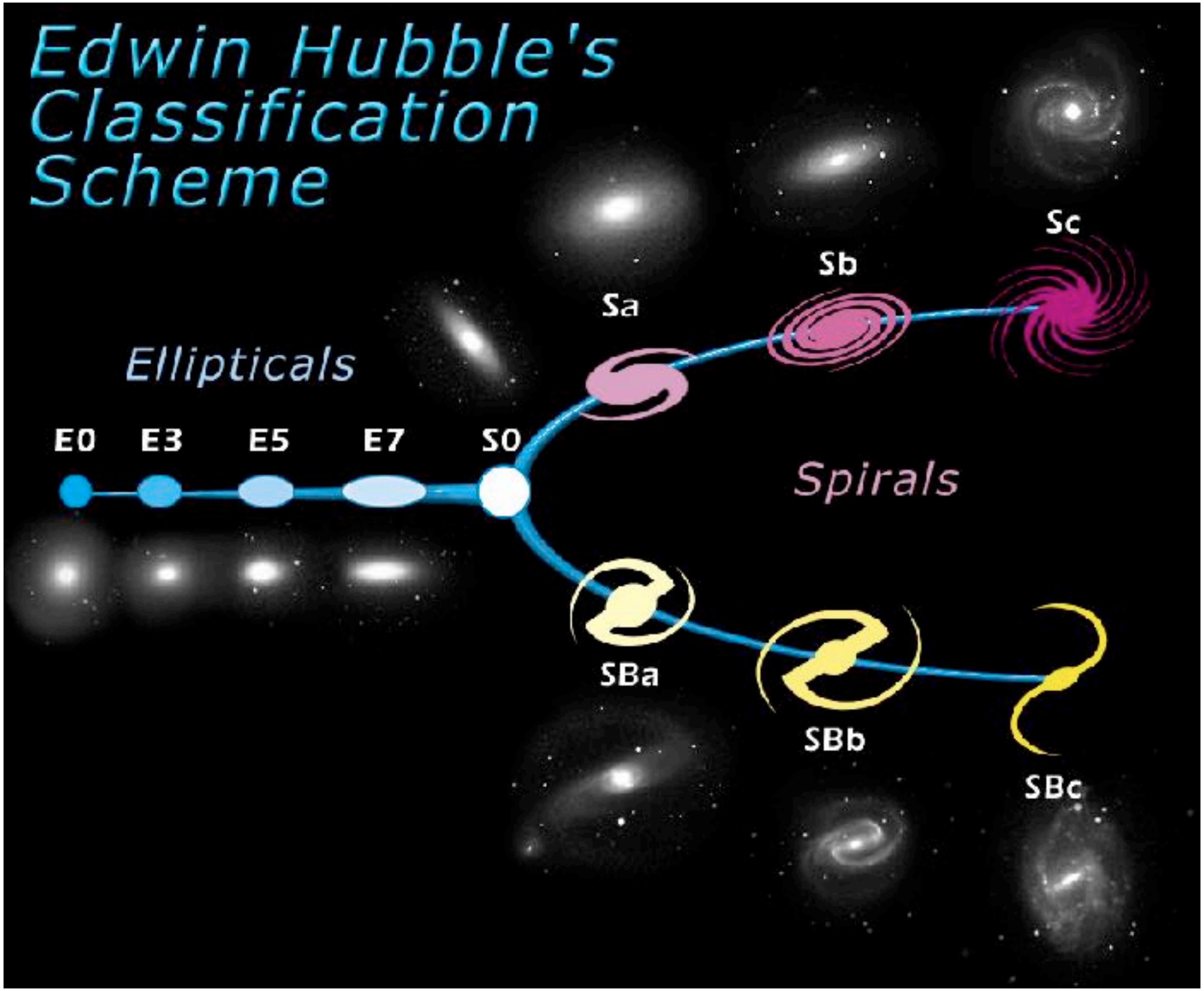

star forming

1. Introduction

tuning-fork diagram

NOTE: we use the more simplistic numerical morphological type (T) classification of RC2 (**de Vaucouleurs 1991**) for the rest of the work

SINGS galaxies by Kennicutt et al. (2003)

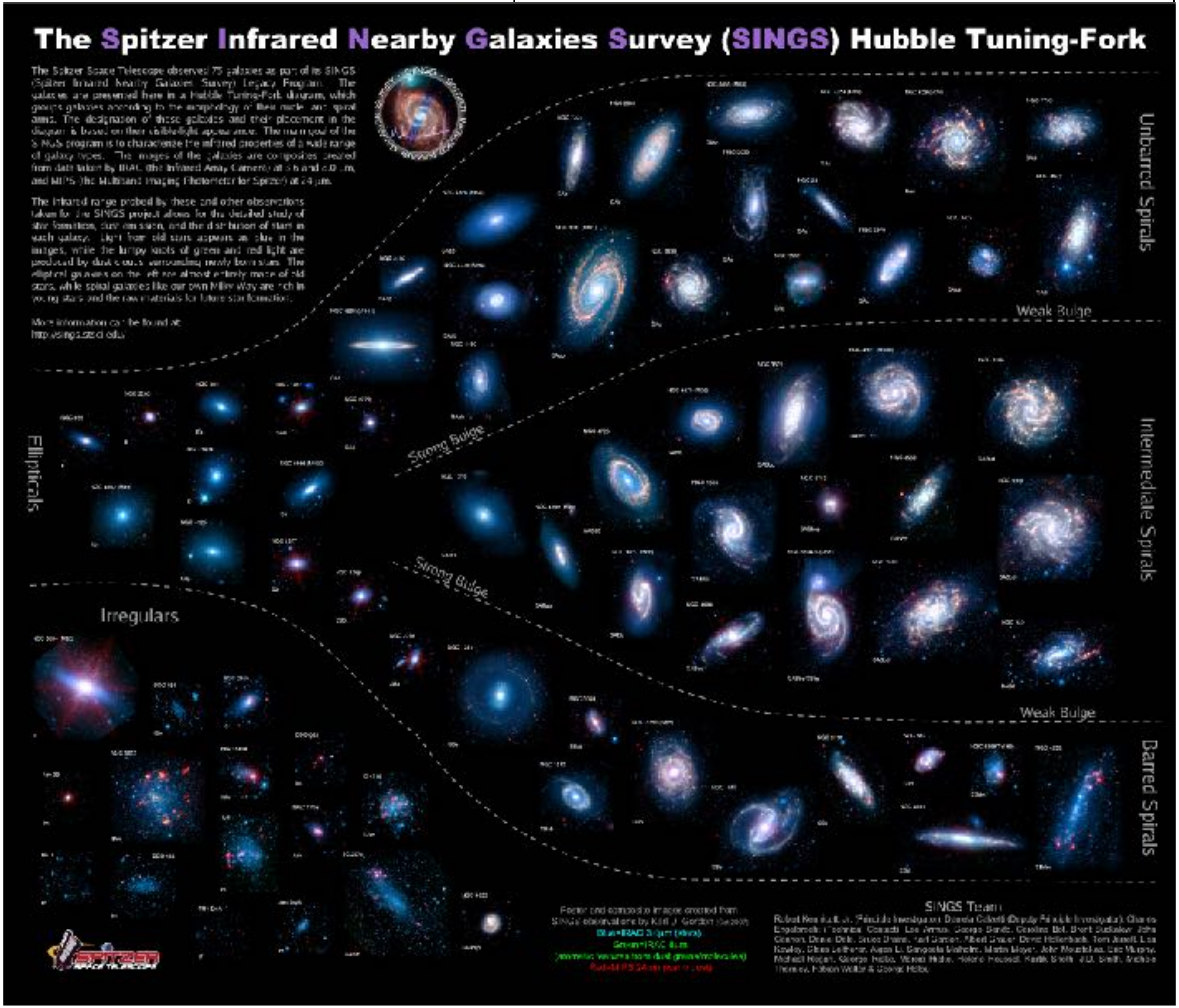

1. Introduction

Numerical morphological types

E = [-5.0; -3.5]
E-S0 = [-3.4; -2.5]
S0 = [-2.4; -1.5]
S0-a = [-1.4; 0.5]
Sa = [0.6; 2.5]
Sb = [2.6; 4.5]
Sc = [4.6; 7.5]
Sd = [7.6; 8.5]
Sm = [8.6; 9.5]
Irr = [9.6;10.0]

NOTE: we use the more simplistic numerical morphological type (T) classification of RC2 (**de Vaucouleurs 1991**) for the rest of the work

1. Introduction

One of the goals of this thesis is to find a way to distinguish between **internal** and **environmental** effects on star formation.

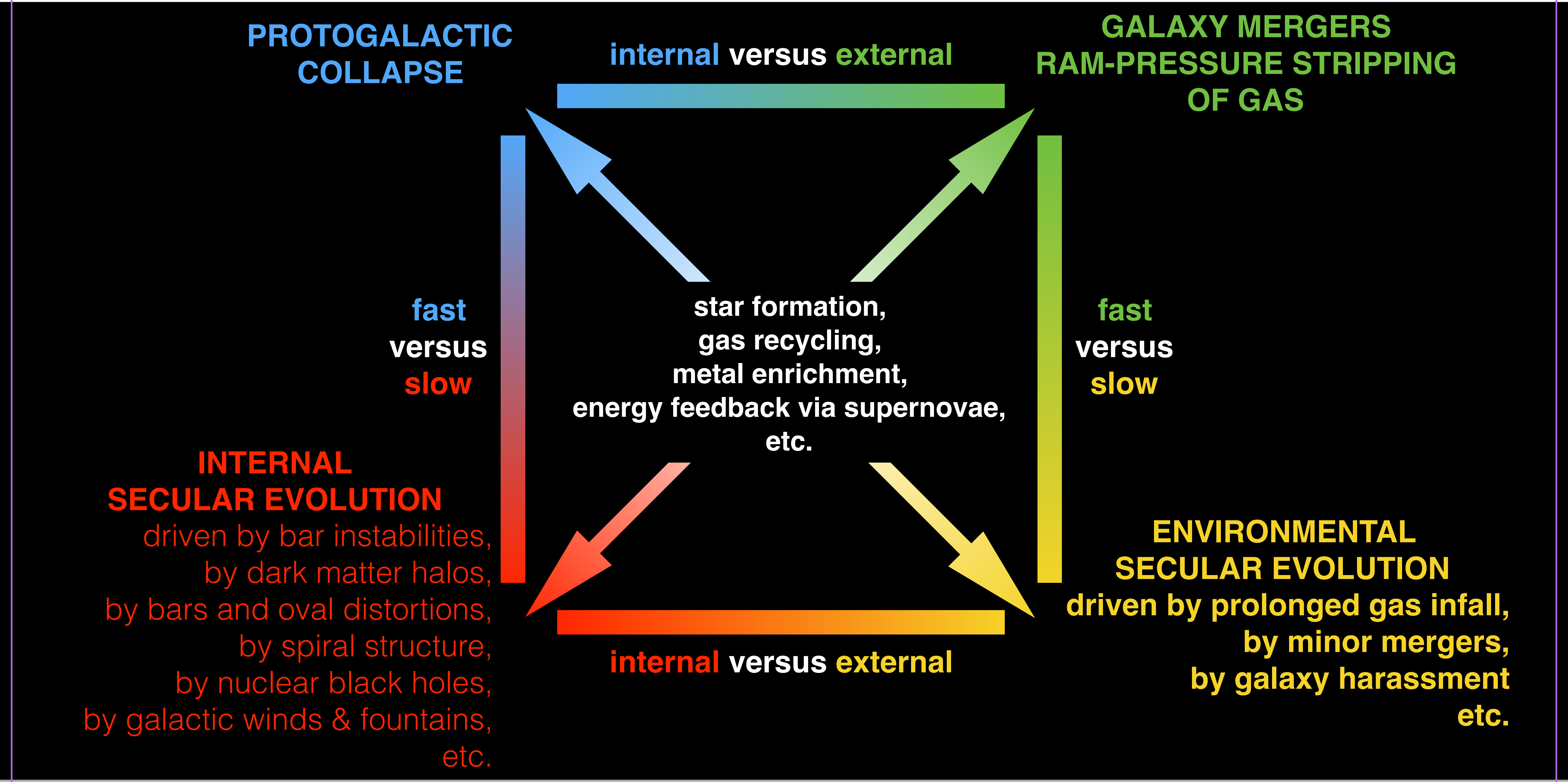

Reproduction of the morphological box (**Zwicky 1957**) of galaxy evolution processes updated by **Kormendy & Kennicutt 2004,** and adapted for this presentation.

1. Introduction

SFRD peaks at z~2 and is seen in both UV and IR bands.

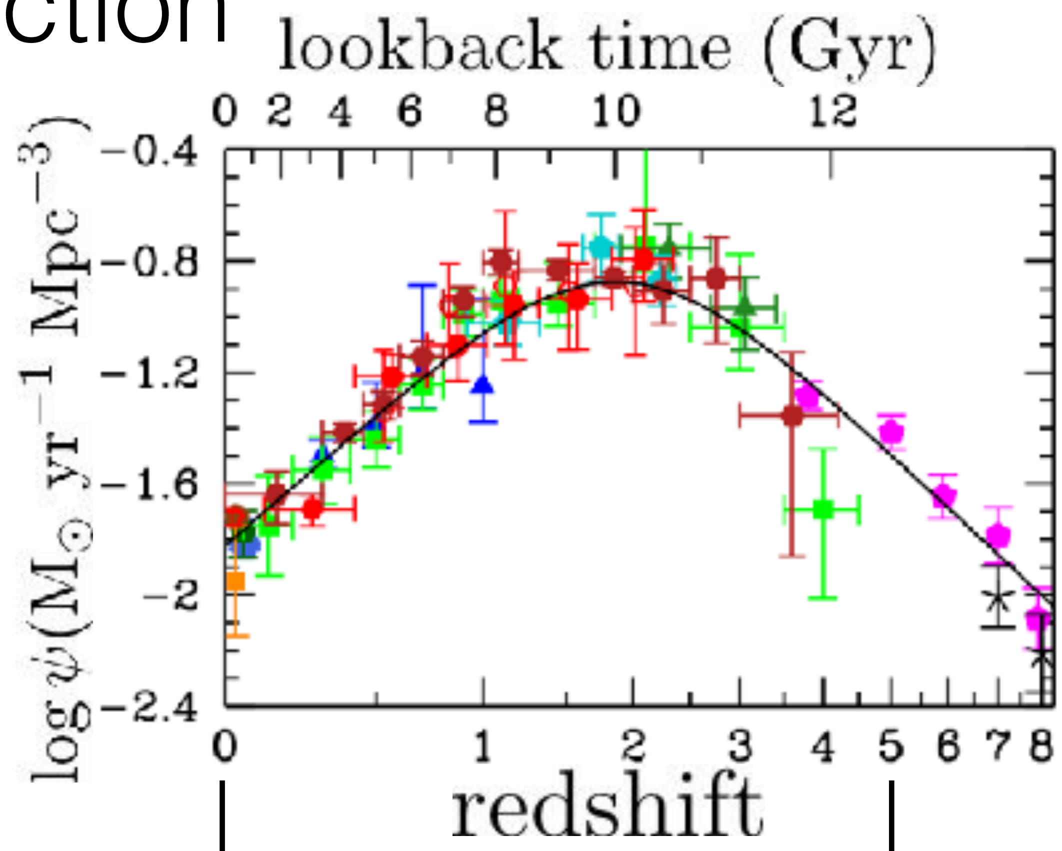

Madau & Dickinson (2014)

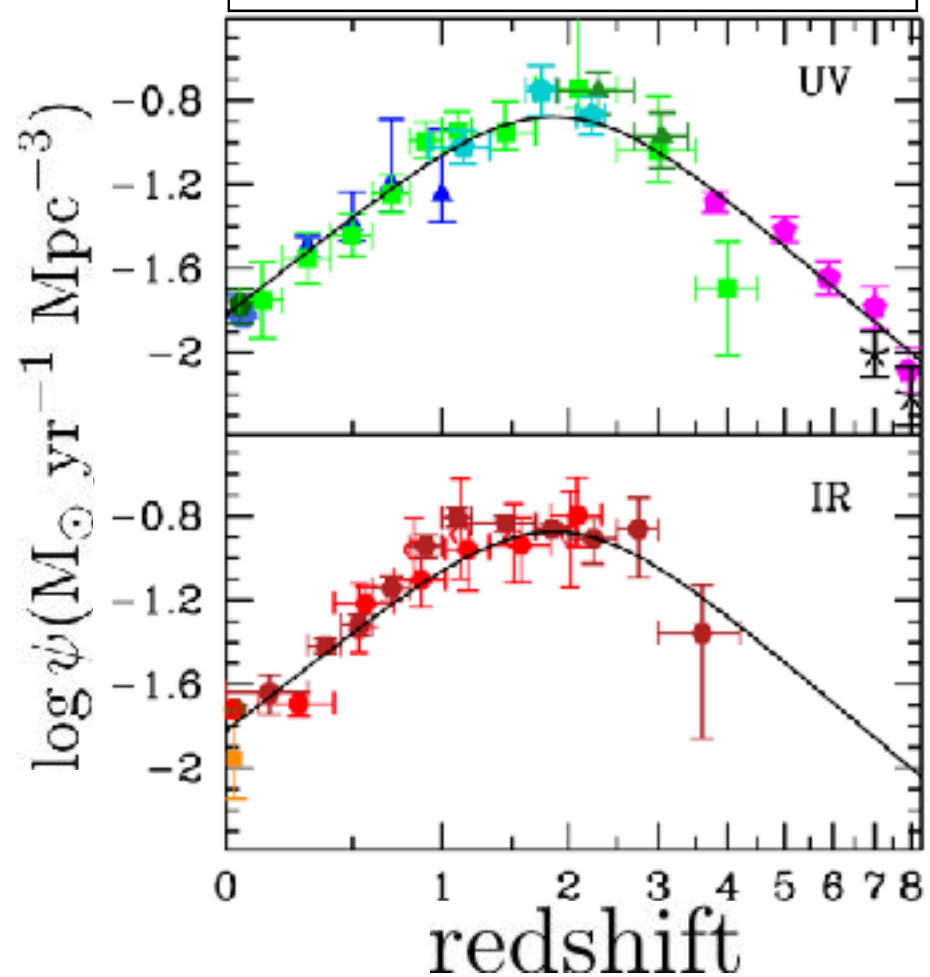

Rejuvenation, mass, and environment driven

Formation phase self-regulated

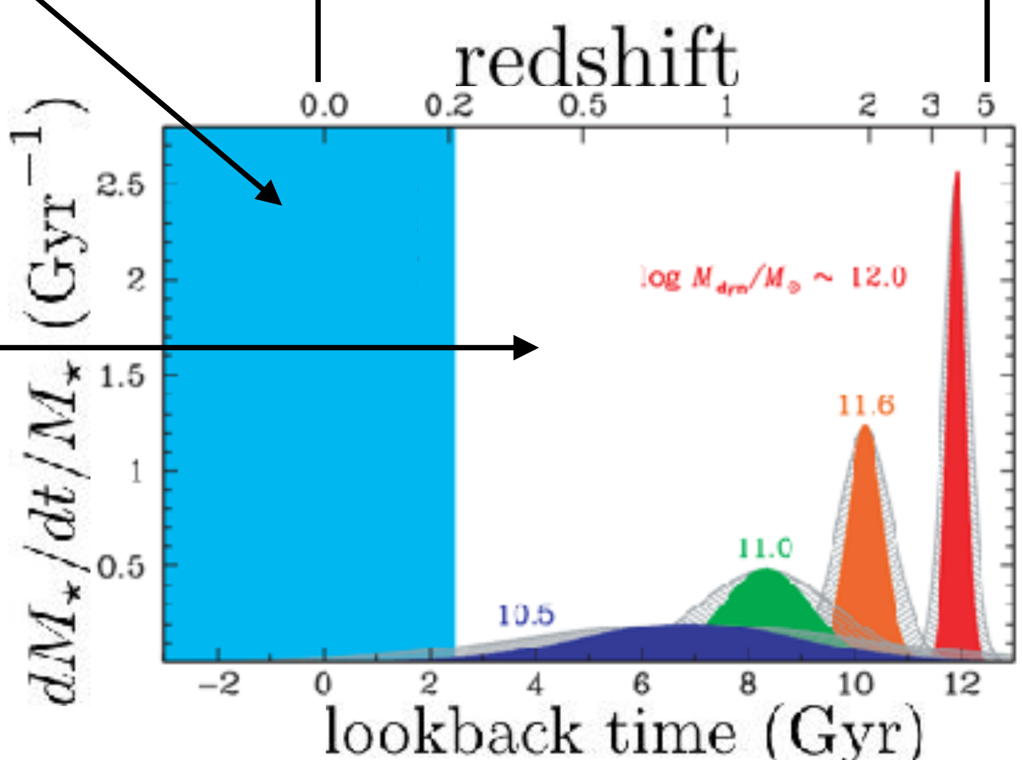

Downsizing is also seen:
i.e. sSFR peaks earlier and lasts shorter for massive (M_{dyn}=12.0 dex M_{Sun}) later in the life of the universe for lower-mass (M_{dyn}<10.5 dex M_{Sun} galaxies.

Thomas et al. (2010)

1. Introduction

Right: nearby galaxies in optical bands

Bottom: distribution of galaxies in optical color-color diagrams per redshift bins

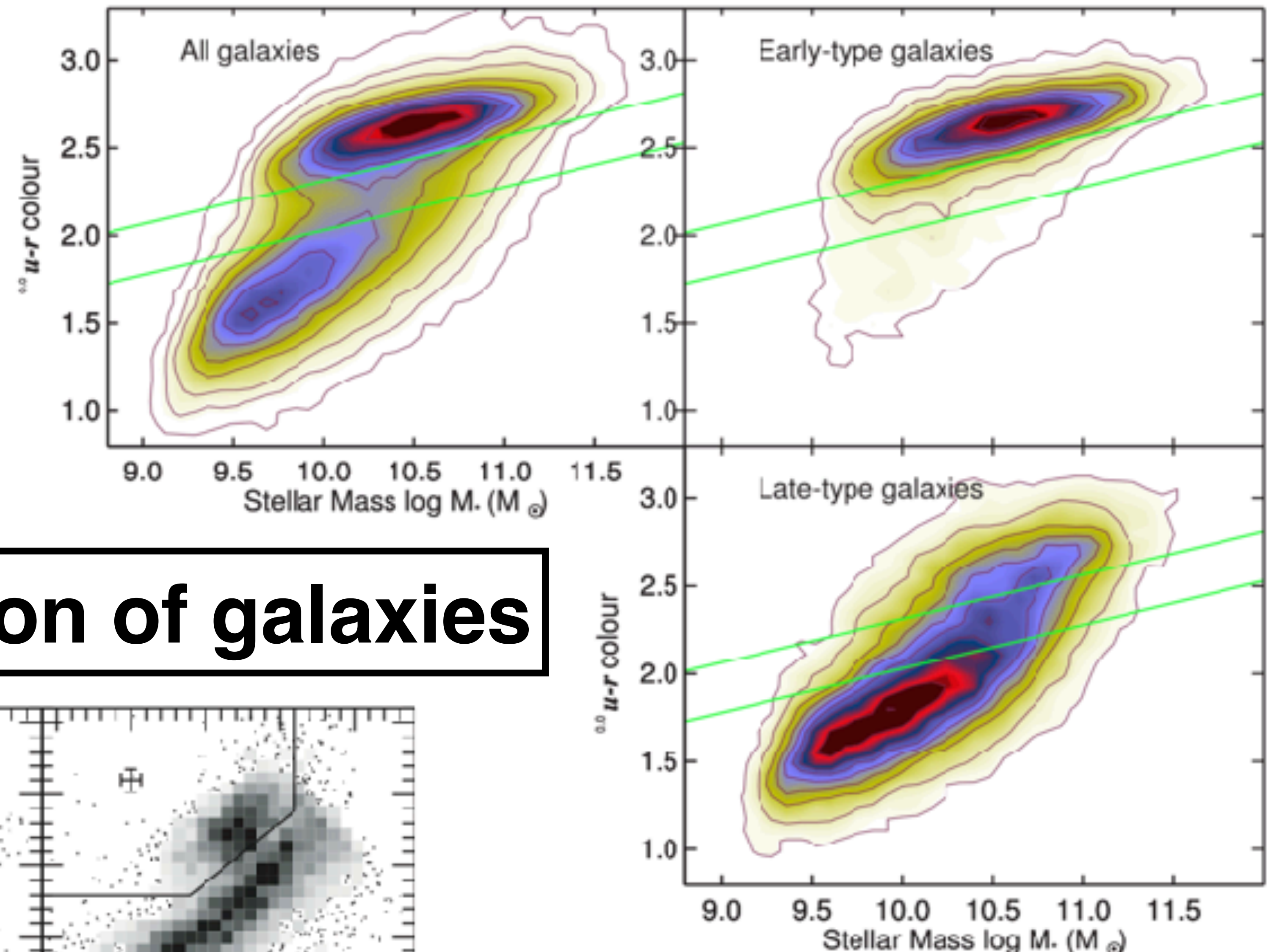

Schawinski et al. (2014)

The bimodal distribution of galaxies

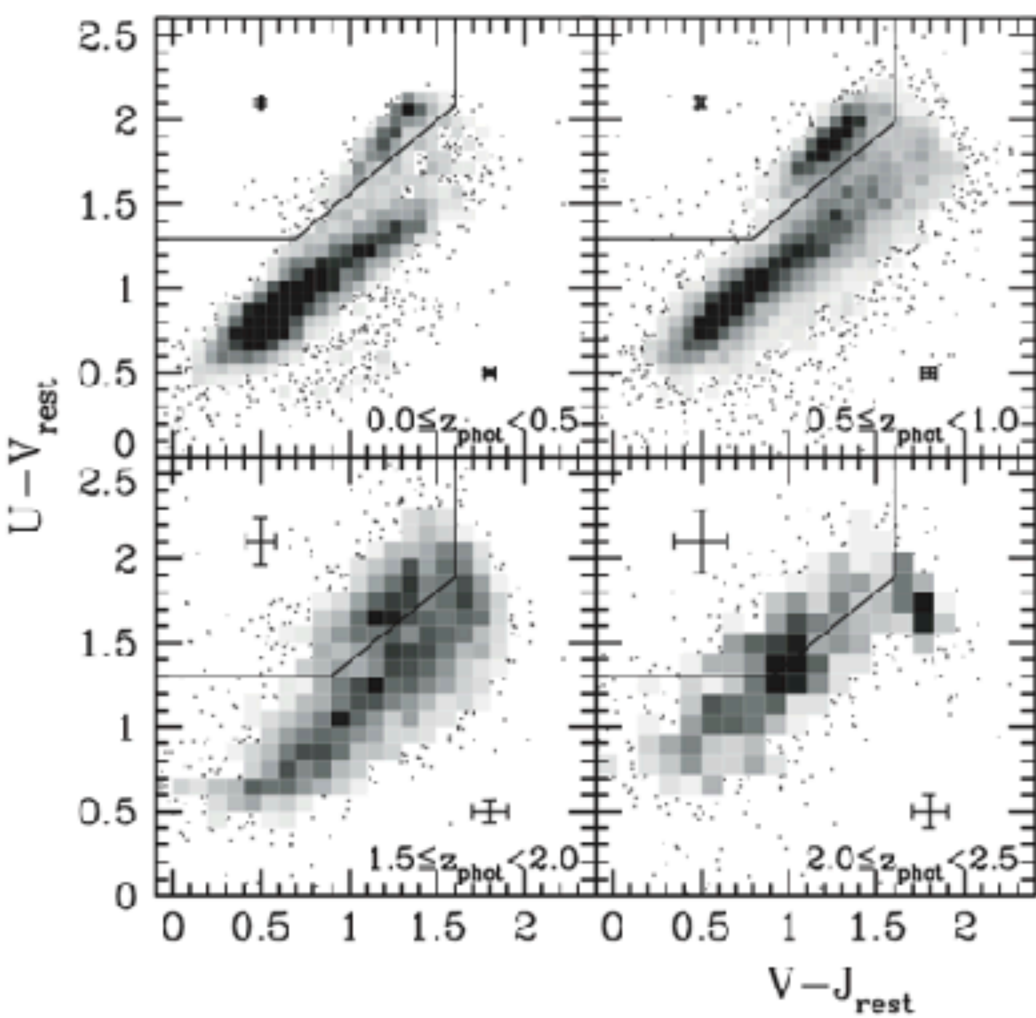

Williams et al. (2009)

But, caveat…:
optical bands are not able to dissociate well between SF, quiescent, and green valley galaxies.

Star formation (in GMC)

1. Introduction

①

collapse of giant molecular cloud and birth of stars (the amount of each depends on the IMF)

②

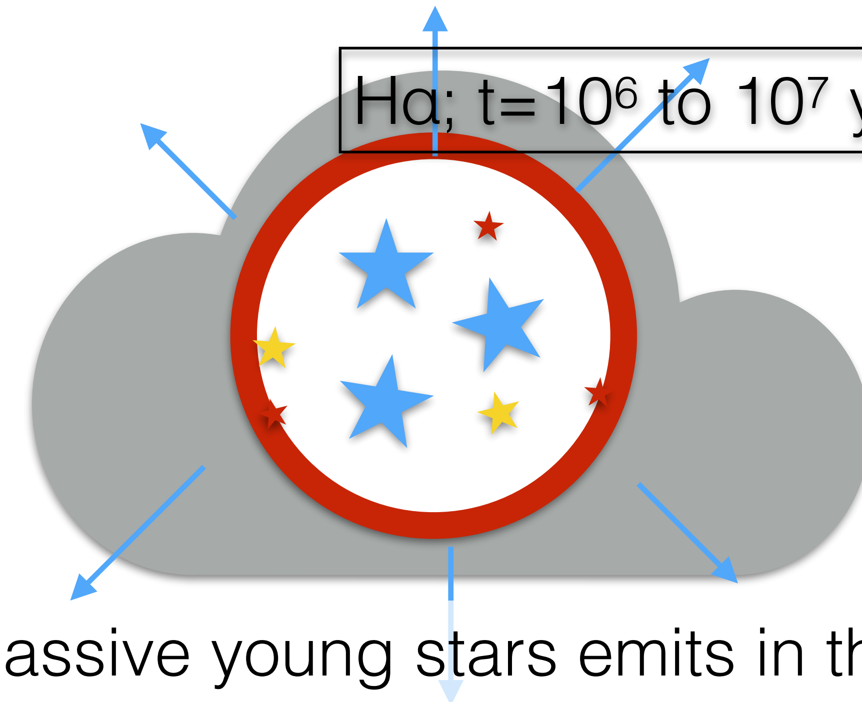

massive young stars emits in the UV ionizing the gas that remains and becomes an HII region

③

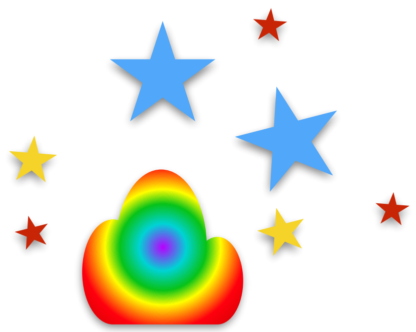

The remaining gas is blown off by SNe+massive stars driven winds after a few Myr

④

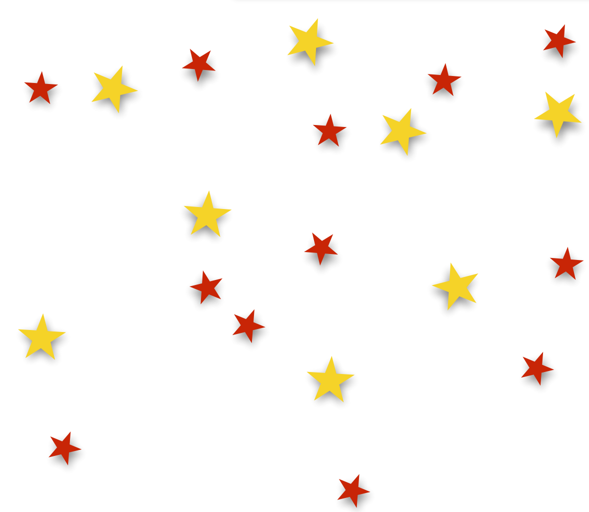

As there is no more gas, we are left with the less-massive stars.

1. Introduction

Young and massive OB associations emit in the UV.
—> GALEX FUV+NUV

Low-mass MS stars and Red Giants emit in the IR.
—> Spitzer/IRAC1

Therefore, FUV, NUV and 3.6 micron are ideal to study young to old stellar populations.

Blackbody curves

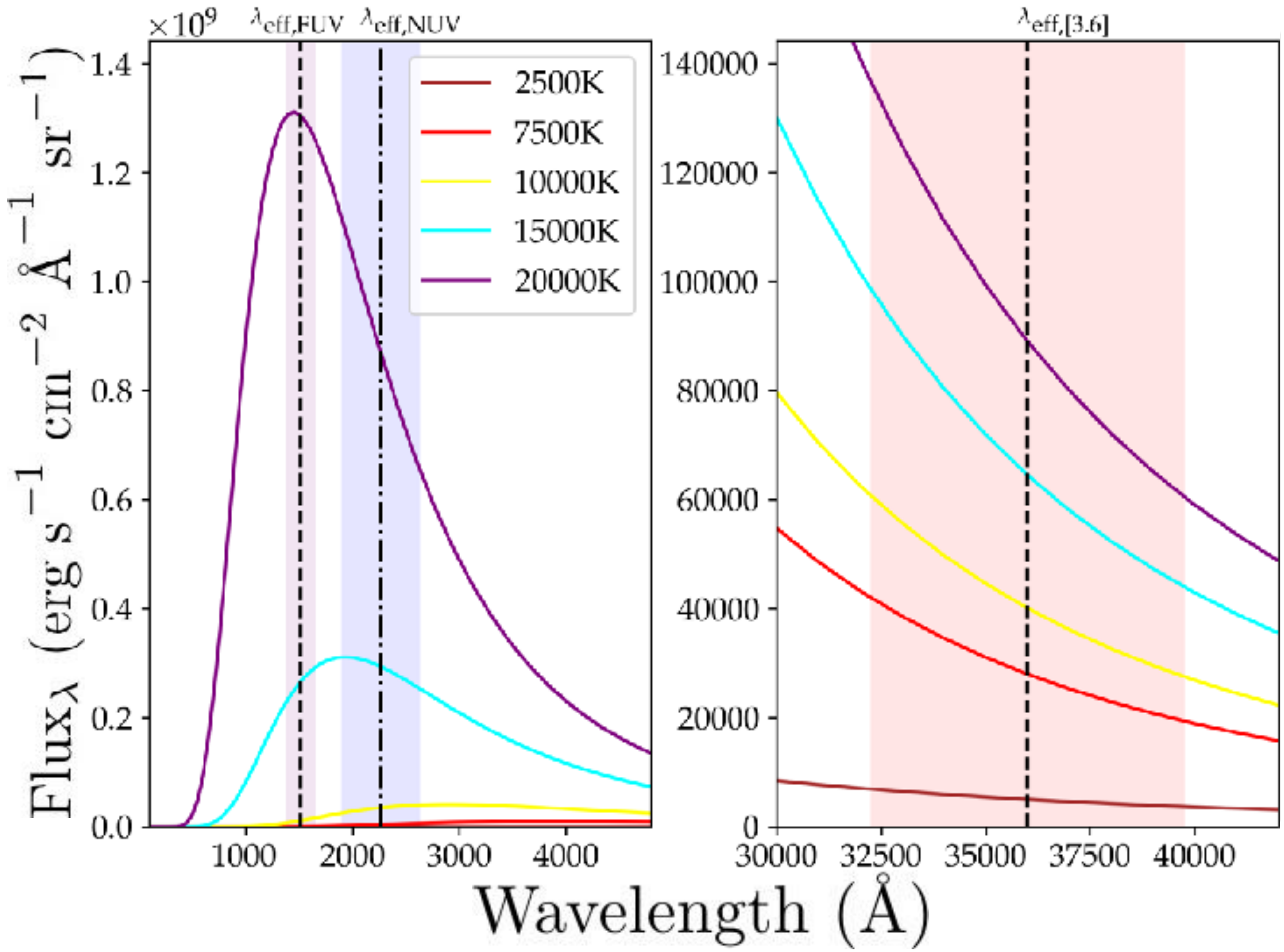

1. Introduction

Young and massive OB associations emit in the UV.
—> GALEX FUV+NUV

Low-mass MS stars and Red Giants emit in the IR.
—> Spitzer/IRAC1

Therefore, FUV, NUV and 3.6 micron are ideal to study young to old stellar populations.

(here assuming a Salpeter IMF)

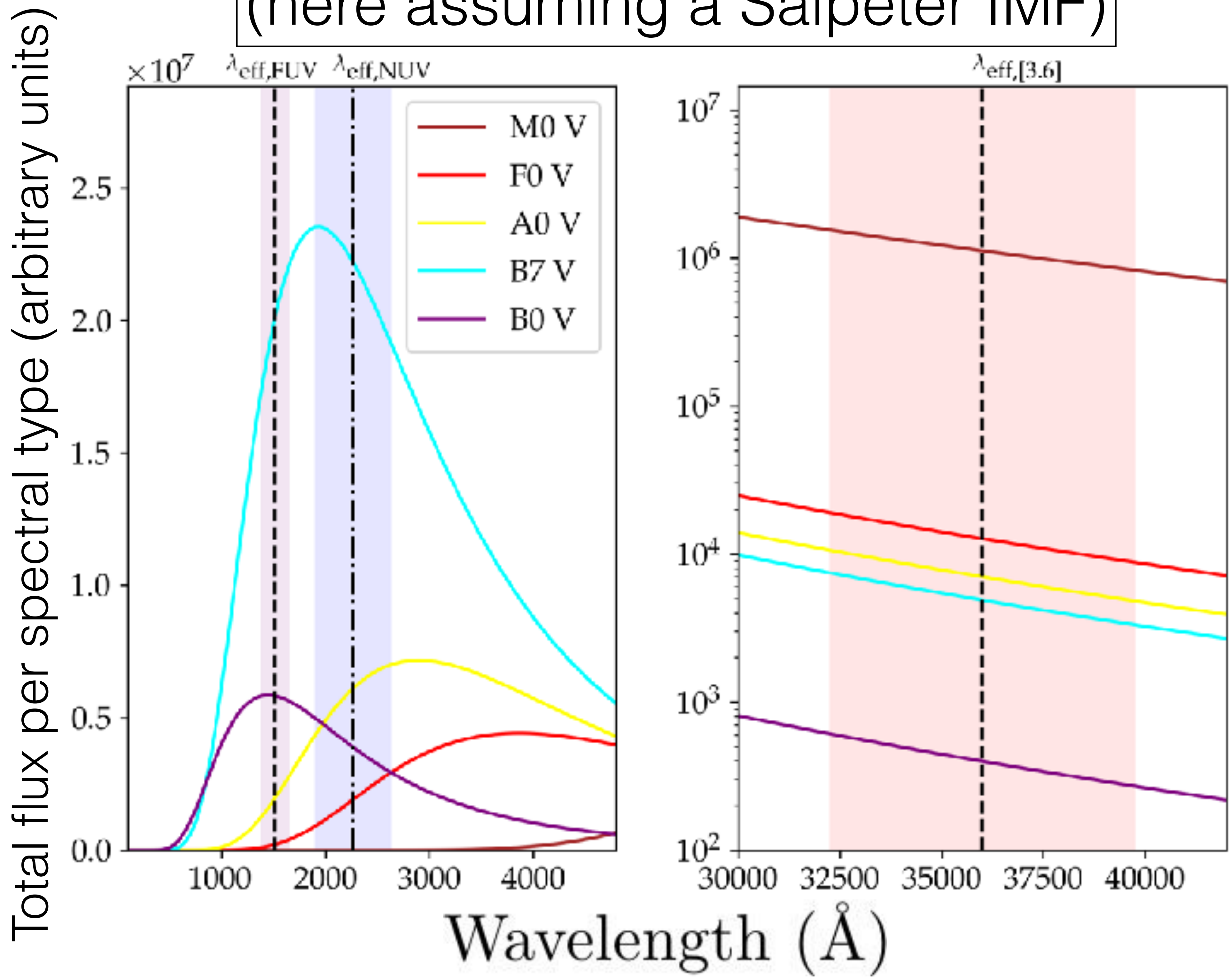

1. Introduction

Young and massive OB associations emit in the UV.
—> GALEX FUV+NUV

Low-mass MS stars and Red Giants emit in the IR.
—> Spitzer/IRAC1

Therefore, FUV, NUV and 3.6 micron are ideal to study young to old stellar populations.

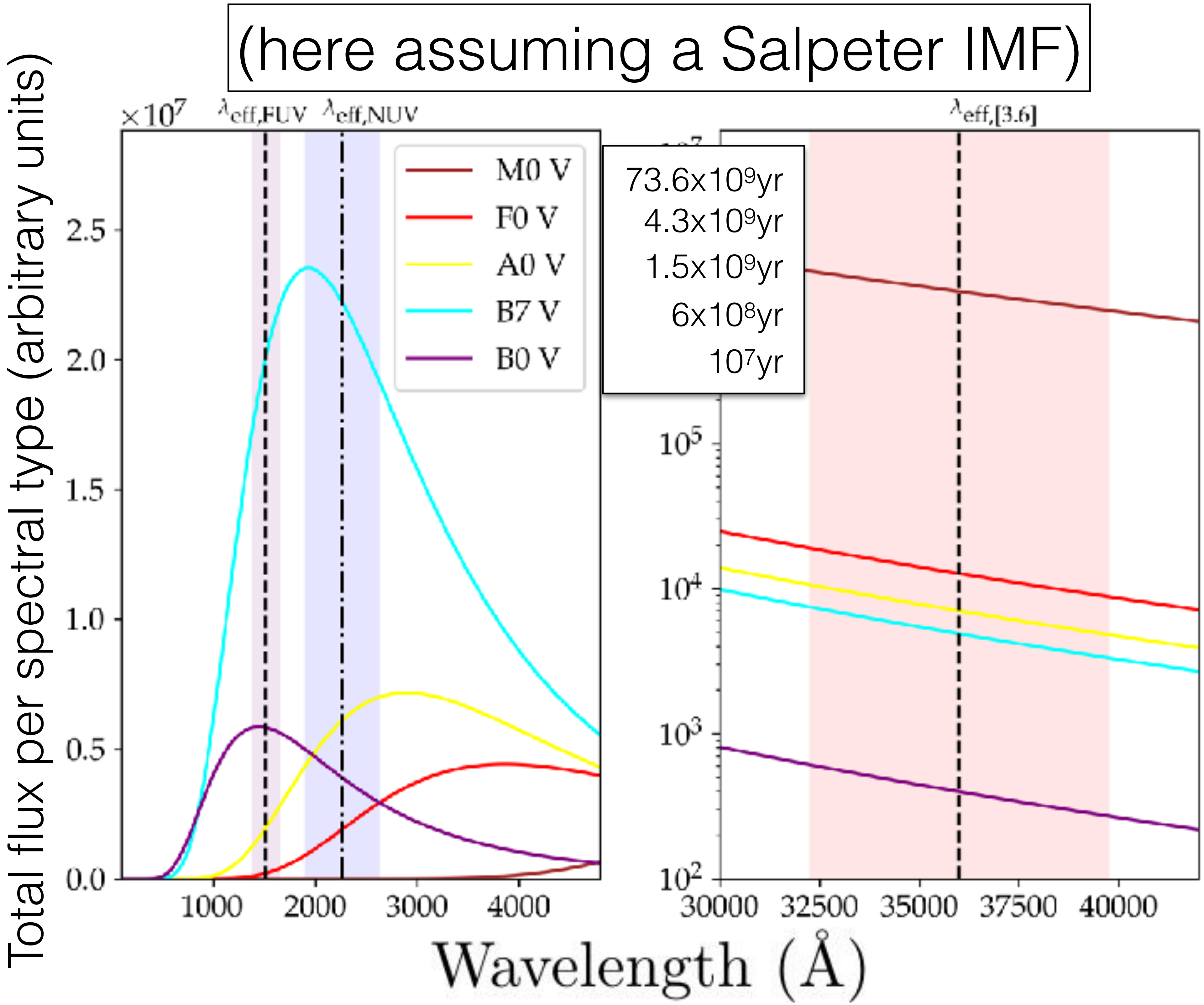

1. Introduction

Observing galaxies in the UV:

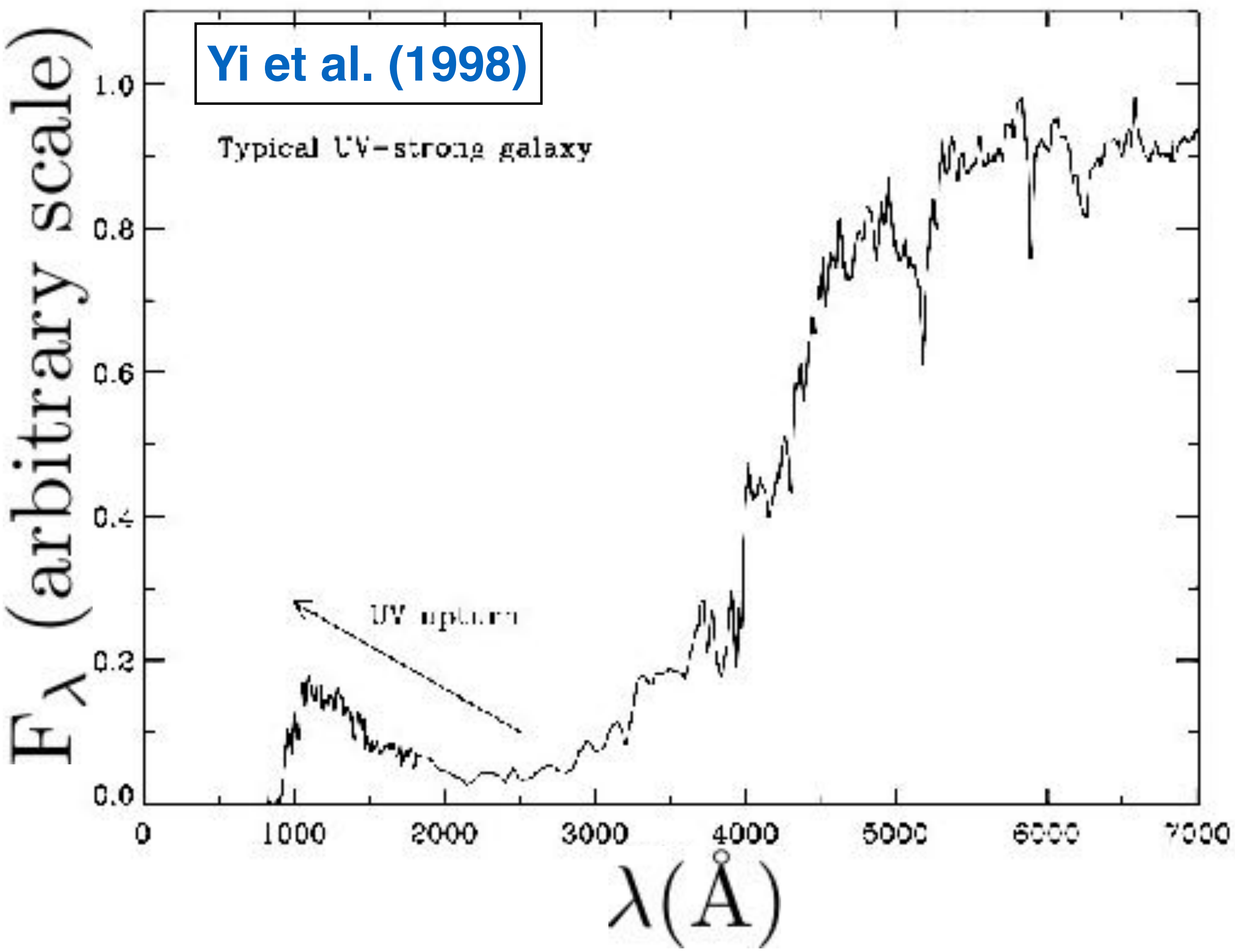

The UV upturn phenomenon in ETGs

- possibly caused by old low-mass stars of the Extreme Horizontal Branch (EHB)
- strength of upturn correlates with line-strength of Mg_2 (**Burstein et al., 1988**)
- also with mass (**Boselli et al., 2015**)

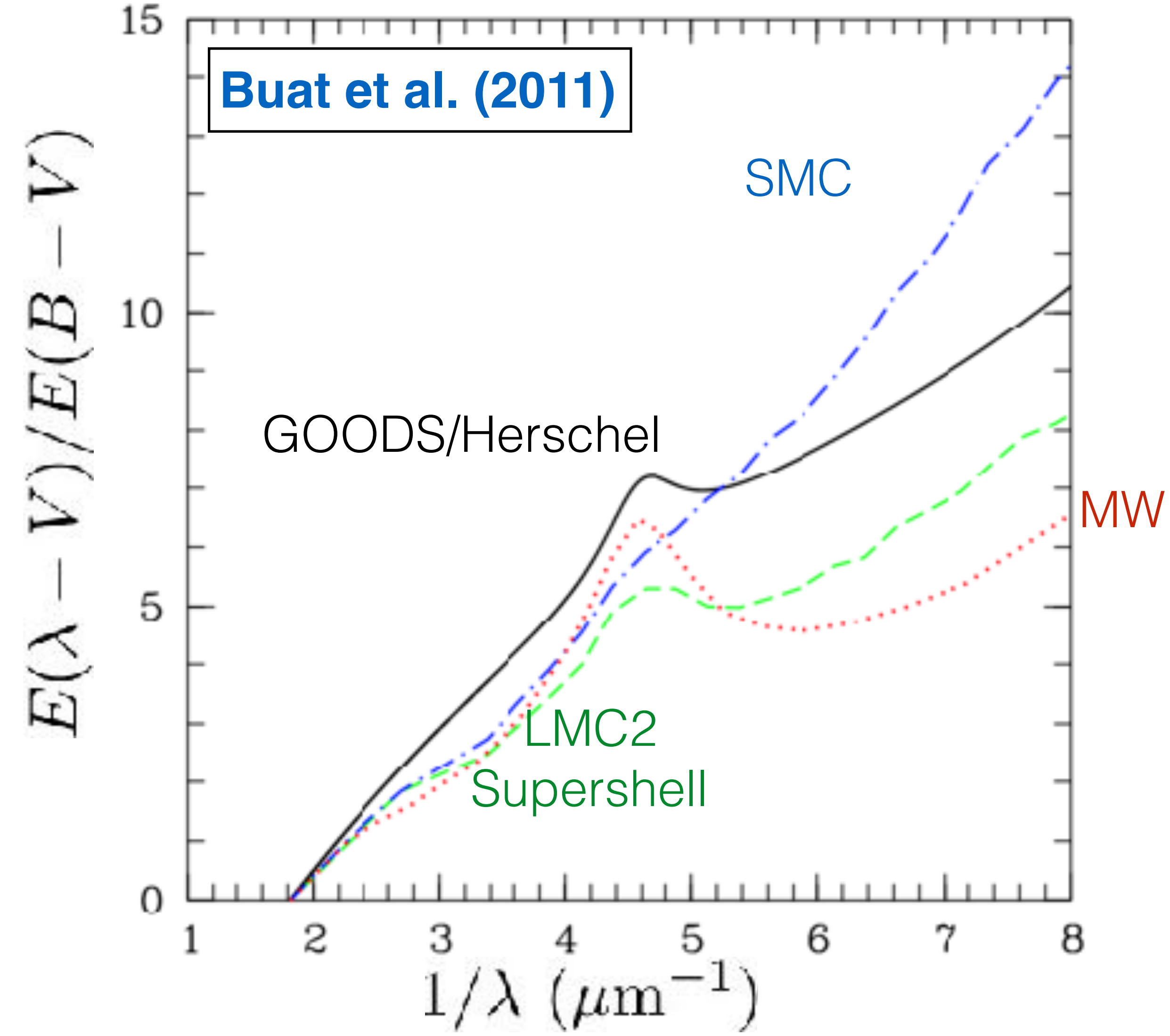

The NUV bump and FUV rise

- relative extinctions are compared
- “bump” at 2175Å

1. Introduction

Environmental effects:
Ram pressure stripping, dry/wet, major/minor mergers (and other interactions with companions), harassment, strangulation, near-collisions (fly-bys).

Tail of ionized gas in NGC 4569.
Boselli et al. (2016)

The "jellyfish" galaxy ESO137-001.
Credit: **NASA/ESA, Ming Sun (UAH), and Serge Meunier. (2014)**

2. Sample

We use the **Spitzer Survey of Stellar Structure in Galaxies (S4G)** sample of nearby galaxies as a base (**Sheth et al. 2010**).

The S4G is a volume-limited, size-limited, magnitude-limited sample and goes to unprecedented depth of ~26.5 mag arcsec^{-2} in the IRAC1 channel

Artist rendition of the Spitzer Space Telescope

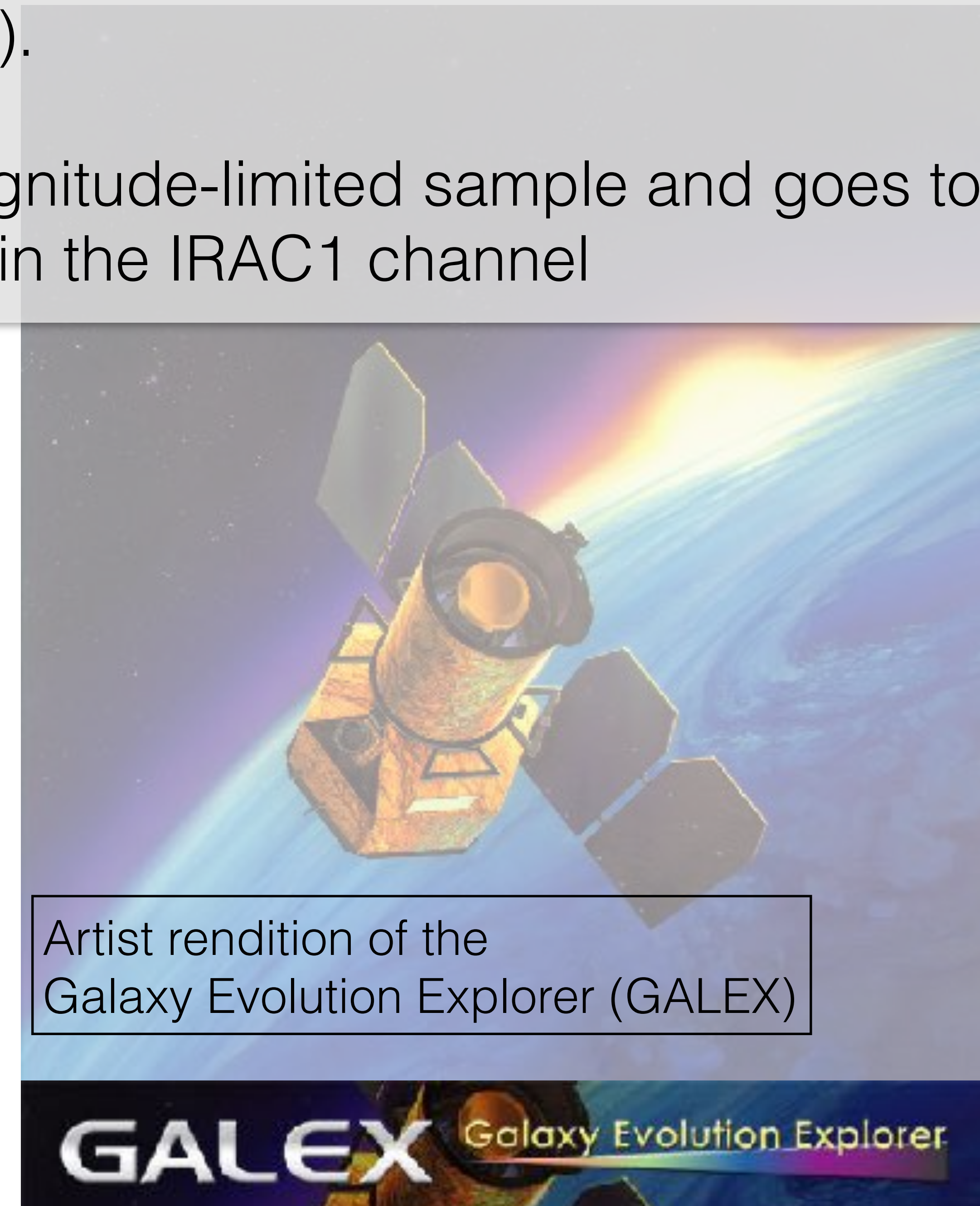

Artist rendition of the Galaxy Evolution Explorer (GALEX)

2. Sample

scripts credit: **Erik Tollerud**
Data: Cosmicflows-2 (**Tully et al., 2013**)
S^4G (**Sheth et al., 2010**)

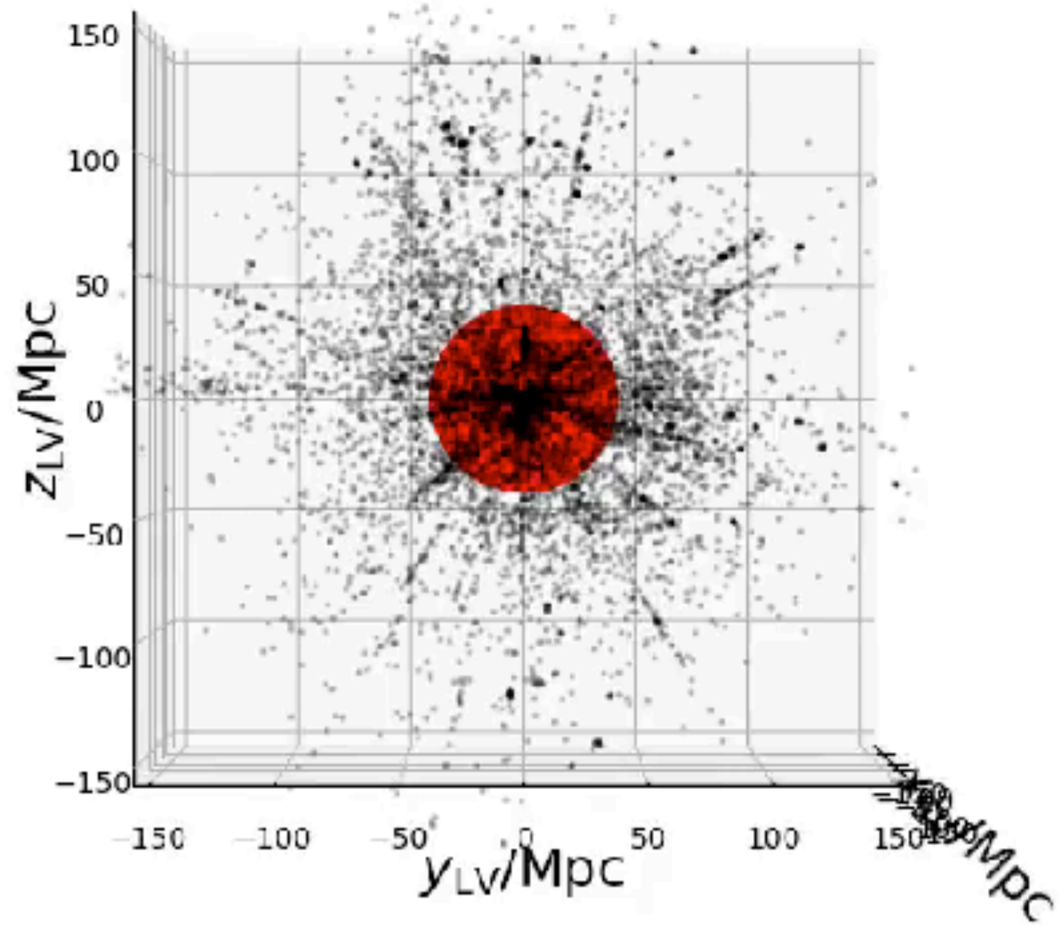

The S^4G sample
size N = 2352 galaxies
Galactic latitude $|b| \geq 30^\circ$
Angular diameter $D_{25} > 1'$
Radial velocity vrad < 3000 km s^{-1}
(corresponds to ~40 Mpc)
(obtained from HI 21cm obs.)

Photometry obtained with
the Infrared Array Camera (IRAC)
in channel 1 (3.6 μm) and 2 (4.5 μm)
by Muñoz Mateos et al., 2015

We gather GALEX raw product tiles from GR6/7 for the S4G galaxies via the publicly available online tool GalexView:
http://galex.stsci.edu/galexview/

2. Sample

scripts credit: **Erik Tollerud**
Data: Cosmicflows-2 (**Tully et al., 2013**)
S^4G (**Sheth et al., 2010**)

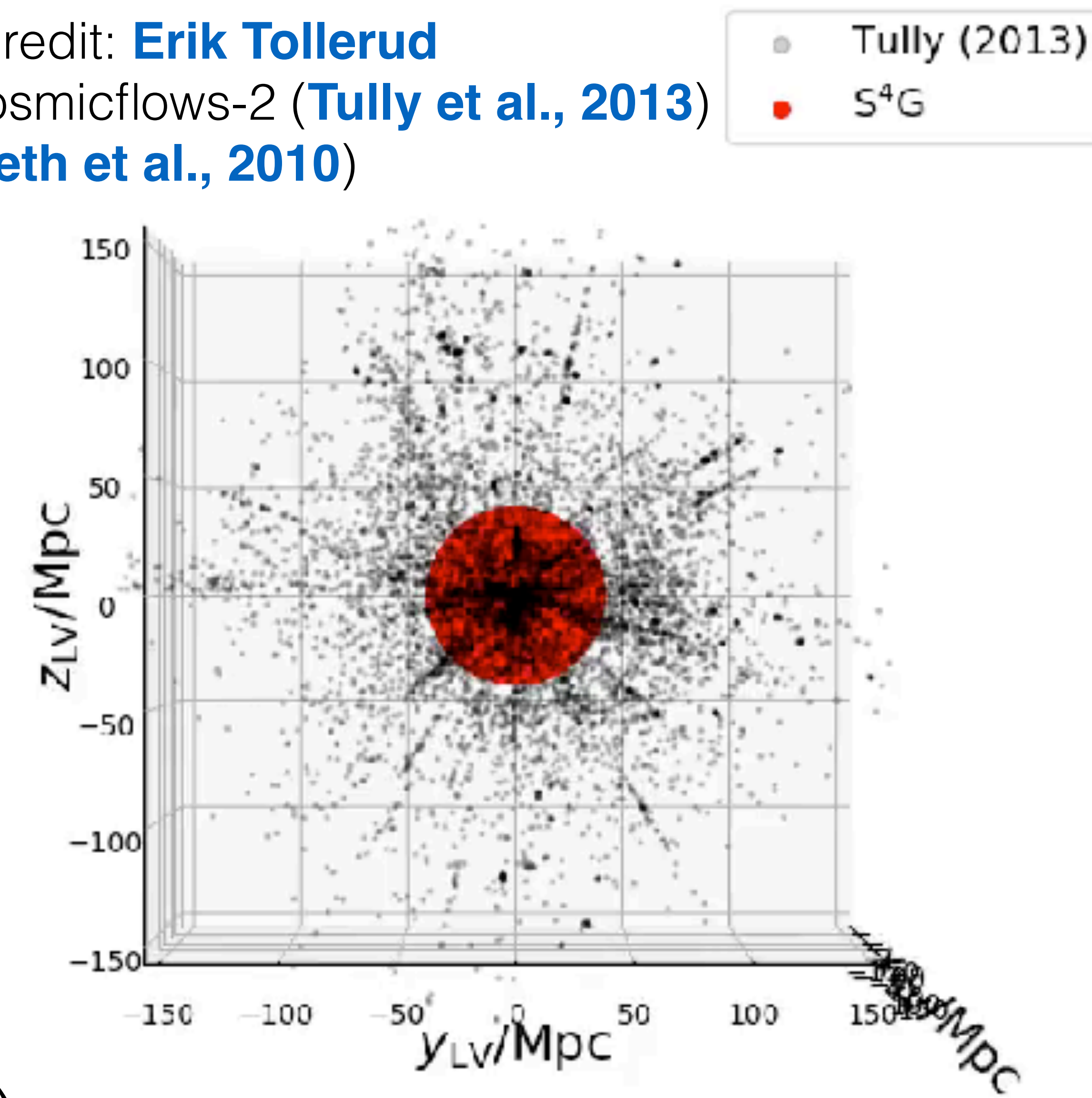

The S^4G sample
size N = 2352 galaxies
Galactic latitude |b| ≥ 30˚
Angular diameter D_{25} > 1’
Radial velocity vrad < 3000 km s^{-1}
(corresponds to ~40 Mpc)
(obtained from HI 21cm obs.)

Photometry obtained with
the Infrared Array Camera (IRAC)
in channel 1 (3.6 μm) and 2 (4.5 μm)
by Muñoz Mateos et al., 2015

We gather GALEX raw product tiles from GR6/7 for the S4G galaxies via the publicly available online tool GalexView:
http://galex.stsci.edu/galexview/

INFRARED ARRAY CAMERA
SPITZER SPACE TELESCOPE

2. Sample

scripts credit: **Erik Tollerud**
Data: Cosmicflows-2 (**Tully et al., 2013**)
S^4G (**Sheth et al., 2010**)

The S^4G sample
size N = 2352 galaxies
Galactic latitude |b| ≥ 30˚
Angular diameter D_{25} > 1'
Radial velocity vrad < 3000 km s^{-1}
(corresponds to ~40 Mpc)
(obtained from HI 21cm obs.)

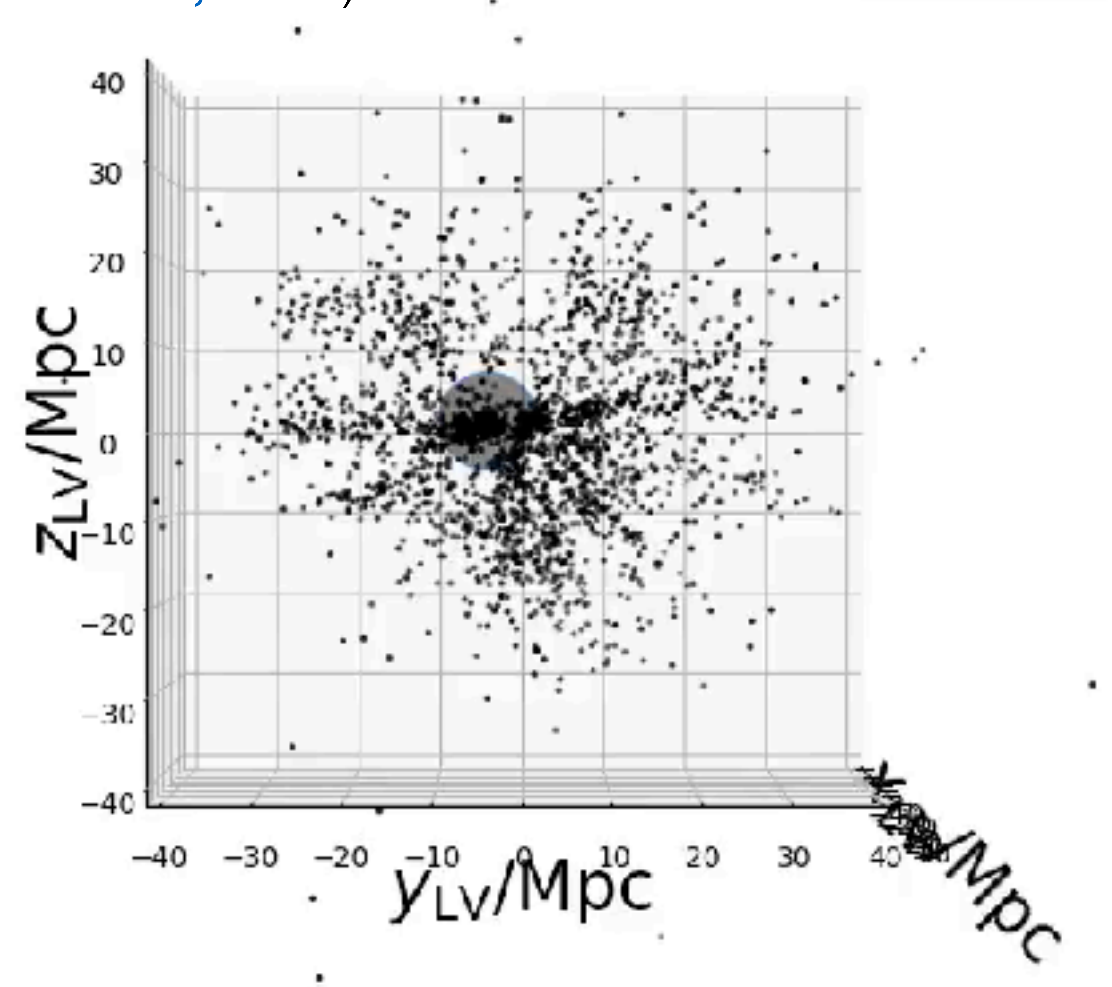

Photometry obtained with
the Infrared Array Camera (IRAC)
in channel 1 (3.6 μm) and 2 (4.5 μm)
by Muñoz Mateos et al., 2015

We gather GALEX raw product tiles from GR6/7
for the S4G galaxies via the publicly available
online tool GalexView:
http://galex.stsci.edu/galexview/

3. Data analysis

Data Preparations
Sky measurement
Semi-automatic masking
Photometry

→

Data products
Surface brightness profiles
Color profiles
false-color RGB images

→

Analysis
Linear fittings
Comparisons with models
M_*, SFR, sSFR conversion

3. Data analysis — Preparations

Sky Measurement

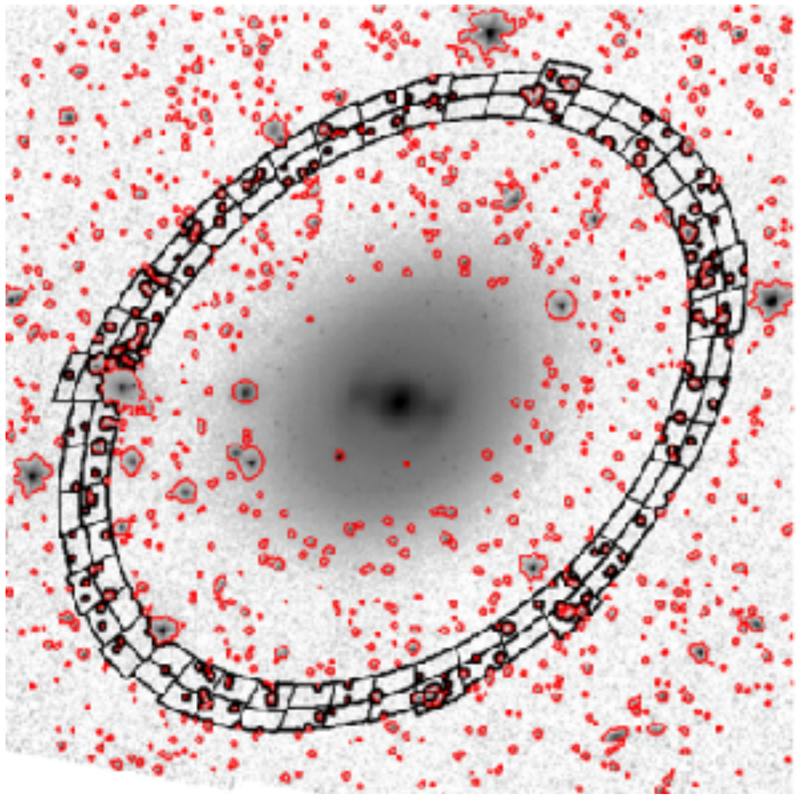

An elliptical ring-annulus is placed at 1.5xD25 and divided into 90 boxes.

The average is computed in each box, which is then averaged using all the boxes.

Masking

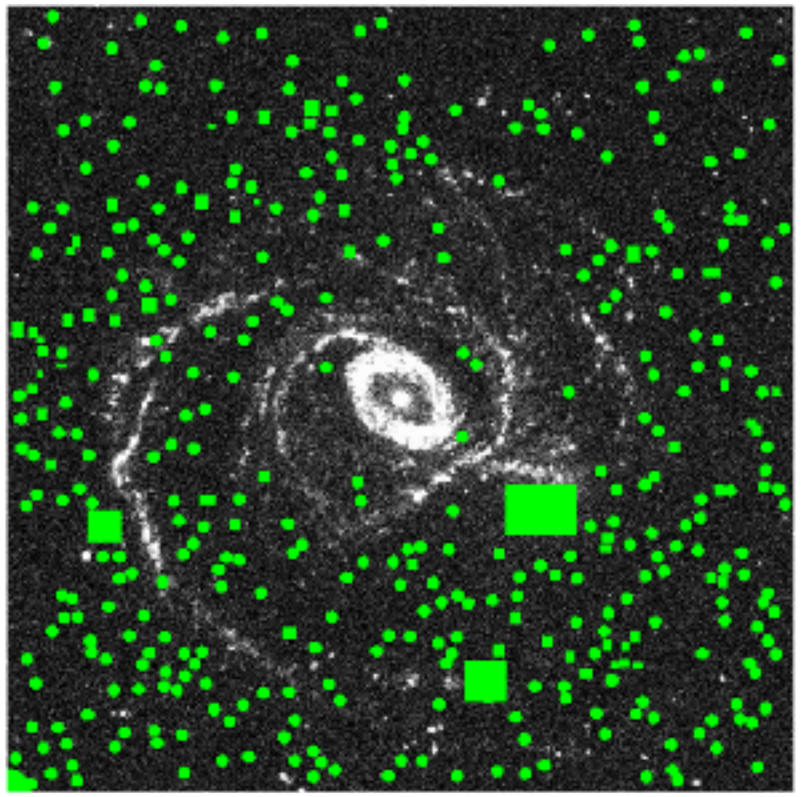

Semi-automatic masking based on (FUV - NUV) color.

Each mask is visually checked and corrected for false-detection, companions, and foreground stars.

Interpolation

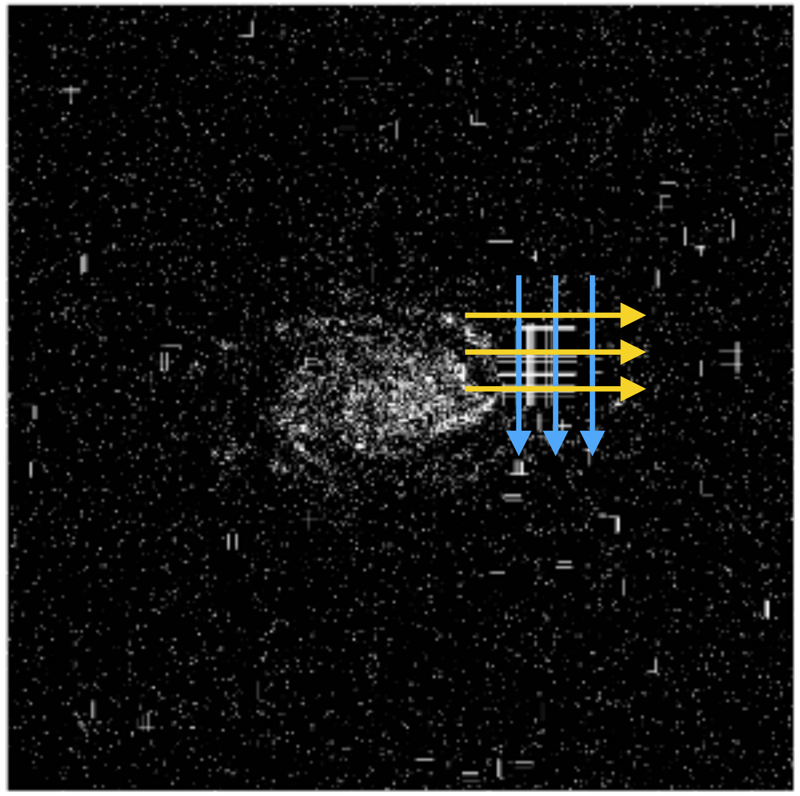

The masked regions are then interpolated using the average of neighbor pixels, vertically and horizontally.

3. Data analysis — Measurements

Photometry

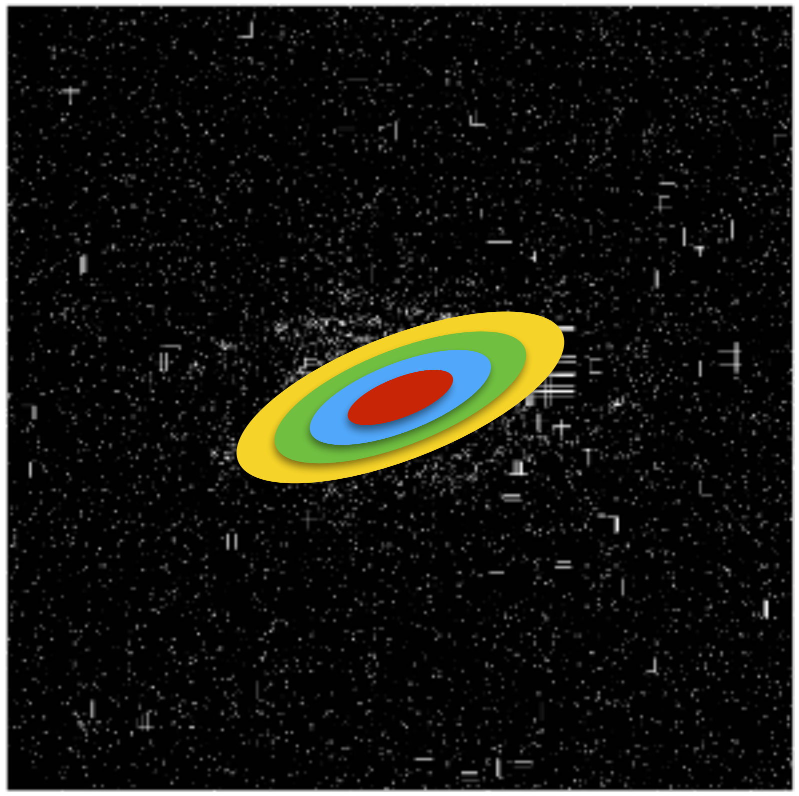

Photometry is performed in fixed PA and ϵ elliptical ring-annuli with 6" steps. The average is computed for each ring.

For the FUV and NUV, we use the same apertures as the ones used to do the 3.6 µm photometry.

Data products

- False-color RGB images
- Surface brightness profiles
- Color profiles
- Growth curves
- Asymptotic magnitudes

- Spatial resolution of data: 6 arcsec
- corrected for foreground MW attenuation using A_{FUV}=7.9E(B-V) and A_{NUV}=8.0E(B-V).
- Final galaxy count: 1931 with homogenized FUV, NUV, and 3.6 µm data

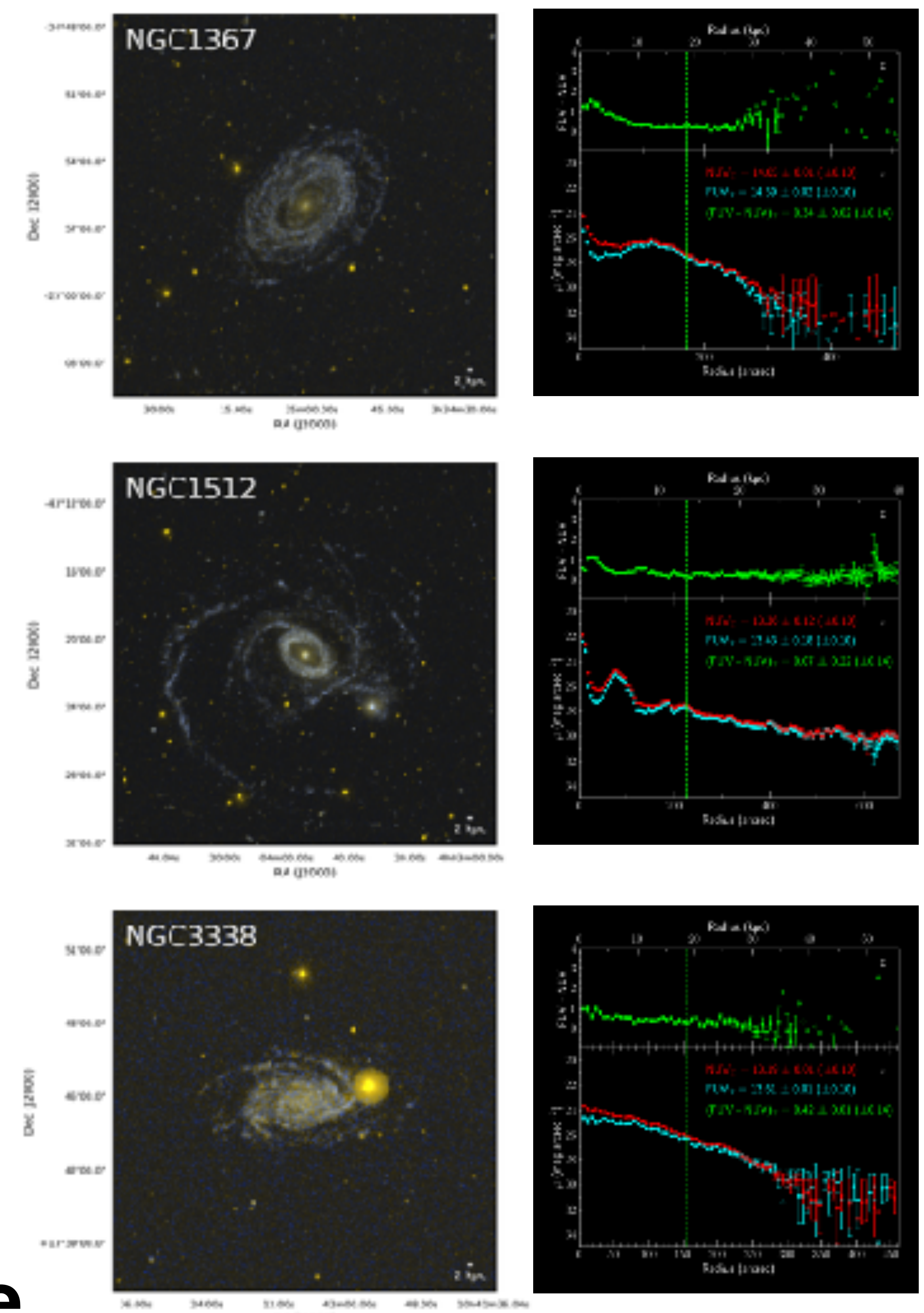

We call this the
GALEX/S4G sample

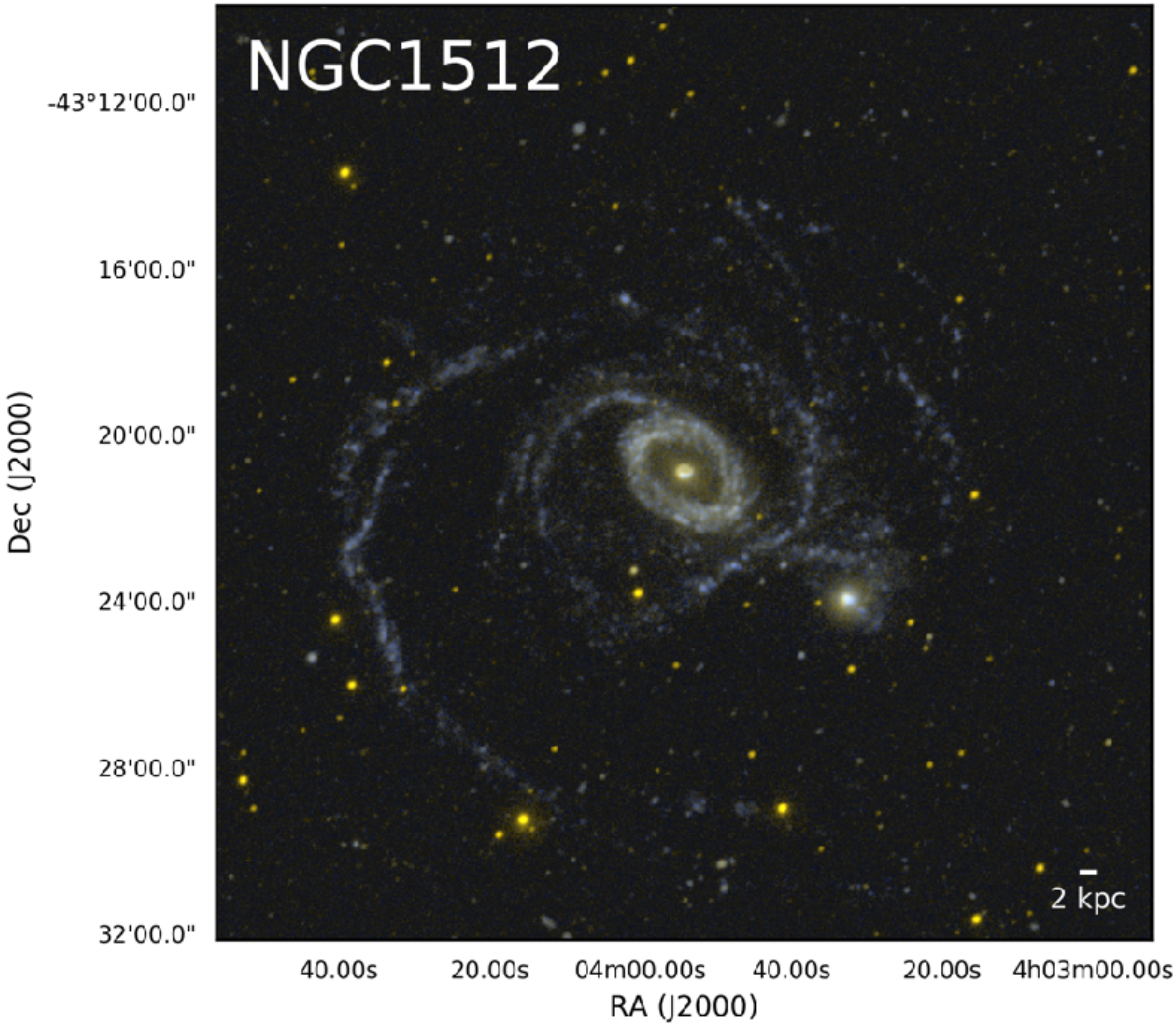
NGC1512
-43°12'00.0"
16'00.0"
20'00.0"
24'00.0"
28'00.0"
32'00.0"
Dec (J2000)
40.00s
20.00s
04m00.00s
40.00s
20.00s
4h03m00.00s
RA (J2000)
2 kpc

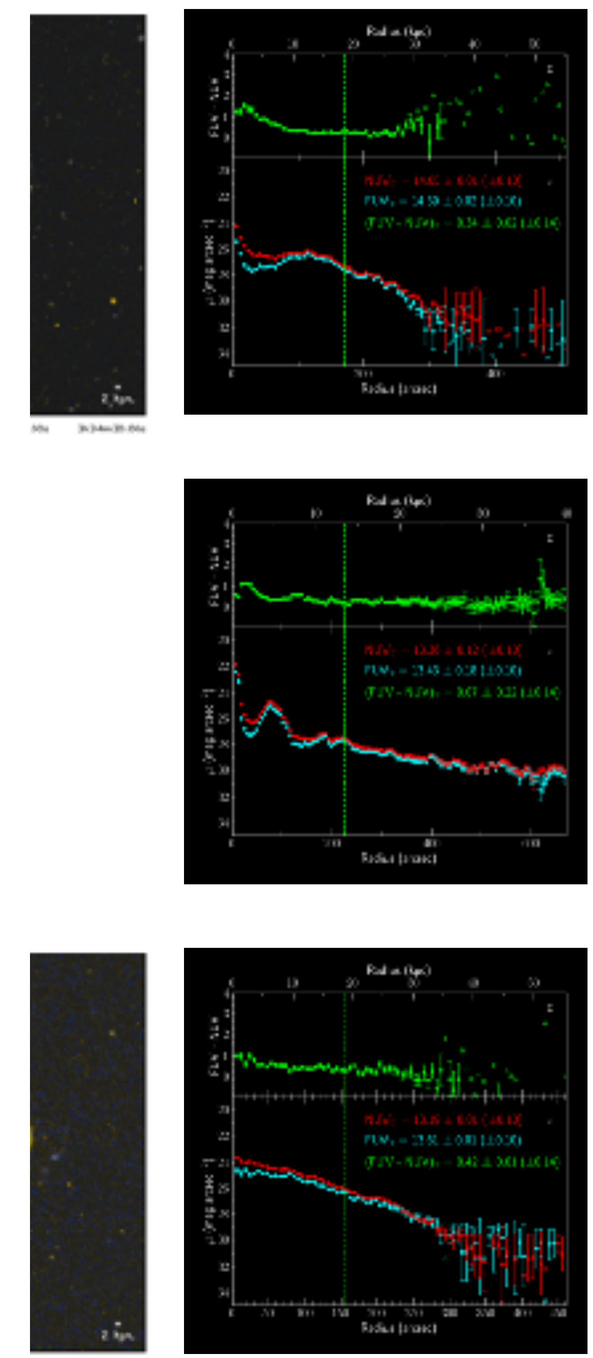

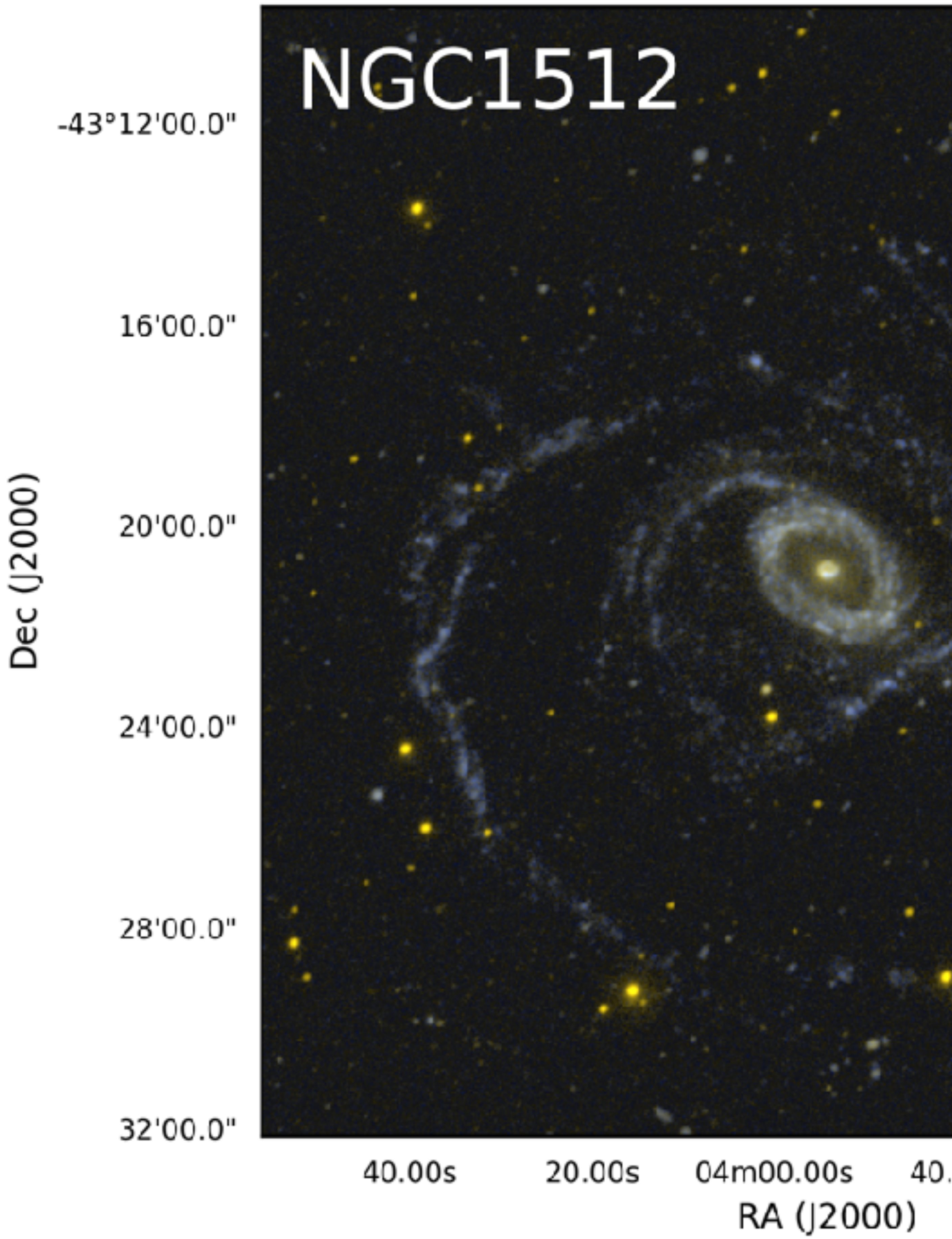
NGC1512
-43°12'00.0"
16'00.0"
20'00.0"
24'00.0"
28'00.0"
32'00.0"
Dec (J2000)
40.00s
20.00s
04m00.00s
40.00s
20.00s
4h03m00.00s
RA (J2000)
2 kpc

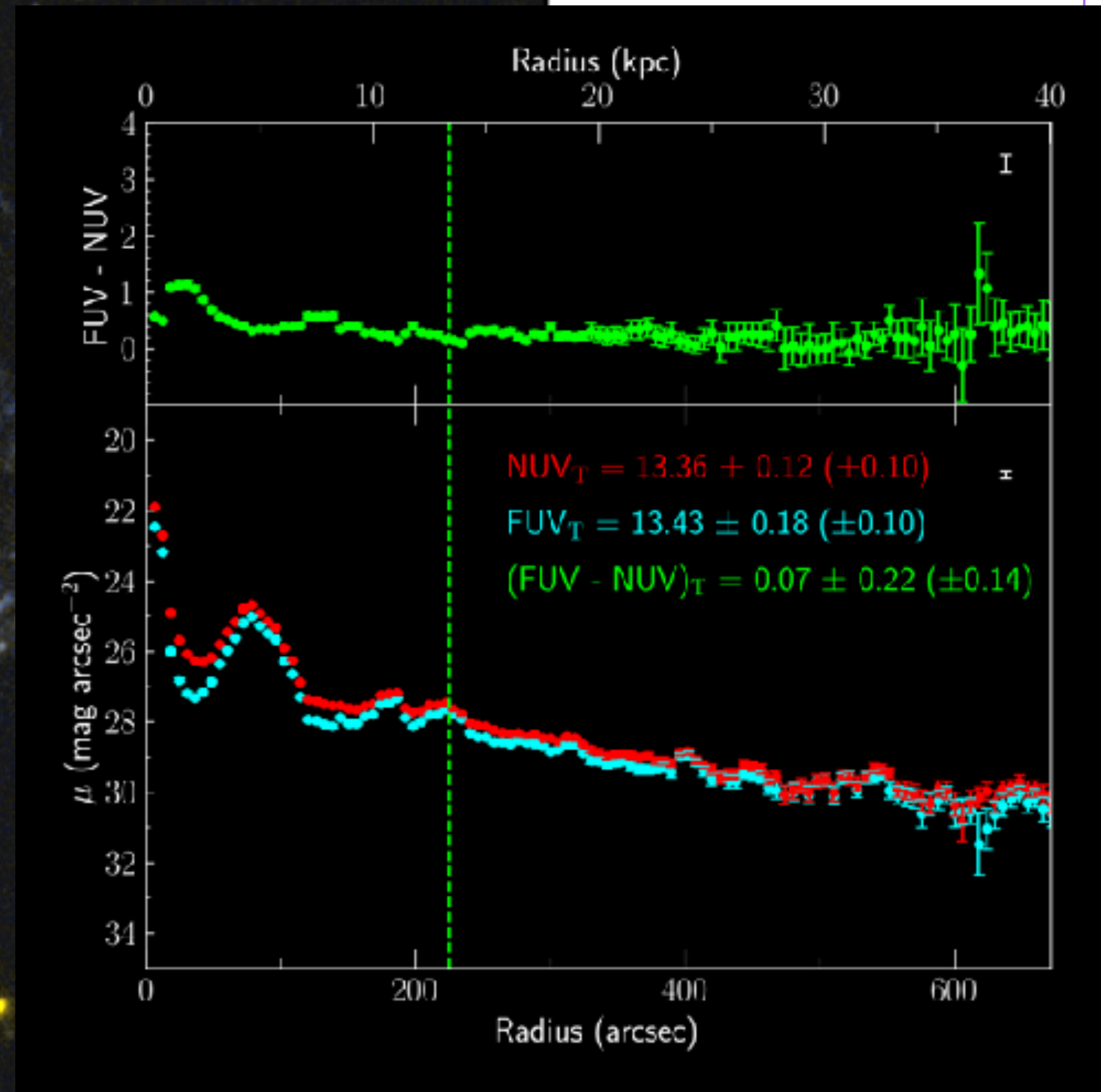
Radius (kpc)
0
10
20
30
40
FUV - NUV
4
3
2
1
0
20
22
24
26
28
30
32
34
μ (mag arcsec^{-2})
$NUV_T = 13.36 \pm 0.12 (\pm 0.10)$
$FUV_T = 13.43 \pm 0.18 (\pm 0.10)$
$(FUV - NUV)_T = 0.07 \pm 0.22 (\pm 0.14)$
0
200
400
600
Radius (arcsec)

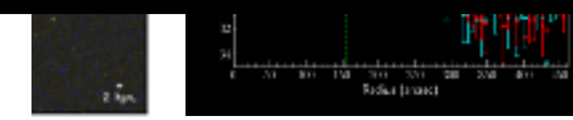

3. Data analysis — Models

Complemented by
- **environmental info of Tully et al. (2013) and Laine et al. (2014)**
- **SSP from Bruzual & Charlot (2003) and (2007)**
- **Ram-pressure stripping model from Boissier (2006)**
- **Disk-models from Boissier & Prantzos (2000)**
- **Kinematic data from HyperLEDA**

Below: 3.6 µm surface brightnesses of disk models from **Boissier & Prantzos (2000)**

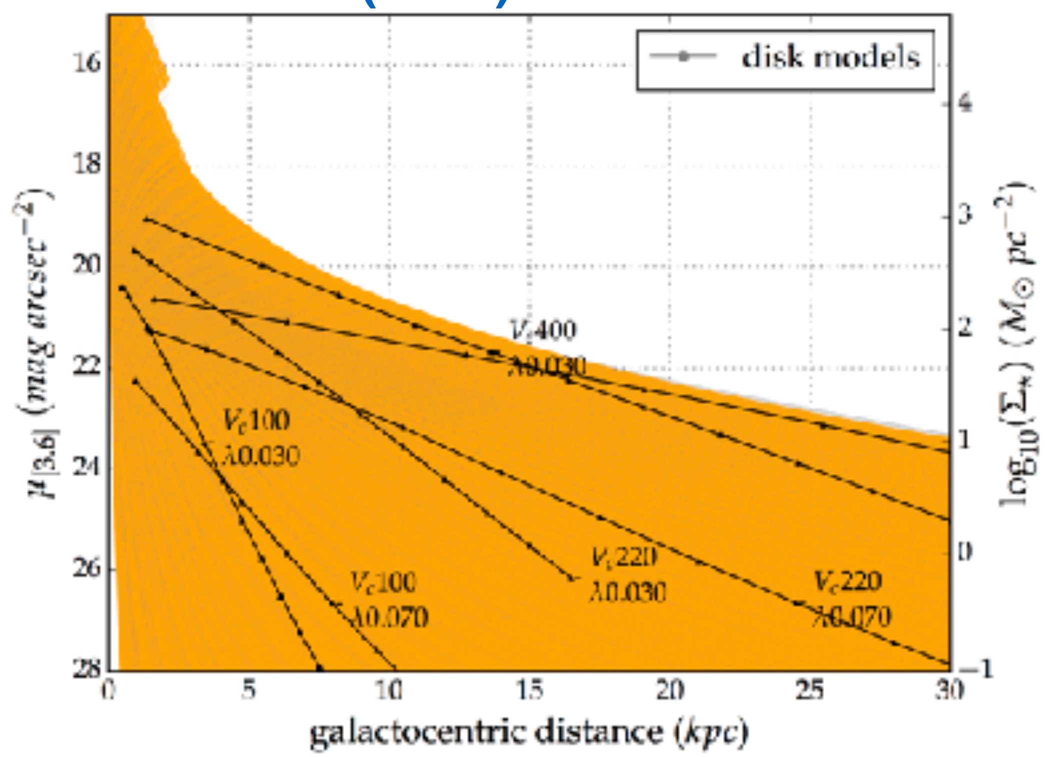

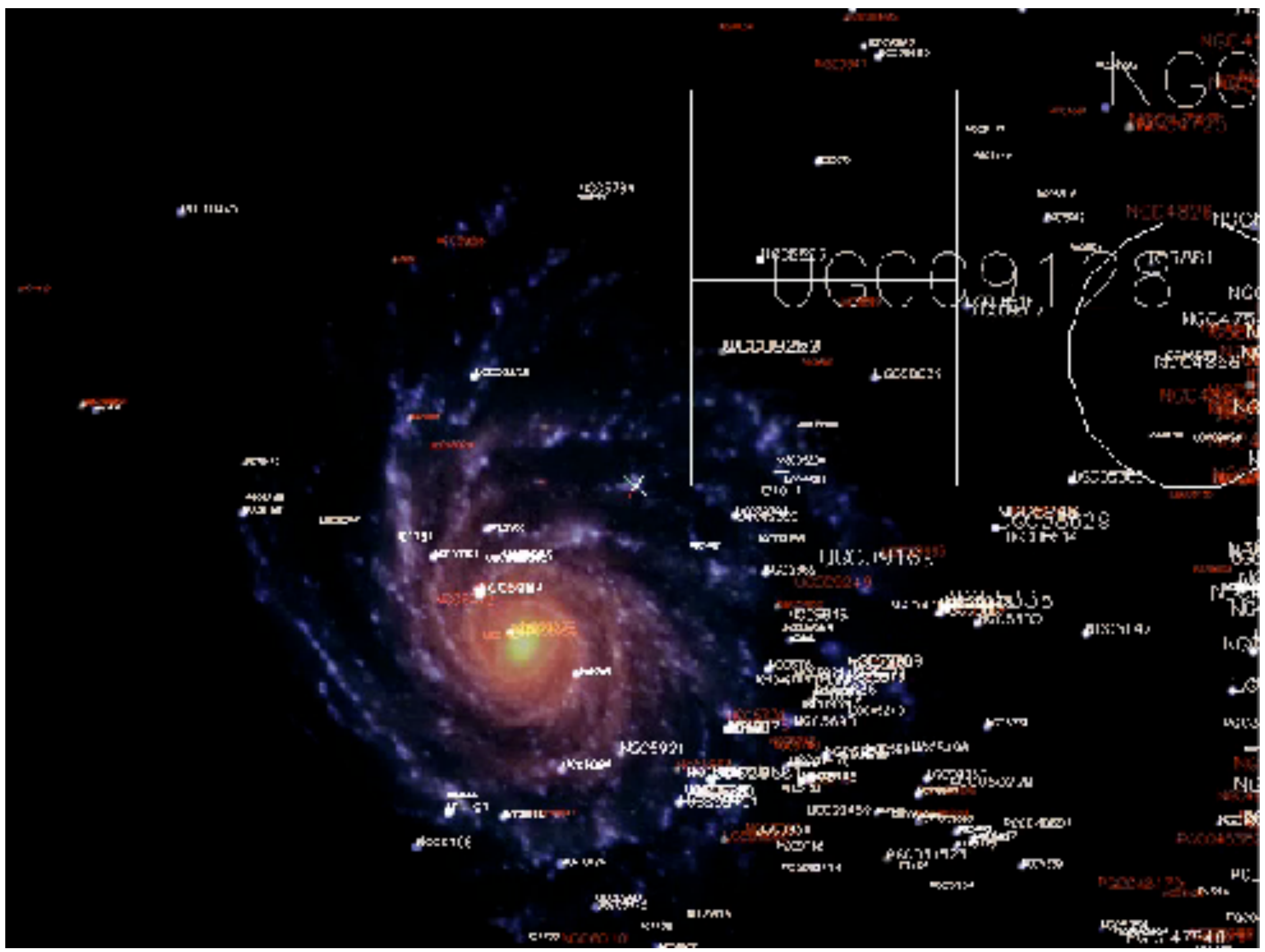

created with PartiView

Left:
red = S4G sample (**Sheth+ 2010**),
white, blue = GALEX/S4G sample (**Bouquin+ 2015**)
colors = Cosmicflows-2 samples (**Tully+ 2013**)

3. Data analysis — Models

Complemented by

- **environmental info of Tully et al. (2013) and Laine et al. (2014)**
- **SSP from Bruzual & Charlot (2003) and (2007)**
- **Ram-pressure stripping model from Boissier (2006)**
- **Disk-models from Boissier & Prantzos (2000)**
- **Kinematic data from HyperLEDA**

Below: 3.6 µm surface brightnesses of disk models from **Boissier & Prantzos (2000)**

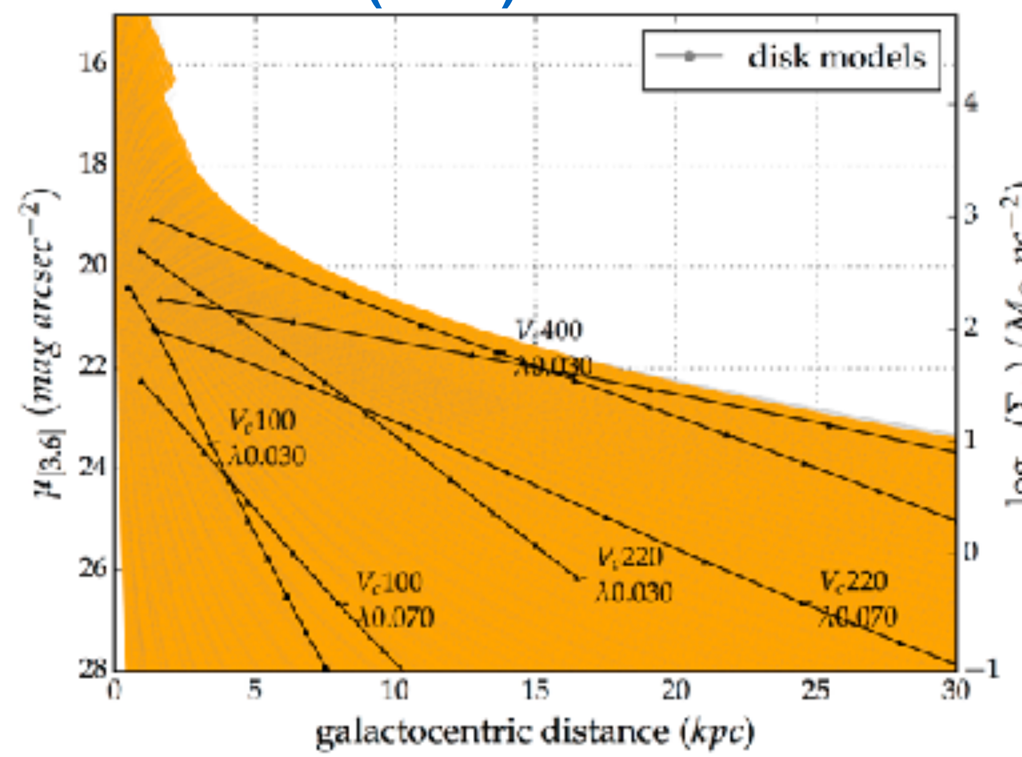

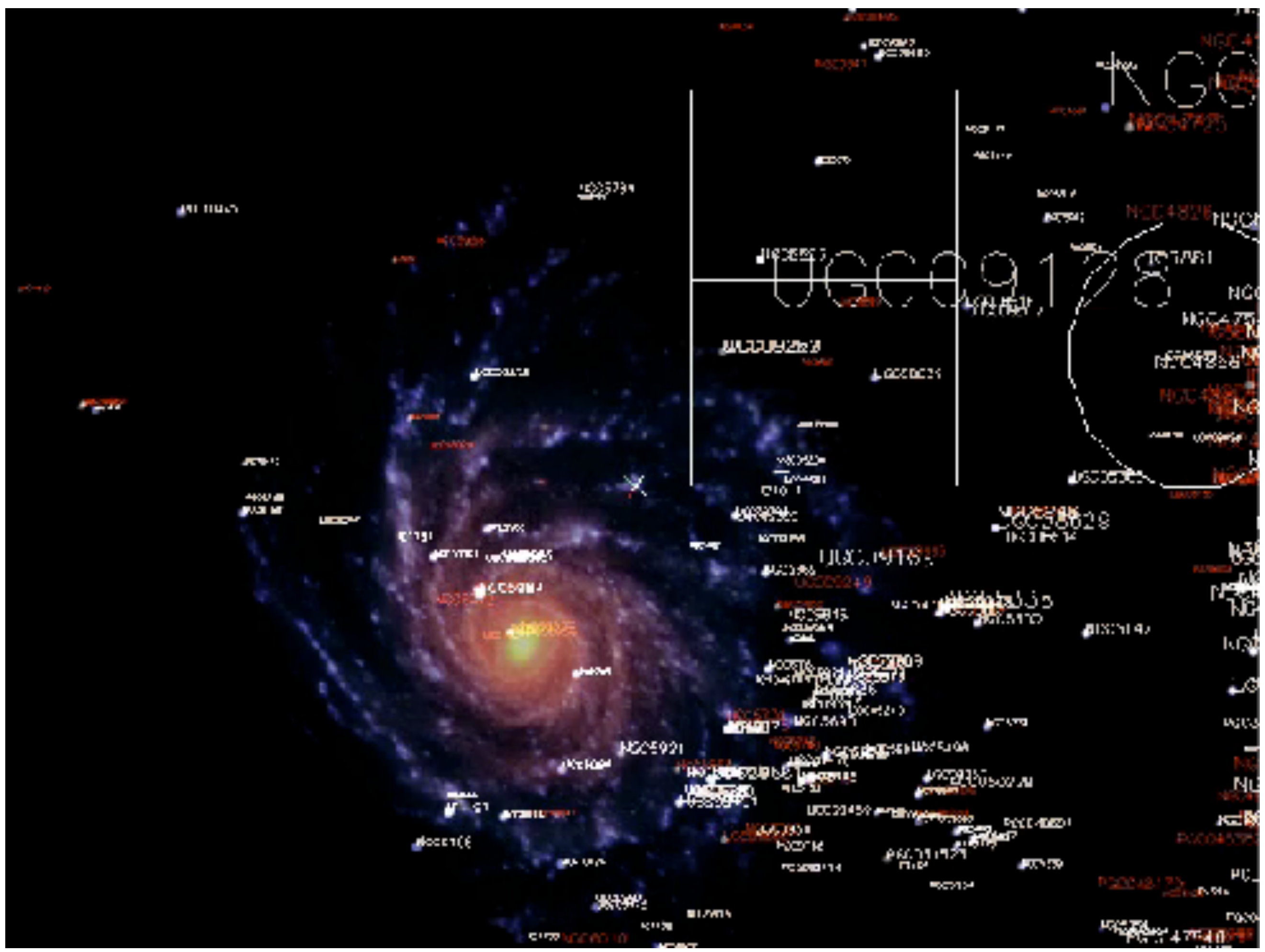

created with PartiView

Left:
red = S4G sample (**Sheth+ 2010**),
white, blue = GALEX/S4G sample (**Bouquin+ 2015**)
colors = Cosmicflows-2 samples (**Tully+ 2013)**

3. Data analysis — Database

Detailed Anatomy of GALaxies

The DAGAL database http://www.astro.rug.nl/~dagal/

FITS image repository

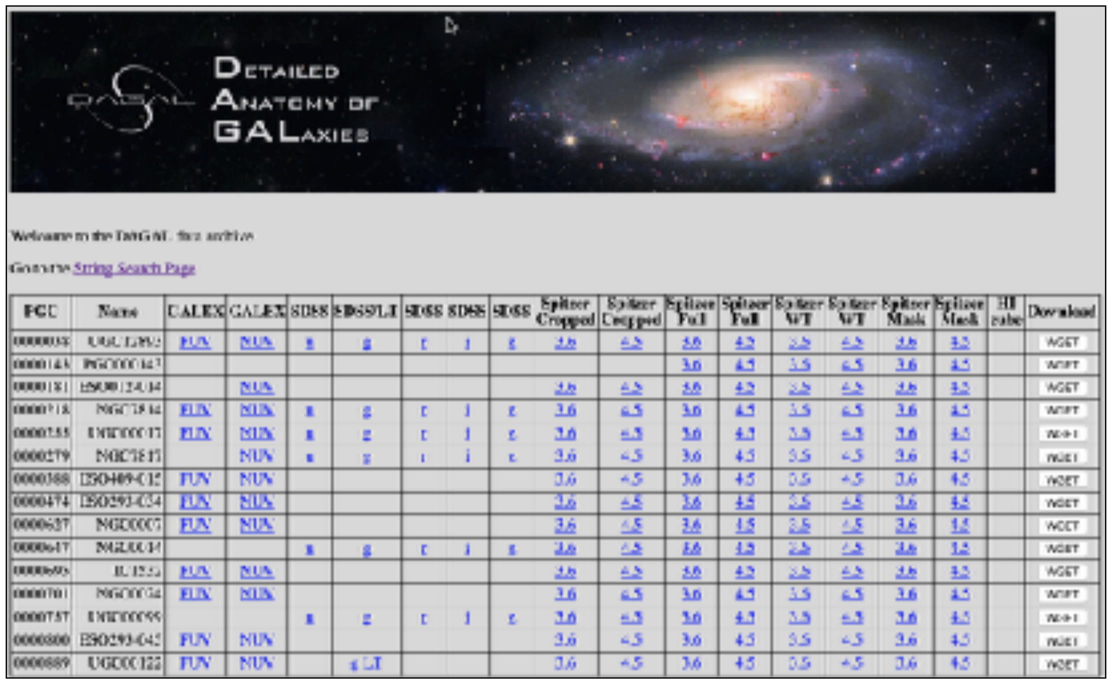

Searchable database with filters

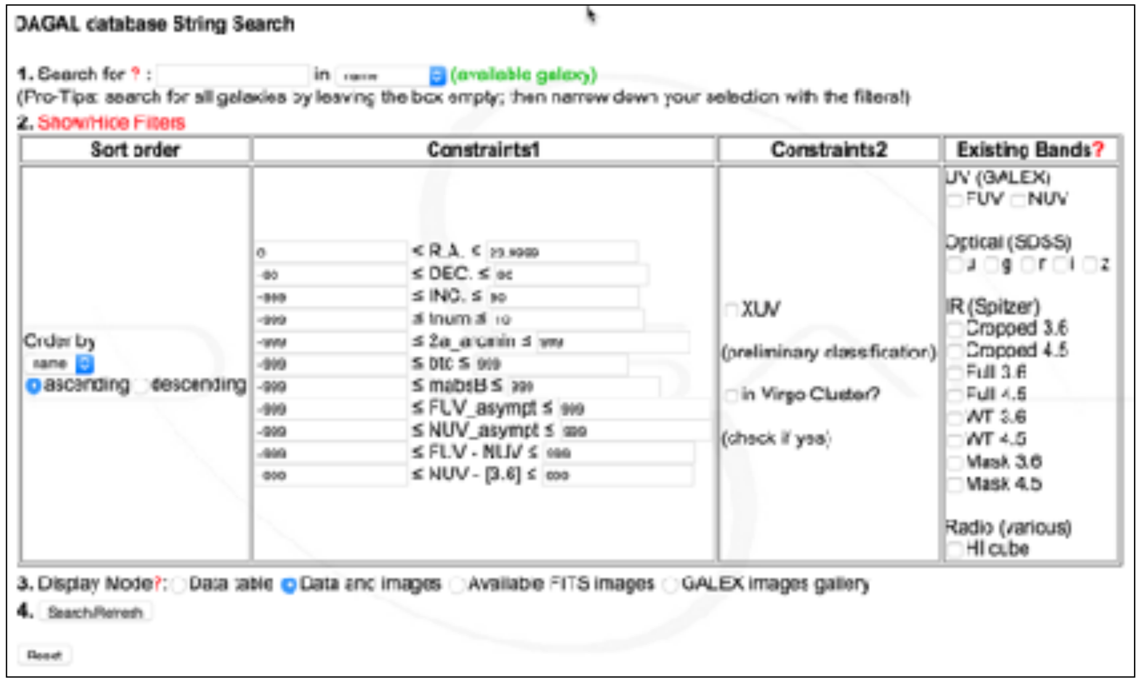

Various display modes of the results

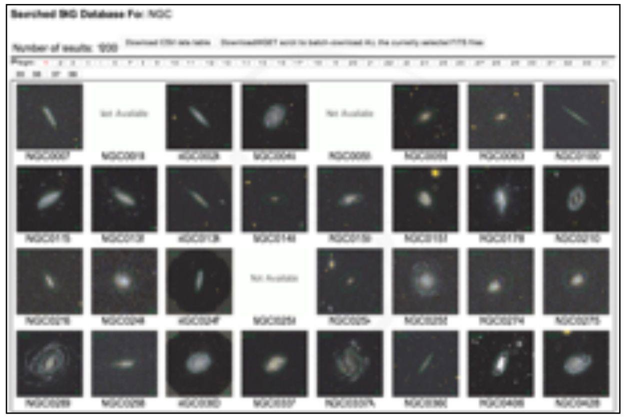

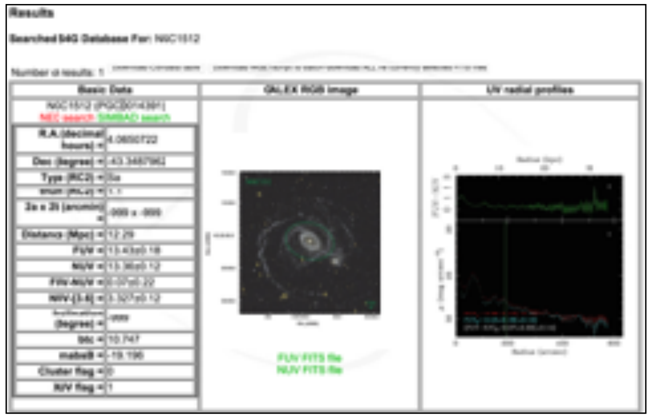

4.1 Results: Global properties

Publication

Bouquin et al. 2015, ApJL, 800, 19

“The *GALEX*/S4G UV-IR color-color diagram: catching spiral galaxies away from the blue sequence”


THE GALEX/S4G UV–IR COLOR–COLOR DIAGRAM: CATCHING SPIRAL GALAXIES AWAY FROM THE BLUE SEQUENCE

ABSTRACT

1. INTRODUCTION

2. SAMPLE

4.1 Results: Global properties

Sample comparisons: S4G (n=2352) vs. *GALEX*/S4G (n=1931) (82%)

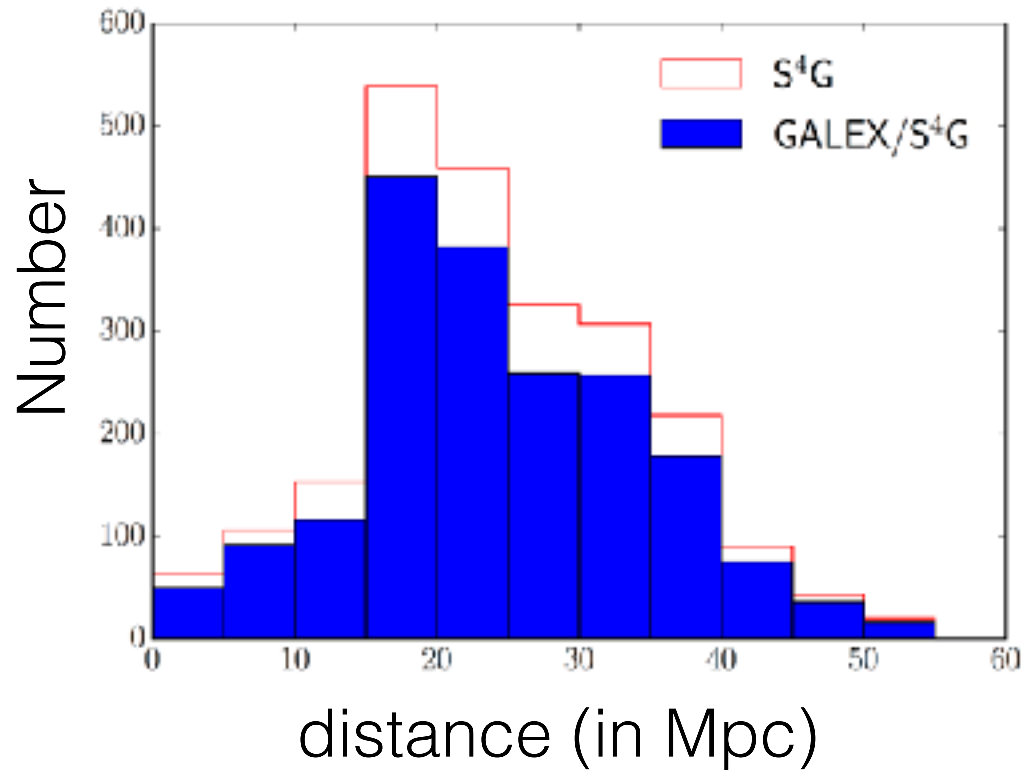

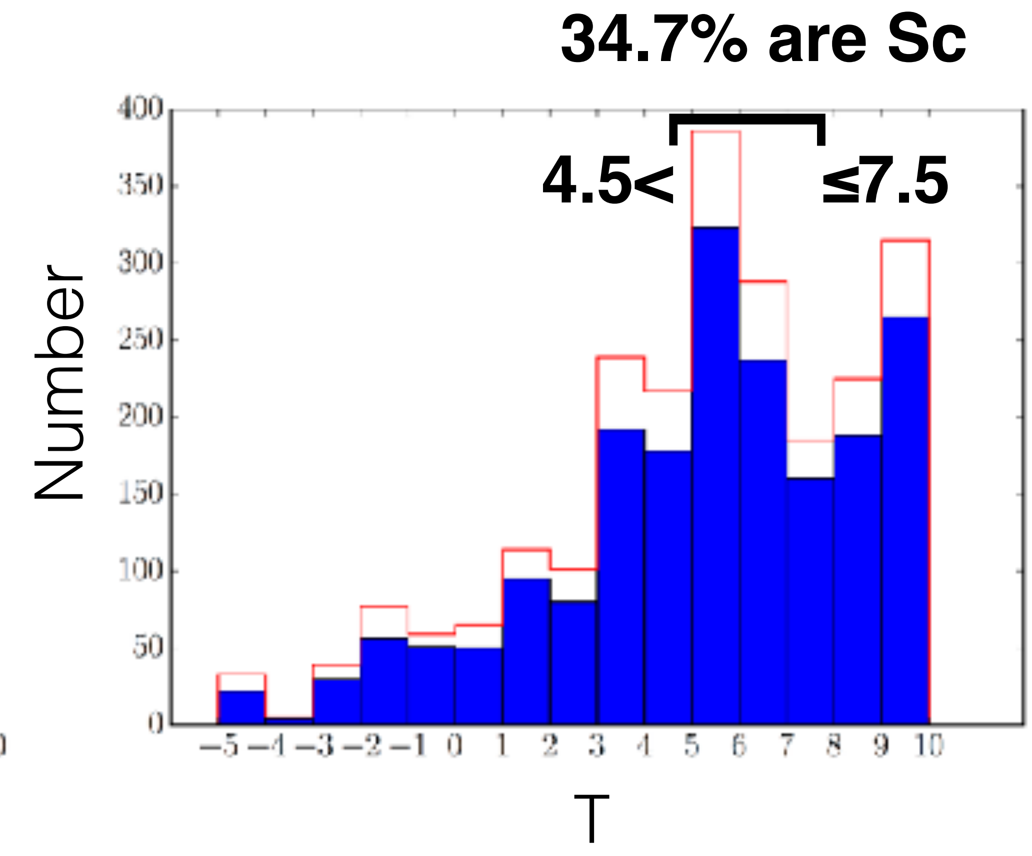

The distribution of the *GALEX*/S4G sample (blue) in various dimensions is comparable to that of the S4G sample (red)

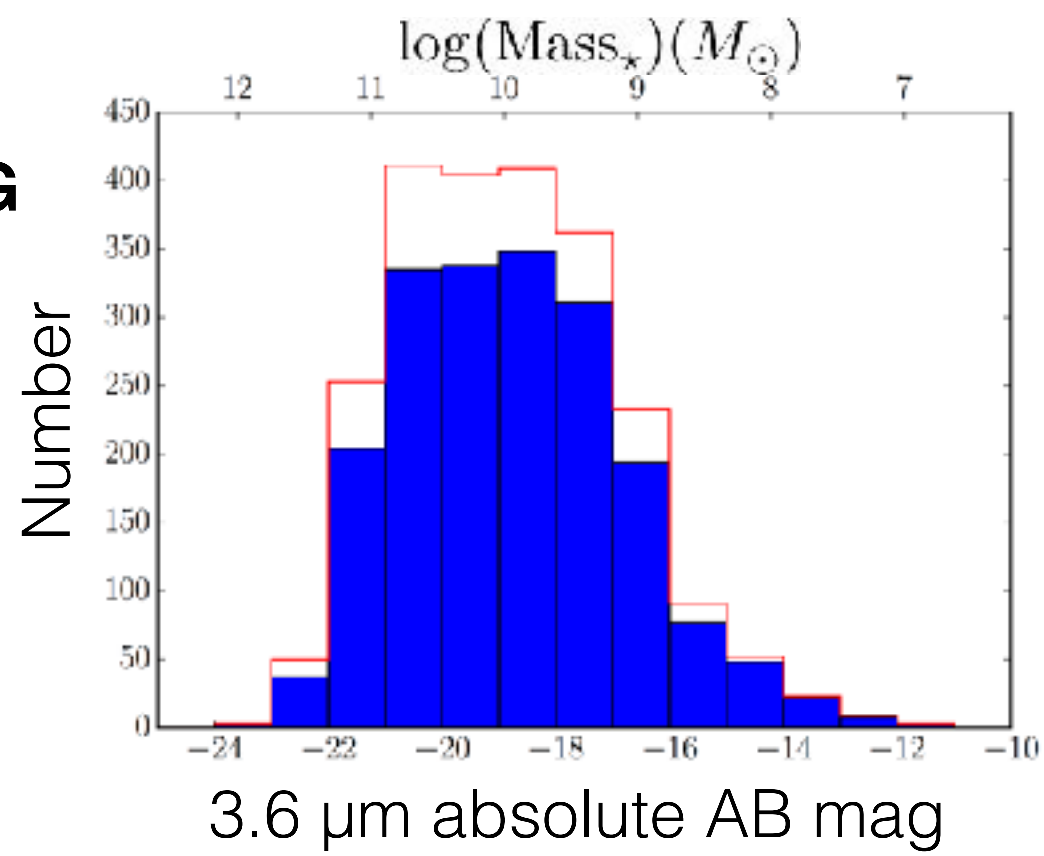

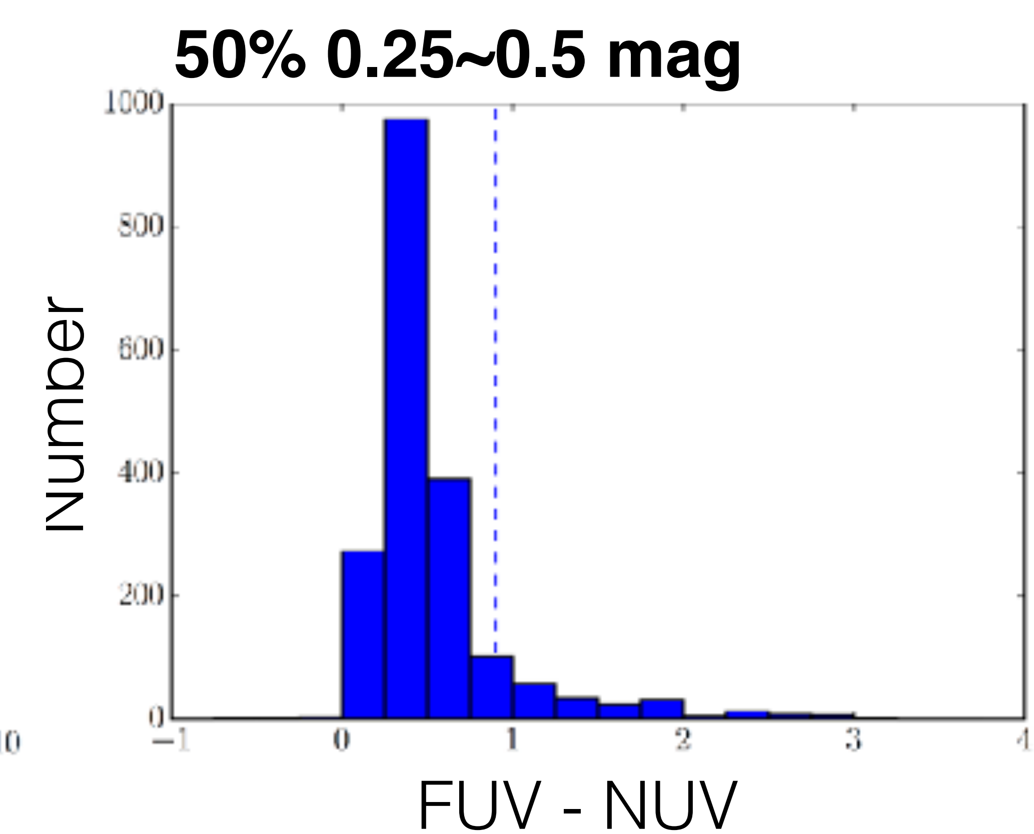

4.1 Results: Global properties

Bouquin et al. 2015

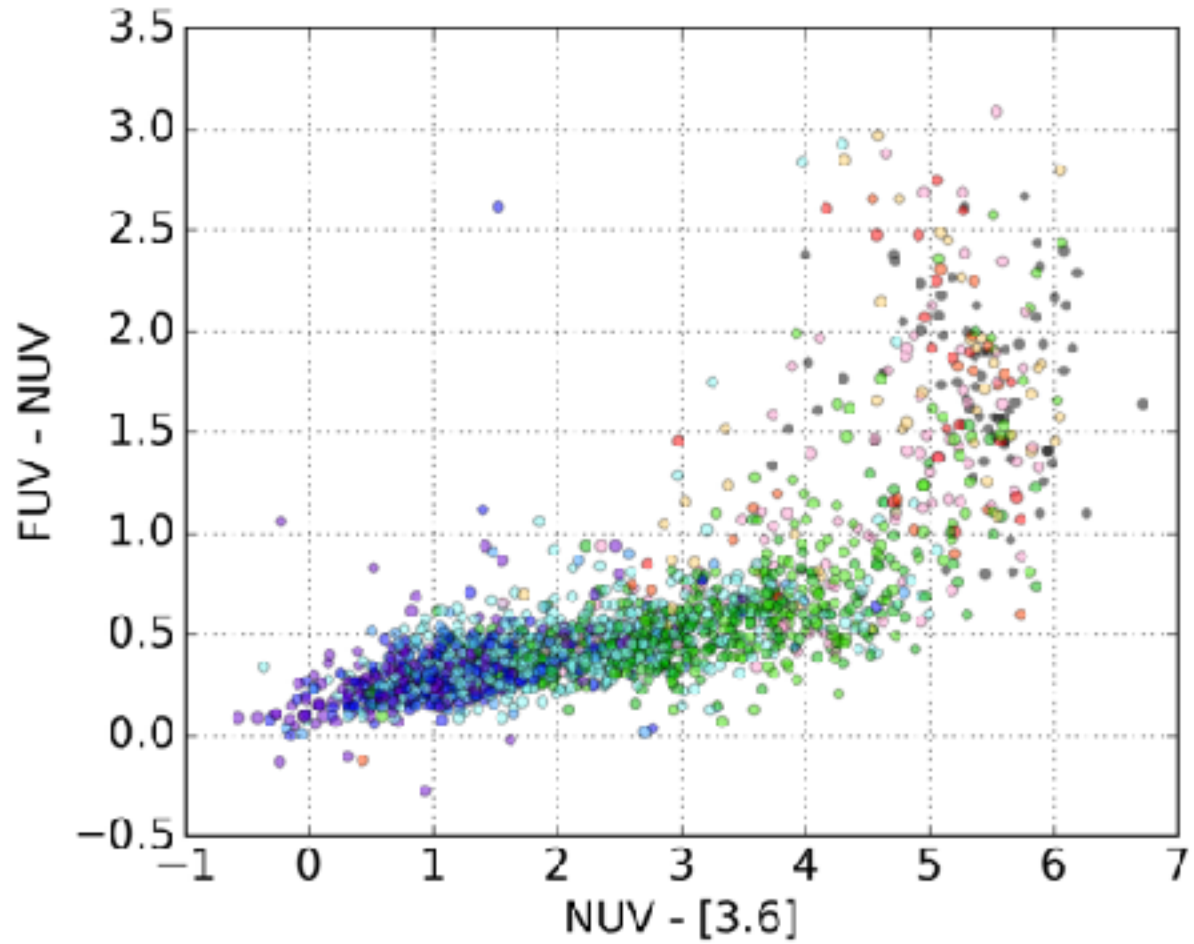

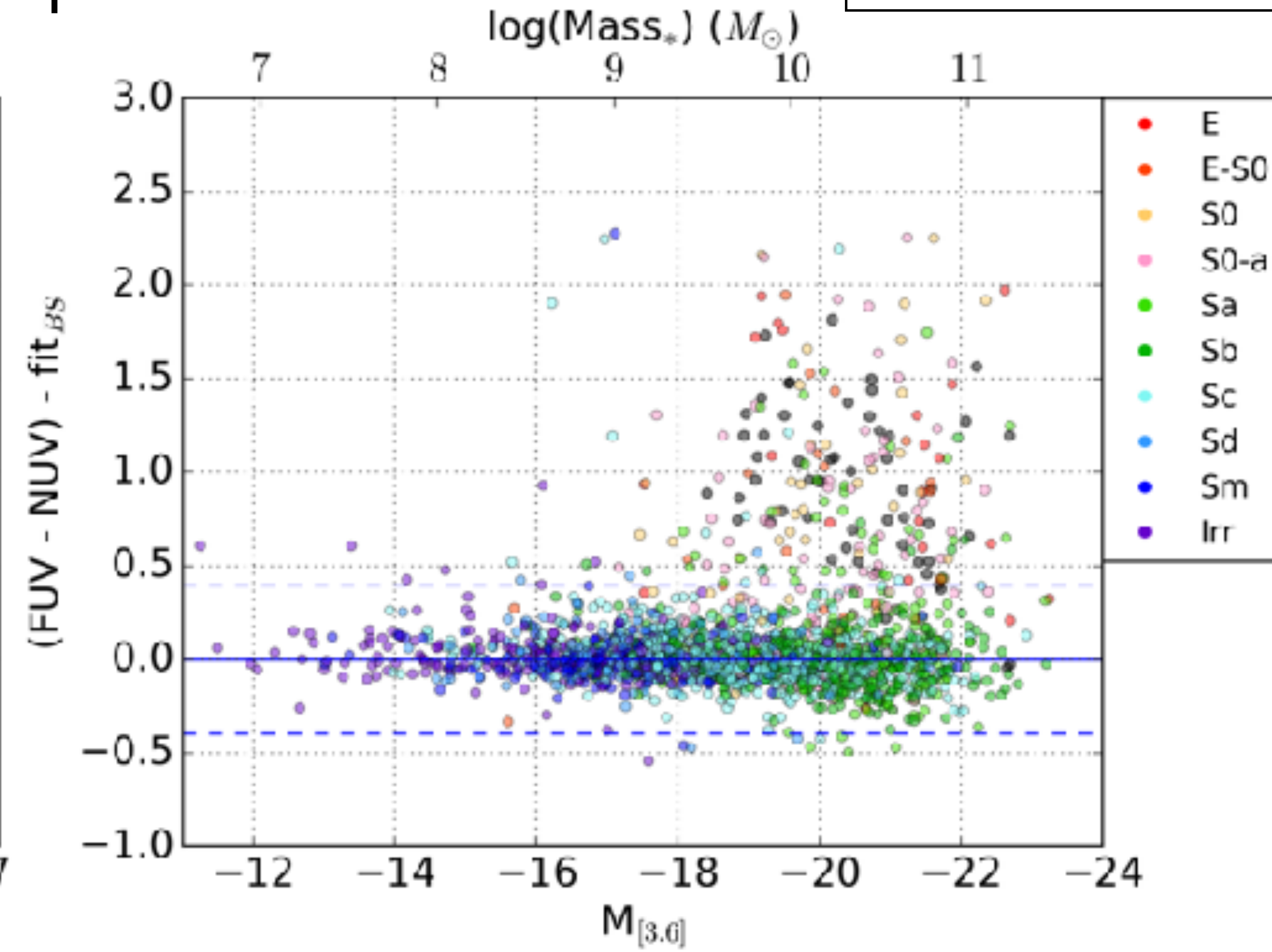

The (FUV - NUV) vs. (NUV - [3.6]) color-color diagram shows the bimodal distribution of galaxies with narrower sequences than the 'classical' (optical) one.

Important: NOT corrected for internal dust attenuation. For Av=0.5 mag, using the Calzetti (1994) attenuation law, (NUV-[3.6]) would change by -1, and (FUV-NUV) by -0.25. The correction is degenerated in the sense that it follows a similar slope than that of the Blue Sequence.

We define the GALEX Blue Sequence (GBS), GALEX Red Sequence (GRS) and GALEX Green Valley (GGV) as follows:

GBS: $0.12x + 0.16 - 2\sigma_{\rm GBS} \le y \le 0.12x + 0.16 + 2\sigma_{\rm GBS}$

GRS: $-0.23y + 5.63 - 1\sigma_{\rm GRS} \le x \le -0.23y + 5.63 + 1\sigma_{\rm GRS}$

GGV: $y > 0.12x + 0.16 + 2\sigma_{\rm GBS}$ and $x < -0.23y + 5.63 - 1\sigma_{\rm GRS}$

where $\sigma_{\rm GBS} = 0.2$ $\quad x = (\text{NUV - [3.6]})$

and $\sigma_{\rm GRS} = 0.45$ $\quad y = (\text{FUV - NUV})$

4.1 Results: Global properties

Bouquin et al. 2015

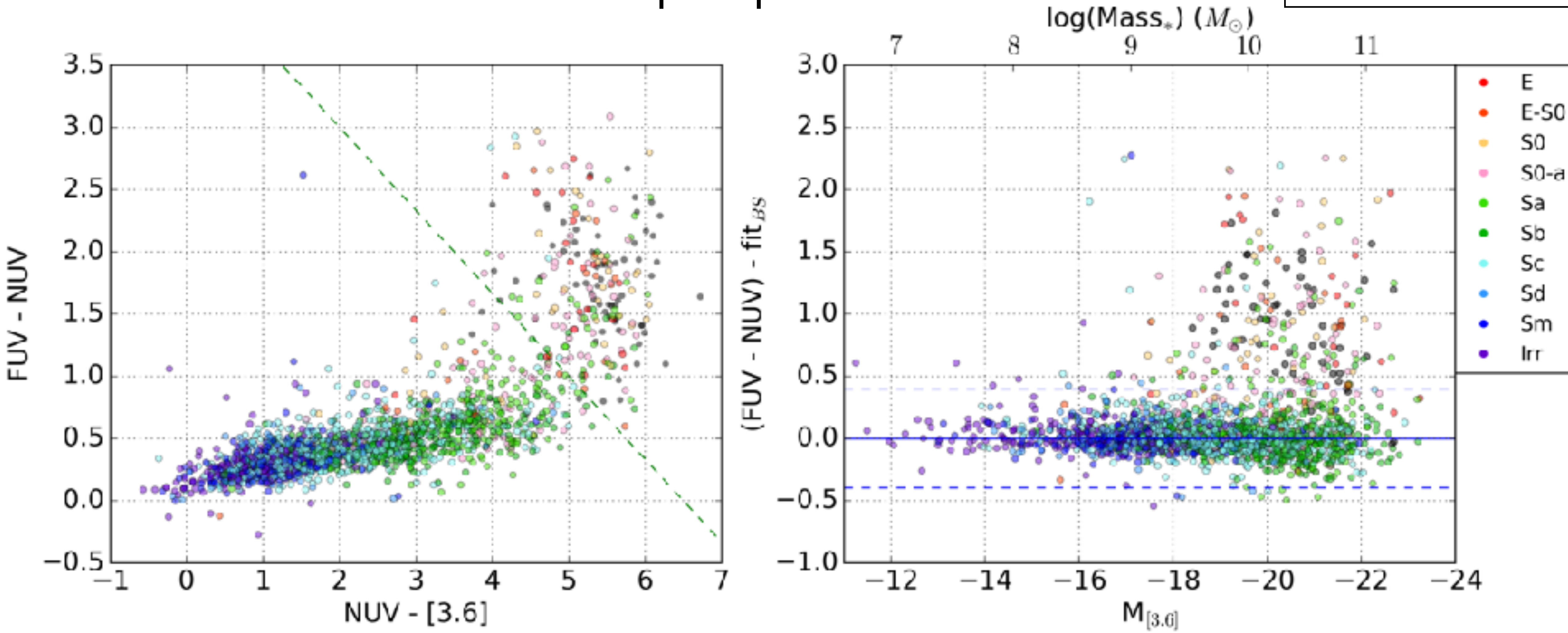

The (FUV - NUV) vs. (NUV - [3.6]) color-color diagram shows the bimodal distribution of galaxies with narrower sequences than the 'classical' (optical) one.

Important: NOT corrected for internal dust attenuation. For Av=0.5 mag, using the Calzetti (1994) attenuation law, (NUV-[3.6]) would change by -1, and (FUV-NUV) by -0.25. The correction is degenerated in the sense that it follows a similar slope than that of the Blue Sequence.

We define the GALEX Blue Sequence (GBS), GALEX Red Sequence (GRS) and GALEX Green Valley (GGV) as follows:

$$\text{GBS: } 0.12x + 0.16 - 2\sigma_{\text{GBS}} \leq y \leq 0.12x + 0.16 + 2\sigma_{\text{GBS}}$$

$$\text{GRS: } -0.23y + 5.63 - 1\sigma_{\text{GRS}} \leq x \leq -0.23y + 5.63 + 1\sigma_{\text{GRS}}$$

$$\text{GGV: } y > 0.12x + 0.16 + 2\sigma_{\text{GBS}} \text{ and } x < -0.23y + 5.63 - 1\sigma_{\text{GRS}}$$

where $\sigma_{\text{GBS}} = 0.2 \quad x = (\text{NUV - [3.6]})$

and $\sigma_{\text{GRS}} = 0.45 \quad y = (\text{FUV - NUV})$

4.1 Results: Global properties

Bouquin et al. 2015

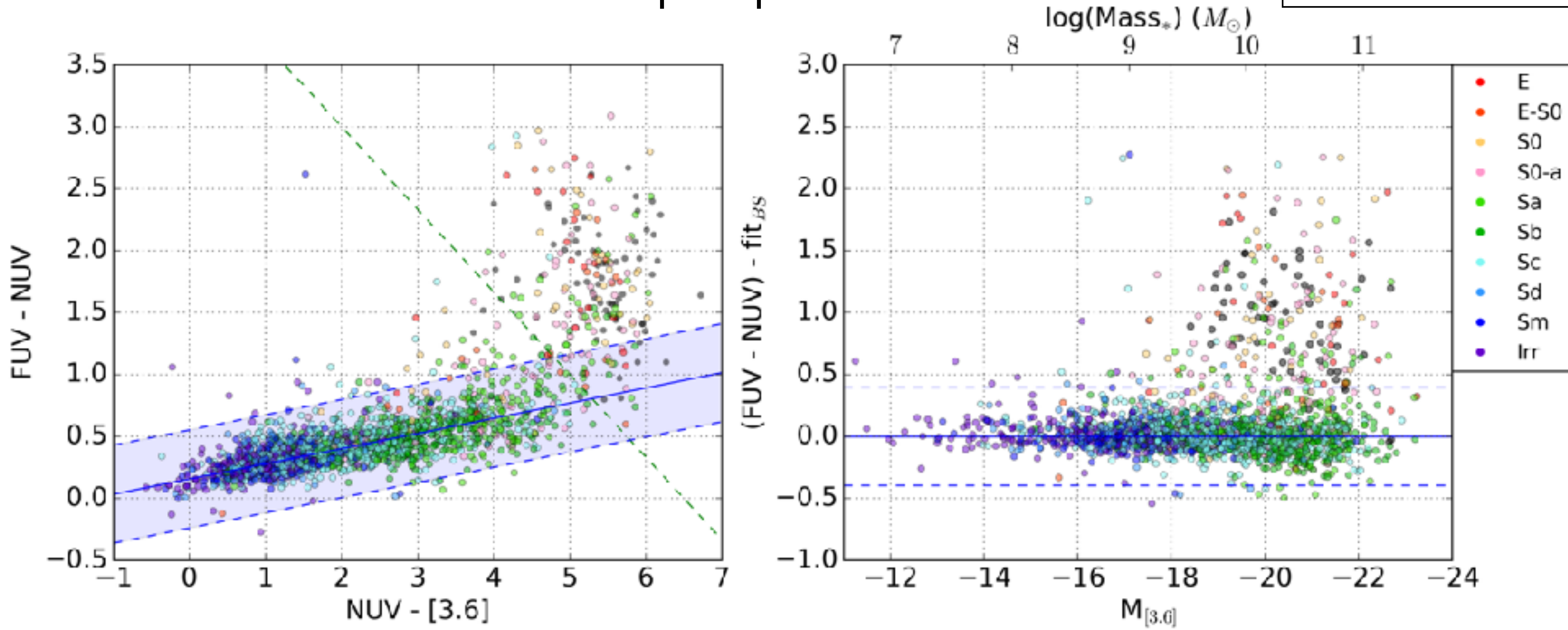

The (FUV - NUV) vs. (NUV - [3.6]) color-color diagram shows the bimodal distribution of galaxies with narrower sequences than the 'classical' (optical) one.

Important: NOT corrected for internal dust attenuation. For Av=0.5 mag, using the Calzetti (1994) attenuation law, (NUV-[3.6]) would change by -1, and (FUV-NUV) by -0.25. The correction is degenerated in the sense that it follows a similar slope than that of the Blue Sequence.

We define the GALEX Blue Sequence (GBS), GALEX Red Sequence (GRS) and GALEX Green Valley (GGV) as follows:

$$\text{GBS: } 0.12x + 0.16 - 2\sigma_{\text{GBS}} \leq y \leq 0.12x + 0.16 + 2\sigma_{\text{GBS}}$$

$$\text{GRS: } -0.23y + 5.63 - 1\sigma_{\text{GRS}} \leq x \leq -0.23y + 5.63 + 1\sigma_{\text{GRS}}$$

$$\text{GGV: } y > 0.12x + 0.16 + 2\sigma_{\text{GBS}} \text{ and } x < -0.23y + 5.63 - 1\sigma_{\text{GRS}}$$

where $\sigma_{\text{GBS}} = 0.2$ $\quad x = (\text{NUV - [3.6]})$
and $\sigma_{\text{GRS}} = 0.45$ $\quad y = (\text{FUV - NUV})$

4.1 Results: Global properties

Bouquin et al. 2015

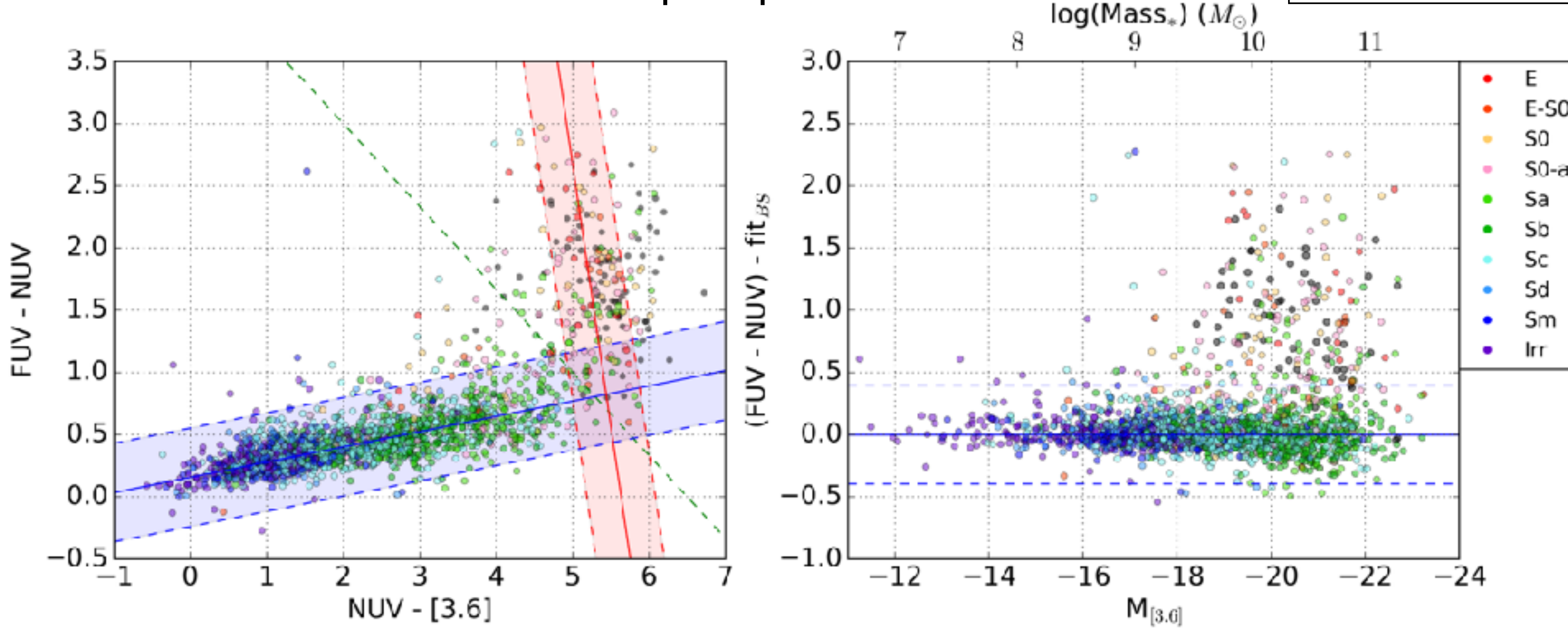

The (FUV - NUV) vs. (NUV - [3.6]) color-color diagram shows the bimodal distribution of galaxies with narrower sequences than the 'classical' (optical) one.

Important: NOT corrected for internal dust attenuation. For Av=0.5 mag, using the Calzetti (1994) attenuation law, (NUV-[3.6]) would change by -1, and (FUV-NUV) by -0.25. The correction is degenerated in the sense that it follows a similar slope than that of the Blue Sequence.

We define the GALEX Blue Sequence (GBS), GALEX Red Sequence (GRS) and GALEX Green Valley (GGV) as follows:

$$\text{GBS: } 0.12x + 0.16 - 2\sigma_{\text{GBS}} \leq y \leq 0.12x + 0.16 + 2\sigma_{\text{GBS}}$$

$$\text{GRS: } -0.23y + 5.63 - 1\sigma_{\text{GRS}} \leq x \leq -0.23y + 5.63 + 1\sigma_{\text{GRS}}$$

$$\text{GGV: } y > 0.12x + 0.16 + 2\sigma_{\text{GBS}} \text{ and } x < -0.23y + 5.63 - 1\sigma_{\text{GRS}}$$

where $\sigma_{\text{GBS}} = 0.2$ $\quad x = (\text{NUV - [3.6]})$
and $\sigma_{\text{GRS}} = 0.45$ $\quad y = (\text{FUV - NUV})$

4.1 Results: Global properties

Bouquin et al. 2015

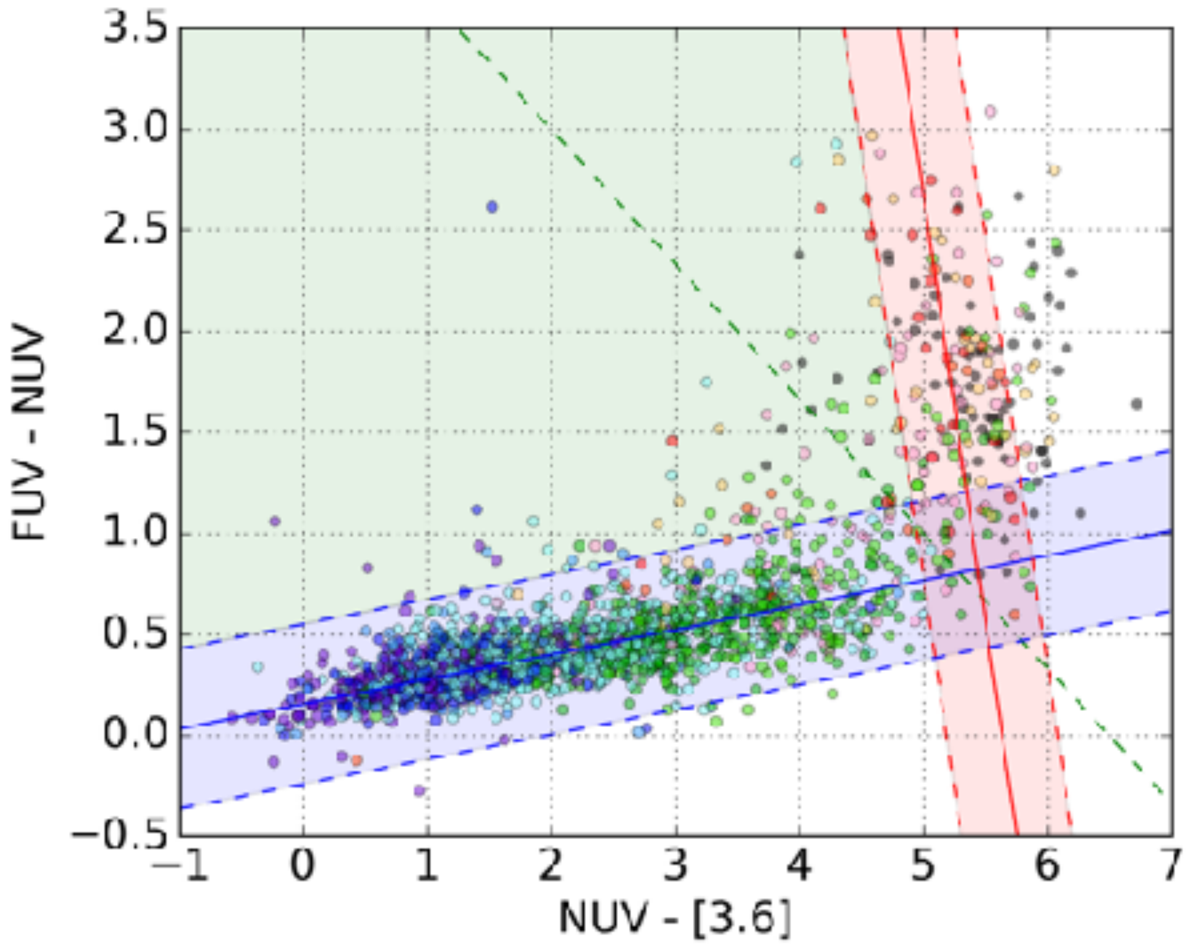

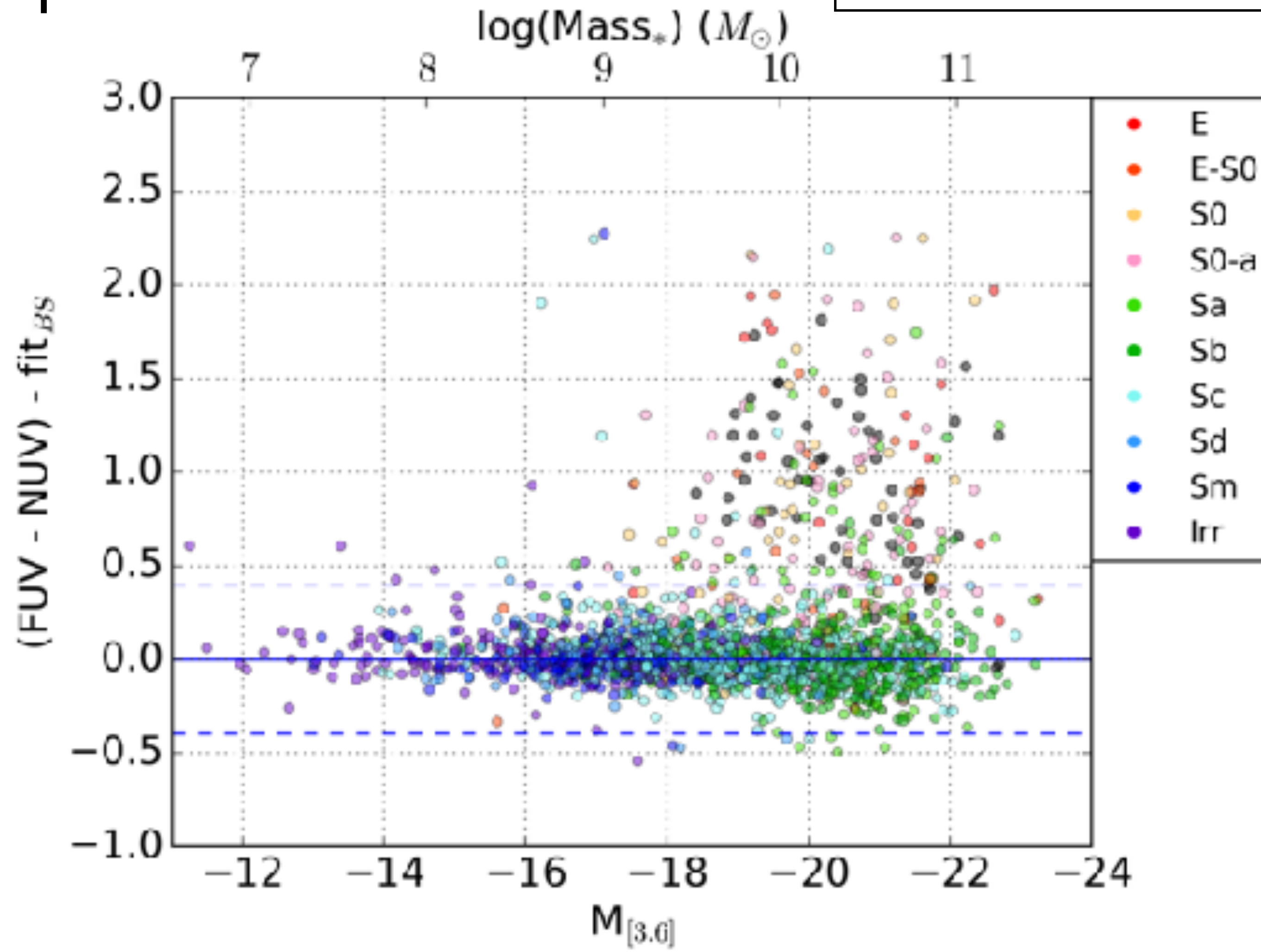

The (FUV - NUV) vs. (NUV - [3.6]) color-color diagram shows the bimodal distribution of galaxies with narrower sequences than the 'classical' (optical) one.

Important: NOT corrected for internal dust attenuation. For Av=0.5 mag, using the Calzetti (1994) attenuation law, (NUV-[3.6]) would change by -1, and (FUV-NUV) by -0.25. The correction is degenerated in the sense that it follows a similar slope than that of the Blue Sequence.

We define the GALEX Blue Sequence (GBS), GALEX Red Sequence (GRS) and GALEX Green Valley (GGV) as follows:

$$\text{GBS: } 0.12x + 0.16 - 2\sigma_{\text{GBS}} \leq y \leq 0.12x + 0.16 + 2\sigma_{\text{GBS}}$$

$$\text{GRS: } -0.23y + 5.63 - 1\sigma_{\text{GRS}} \leq x \leq -0.23y + 5.63 + 1\sigma_{\text{GRS}}$$

$$\text{GGV: } y > 0.12x + 0.16 + 2\sigma_{\text{GBS}} \text{ and } x < -0.23y + 5.63 - 1\sigma_{\text{GRS}}$$

where $\sigma_{\text{GBS}} = 0.2$ and $\sigma_{\text{GRS}} = 0.45$, $x = (\text{NUV - [3.6]})$, $y = (\text{FUV - NUV})$

4.1 Results: Global properties

Bouquin et al. 2015

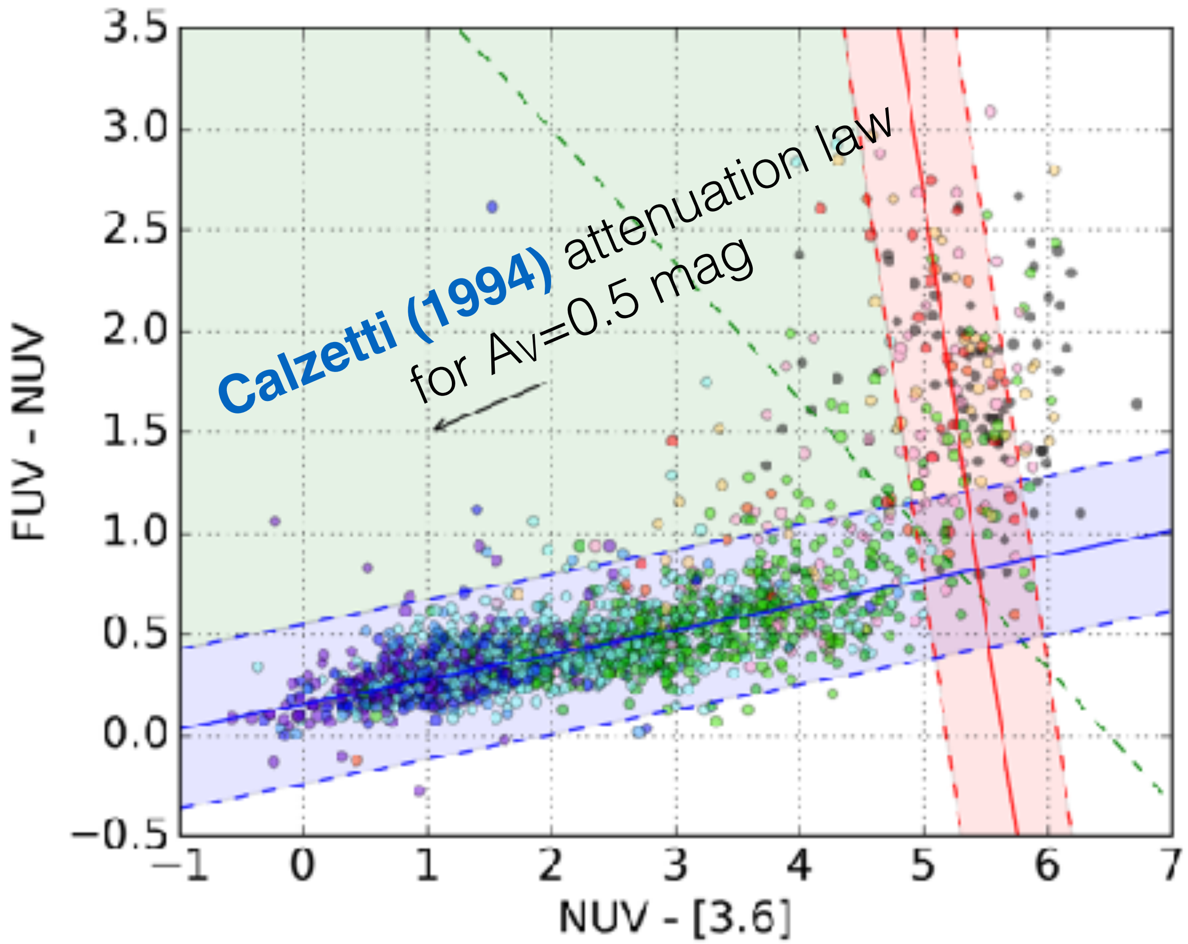

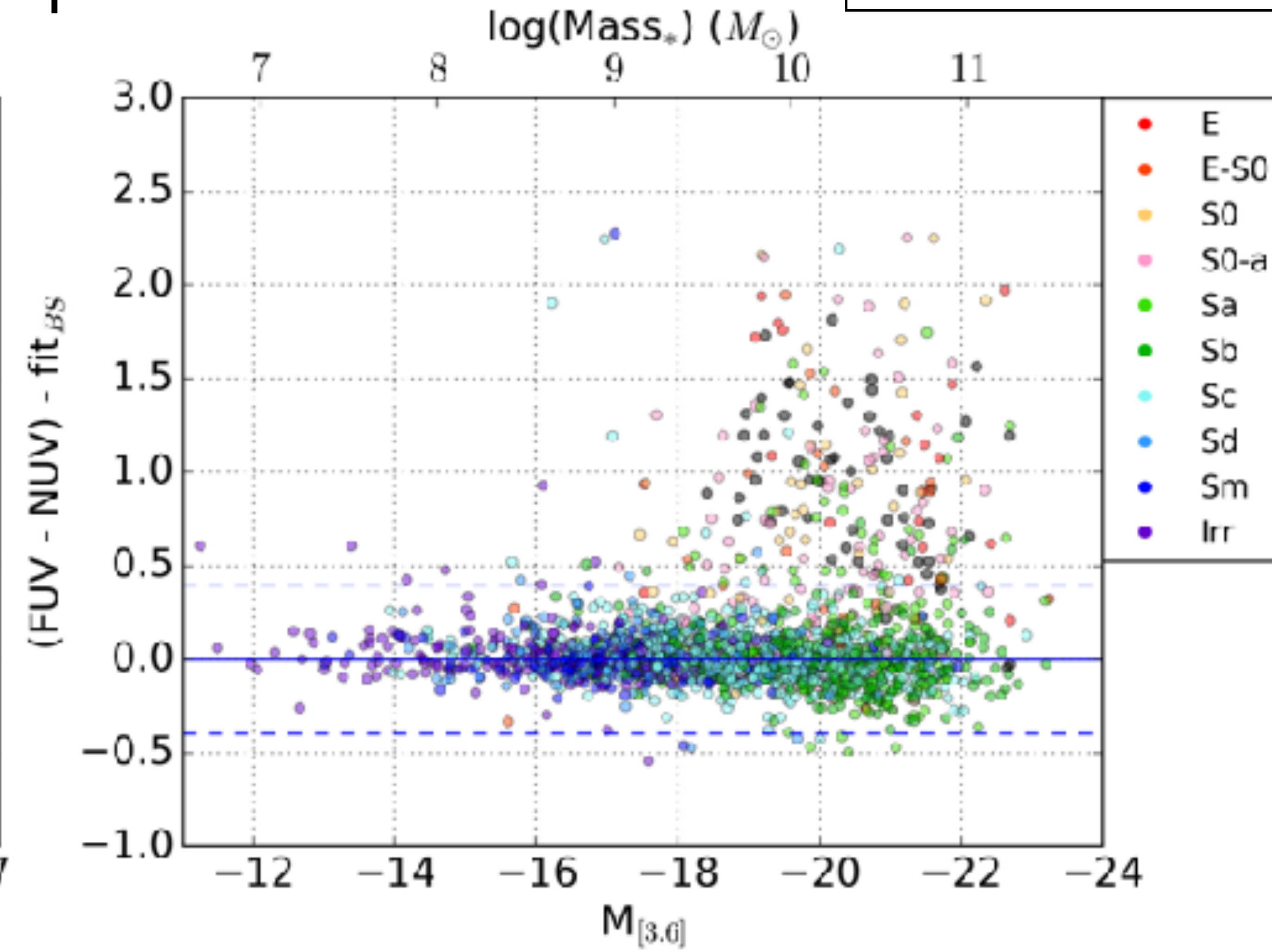

The (FUV - NUV) vs. (NUV - [3.6]) color-color diagram shows the bimodal distribution of galaxies with narrower sequences than the 'classical' (optical) one.

Important: NOT corrected for internal dust attenuation. For Av=0.5 mag, using the Calzetti (1994) attenuation law, (NUV-[3.6]) would change by -1, and (FUV-NUV) by -0.25. The correction is degenerated in the sense that it follows a similar slope than that of the Blue Sequence.

We define the GALEX Blue Sequence (GBS), GALEX Red Sequence (GRS) and GALEX Green Valley (GGV) as follows:

$$\text{GBS: } 0.12x + 0.16 - 2\sigma_{\text{GBS}} \leq y \leq 0.12x + 0.16 + 2\sigma_{\text{GBS}}$$

$$\text{GRS: } -0.23y + 5.63 - 1\sigma_{\text{GRS}} \leq x \leq -0.23y + 5.63 + 1\sigma_{\text{GRS}}$$

$$\text{GGV: } y > 0.12x + 0.16 + 2\sigma_{\text{GBS}} \text{ and } x < -0.23y + 5.63 - 1\sigma_{\text{GRS}}$$

where $\sigma_{\text{GBS}} = 0.2$ $\quad x = (\text{NUV - [3.6]})$
and $\sigma_{\text{GRS}} = 0.45$ $\quad y = (\text{FUV - NUV})$

4.1 Results: Global properties

Bouquin et al. 2015

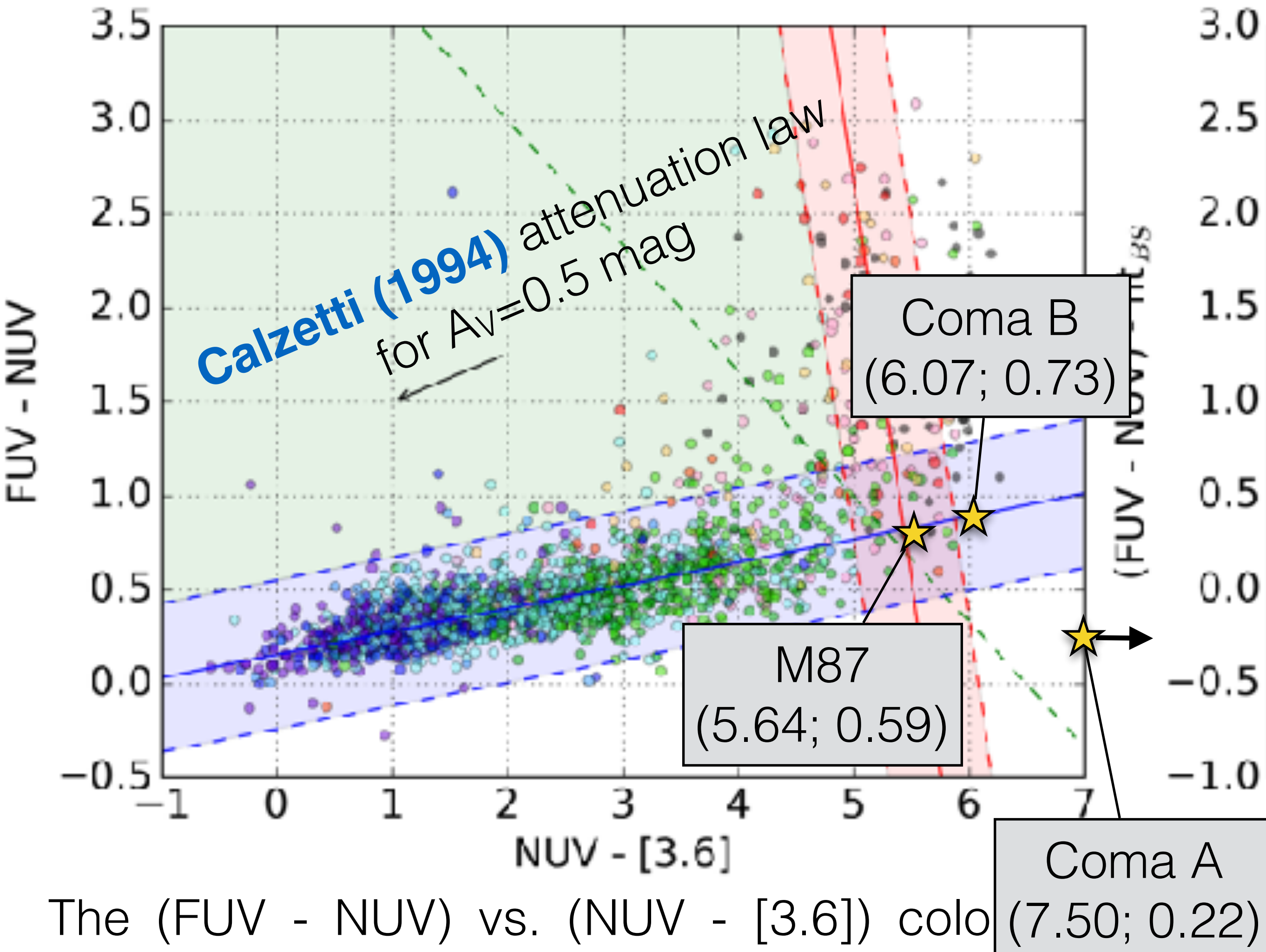

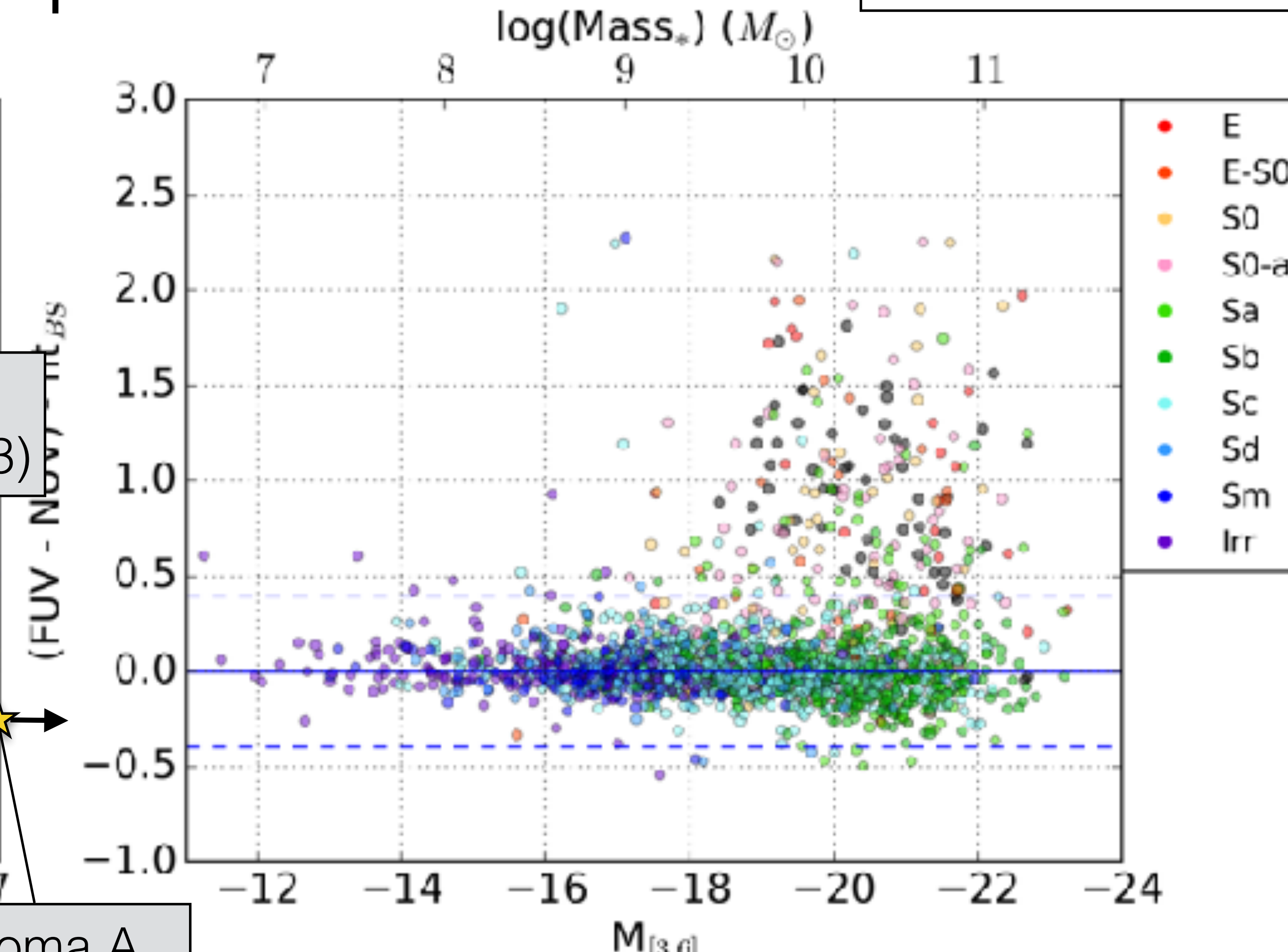

The (FUV - NUV) vs. (NUV - [3.6]) colo color diagram shows the bimodal distribution of galaxies with narrower sequences than the ‘classical’ (optical) one.

Important: NOT corrected for internal dust attenuation. For Av=0.5 mag, using the Calzetti (1994) attenuation law, (NUV-[3.6]) would change by -1, and (FUV-NUV) by -0.25. The correction is degenerated in the sense that it follows a similar slope than that of the Blue Sequence.

efine the GALEX Blue Sequence (GBS), GALEX Red Sequence (GRS) and GALEX Green Valley (GGV) as follows:

$$\text{GBS: } 0.12x + 0.16 - 2\sigma_{\text{GBS}} \leq y \leq 0.12x + 0.16 + 2\sigma_{\text{GBS}}$$

$$\text{GRS: } -0.23y + 5.63 - 1\sigma_{\text{GRS}} \leq x \leq -0.23y + 5.63 + 1\sigma_{\text{GRS}}$$

$$\text{GGV: } y > 0.12x + 0.16 + 2\sigma_{\text{GBS}} \text{ and } x < -0.23y + 5.63 - 1\sigma_{\text{GRS}}$$

where $\sigma_{\text{GBS}} = 0.2$ $\quad x = (\text{NUV - [3.6]})$
and $\sigma_{\text{GRS}} = 0.45$ $\quad y = (\text{FUV - NUV})$

4.1 Results: Global properties

Bouquin et al. 2015

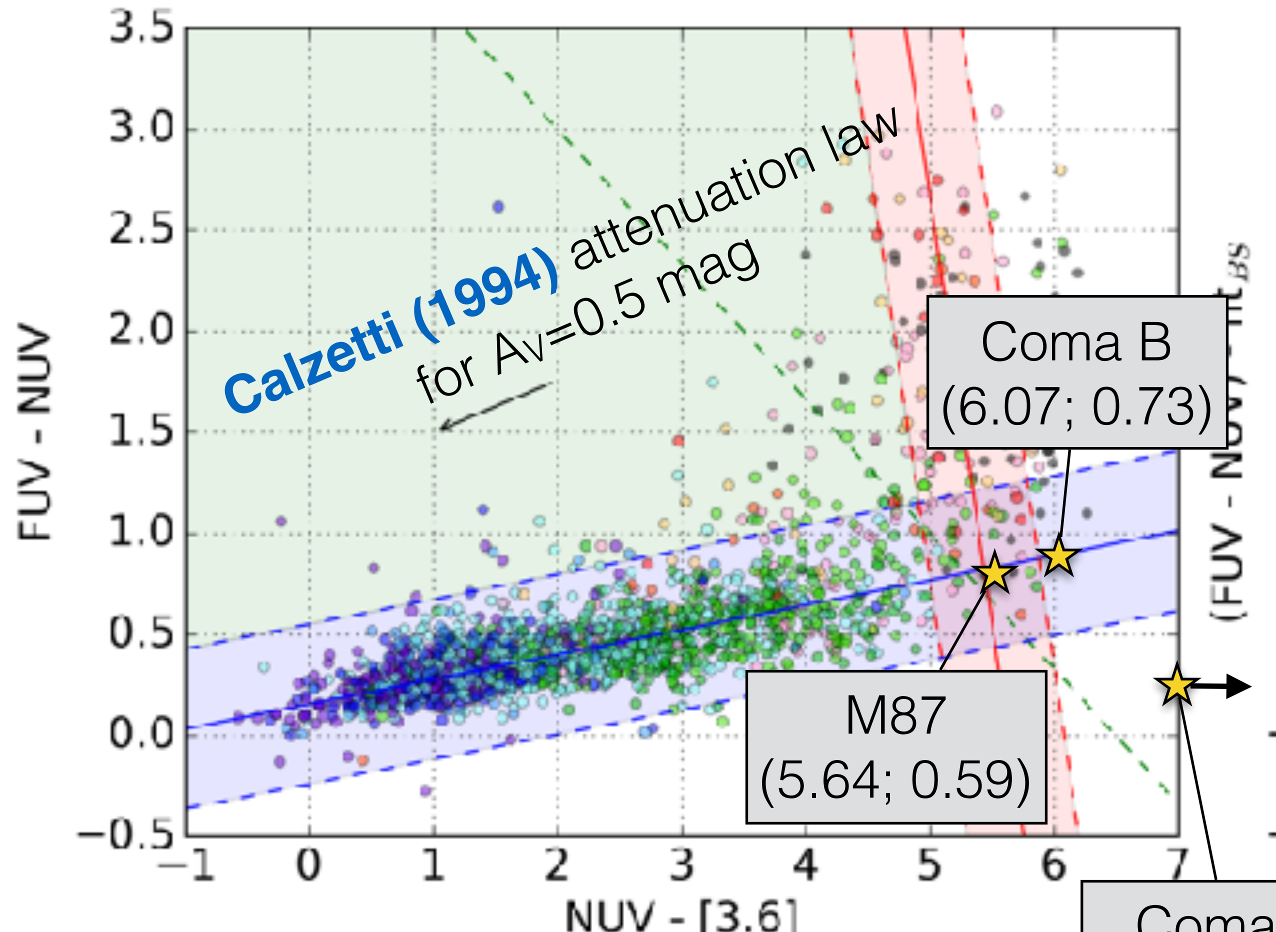

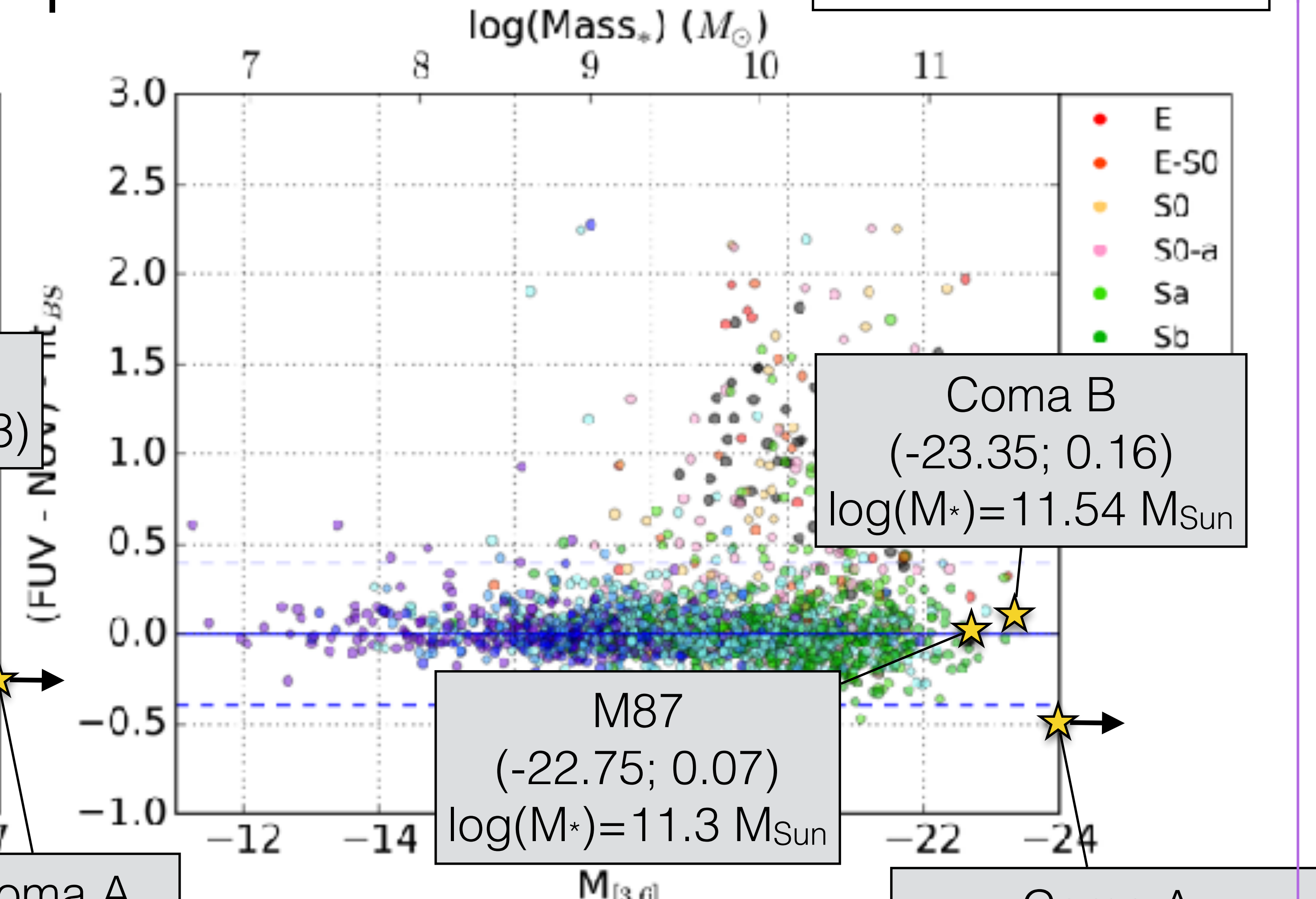

The (FUV - NUV) vs. (NUV - [3.6]) colo[r-] color diagram shows the bimodal distribution of galaxies with narrower sequences than the 'classical' (optical) one.

Important: NOT corrected for internal dust attenuation. For Av=0.5 mag, using the Calzetti (1994) attenuation law, (NUV-[3.6]) would change by -1, and (FUV-NUV) by -0.25. The correction is degenerated in the sense that it follows a similar slope than that of the Blue Sequence.

...efine the **GALEX Blue Sequenc**... **Red Sequence (GRS)** and **GALEX Gre**... as follows:

GBS: $0.12x + 0.16 - 2\sigma_{\rm GBS} \leq y \leq 0.12x + 0.16 + 2\sigma_{\rm GBS}$

GRS: $-0.23y + 5.63 - 1\sigma_{\rm GRS} \leq x \leq -0.23y + 5.63 + 1\sigma_{\rm GRS}$

GGV: $y > 0.12x + 0.16 + 2\sigma_{\rm GBS}$ and $x < -0.23y + 5.63 - 1\sigma_{\rm GRS}$

where $\sigma_{\rm GBS} = 0.2$ $\quad x = ({\rm NUV - [3.6]})$

and $\sigma_{\rm GRS} = 0.45$ $\quad y = ({\rm FUV - NUV})$

4.1 Results: Global properties

Bouquin et al. 2015

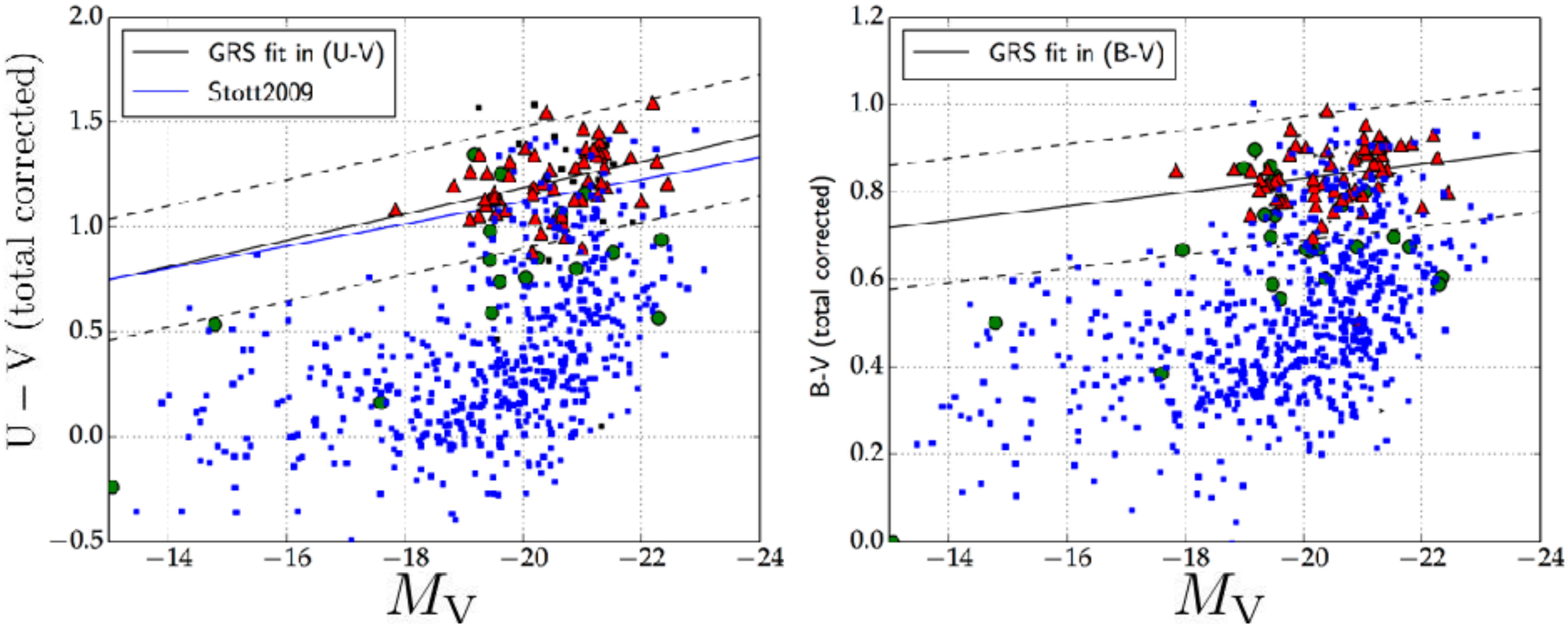

These are ‘**classical**’ (optical) color-magnitude diagrams showing the ‘red sequence’ and ‘blue cloud’.

▲ = galaxies identified in the GALEX Red Sequence
● = galaxies identified in the GALEX Green Valley
■ = galaxies identified in the GALEX Blue Sequence

Caveats of optical colors:
(1) hard to classify Red Sequence, Green Valley, Blue Cloud galaxies
(2) many GBS galaxies appear in the optical Red Sequence

4.1 Results: Global properties

Bouquin et al. 2015

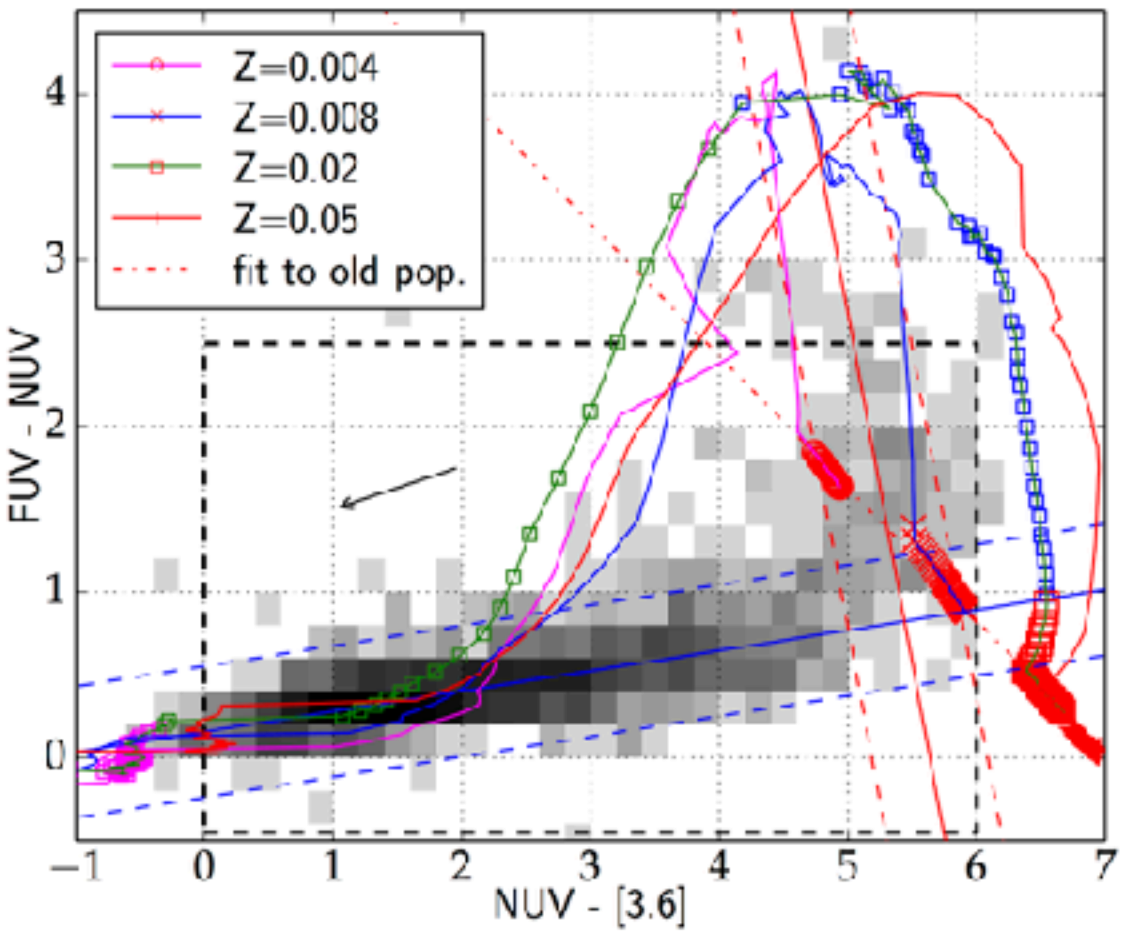

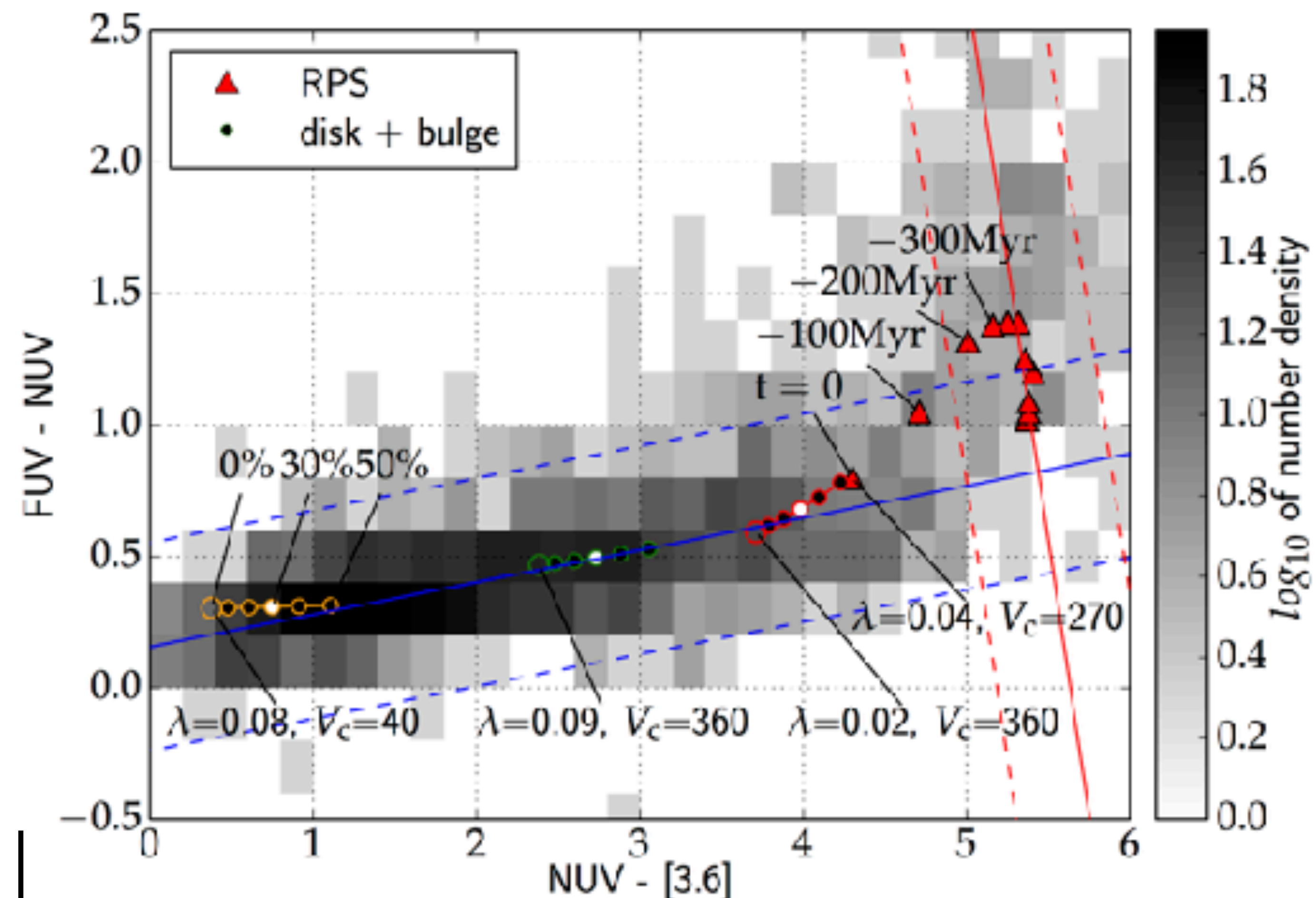

Left: evolution of SSP models of **Bruzual and Charlot (2003)** of various metallicities in the (FUV - NUV) and (NUV - [3.6]) colors.

Highly-evolved systems (>10^{10} Gyr) are shown in red.

Right: evolution of UV+IR colors for disk+bulge models and a Ram-Pressure Stripping (RPS) model. The disks are from **Boissier & Prantzos, 2000,** and are controlled by two parameters: *circular velocity v_c* and *spin parameter λ*.
We simulate a bulge by taking a highly-evolved SSP and by varying the B/T ratio of **Laurikainen et al., 2007**.
An RPS model of **Boselli et al., 2006** is also shown (red triangles).

4.1 Results: Global properties

Bouquin et al. 2015

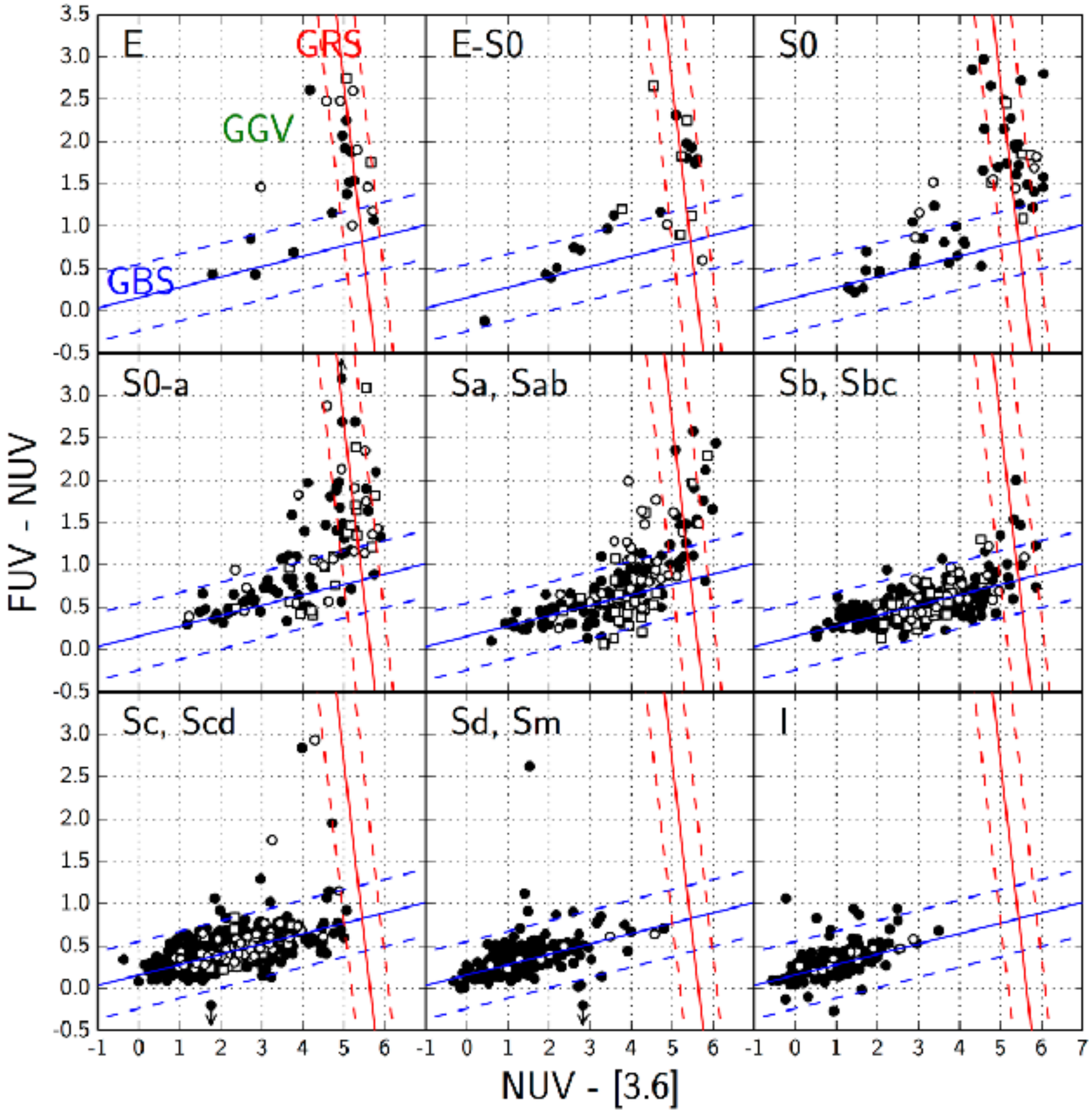

The distribution of the GALEX/S4G galaxies in the (FUV - NUV) vs. (NUV - [3.6]) CCD per morphological type.

○: galaxies in the Virgo cluster.

□: galaxies in high-density regions as defined by **Laine et al. (2014)**.

●: field galaxies

We find a **higher fraction** (29%) of GGV galaxies in our sample to be in the Virgo cluster, as compared to the GBS (7%) or the GRS (14%) galaxies, and 162/1931 (8%) galaxies overall.

4.1 Results: Global properties

Conclusions of 4.1:

- Galaxies are distributed into **two narrow sequences** in the (FUV - NUV) versus (NUV - [3.6]) color-color diagram: **the GALEX Blue Sequence (GBS)** is populated by actively star-forming late-type galaxies and **the GALEX Red Sequence (GRS)** is populated by quiescent early-type galaxies.

- In the region of intermediate-colors, **the GALEX Green Valley (GGV),** a large fraction of galaxies are early-type spirals of type Sa and S0-a.

- The GGV can be interpreted as **a zone of rapid transition (≤1 Gyr)** due to the quenching or damping of star formation in the disk resulting in its reddening, consistent with timescales of ram-pressure stripping in denser environment. It is worth noting, however that these results do not exclude the possibility of having rejuvenated galaxies from the GRS to fall into the GGV as well.

- We also find that a **higher fraction** of galaxies in the GGV (compared to the GBS or the GRS) **belong to the Virgo** cluster, suggesting that the **environment is at play**.

4.2 Results: UV-color and stellar M/L ratio correlation in ETGs

Publications:

Zaritsky, Gil de Paz, Bouquin 2014, ApJL, 780, 1

“An empirical connection between ultraviolet color of early-type galaxies and the stellar initial mass function”

Zaritsky, Gil de Paz, Bouquin 2015, MNRAS, 446, 2030

“The connection between the UV colour of early type galaxies and the stellar initial mass function revisited”

The connection between the UV colour of early-type galaxies and the stellar initial mass function revisited

4.2 Results: UV-color and stellar M/L ratio correlation in ETGs

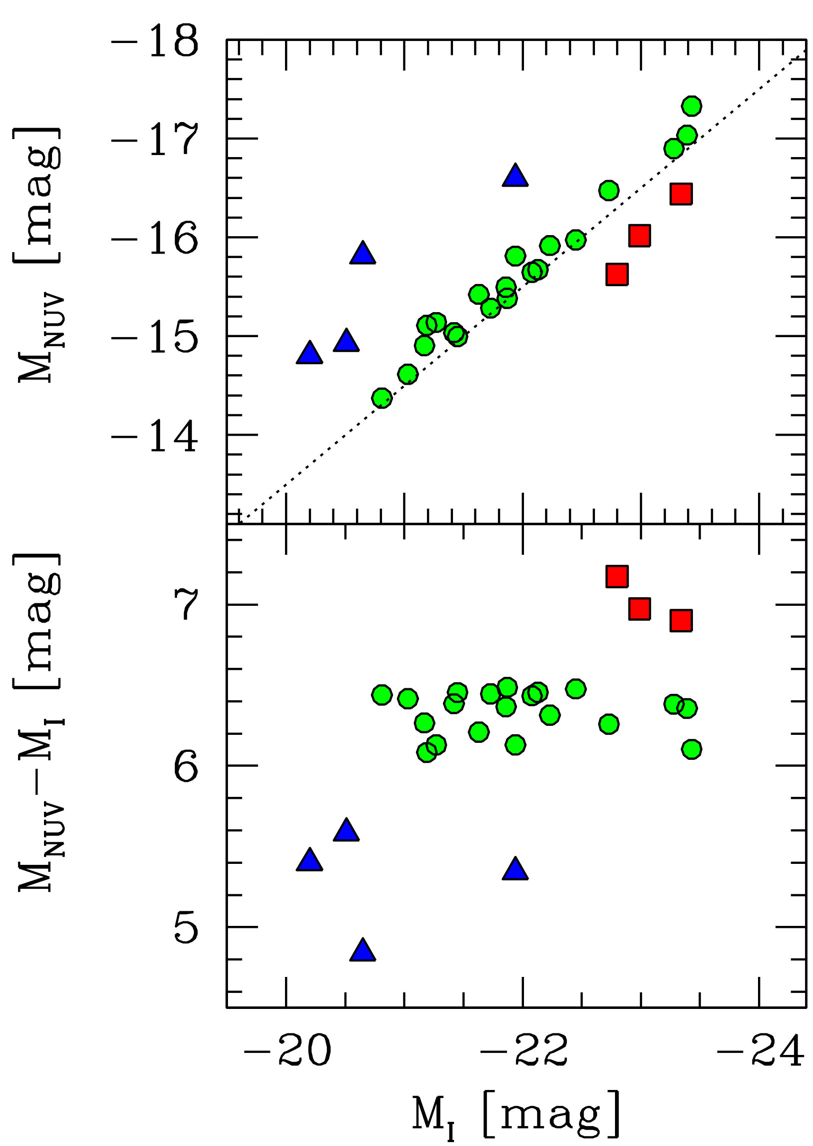

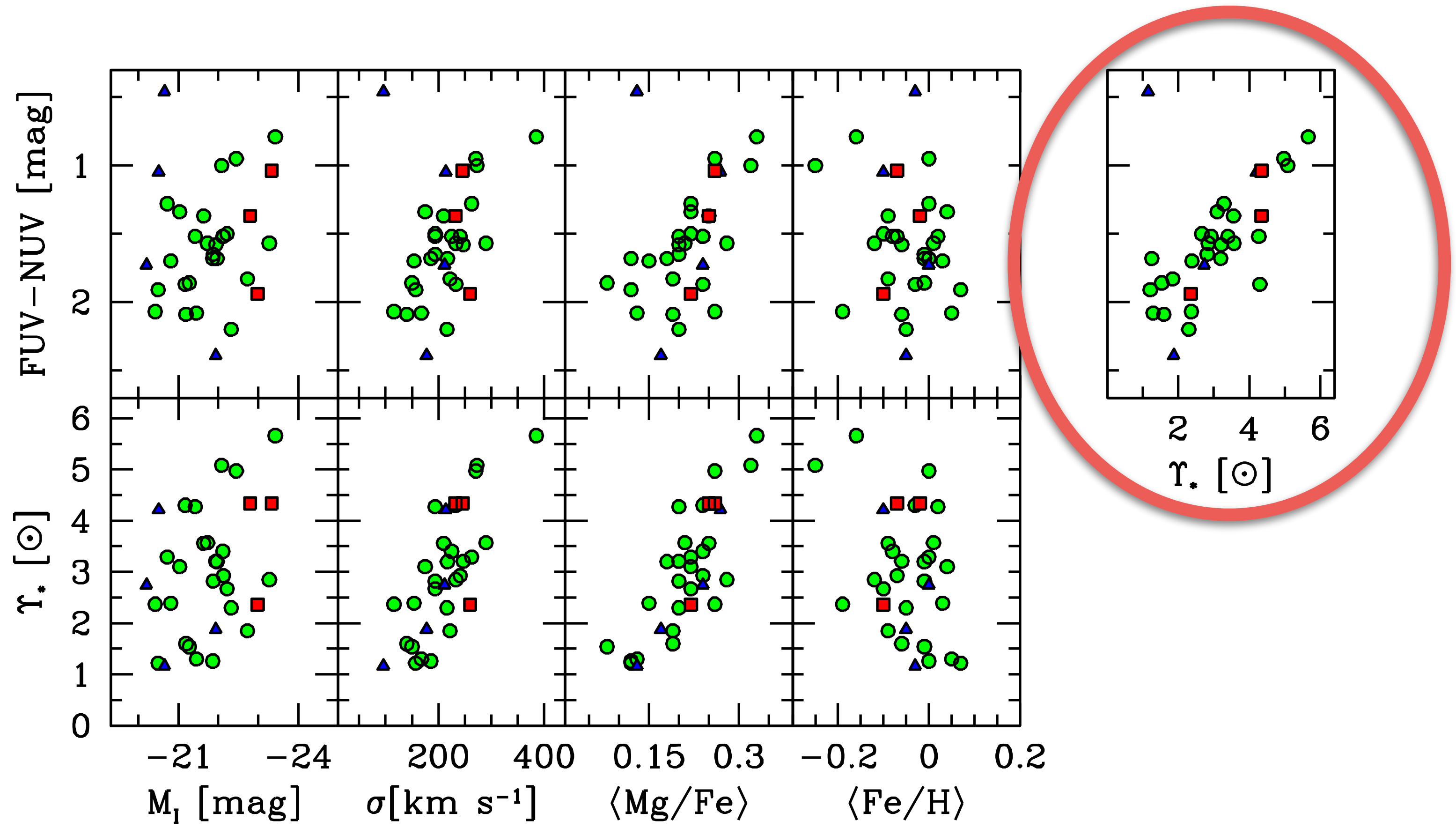

UV color and M*/L* versus I-band mag, internal vel.disp., Mg/Fe, Fe/H

mag-mag and color-mag diagrams.

▲ = Blue outliers

■ = Red outliers

N=32 galaxies

4.2 Results: UV-color and stellar M/L ratio correlation in ETGs

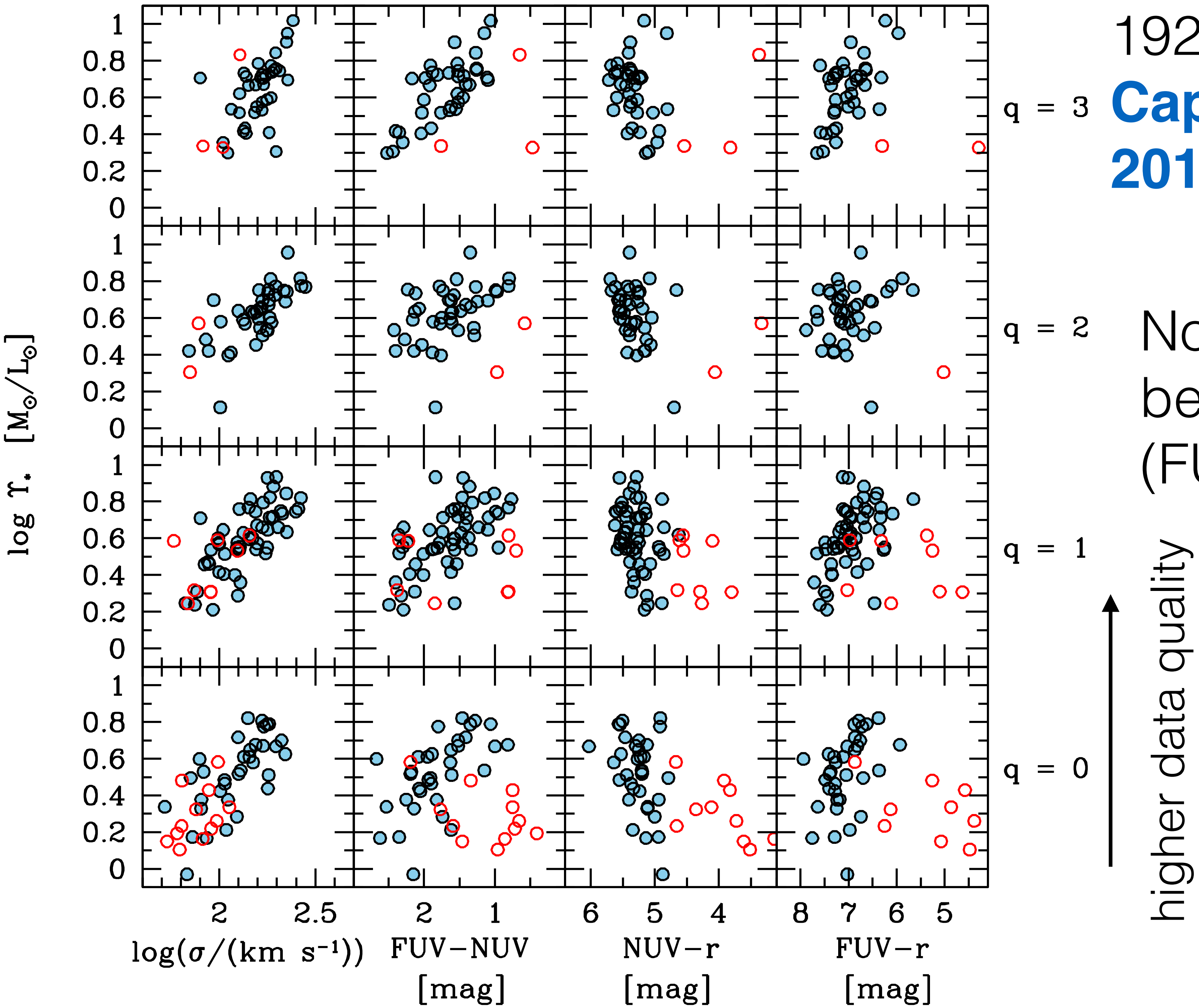

Correlations revisited
192 galaxies of ATLAS3D
Cappellari et al. (2013, 2014)

Note the reversal of trend between
(FUV - r) and (NUV - r)

○ = points excluded on the basis of their (NUV - K) color ≤7.5 cut to select only reddest systems with low H_2 content.

4.2 Results: UV-color and stellar M/L ratio correlation in ETGs

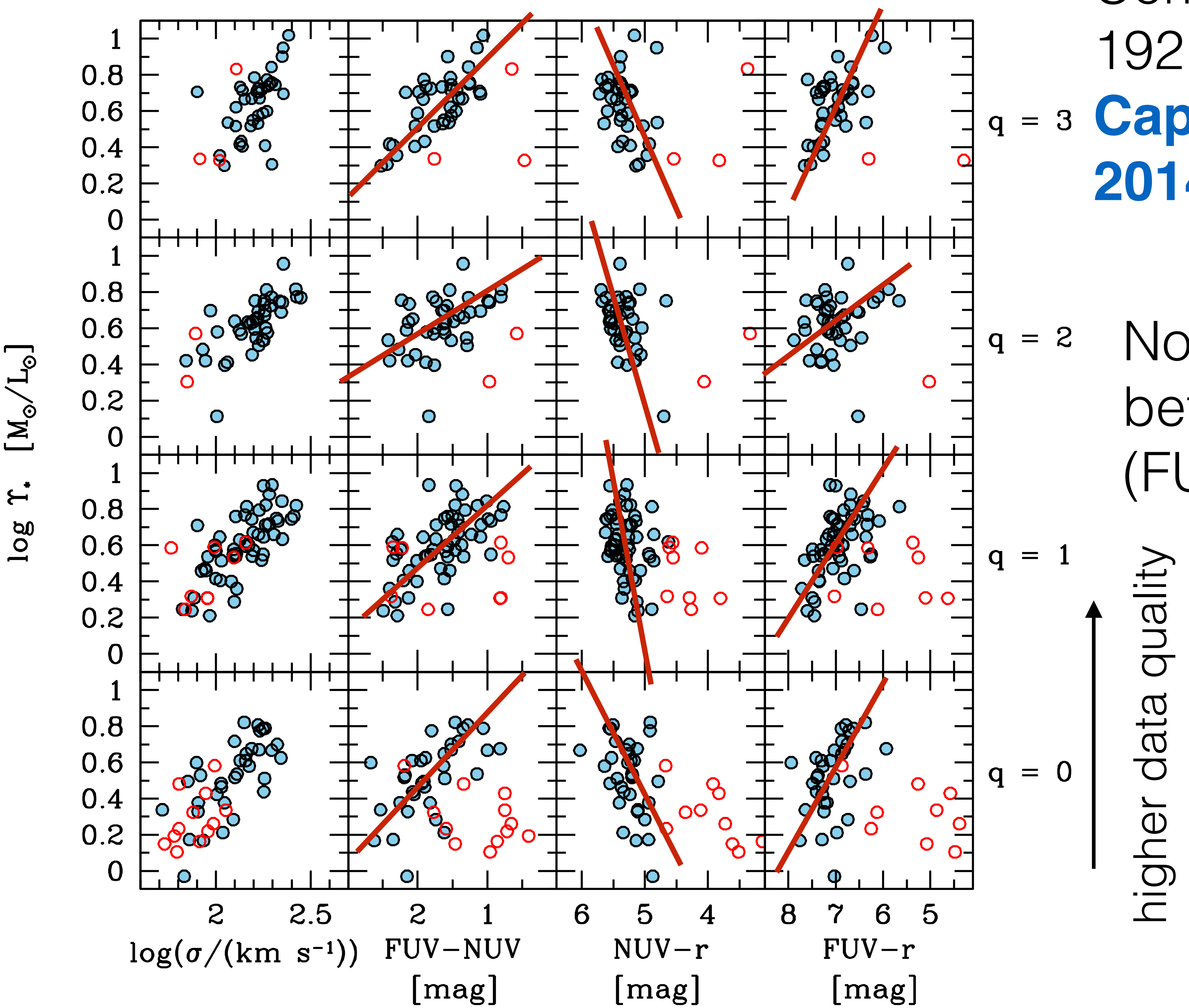

Correlations revisited
192 galaxies of ATLAS[3D]
Cappellari et al. (2013, 2014)

Note the reversal of trend between
(FUV - r) and (NUV - r)

○ = points excluded on the basis of their (NUV - K) color ≤7.5 cut to select only reddest systems with low H_2 content.

4.2 Results: UV-color and stellar M/L ratio correlation in ETGs

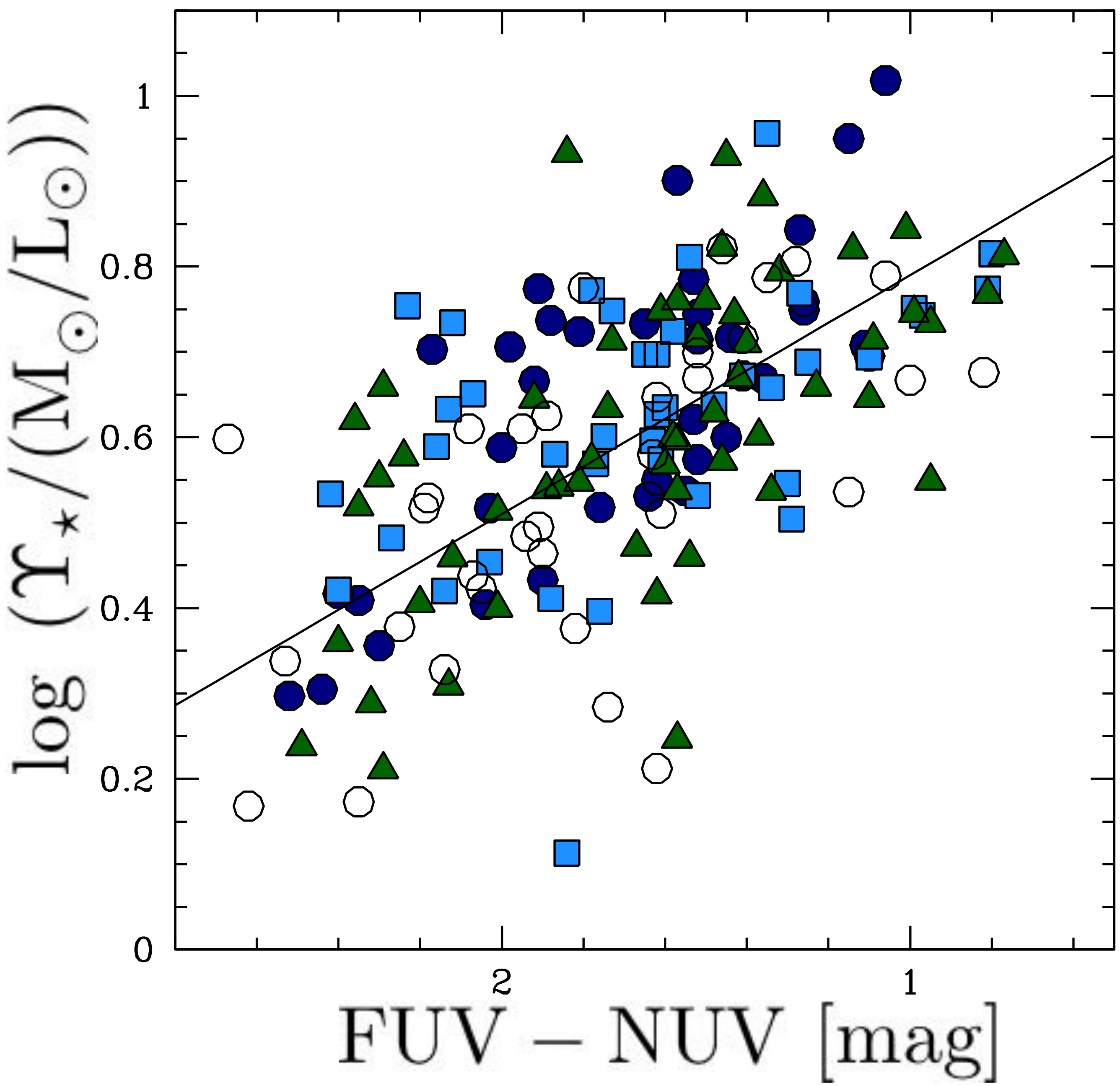

Different points=
different quality of data from high to low:
filled circles, filled squares, filled triangles,
and open circles

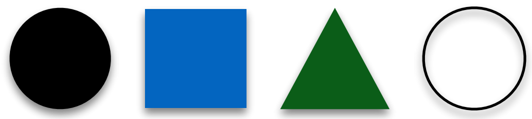

Regression line:

$$\log(\Upsilon_\star) = 1.07 - 0.28(\mathrm{FUV} - \mathrm{NUV})$$

The bluer the (FUV - NUV) color,
the larger the stellar mass-to-light ratio.

4.2 Results: UV-color and stellar M/L ratio correlation in ETGs

Conclusions of 4.2:
A strong empirical correlation is found between (FUV - NUV) color and the stellar M/L in ETGs, in the sense that **a bluer color** yields **a higher stellar M/L**.

UV-upturn stars are thought to be the main contributors of the UV emission in ETGs. The amount of UV-upturn stars depends on the low-mass end of the IMF.

We conjecture that we can use the (FUV - NUV) color to differentiate between ETGs having different IMFs.

4.3 Results: Spatially-resolved properties

Bouquin et al. 2018, ApJS, 234, 18

“The *GALEX*/S⁴G Surface Brightness and Color Profiles Catalog. I. Surface Photometry and Color Gradients of Galaxies”

Online Data available on VizieR


The *GALEX*/S⁴G Surface Brightness and Color Profiles Catalog. I. Surface Photometry and Color Gradients of Galaxies

Abstract

1. Introduction

4.3 Results: Spatially-resolved properties

Surface brightness radial profiles

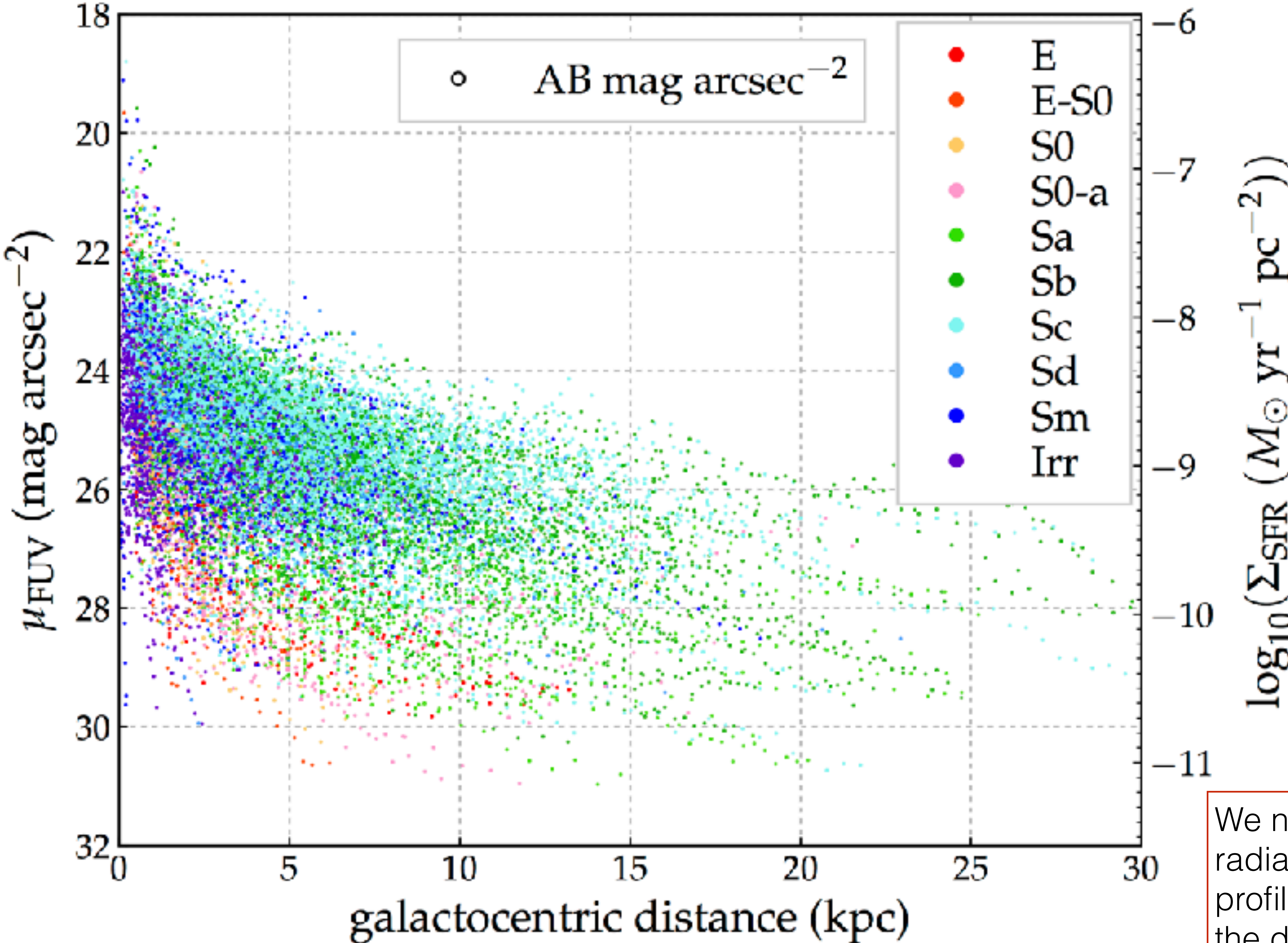

Surface brightness radial profiles

data points are taken at steps of 6 arcsec

data points with associated uncertainties larger than 0.2 mag are ignored

We normalize the 3.6μm radial surface brightness profile to compensate for the discrepancies

4.3 Results: Spatially-resolved properties

Surface brightness radial profiles

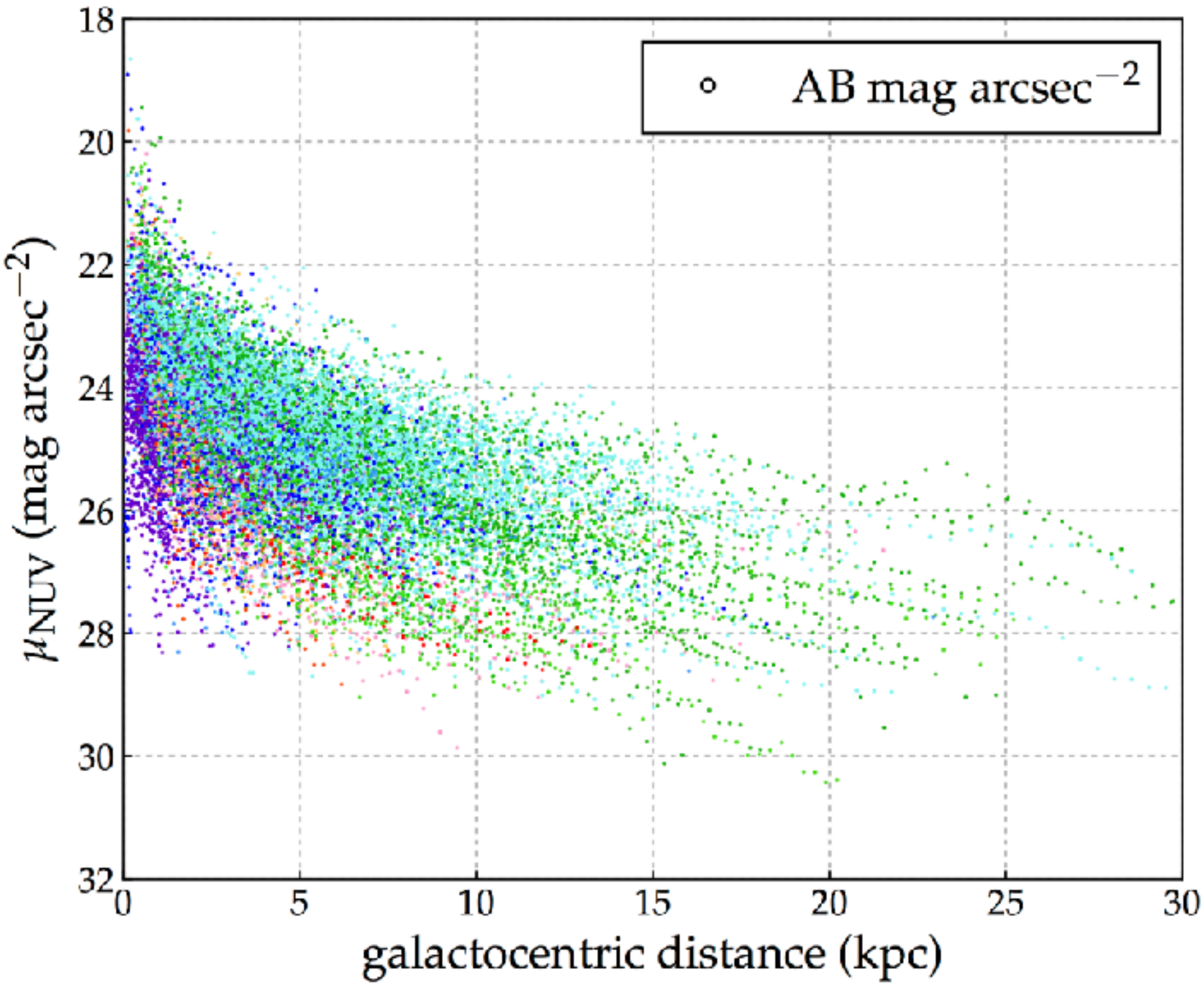

Surface brightness radial profiles

data points are taken at steps of 6 arcsec

data points with associated uncertainties larger than 0.2 mag are ignored

We normalize the 3.6μm radial surface brightness profile to compensate for the discrepancies

4.3 Results: Spatially-resolved properties

Surface brightness radial profiles

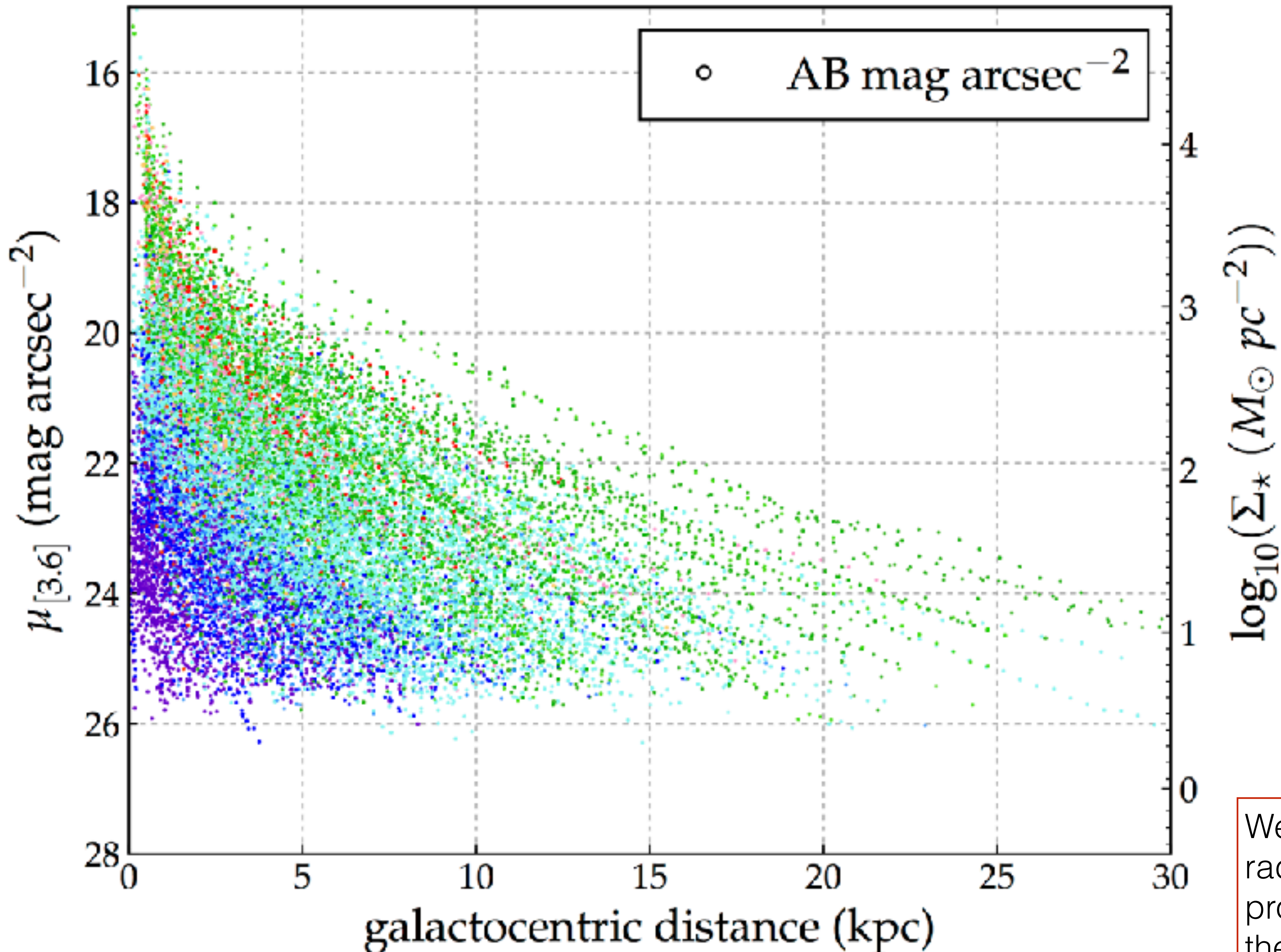

Surface brightness radial profiles

data points are taken at steps of 6 arcsec

data points with associated uncertainties larger than 0.2 mag are ignored

We normalize the 3.6μm radial surface brightness profile to compensate for the discrepancies

4.3 Results: Spatially-resolved properties

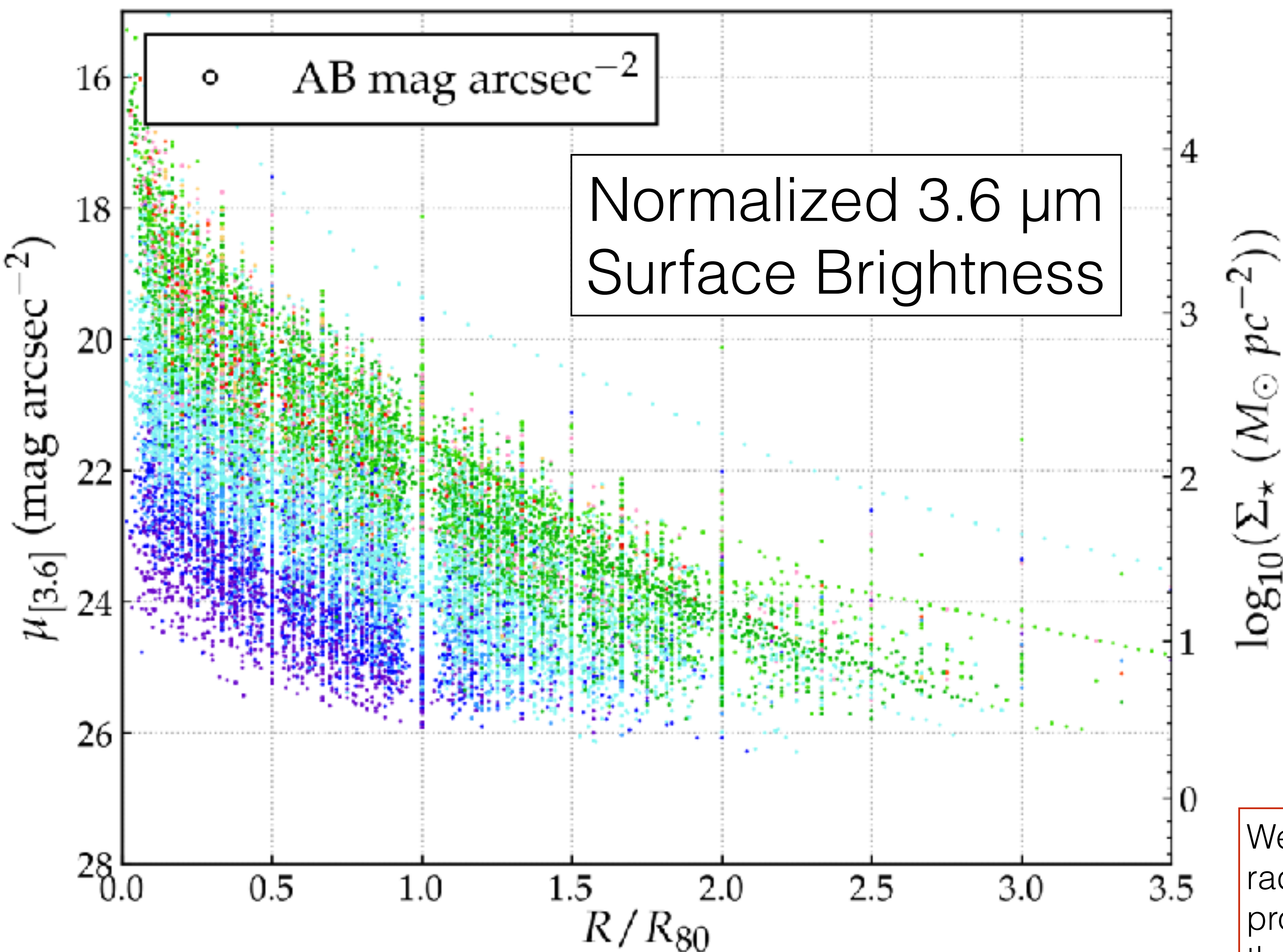

Surface brightness radial profiles

data points are taken at steps of 6 arcsec

data points with associated uncertainties larger than 0.2 mag are ignored

We normalize the 3.6µm radial surface brightness profile to compensate for the discrepancies

4.3 Results: Spatially-resolved properties

Colors radial profiles (normalized to R80)

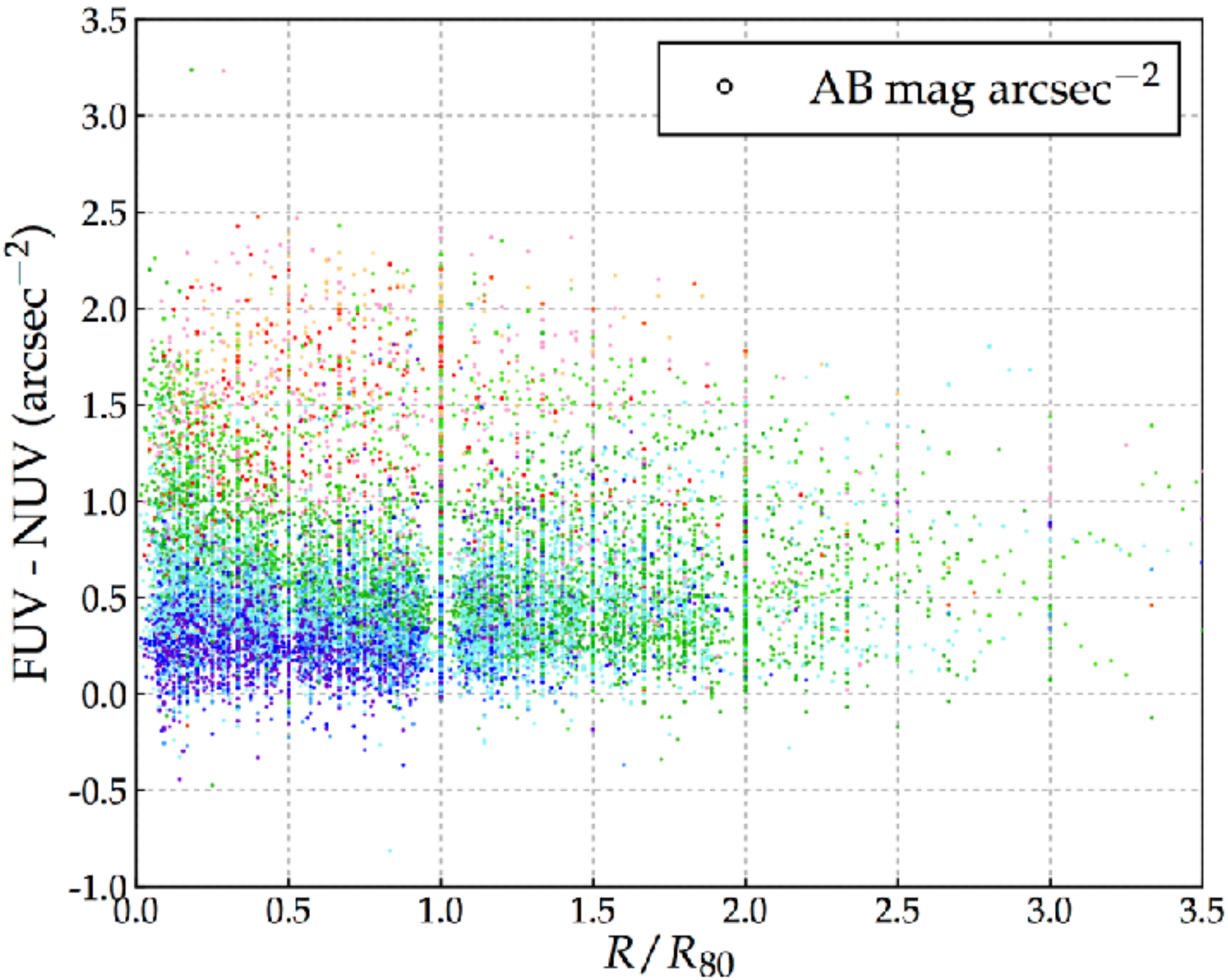

Color radial profiles

data points are taken at steps of 6 arcsec

we normalize the galactocentric distance to R80 unit (radius at which 80% of the IR-light is enclosed)

4.3 Results: Spatially-resolved properties

Colors radial profiles (normalized to R80)

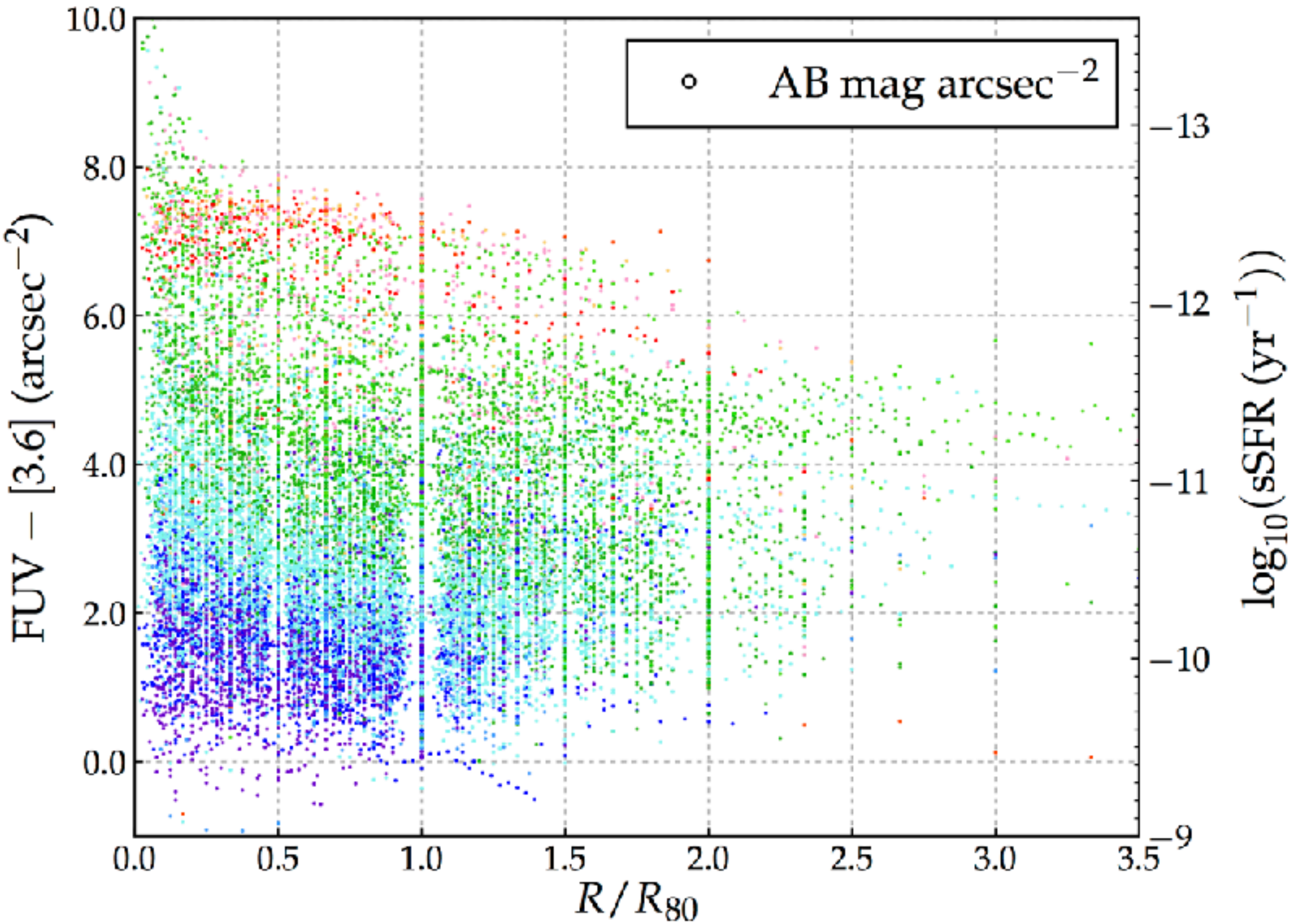

Color radial profiles

data points are taken at steps of 6 arcsec

we normalize the galactocentric distance to R80 unit (radius at which 80% of the IR-light is enclosed)

4.3 Results: Spatially-resolved properties

Colors radial profiles (normalized to R80)

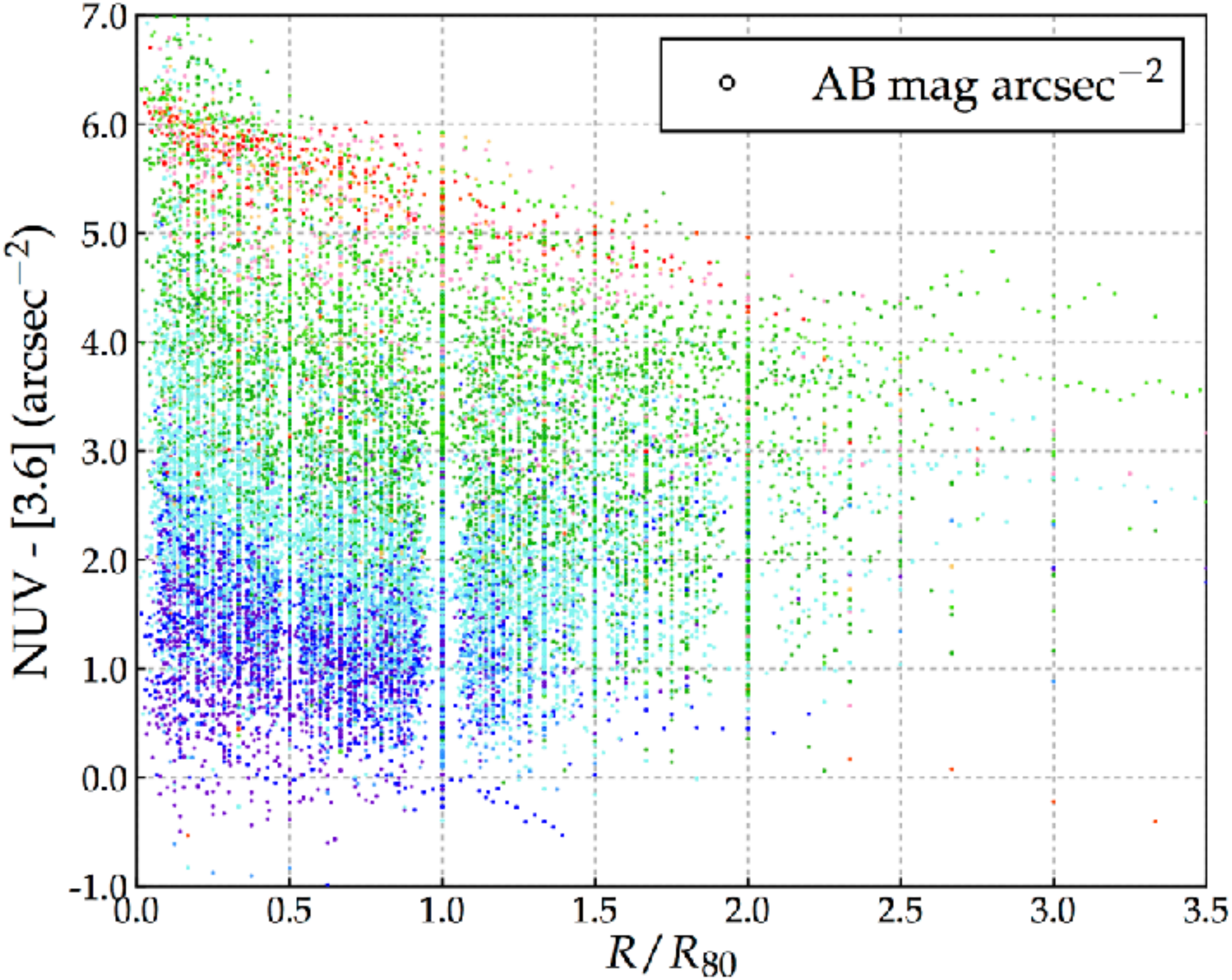

Color radial profiles

data points are taken at steps of 6 arcsec

we normalize the galactocentric distance to R80 unit (radius at which 80% of the IR-light is enclosed)

4.3 Results: Spatially-resolved properties

Average SB and color radial profiles normalized (to R80)

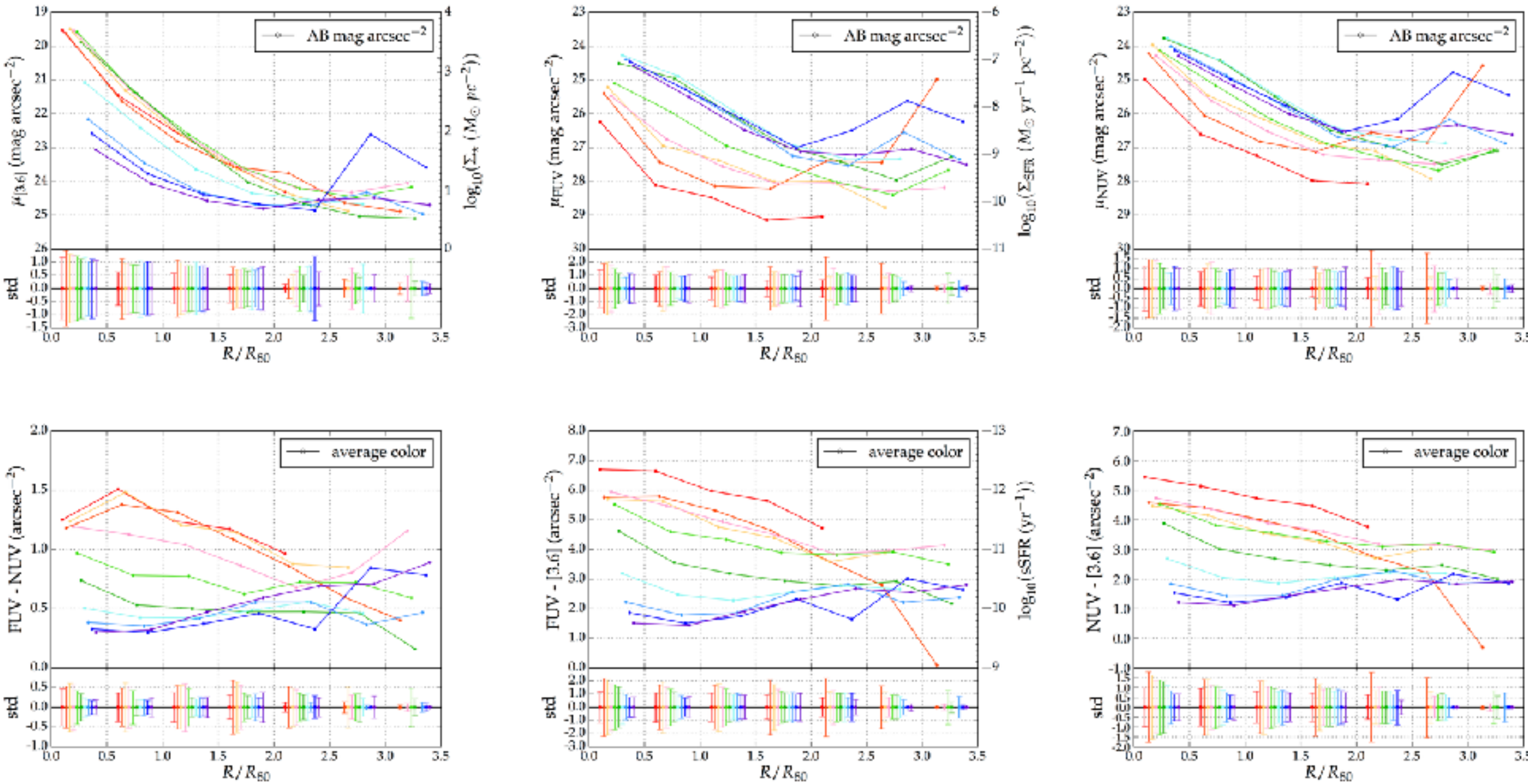

4.3 Results: Spatially-resolved properties

Average SB and color radial profiles normalized (to R80)

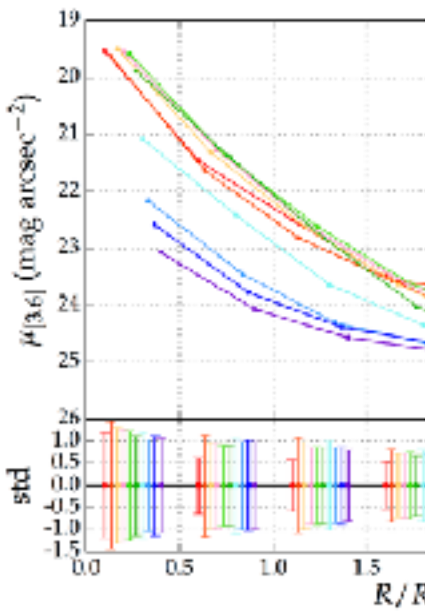

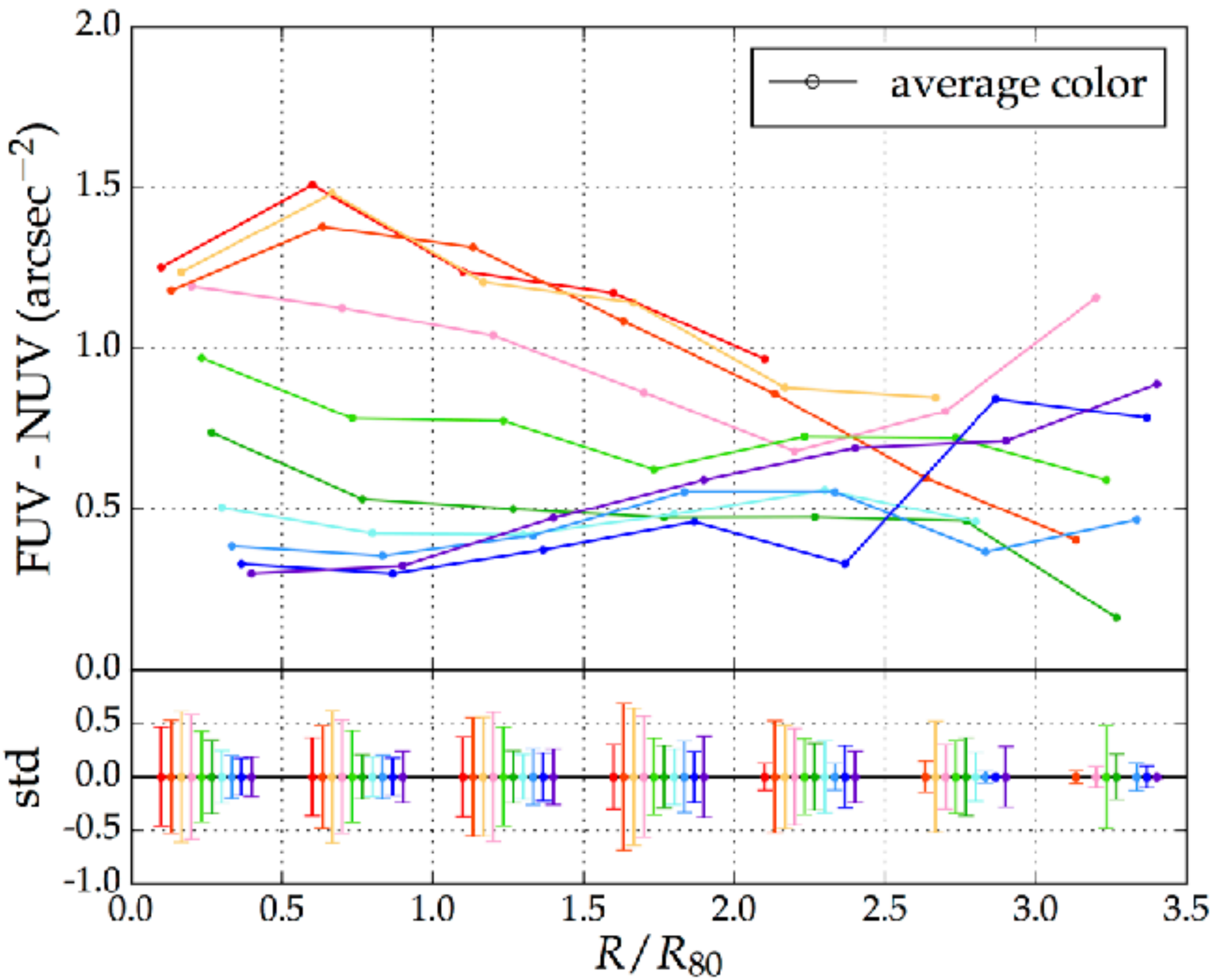

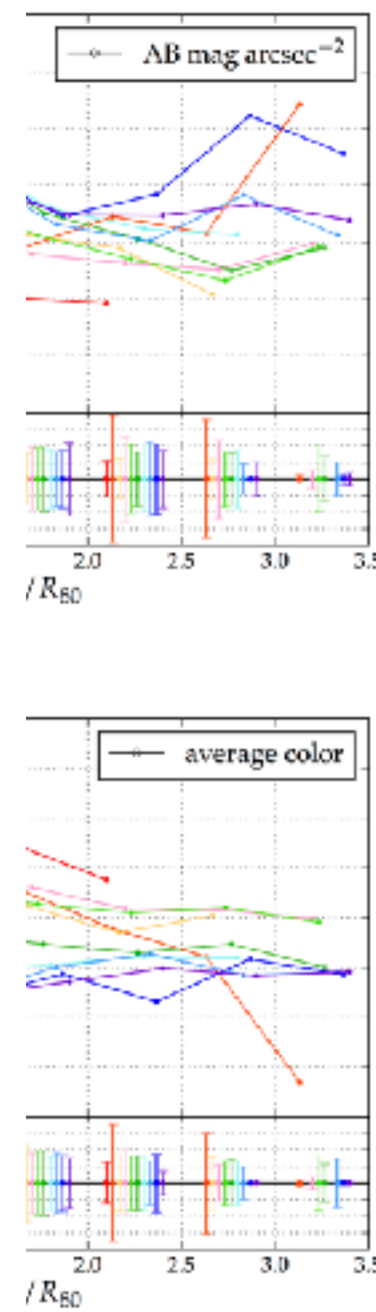

4.3 Results: Spatially-resolved properties

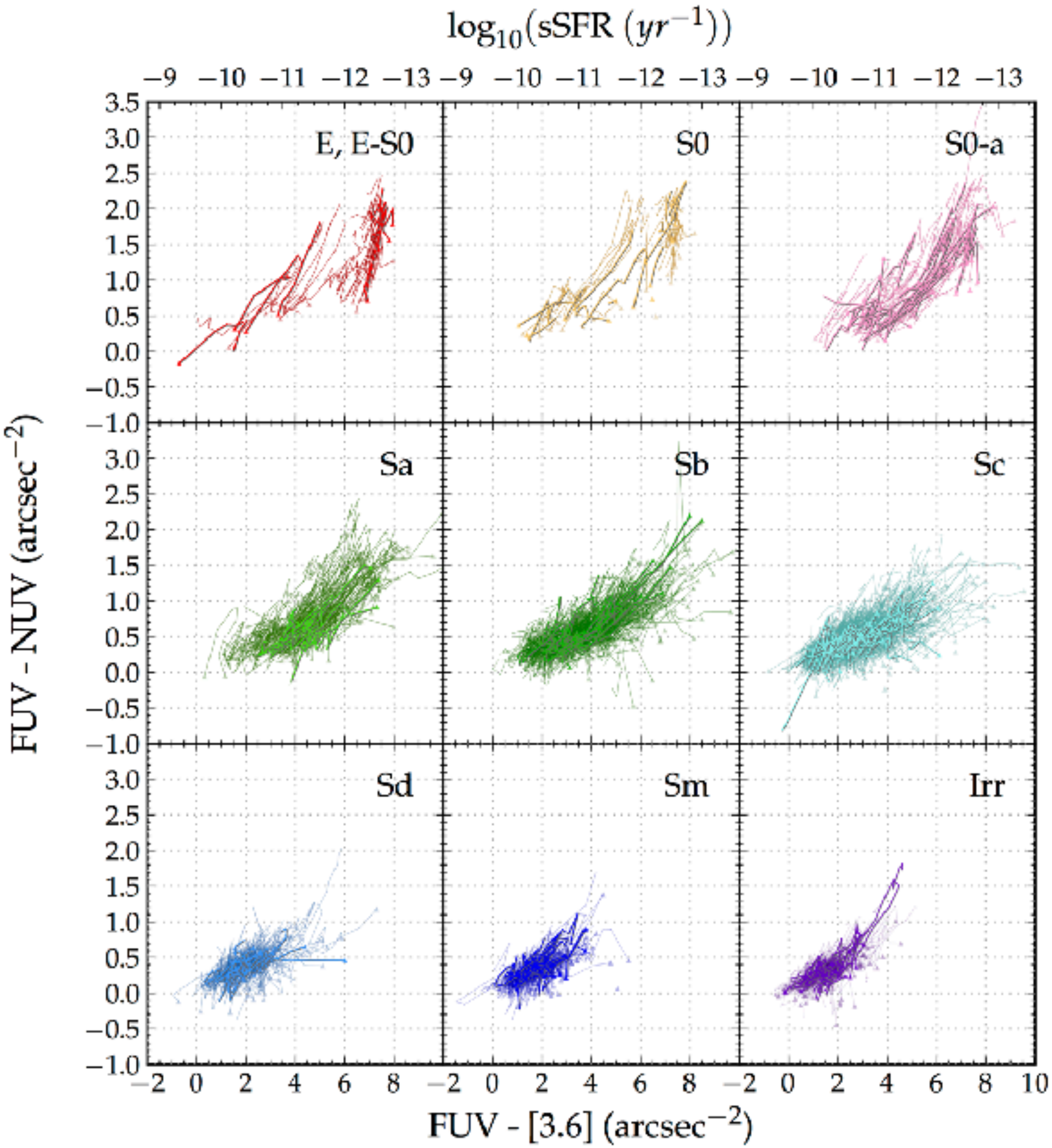

FUV - NUV
vs.
FUV - [3.6]

We readily see the radial color distributions of all our galaxies.
ETGs are clearly populating the 'red-red' corner but still having some bluer component.
Low-mass late-type are only found in the 'blue-blue' corner but some are found with reddened outer disks.

4.3 Results: Spatially-resolved properties

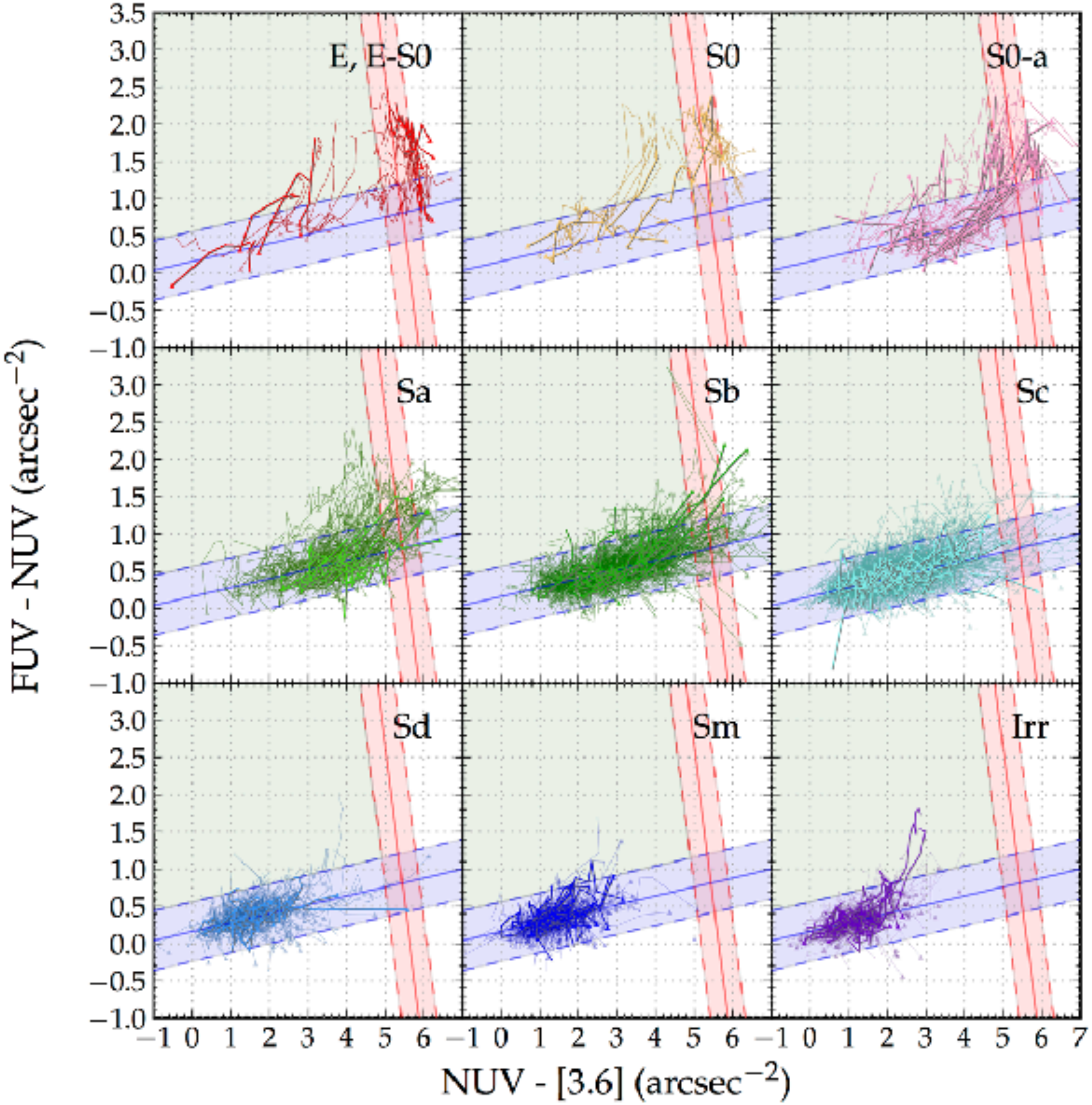

FUV - NUV
vs.
NUV - [3.6]

This helps identifying the regions that are first to move toward the GGV

4.3 Results: Spatially-resolved properties

μ_{FUV} vs. $\mu_{[3.6]}$ per zone

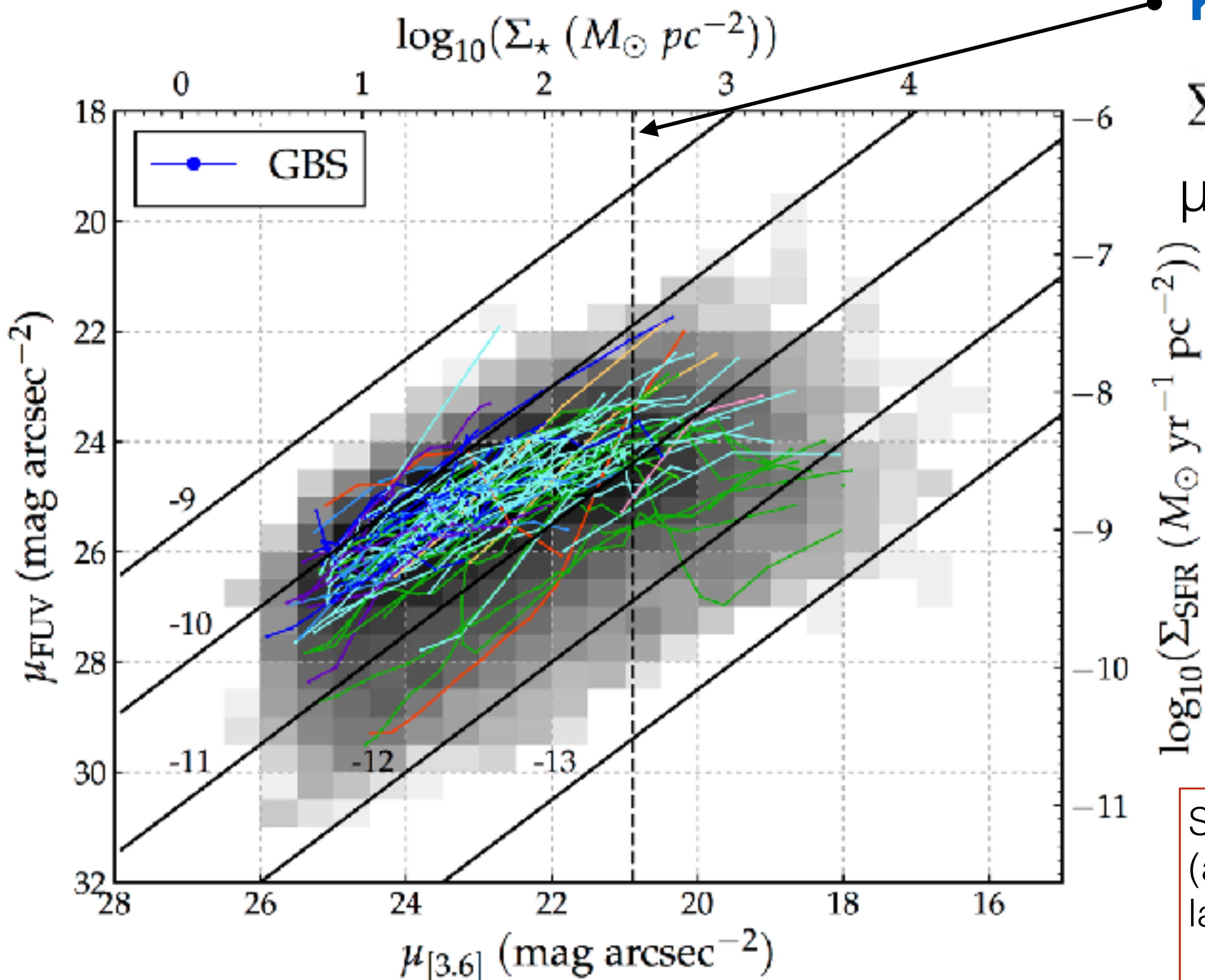

Kauffmann et al. (2006)

$$\Sigma_\star = 3 \times 10^8\ M_\odot\ \mathrm{kpc}^{-2}$$

$\mu_{[3.6]}$=20.89 mag arcsec^{-2}

separates between “inner” and “outer” disk

Star-forming galaxies (all except ETGs) have sSFR larger than log(sSFR)=-12

GGV also have constant sSFR beyond 20.89 mag arcsec^{-2}

4.3 Results: Spatially-resolved properties

μ_{FUV} vs. $\mu_{[3.6]}$ per zone

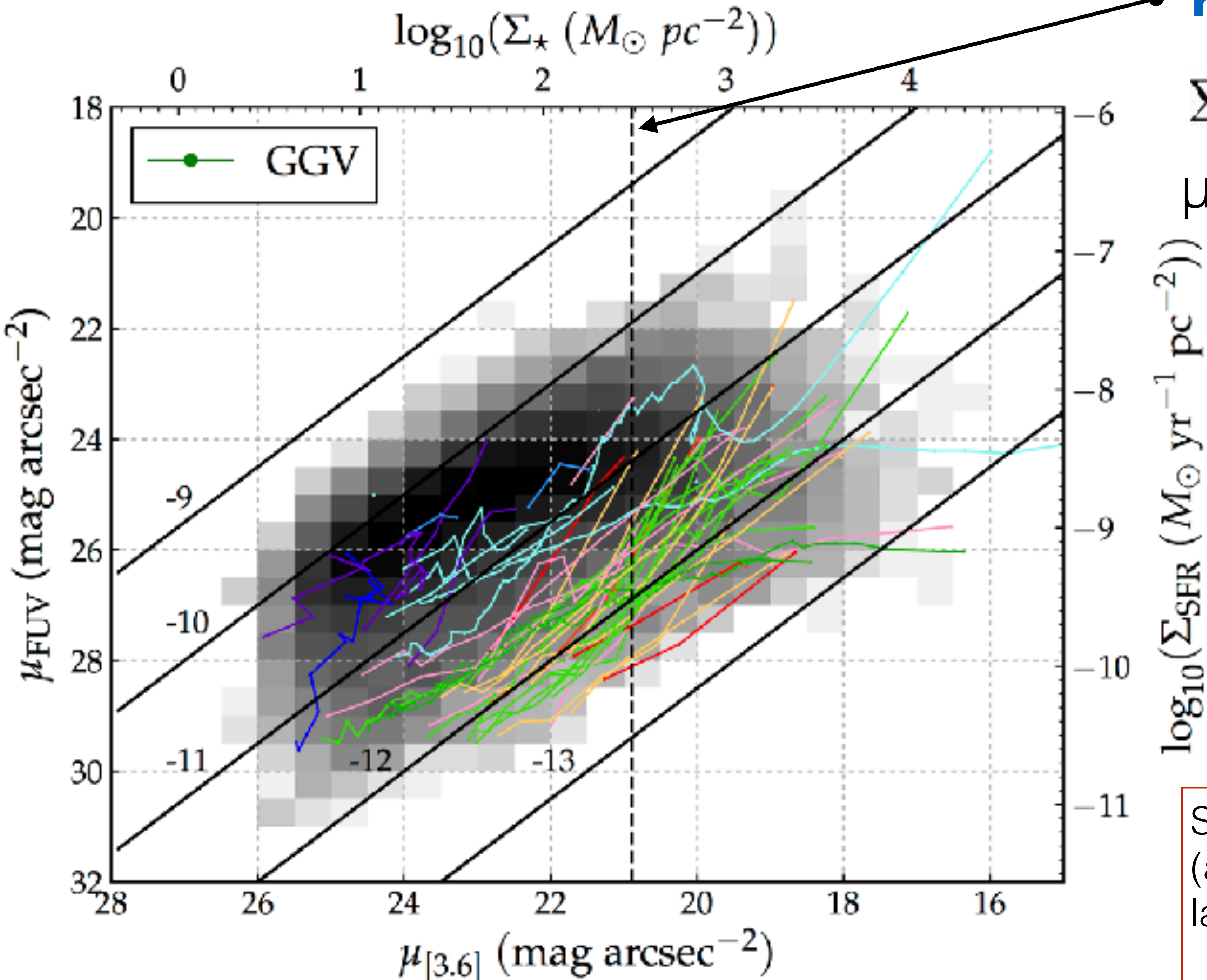

Kauffmann et al. (2006)

$$\Sigma_\star = 3 \times 10^8\ M_\odot\ \mathrm{kpc}^{-2}$$

$\mu_{[3.6]}$=20.89 mag arcsec^{-2}

separates between “inner” and “outer” disk

Star-forming galaxies (all except ETGs) have sSFR larger than log(sSFR)=-12

GGV also have constant sSFR beyond 20.89 mag arcsec^{-2}

4.3 Results: Spatially-resolved properties

μ_{FUV} vs. $\mu_{[3.6]}$ per zone

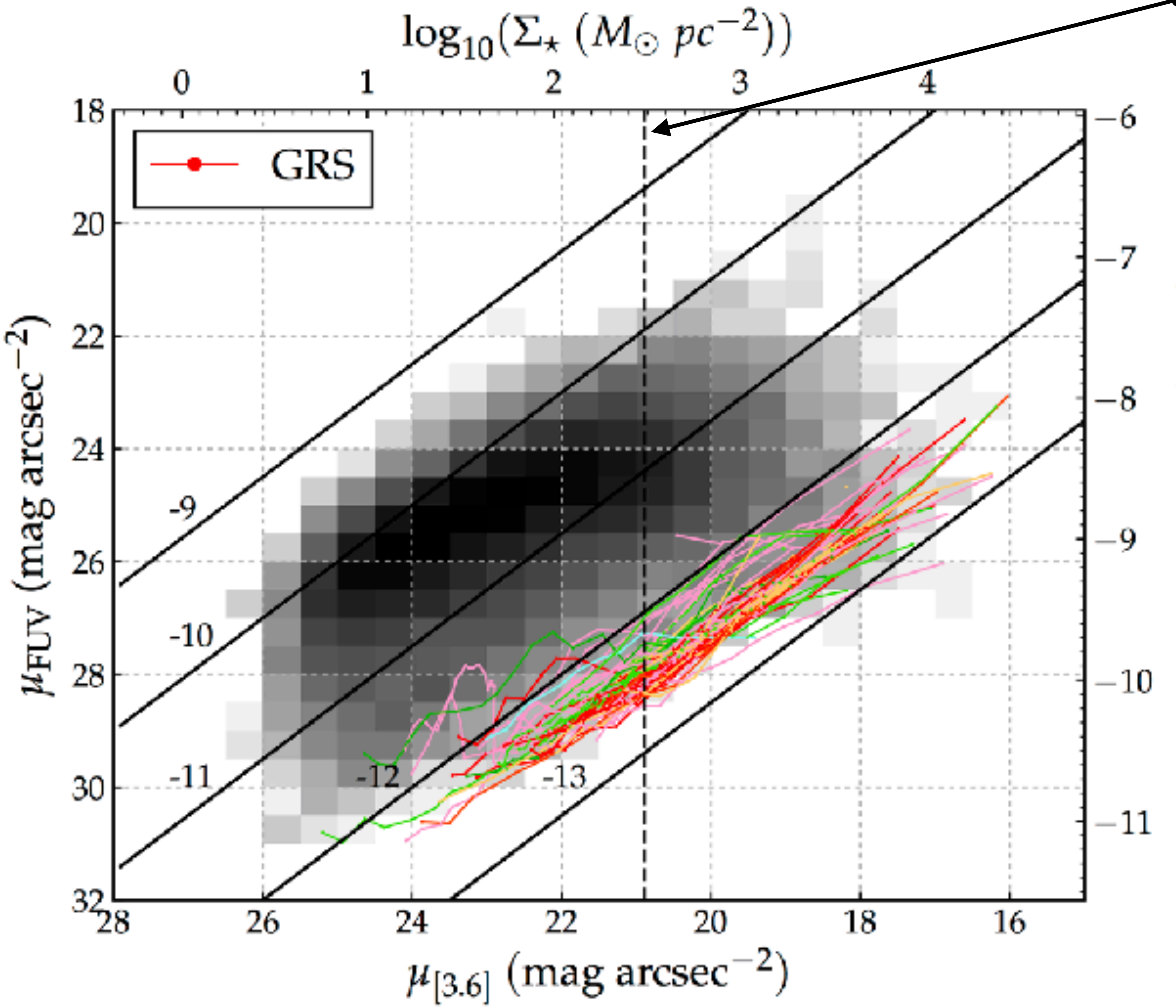

Kauffmann et al. (2006)

$$\Sigma_\star = 3 \times 10^8\ M_\odot\ \mathrm{kpc}^{-2}$$

$\mu_{[3.6]}$=20.89 mag arcsec^{-2}

separates between "inner" and "outer" disk

Star-forming galaxies (all except ETGs) have sSFR larger than log(sSFR)=-12

GGV also have constant sSFR beyond 20.89 mag arcsec^{-2}

4.3 Results: Spatially-resolved properties

Distribution of outer disk sSFR per zone

sSFR of "outer disk", beyond $\mu_{[3.6]}$=20.89 mag arcsec^{-2} of **Kauffmann et al. (2006)**

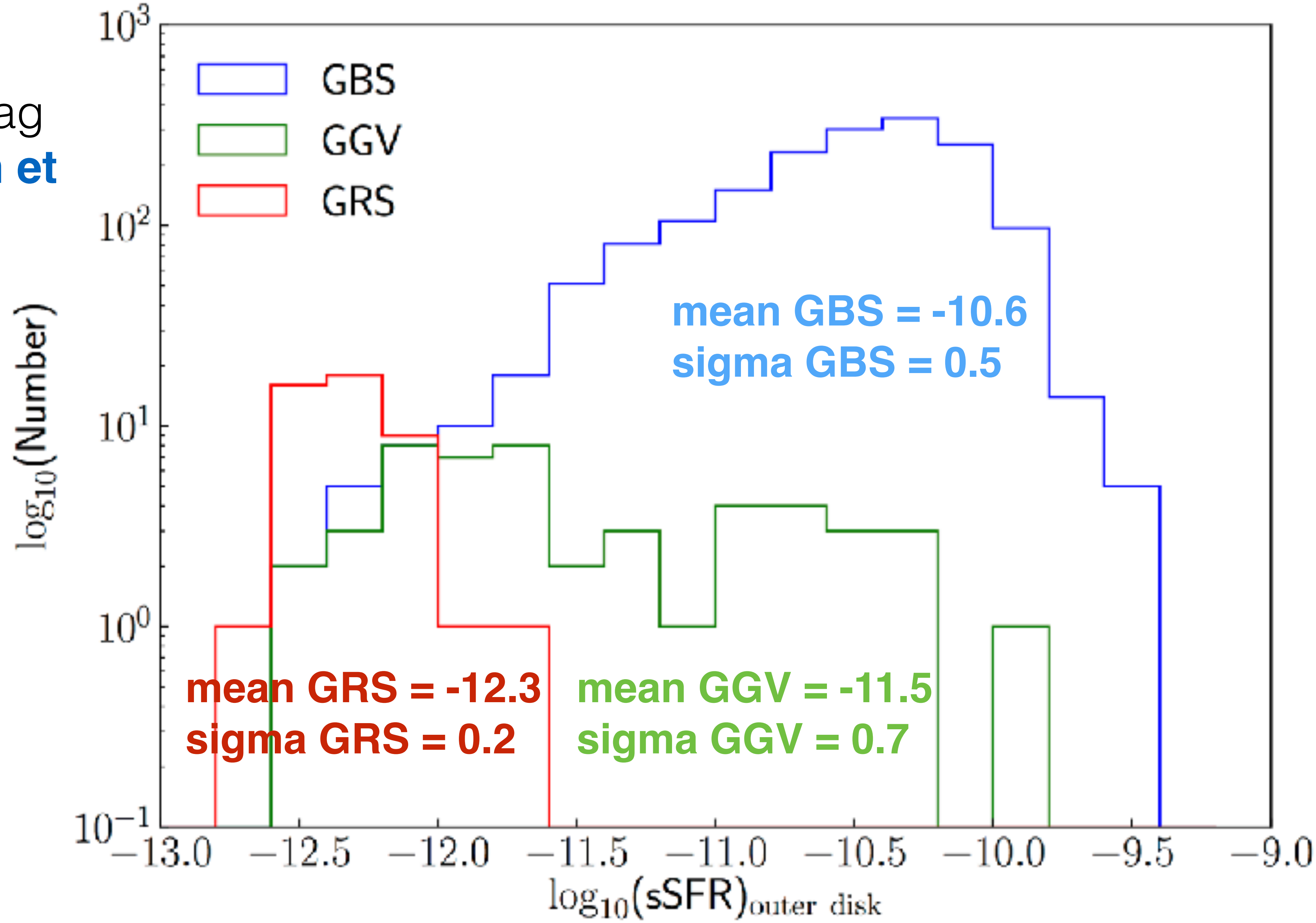

4.3 Results: Spatially-resolved properties

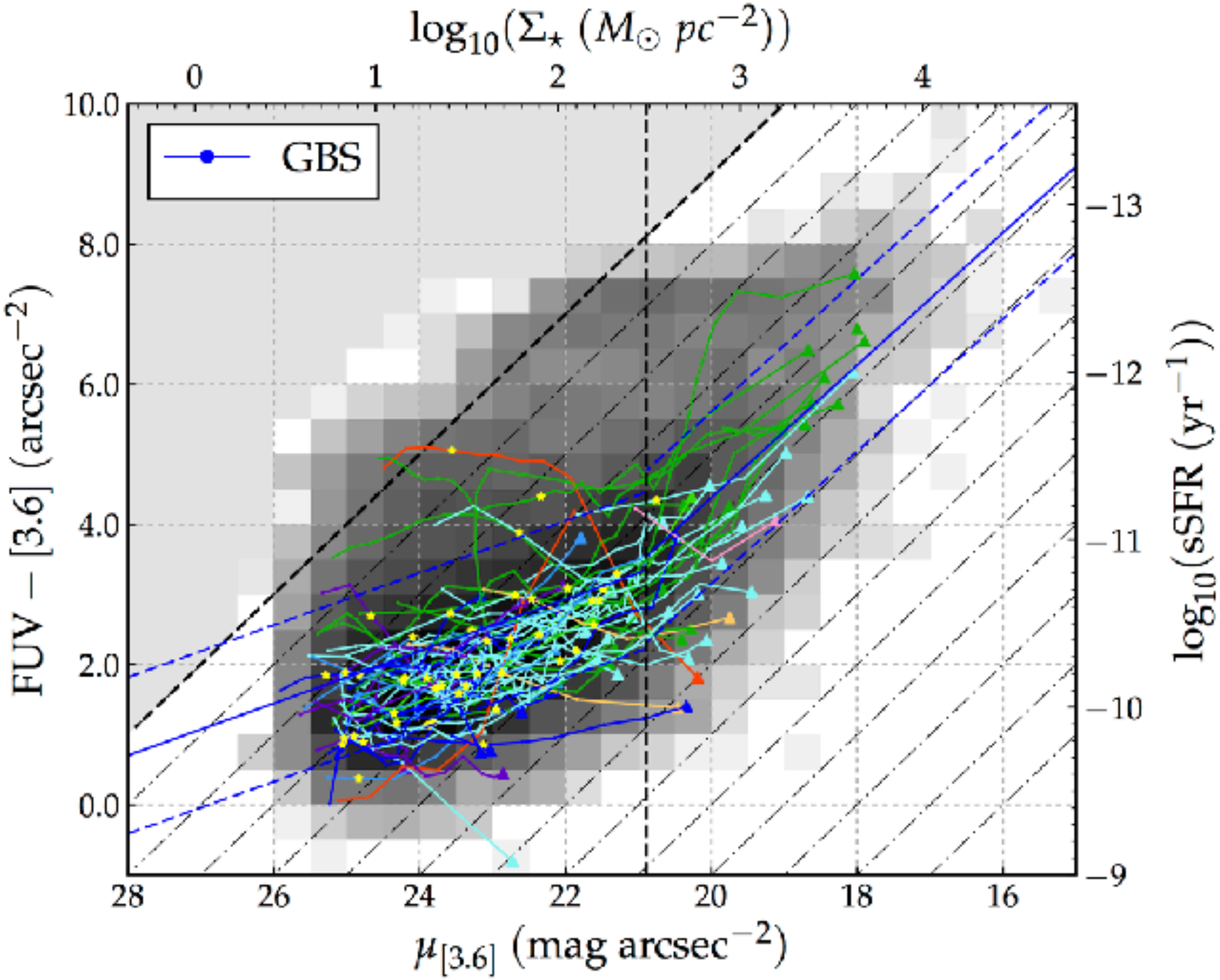

- (FUV - [3.6]) colors vs. $\mu_{[3.6]}$

locus of R80 (yellow star) well separated for GBS, GGV and GRS galaxies

4.3 Results: Spatially-resolved properties

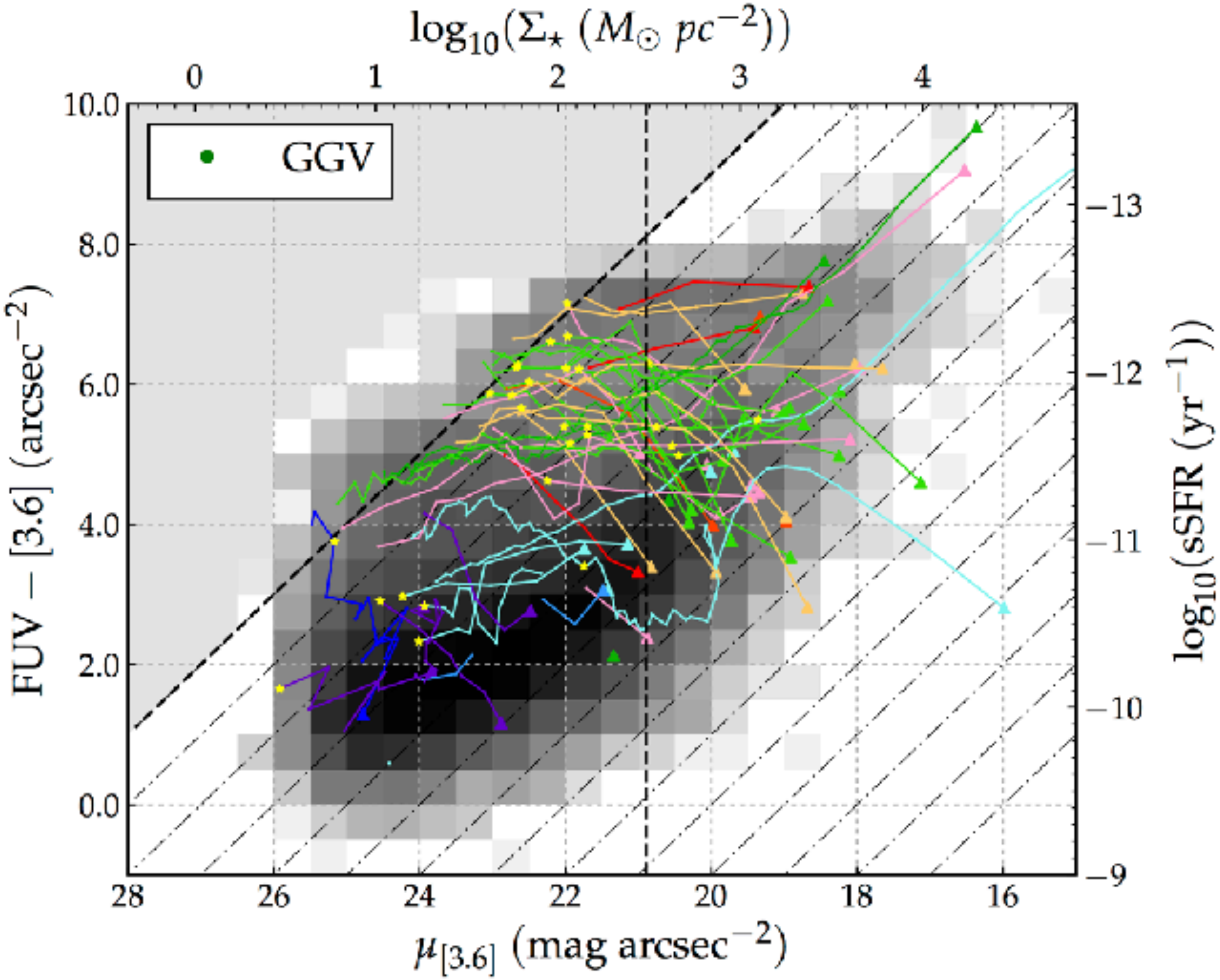

- (FUV - [3.6]) colors vs. $\mu_{[3.6]}$

locus of R80 (yellow star) well separated for GBS, GGV and GRS galaxies

4.3 Results: Spatially-resolved properties

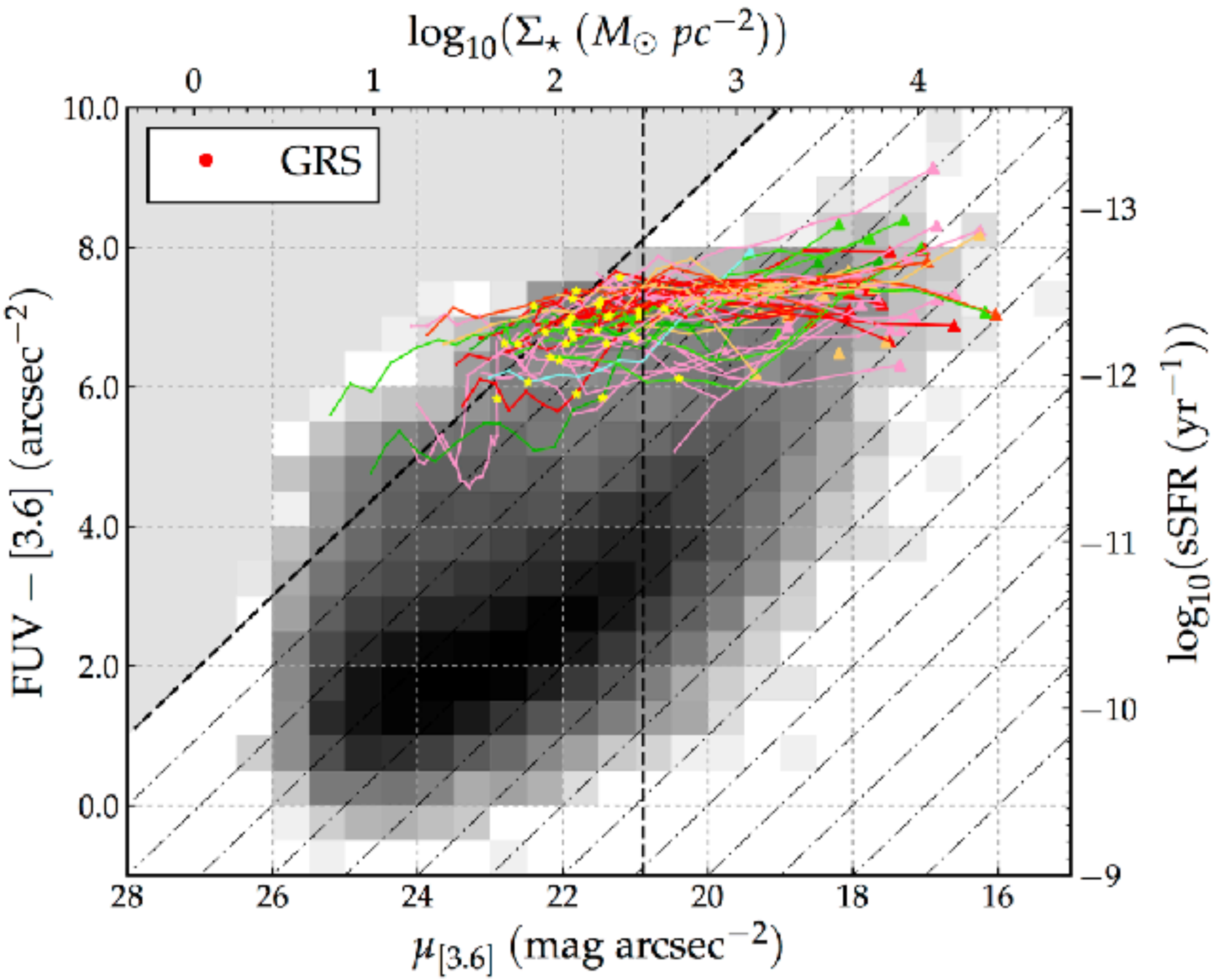

- (FUV - [3.6]) colors vs. $\mu_{[3.6]}$

locus of R80 (yellow star) well separated for GBS, GGV and GRS galaxies

4.3 Results: Spatially-resolved properties

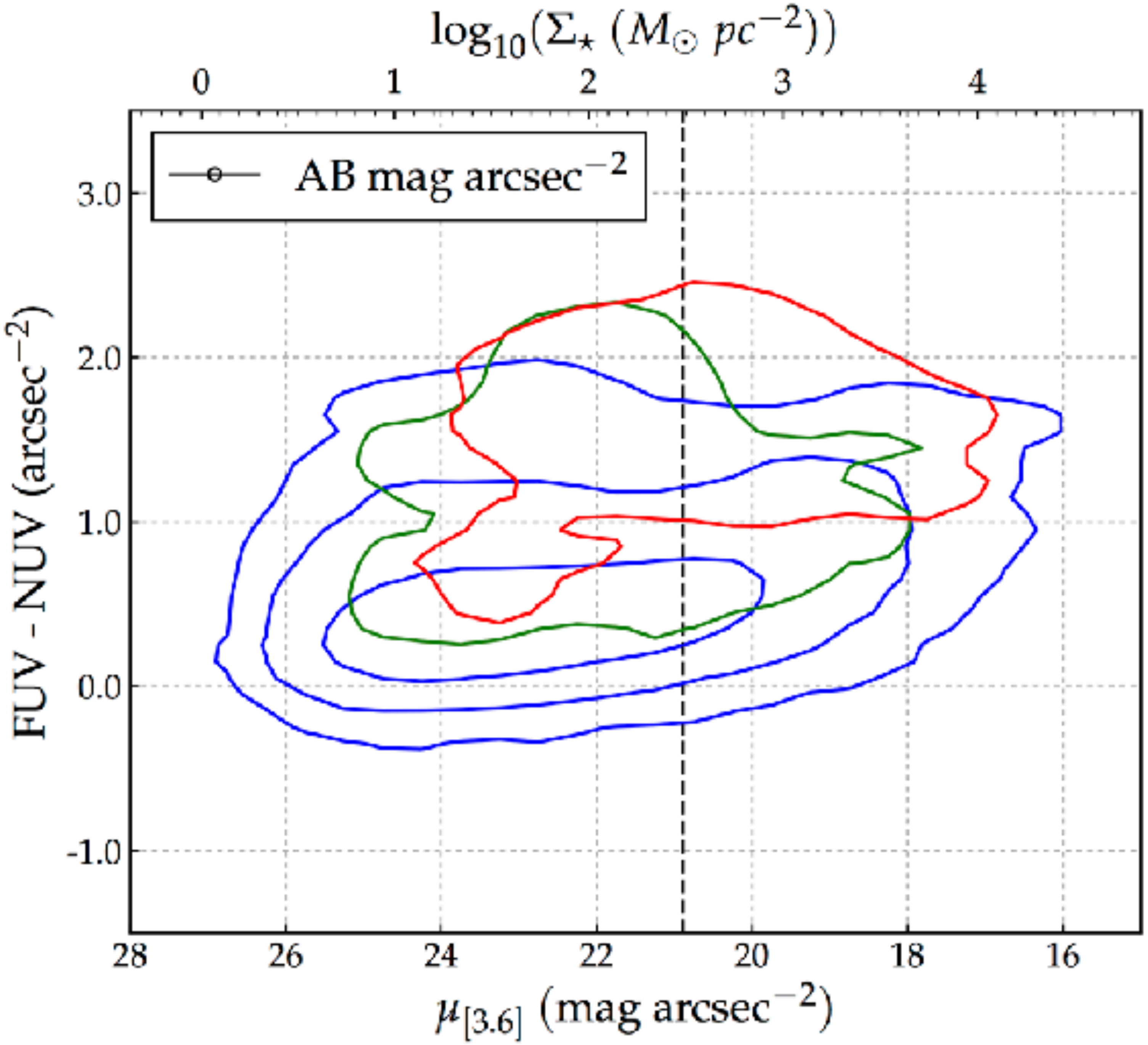

- (FUV - NUV)
- (NUV - [3.6])
- (FUV - [3.6]) colors

vs.

$\mu_{[3.6]}$

4.3 Results: Spatially-resolved properties

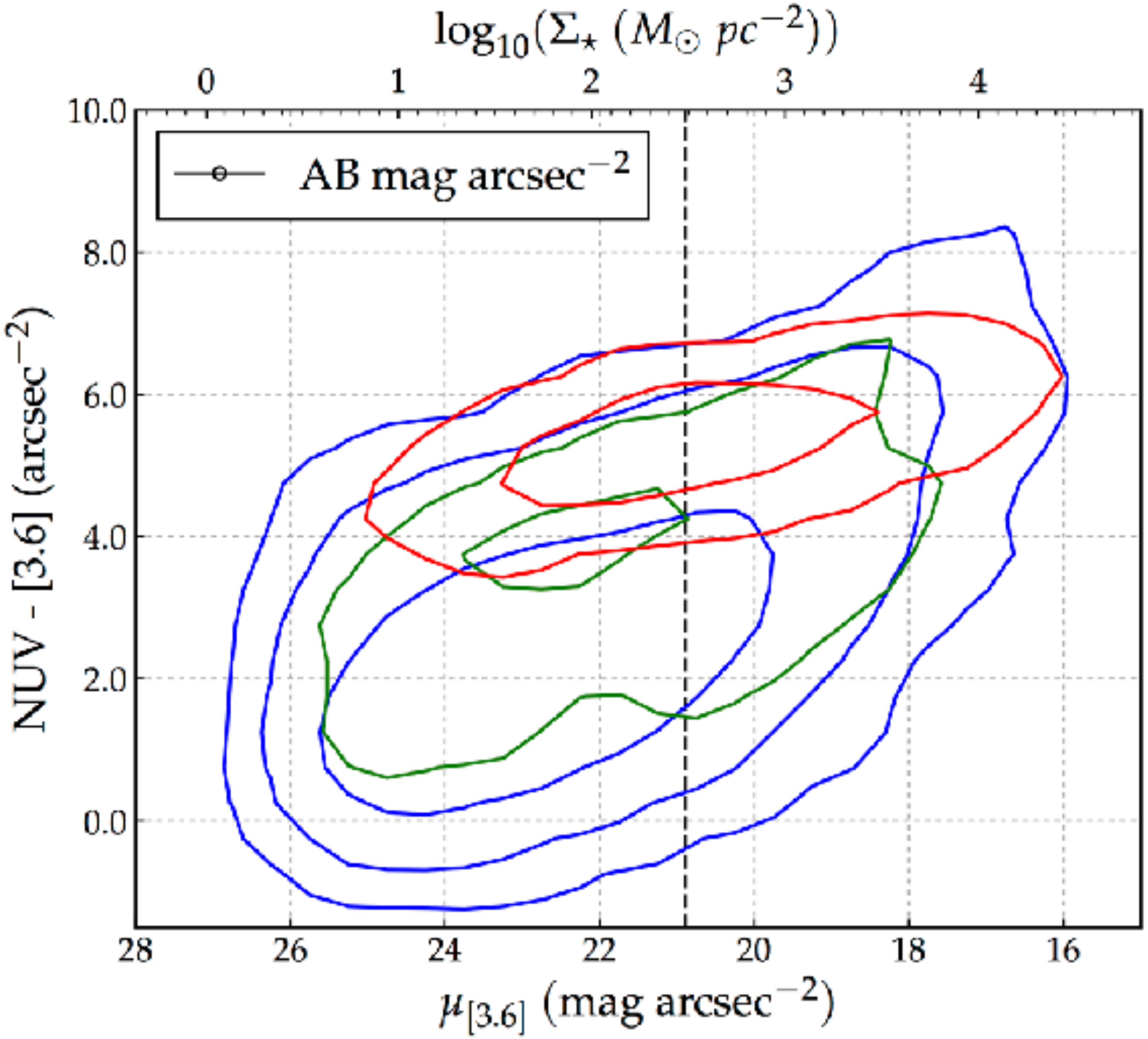

- (FUV - NUV)
- (NUV - [3.6])
- (FUV - [3.6])

colors

vs.

$\mu_{[3.6]}$

4.3 Results: Spatially-resolved properties

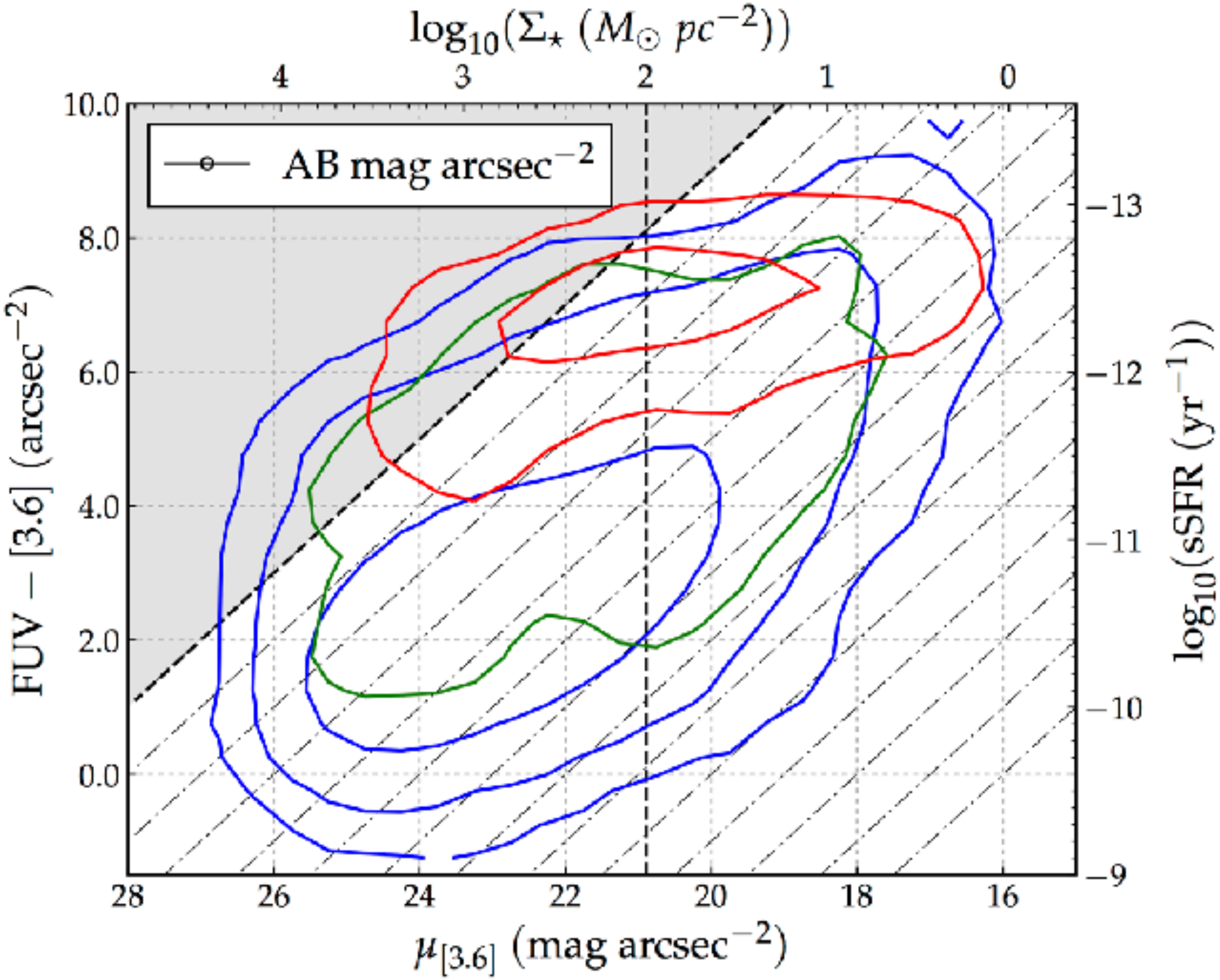

- (FUV - NUV)
- (NUV - [3.6])
- (FUV - [3.6]) colors vs. $\mu_{[3.6]}$

4.3 Results: Spatially-resolved properties

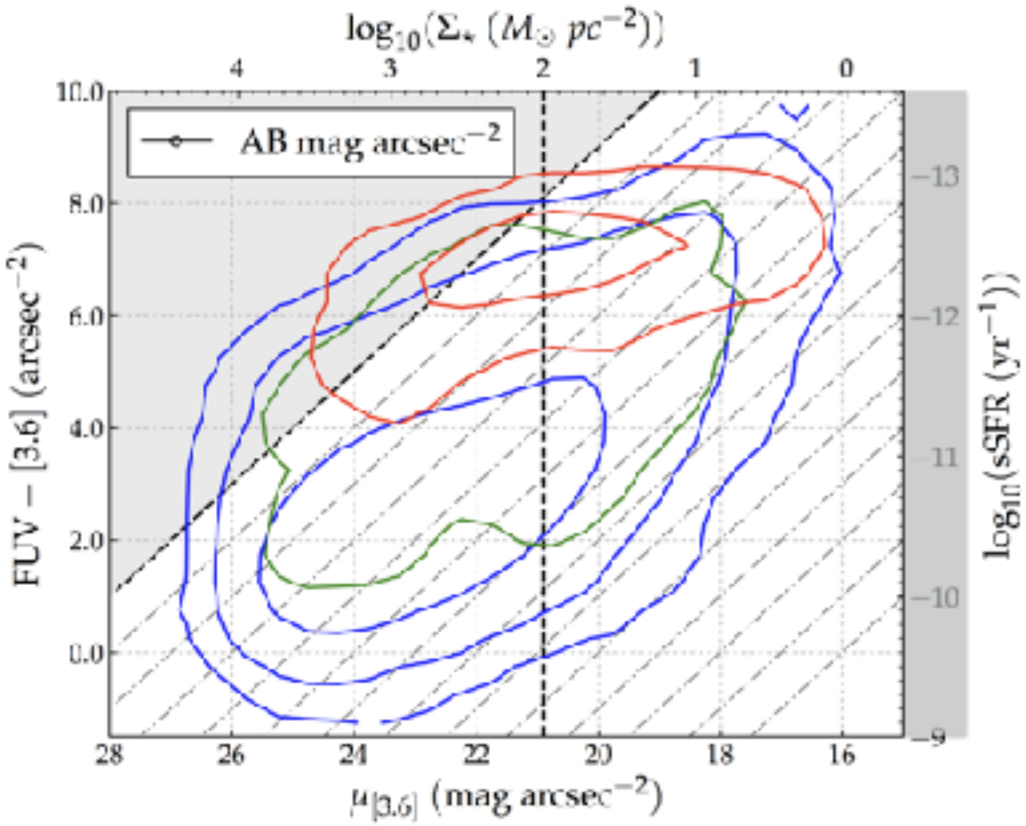

Median color profiles of GBS, GGV, GRS galaxies.

Both GGV and GRS galaxies have reddening disks, followed by a flattening of sSFR @>20.89 mag/arcsec^{-2}

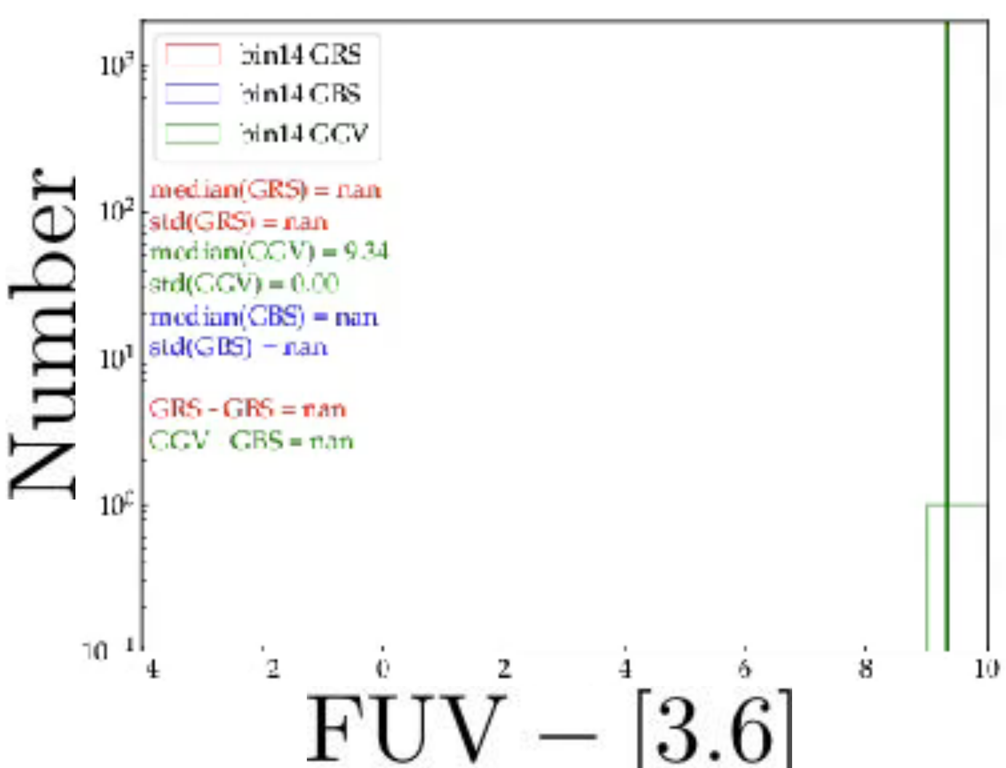

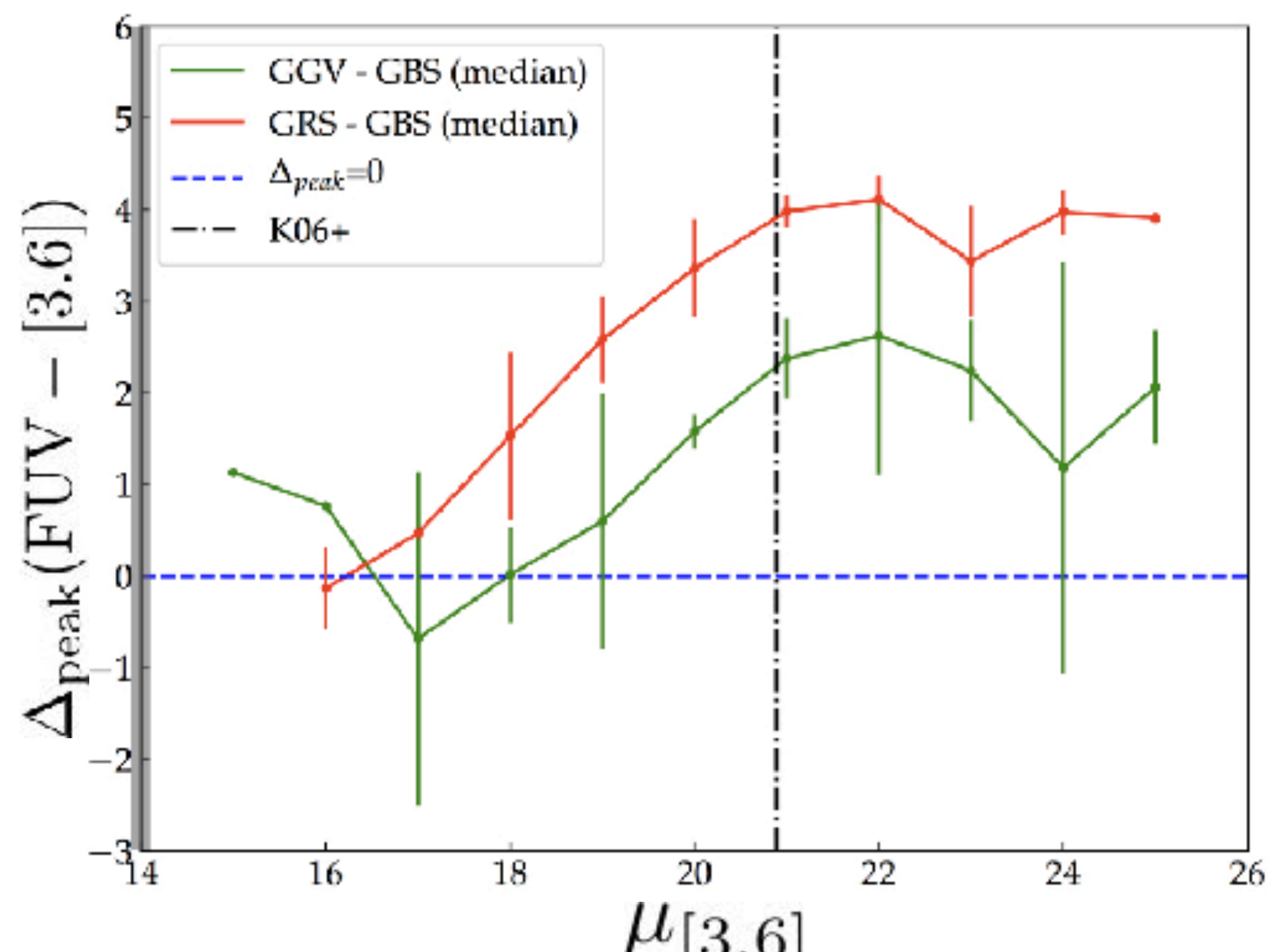

4.3 Results: Spatially-resolved properties

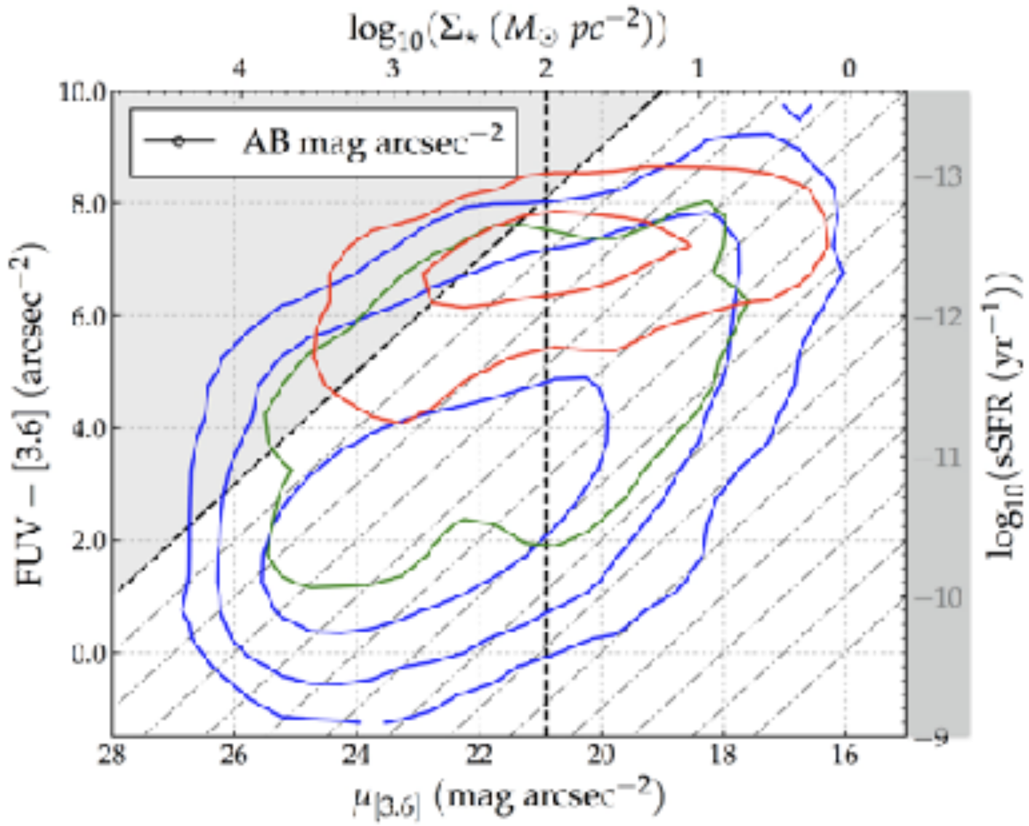

Median color profiles of GBS, GGV, GRS galaxies.

Both GGV and GRS galaxies have reddening disks, followed by a flattening of sSFR @>20.89 mag/arcsec^{-2}

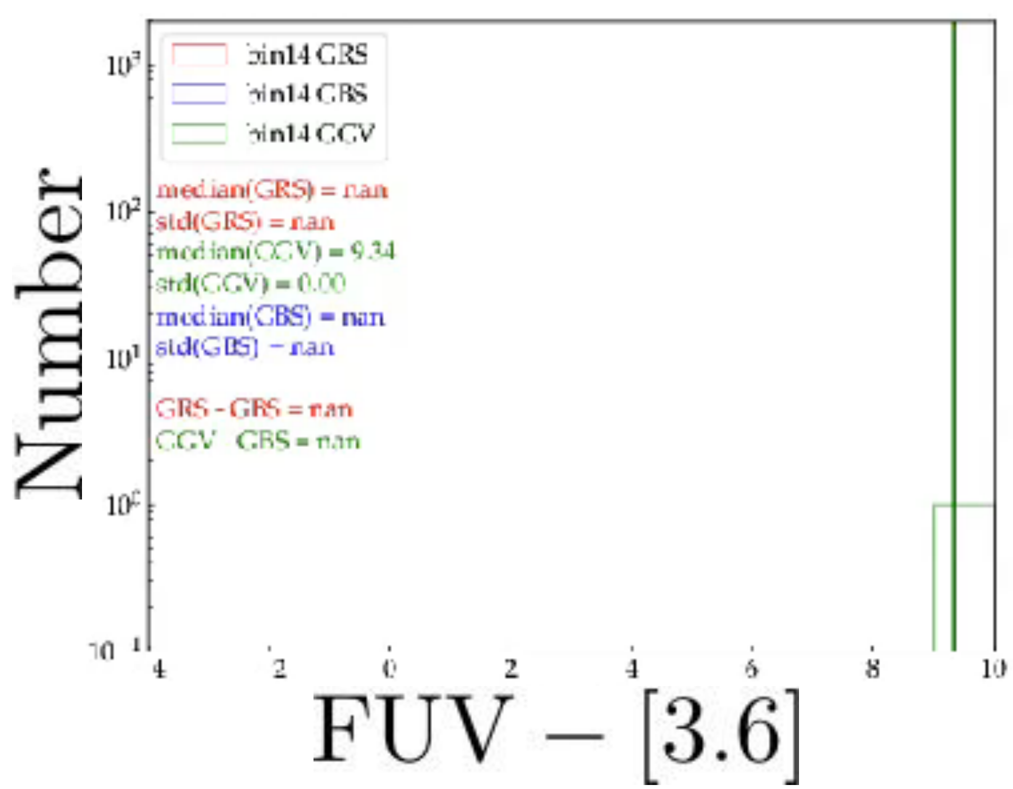

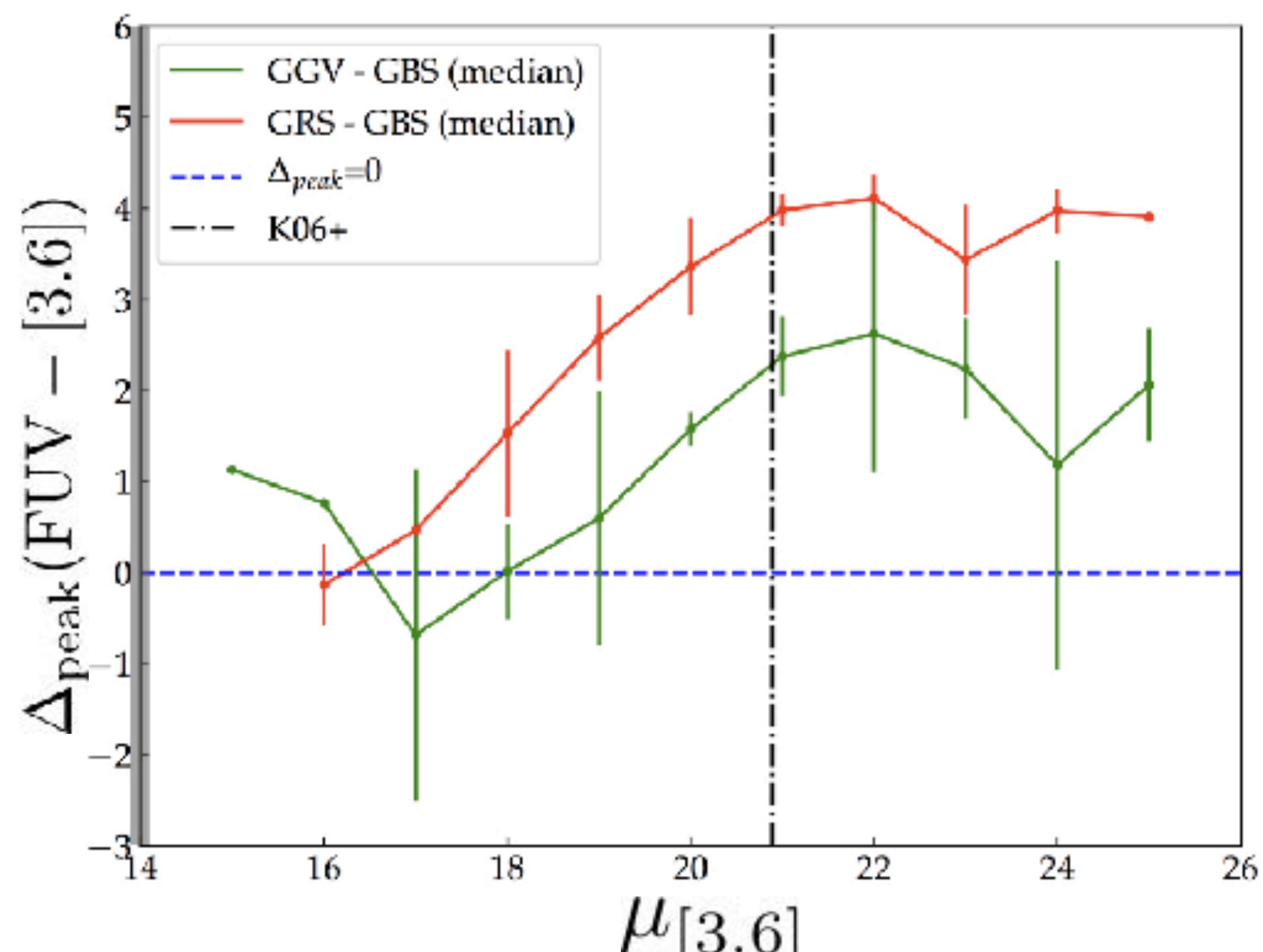

4.3 Results: Spatially-resolved properties

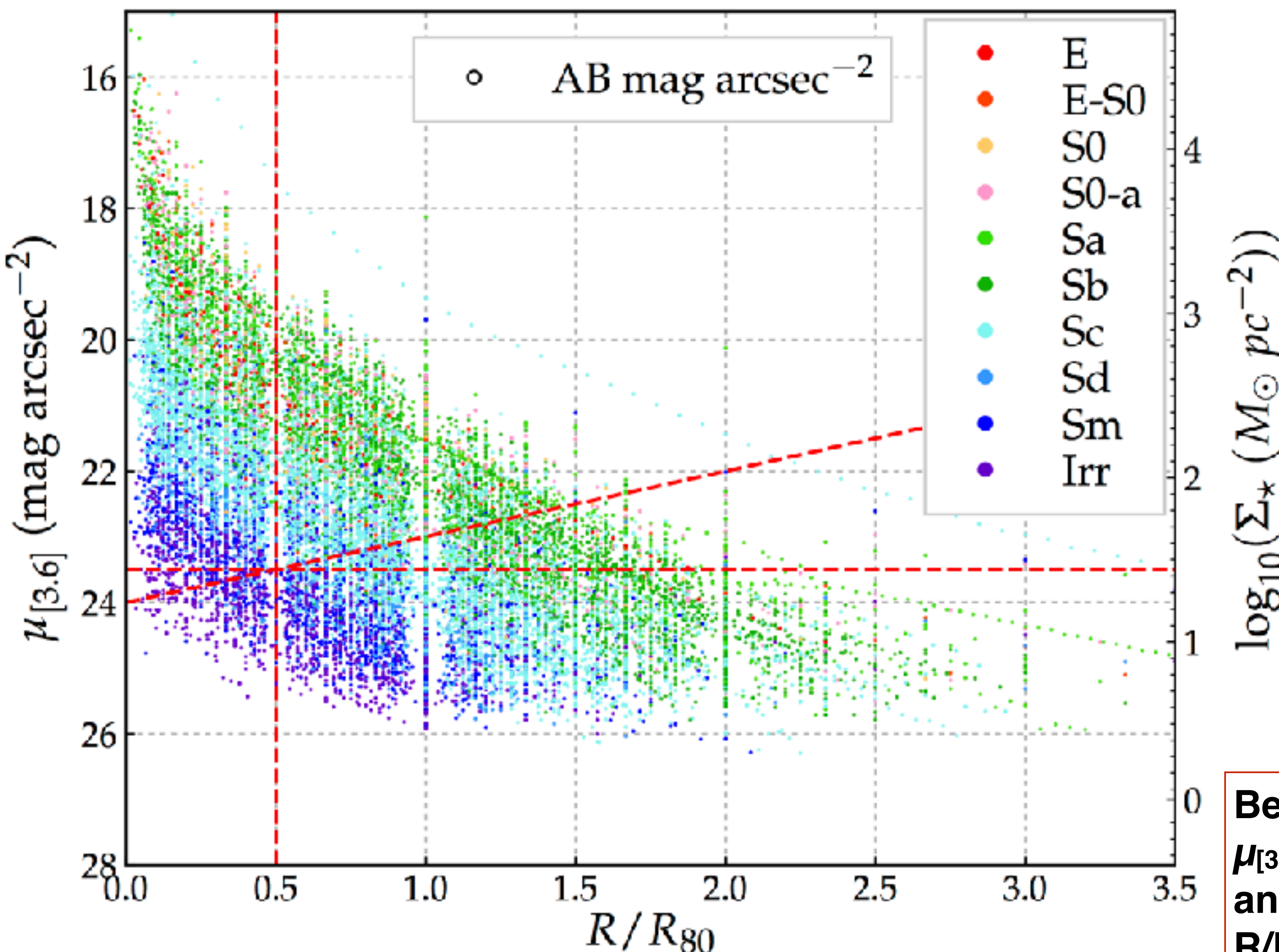

We first isolate the disk component by making vertical/ horizontal cutoffs, and also by making an oblique cutoff.

Best cutoff@
$\mu_{[3.6]}$=23.5 mag arcsec^{-2}
and
R/R80 = 0.5

4.3 Results: Spatially-resolved properties

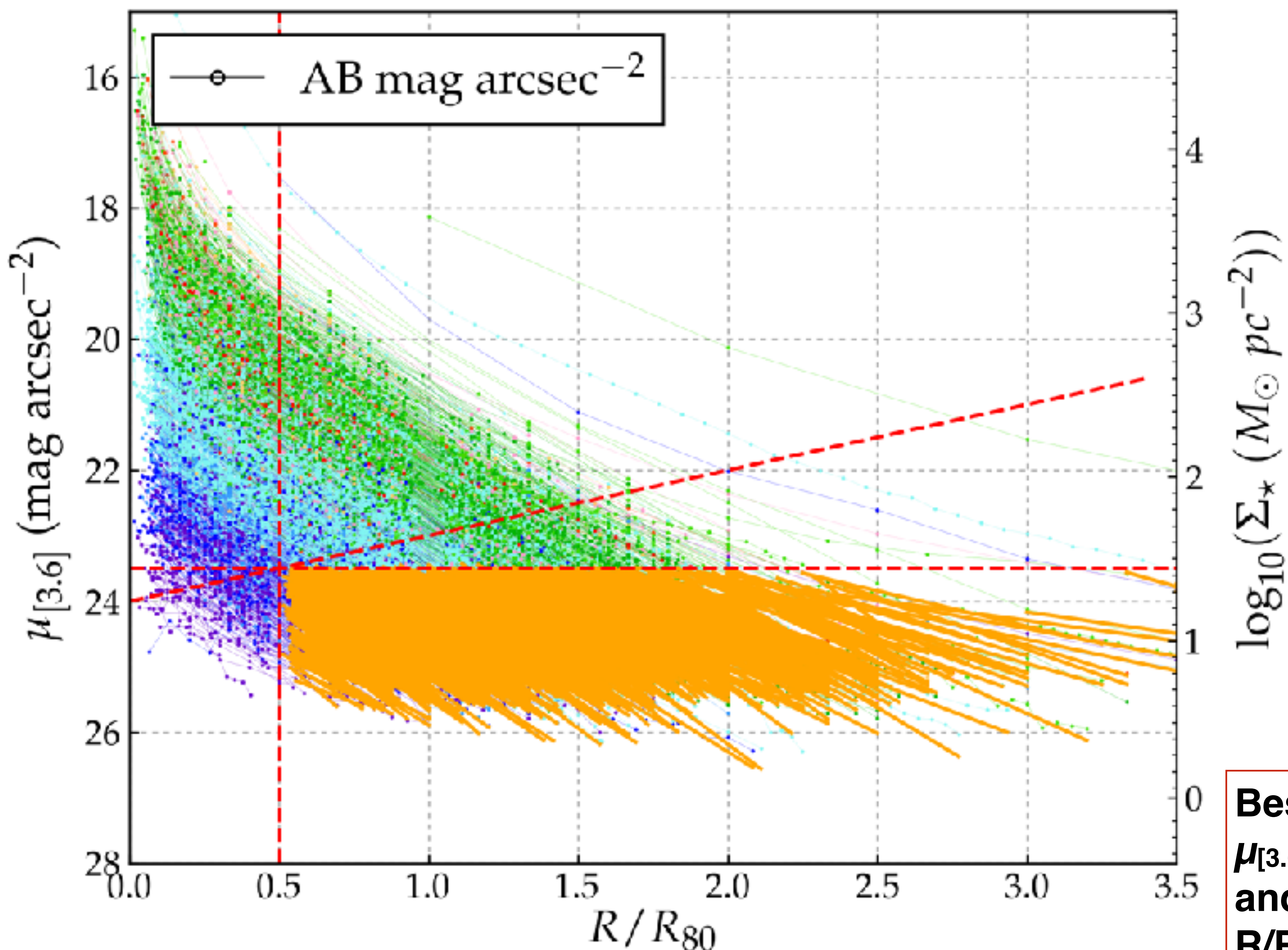

We first isolate the disk component by making vertical/ horizontal cutoffs, and also by making an oblique cutoff.

Best cutoff@
$\mu_{[3.6]}$=23.5 mag arcsec^{-2}
and
R/R80 = 0.5

4.3 Results: Spatially-resolved properties

Average Reduced χ^2 of the Linear Fit with $\mu_{[3.6]}$ and $R/R80$ Cuts

		R/R80 Cutoffs											
		0.00		0.25		0.50		0.75		1.00		1.25	
		$\langle\chi^2\rangle$	N	$\langle\chi^2\rangle$	N	$\langle\chi^2\rangle$	N	$\langle\chi^2\rangle$	N	$\langle\chi^2\rangle$	N	$\langle\chi^2\rangle$	N
$\mu_{[3.6]}$ cutoffs	21.5	26.20	(1577)	20.84	(1554)	15.72	(1451)	9.68	(1240)	4.04	(794)	2.87	(535)
	22	10.64	(1489)	8.63	(1474)	6.97	(1387)	5.85	(1191)	3.26	(781)	2.48	(530)
	22.5	4.89	(1384)	4.28	(1375)	3.54	(1298)	3.11	(1126)	2.02	(756)	1.62	(518)
	23	2.34	(1232)	2.17	(1228)	1.81	(1165)	1.63	(1014)	1.14	(693)	0.98	(482)
	23.5	1.37	(1034)	1.28	(1033)	1.12	(987)	0.96	(863)	0.68	(591)	0.56	(419)
	24	0.78	(755)	0.77	(754)	0.73	(723)	0.67	(630)	0.40	(426)	0.35	(296)

Average Reduced χ^2 of the Linear Fit in the $\mu_{[3.6]}$ vs. $R/R80$ Plane with Oblique Cuts

		Slope (a) Cutoff											
		−6		−5		−4		−3		−2		−1	
		$\langle\chi^2\rangle$	N	$\langle\chi^2\rangle$	N	$\langle\chi^2\rangle$	N	$\langle\chi^2\rangle$	N	$\langle\chi^2\rangle$	N	$\langle\chi^2\rangle$	N
y intercept (b) cutoff	20	777.55	(1717)	649.14	(1716)	569.63	(1713)	469.68	(1712)	393.01	(1707)	304.54	(1699)
	22	205.61	(1697)	158.46	(1691)	129.09	(1684)	88.95	(1668)	52.78	(1644)	27.10	(1592)
	24	61.96	(1633)	44.50	(1607)	28.48	(1563)	13.20	(1528)	5.58	(1412)	2.07	(1233)
	25	33.19	(1578)	23.64	(1540)	11.19	(1482)	6.19	(1375)	2.21	(1202)	0.78	(831)
	26	20.87	(1516)	10.53	(1445)	6.24	(1339)	2.50	(1166)	0.96	(845)	0.44	(219)
	28	6.20	(1260)	3.12	(1090)	1.74	(838)	0.89	(471)	0.79	(127)	0.72	(5)
	30	2.46	(858)	1.56	(596)	0.87	(322)	1.27	(103)	1.04	(8)	…	(0)

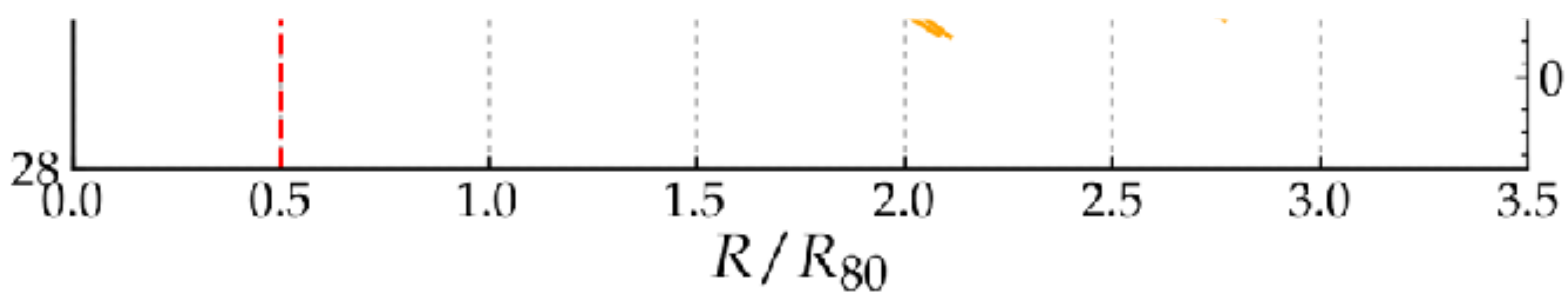

Best cutoff@ $\mu_{[3.6]}$=23.5 mag arcsec^{-2} and R/R80 = 0.5

4.3 Results: Spatially-resolved properties

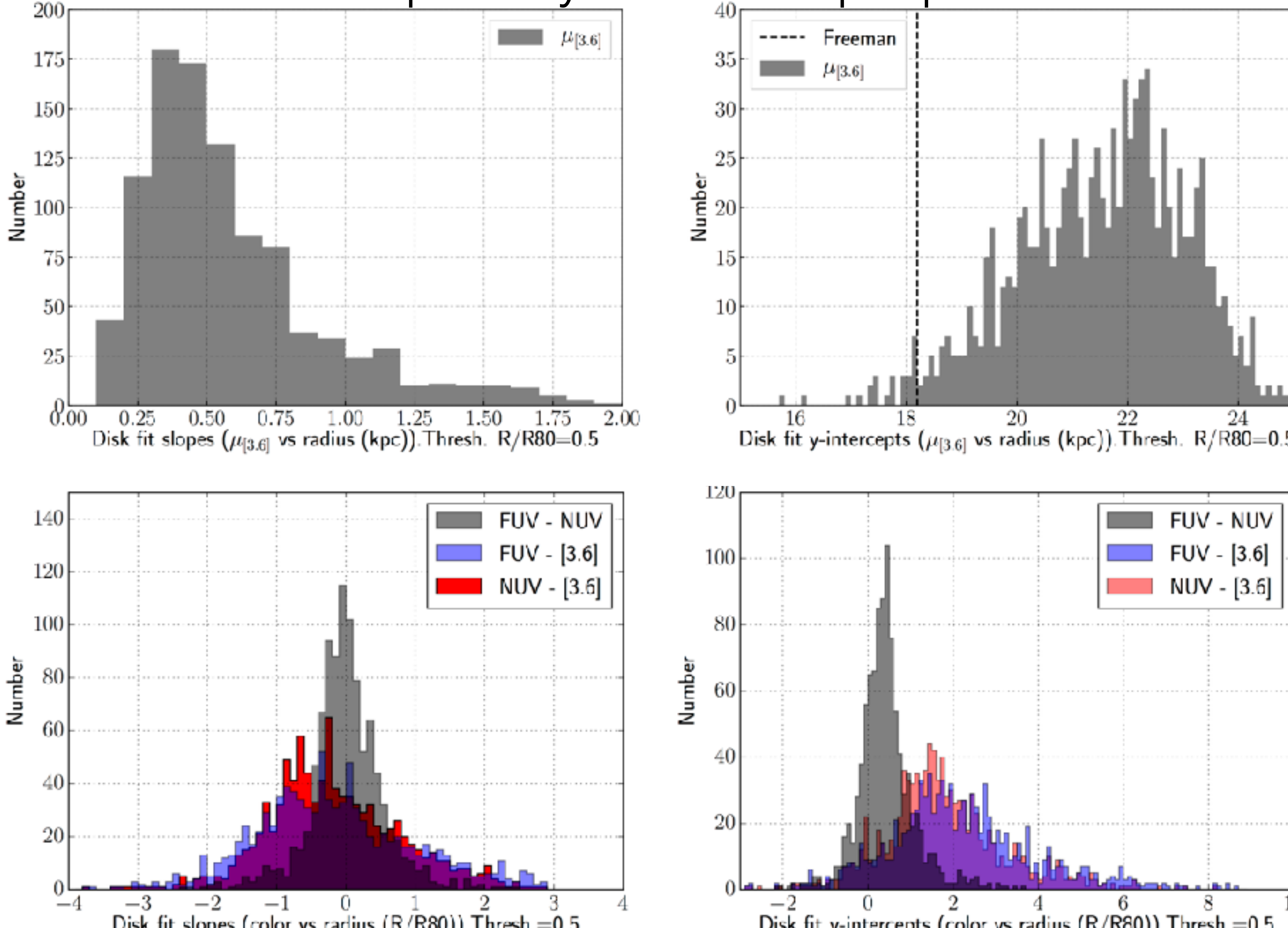

4.3 Results: Spatially-resolved properties

Boissier & Prantzos (2000) disk models.

The SB profiles are generated by varying the circular velocity and spin parameter.

A larger circular velocity translates to a fixed central surface brightness and an increase in the scale length.

$$\frac{v_c}{220} = \left(\frac{M}{M_{\rm MW}}\right)^{1/3}$$

A larger spin parameter translates to a decrease in central surface brightness and an increase in the scale length.

The dimensionless spin parameter λ is defined as:

$$\lambda = J|E|^{1/2}G^{-1}M^{-5/2}$$

where J is the angular momentum,
E is the energy of the halo,
G is the gravitational constant
M is the total baryonic mass

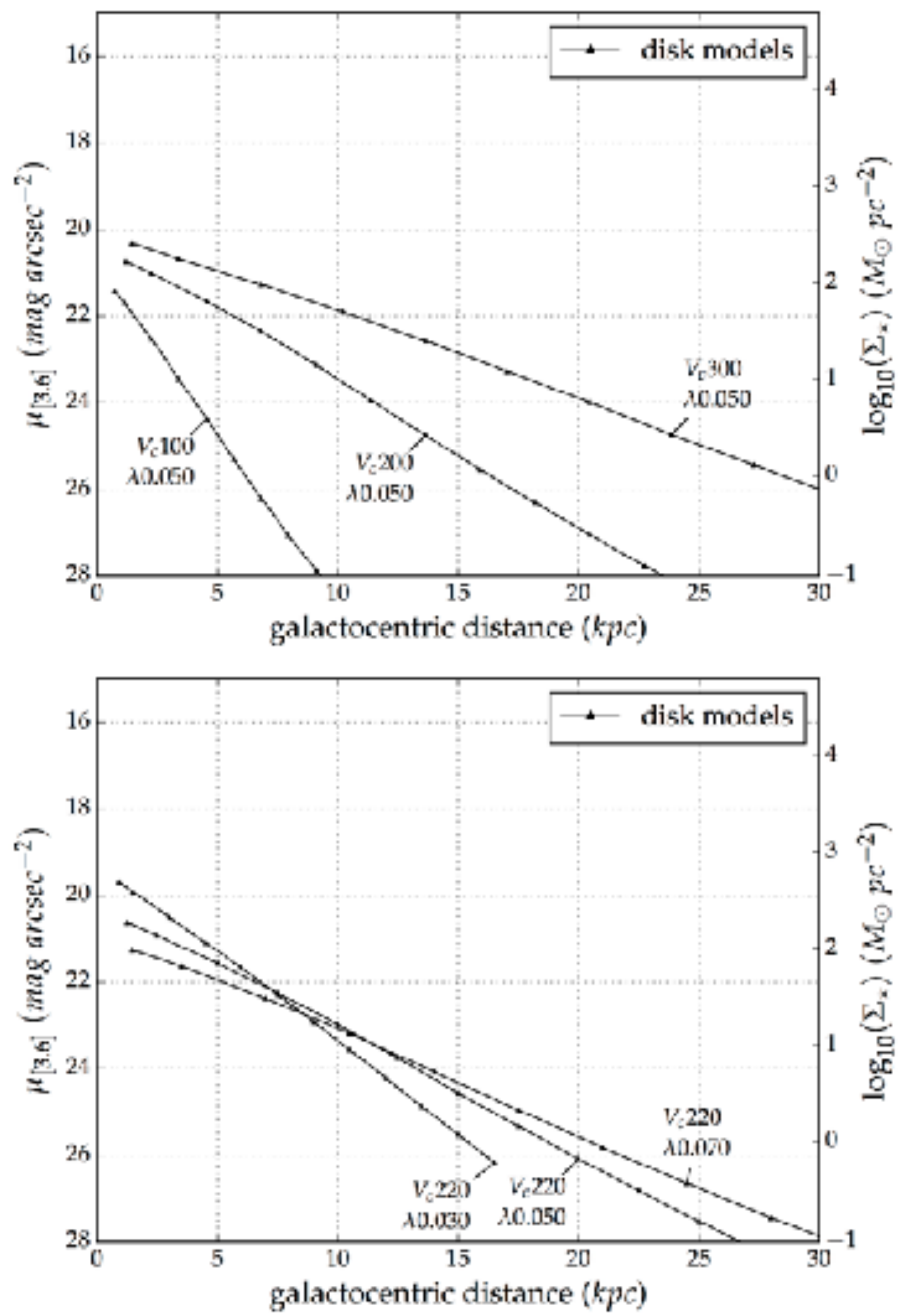

We also fit these disk models and obtain a single pair (slope, y-intercept) for each of them

4.3 Results: Spatially-resolved properties

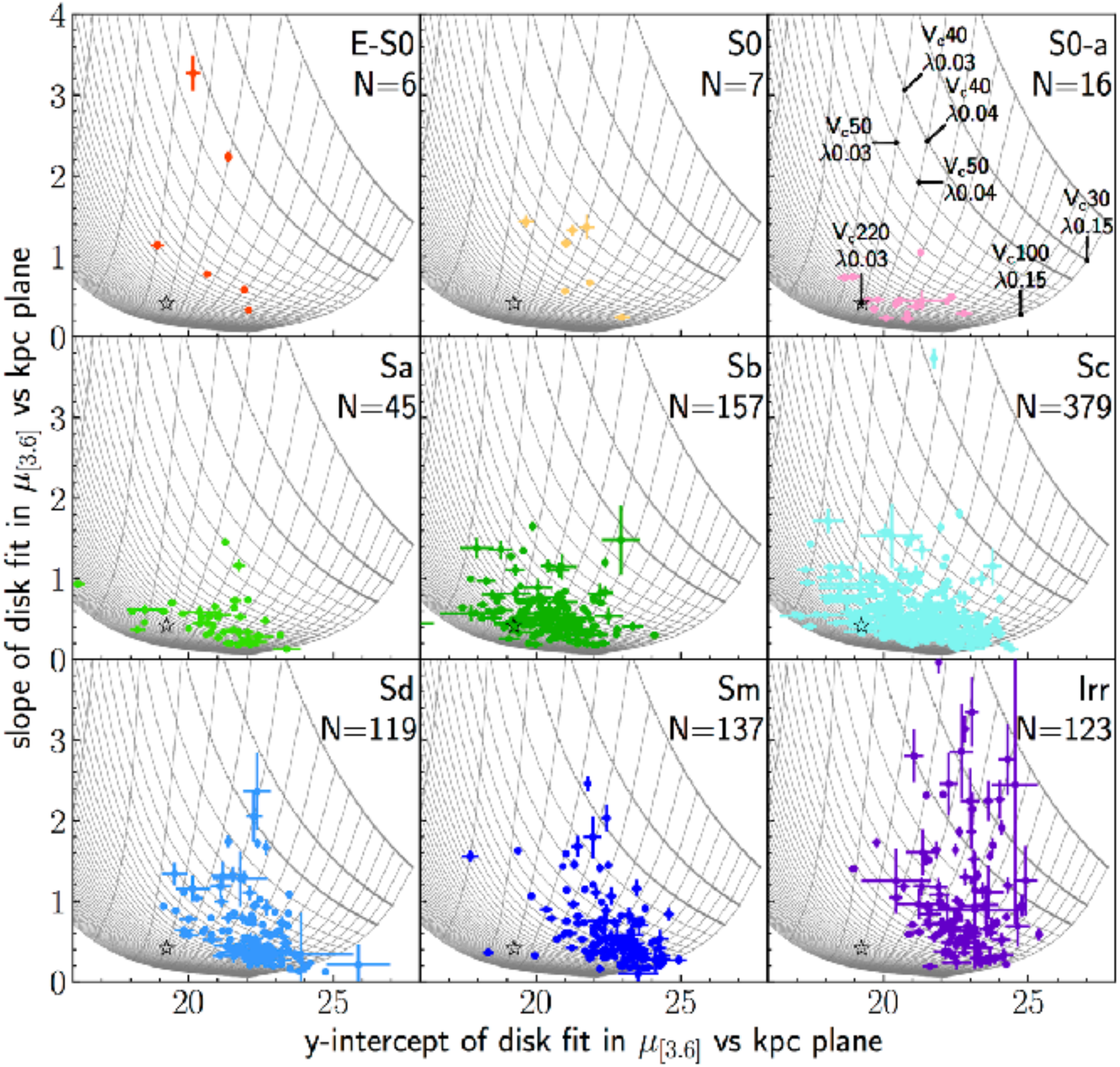

slope vs. y-intercept
per morphological type

grid = **Boissier & Prantzos (2000)** disk models
6258 models created specifically for this project.

value ranges:
$20 \leq v_{circ} \leq 430$ km s^{-1}
(10 km s^{-1} steps)
$0.002 \leq \lambda \leq 0.15$
(0.001 steps)

4.3 Results: Spatially-resolved properties

MC sampling
of 1000 particles (with elliptical 2D Gaussian distribution) and matching with closest disk model's circular velocity and spin parameter.

We then measure the mean (red), median (blue) and mode (purple) of these distributions.

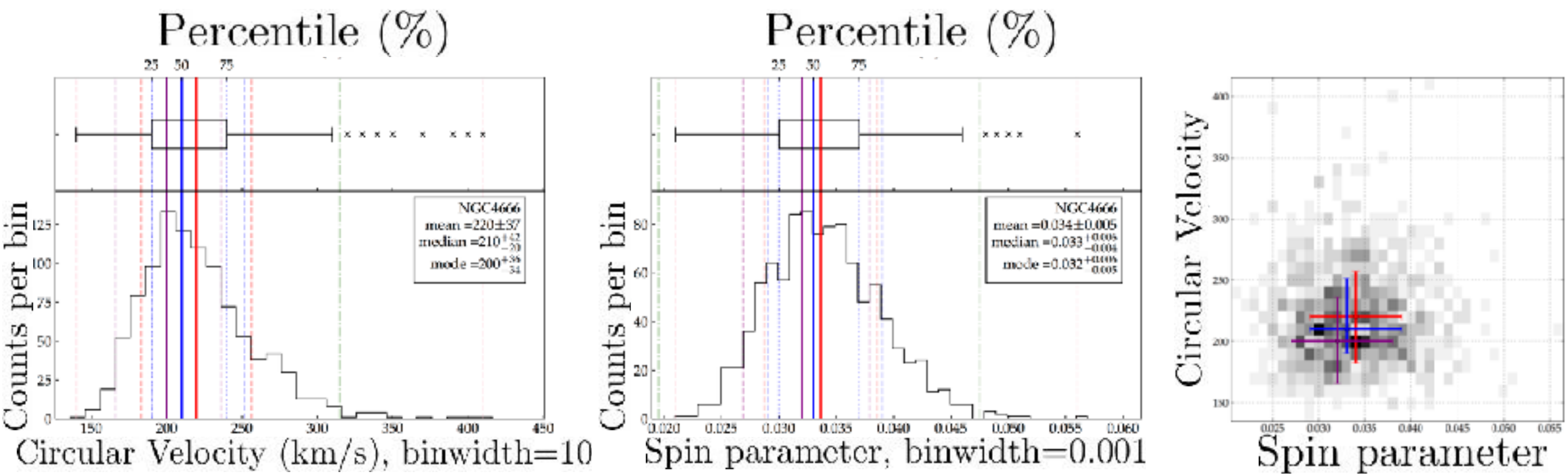

4.3 Results: Spatially-resolved properties

MC sampling
of 1000 particles (with elliptical 2D Gaussian distribution) and matching with closest disk model’s circular velocity and spin parameter.

We then measure the mean (red), median (blue) and mode (purple) of these distributions.

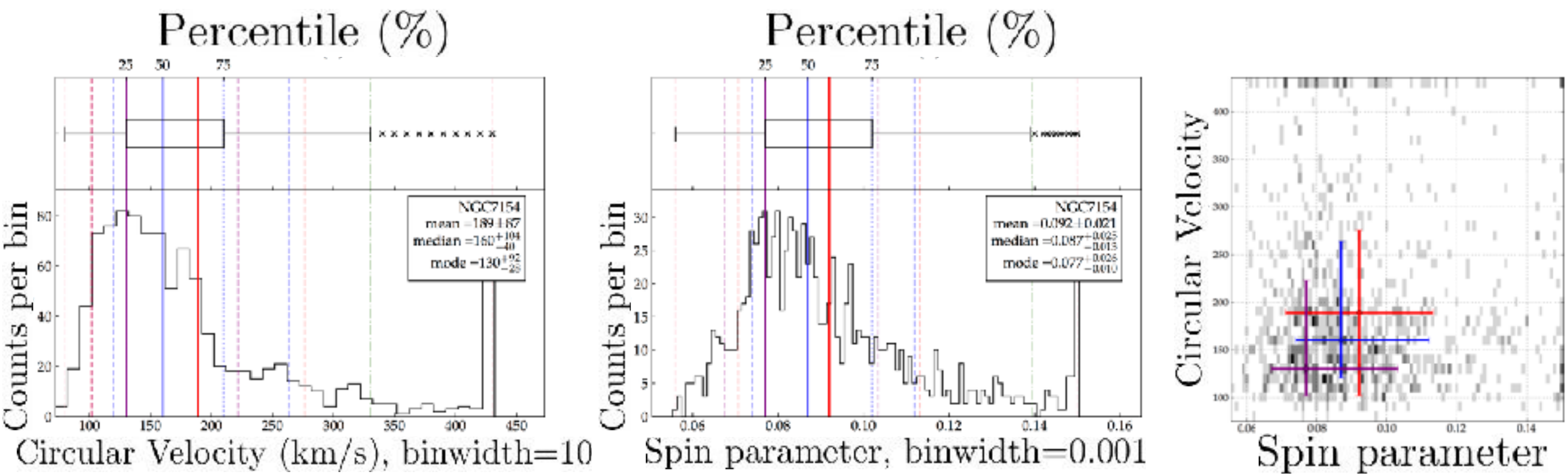

4.3 Results: Spatially-resolved properties

MC sampling
of 1000 particles (with elliptical 2D Gaussian distribution) and matching with closest disk model's circular velocity and spin parameter.

We then measure the mean (red), median (blue) and mode (purple) of these distributions.

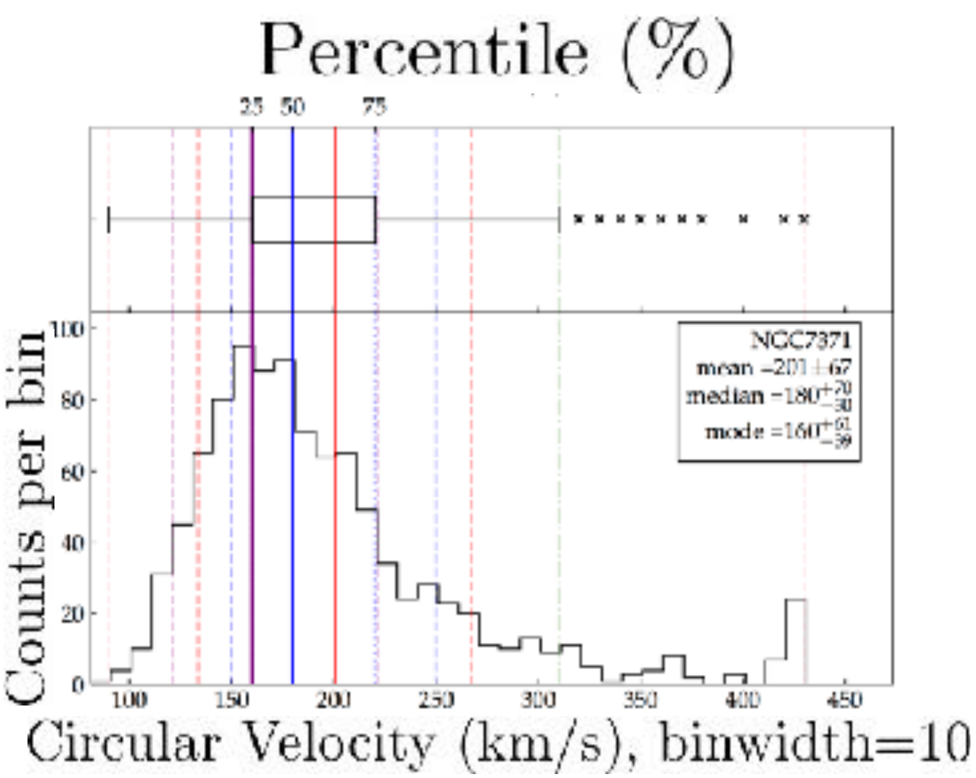

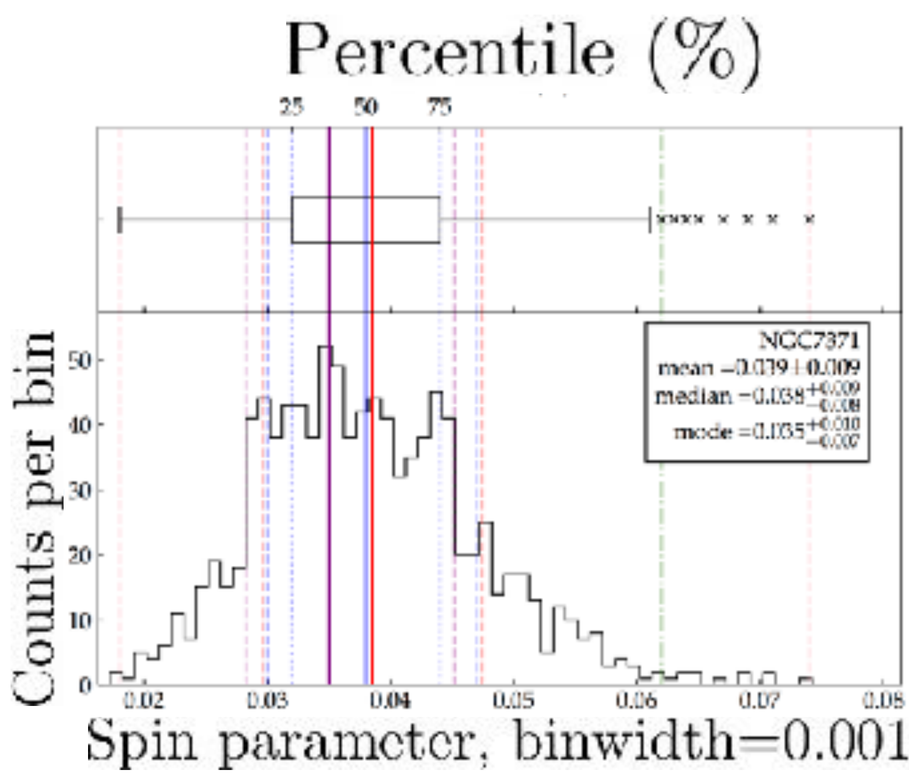

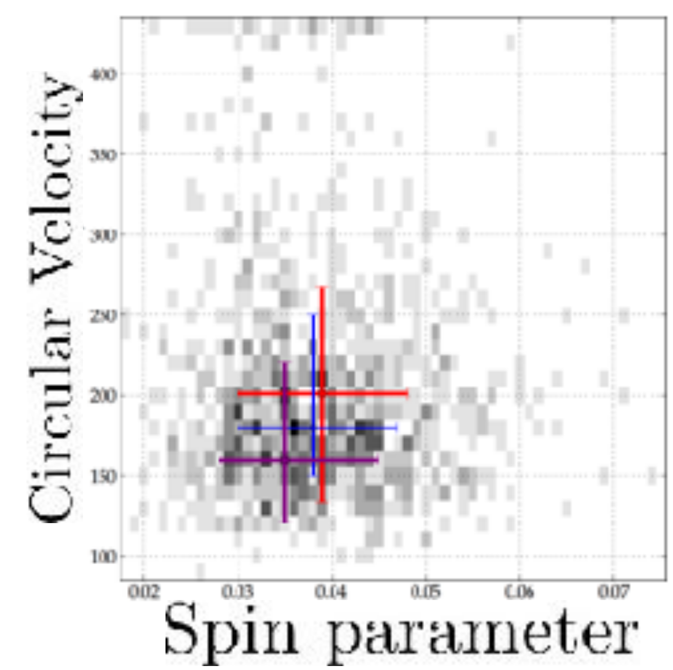

4.3 Results: Spatially-resolved properties

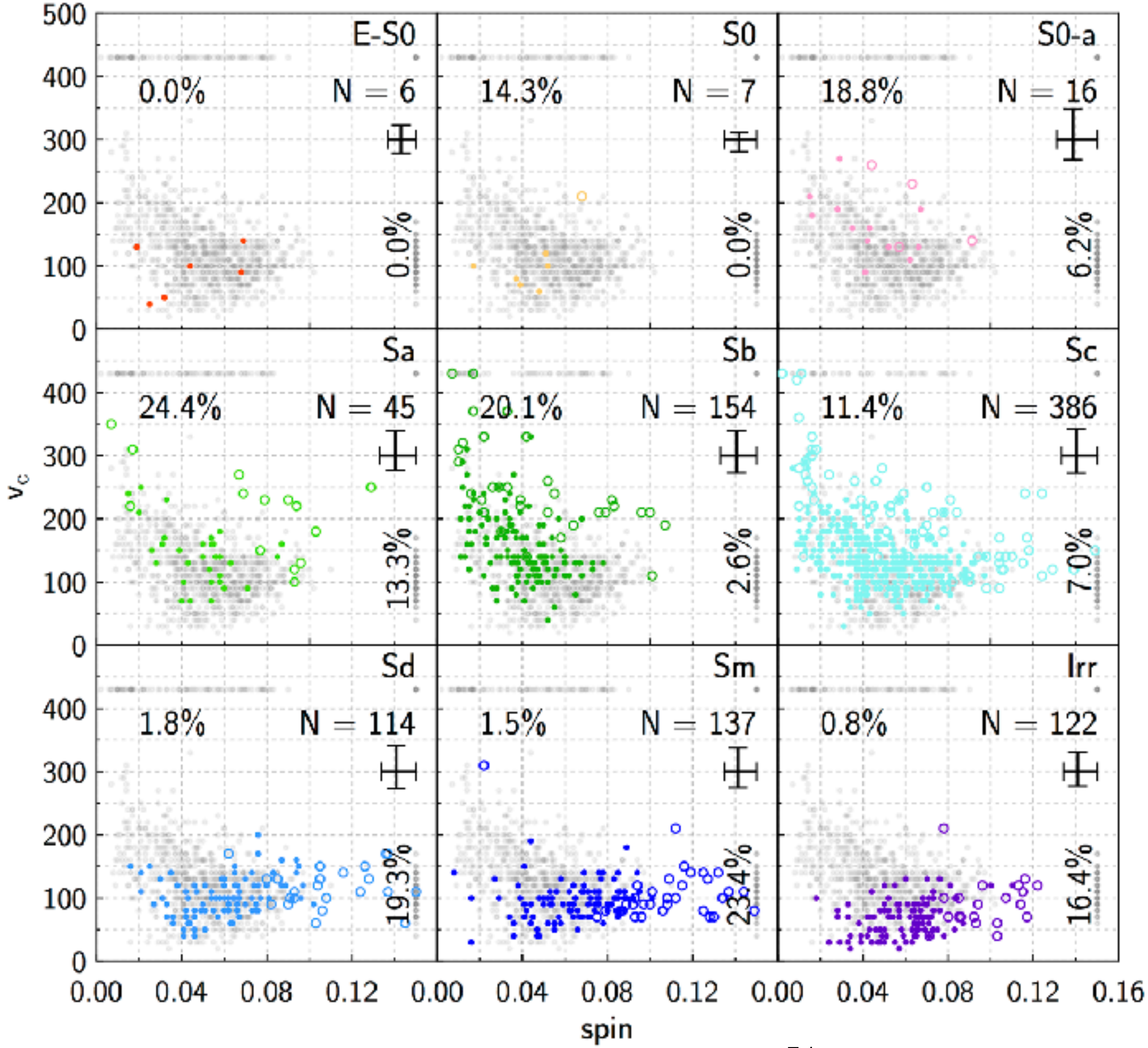

circular velocity v_c
vs.
spin parameter λ
per morphological type

● = mode values.

○ = extreme values in either v_c or λ; using central values instead.

low-mass galaxies clearly have low circular velocities

4.3 Results: Spatially-resolved properties

Comparisons with observations:
the median yields larger scatter than when using the mode due to the skewness of the circular velocity distribution. The mode however yields a good estimate (within factor of 2) of the circular velocity.

From the simple linear fitting of the 3.6 μm SB profile of a galaxy, we are able to obtain its circular velocity.

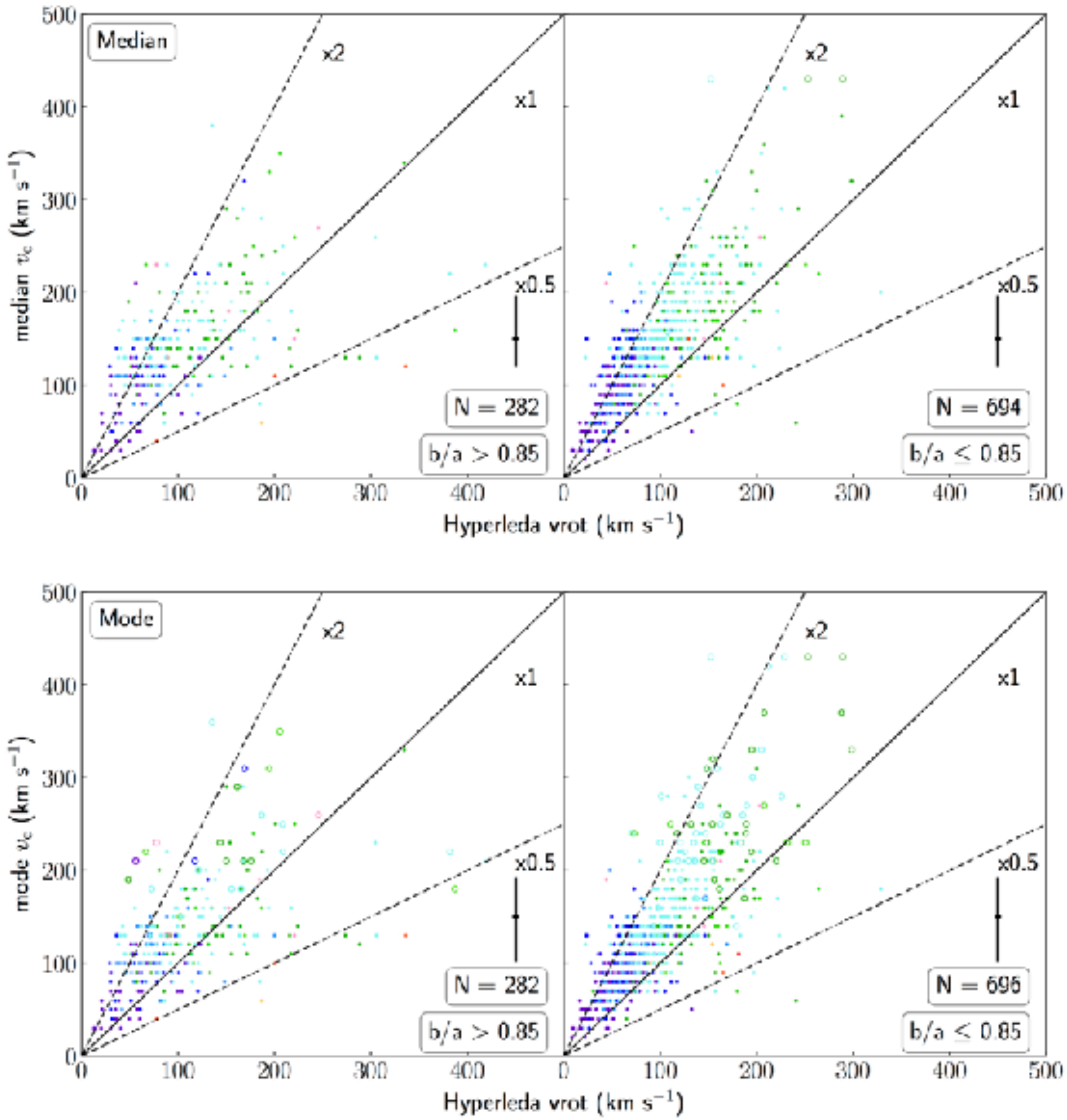

4.3 Results: Spatially-resolved properties

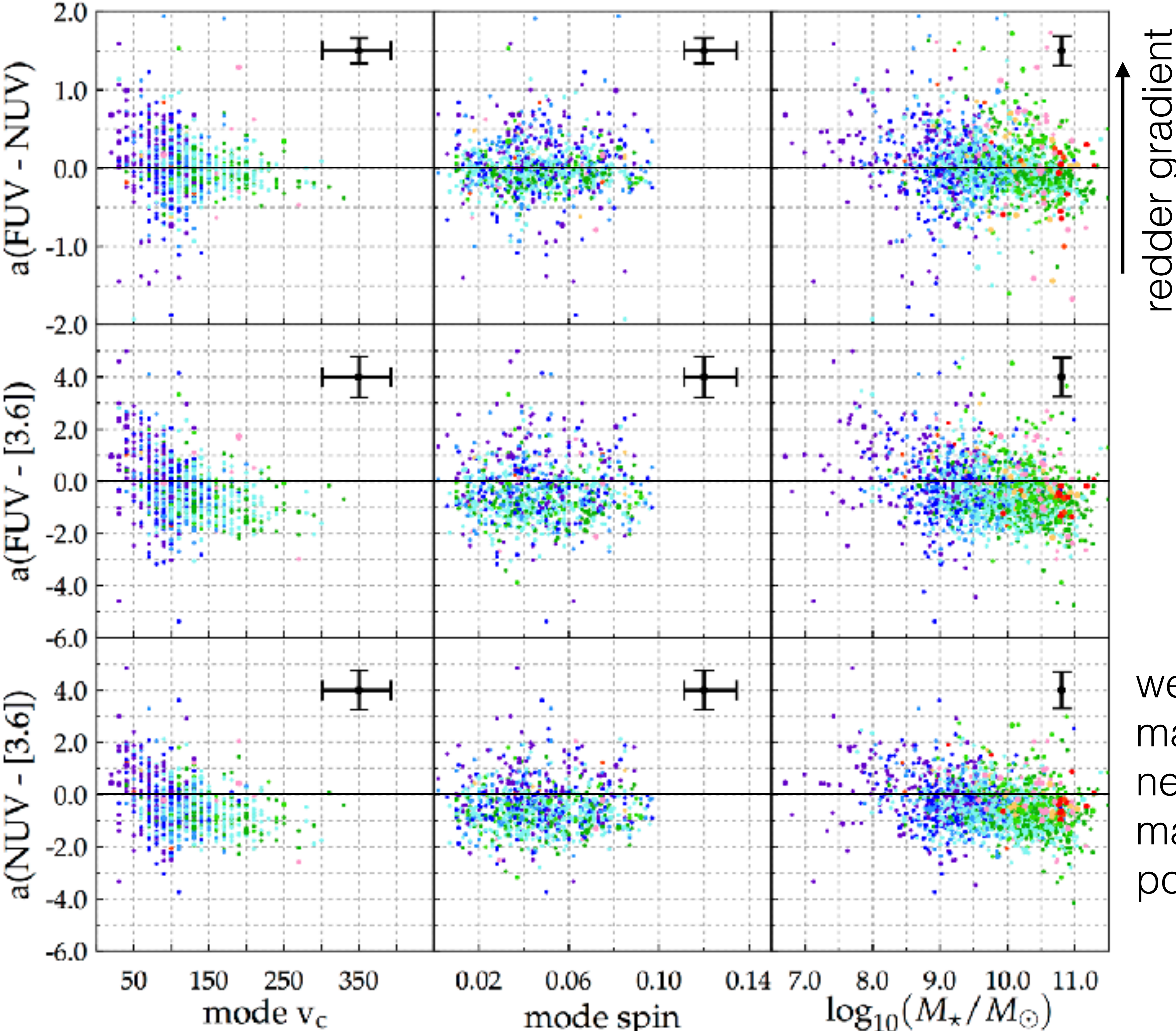

Color gradients (slopes) vs.

- circular velocity v_C (mode)
- spin λ (mode)
- stellar mass (log)

we see that most low-mass galaxies and a non-negligible fraction of massive galaxies show positive gradients.

4.3 Results: Spatially-resolved properties

Conclusions:

- We see **disk-reddening occurring in both GRS and GGV galaxies**, with GGV galaxies slightly bluer than the GRS, but definitively redder than GBS.
- Galaxies are well-separated in the μ_{FUV} vs. $\mu_{[3.6]}$ (spatially-resolved "star-forming main sequence")
- Galaxies are well-separated in the spatially-resolved (FUV - [3.6]) vs. $\mu_{[3.6]}$. This diagram seems to indicate **a clear cut at 10^{-12} yr^{-1} in sSFR**. Moreover, GGV and GRS galaxies remain with a constant radial values sSFR below 10^{-12}, beyond $\mu_{[3.6]}$=20.89 mag arcsec^{-2}.
- From the slopes and y-intercepts of the outerdisk linear fits and comparing them to the disk models of **Boissier & Prantzos (2000) we are able to obtain circular velocity and spin parameters within a factor of 2** to the truly-measured ones. This could be a powerful technique for much larger surveys.

4.4 Results: XUV-disk galaxies classification

Discovery: **Gil de Paz et al. 2005**, **Thilker et al. 2005**

Classification: **Thilker et al. 2007**

NGC4625

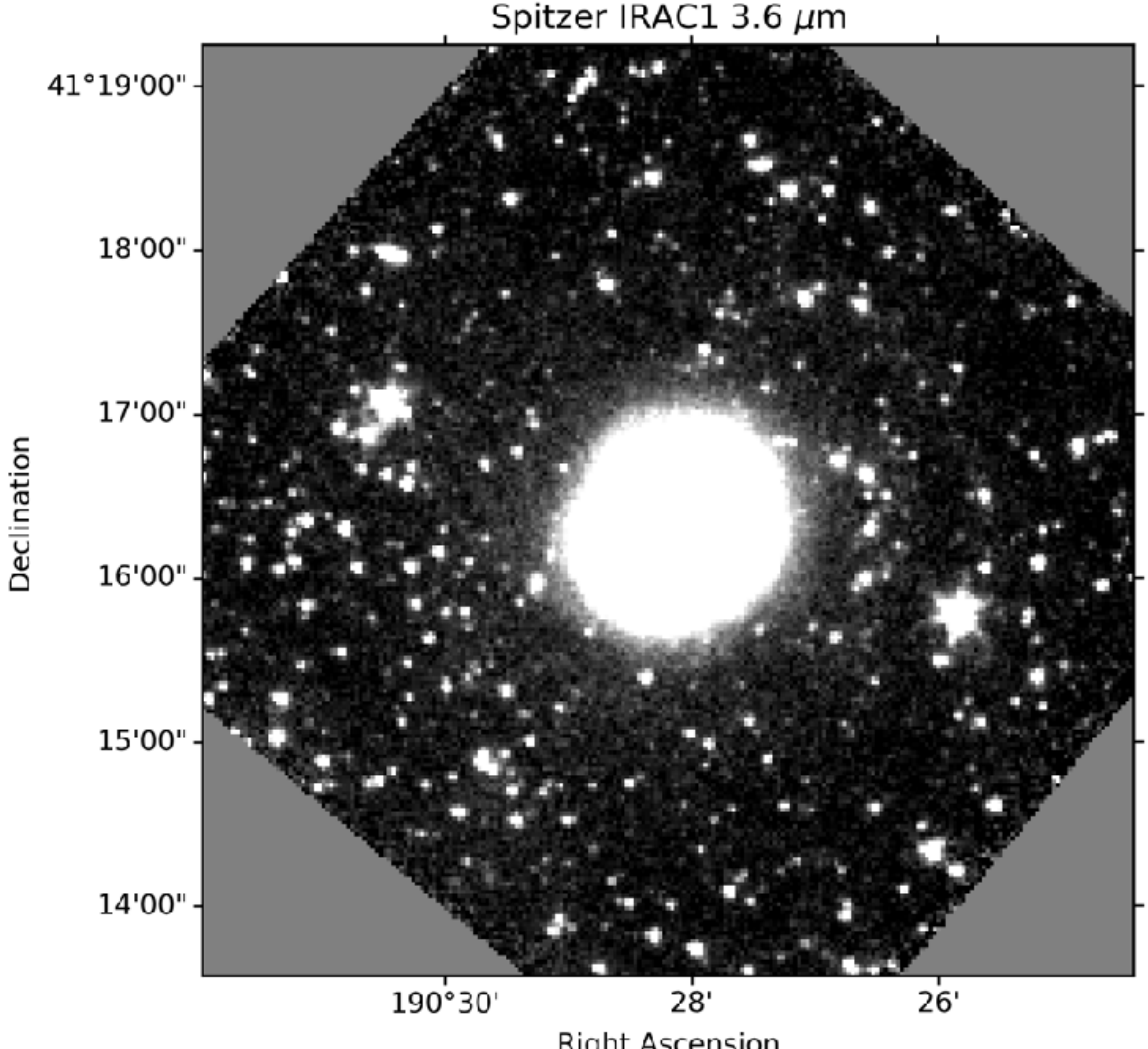
Spitzer IRAC1 3.6 μm
41°19'00"
18'00"
17'00"
16'00"
15'00"
14'00"
Declination
190°30'
28'
26'
Right Ascension

NGC4625

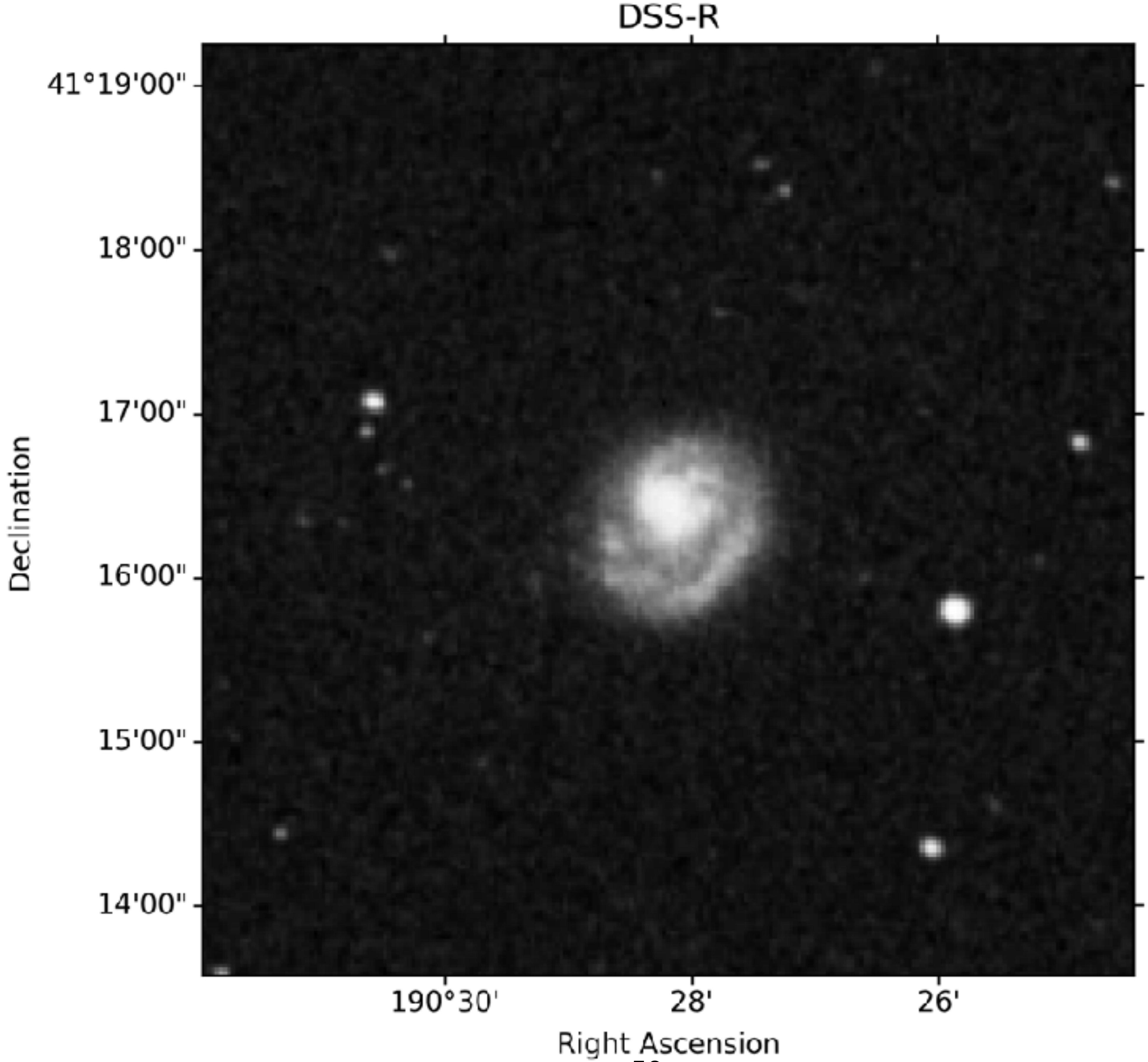
DSS-R
41°19'00"
18'00"
17'00"
16'00"
15'00"
14'00"
Declination
190°30'
28'
26'
Right Ascension

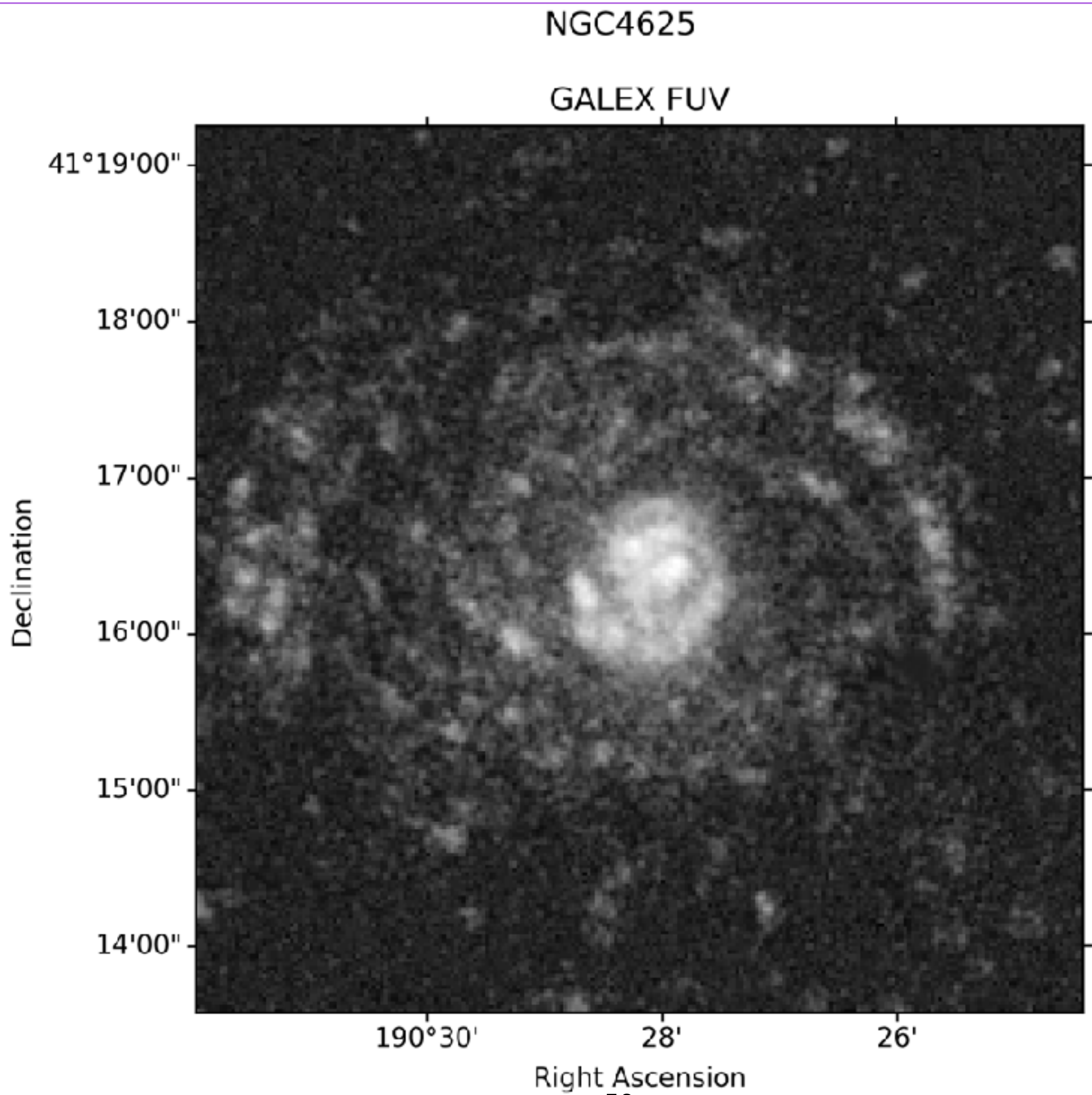
NGC4625
GALEX FUV
41°19'00"
18'00"
17'00"
16'00"
15'00"
14'00"
Declination
190°30'
28'
26'
Right Ascension

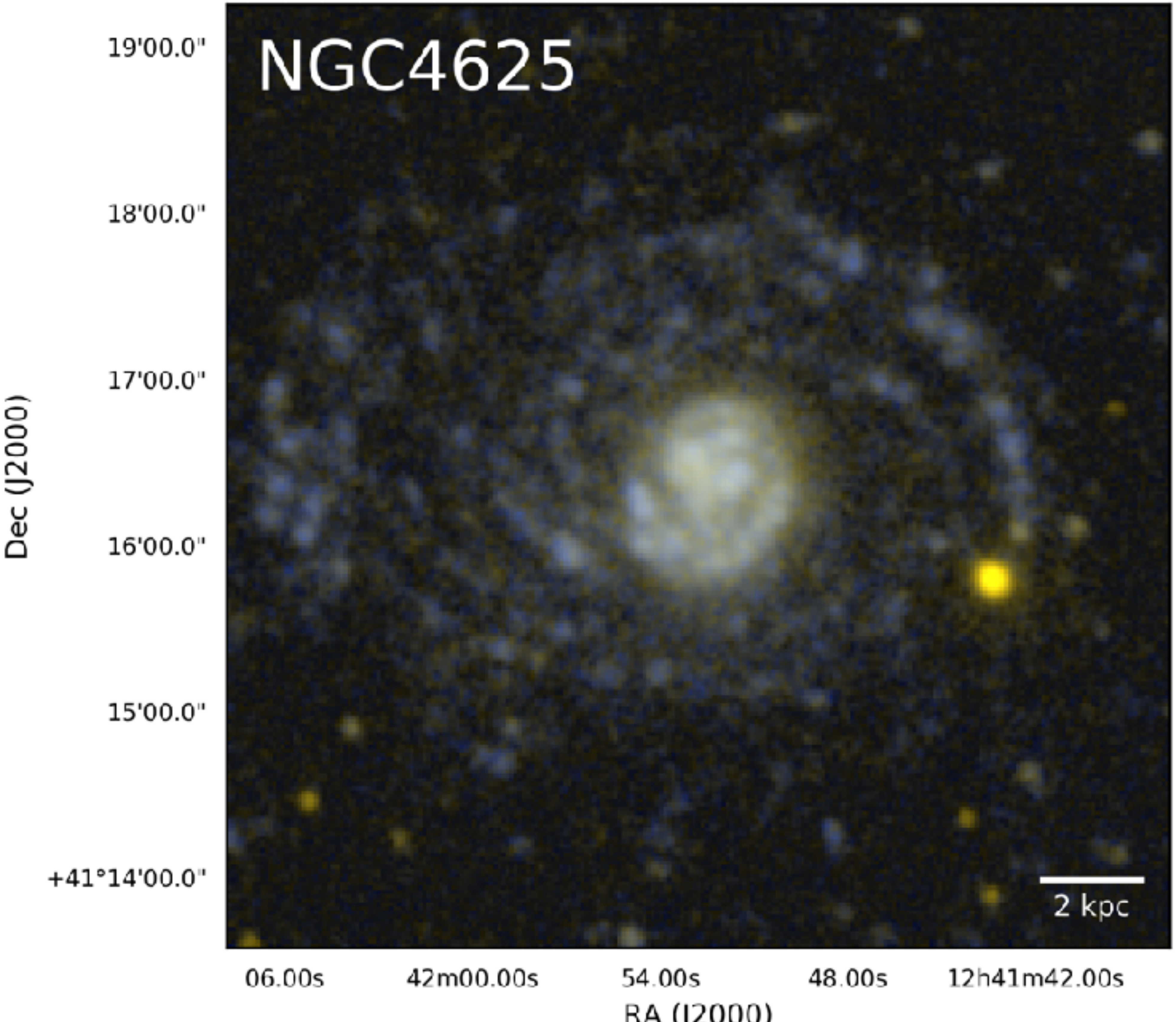
NGC4625
2 kpc
19'00.0"
18'00.0"
17'00.0"
16'00.0"
15'00.0"
+41°14'00.0"
Dec (J2000)
06.00s
42m00.00s
54.00s
48.00s
12h41m42.00s
RA (J2000)

4.4 Results: XUV-disk galaxies classification

Visual classification of **Type 1 (Outer-Structure) XUVs**
Comparison between μ_{FUV}=27.25 AB mag arcsec^{-2} and optical DSS-R band.

Type1 XUV Criteria:
1) structures are seen beyond the μ_{FUV} contour
2) structures are also beyond the D25 ellipse,
3) structures are invisible in the DSS-R image

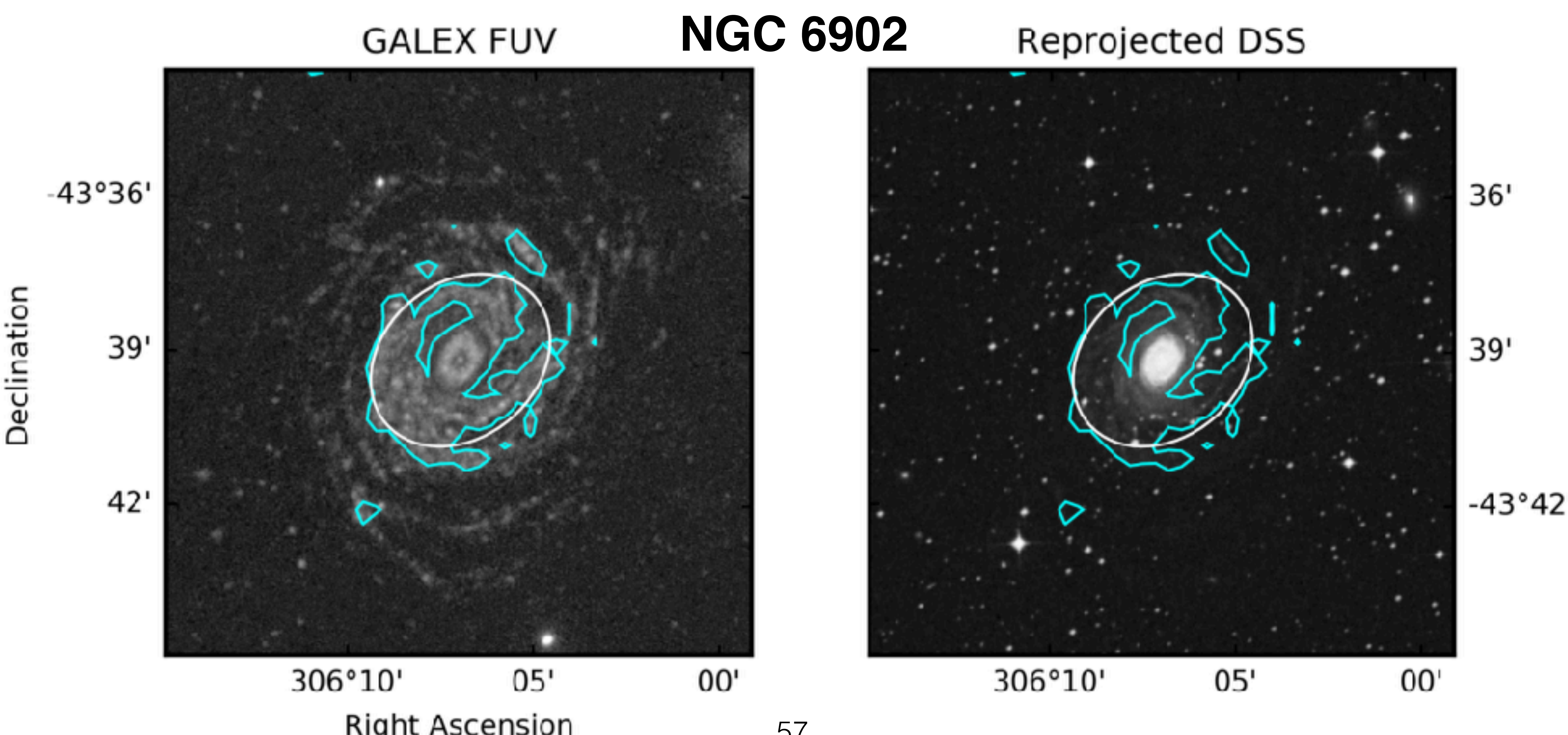

4.4 Results: XUV-disk galaxies classification

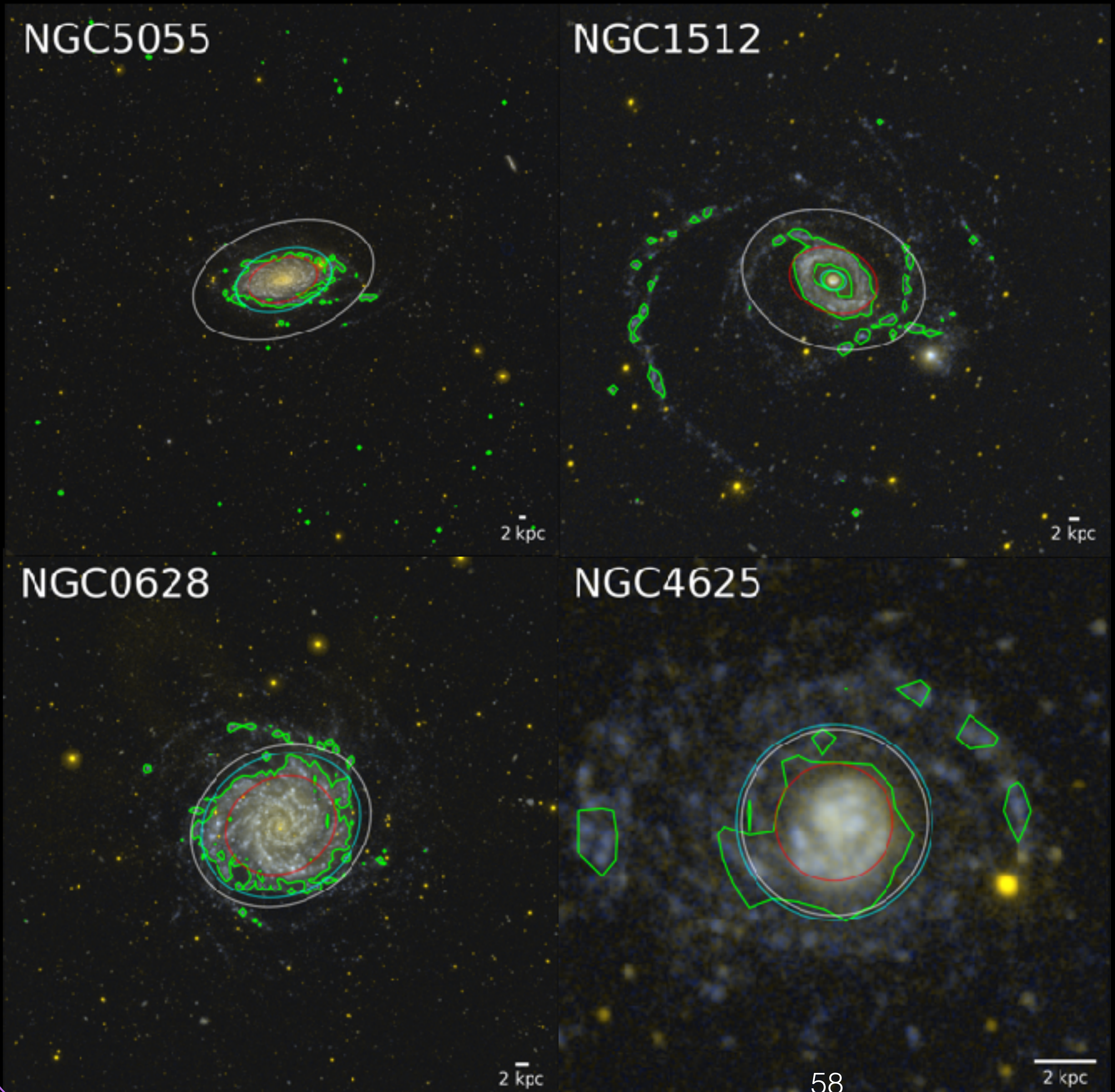

Examples of Type 1 XUV-disk galaxies

TOTAL in the GALEX/S4G sample: 217/1931 (11%)

4.4 Results: XUV-disk galaxies classification

Type 2 (Blue Disk) XUVs matching with 17 “classical” Type 2

e.g.: NGC 2541

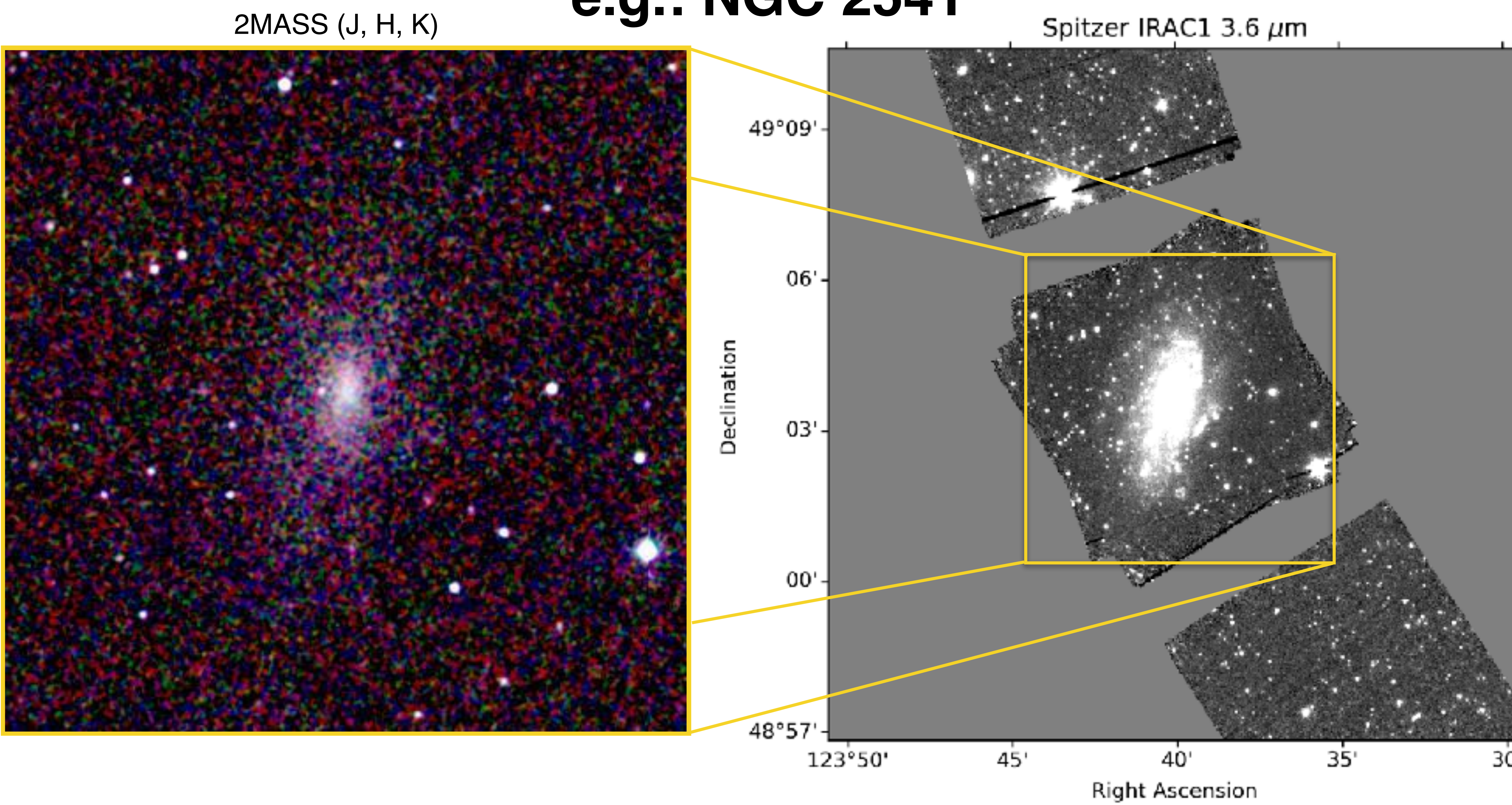

4.4 Results: XUV-disk galaxies classification

Type 2 (Blue Disk) XUVs matching with 17 “classical” Type 2

e.g.: NGC 2541

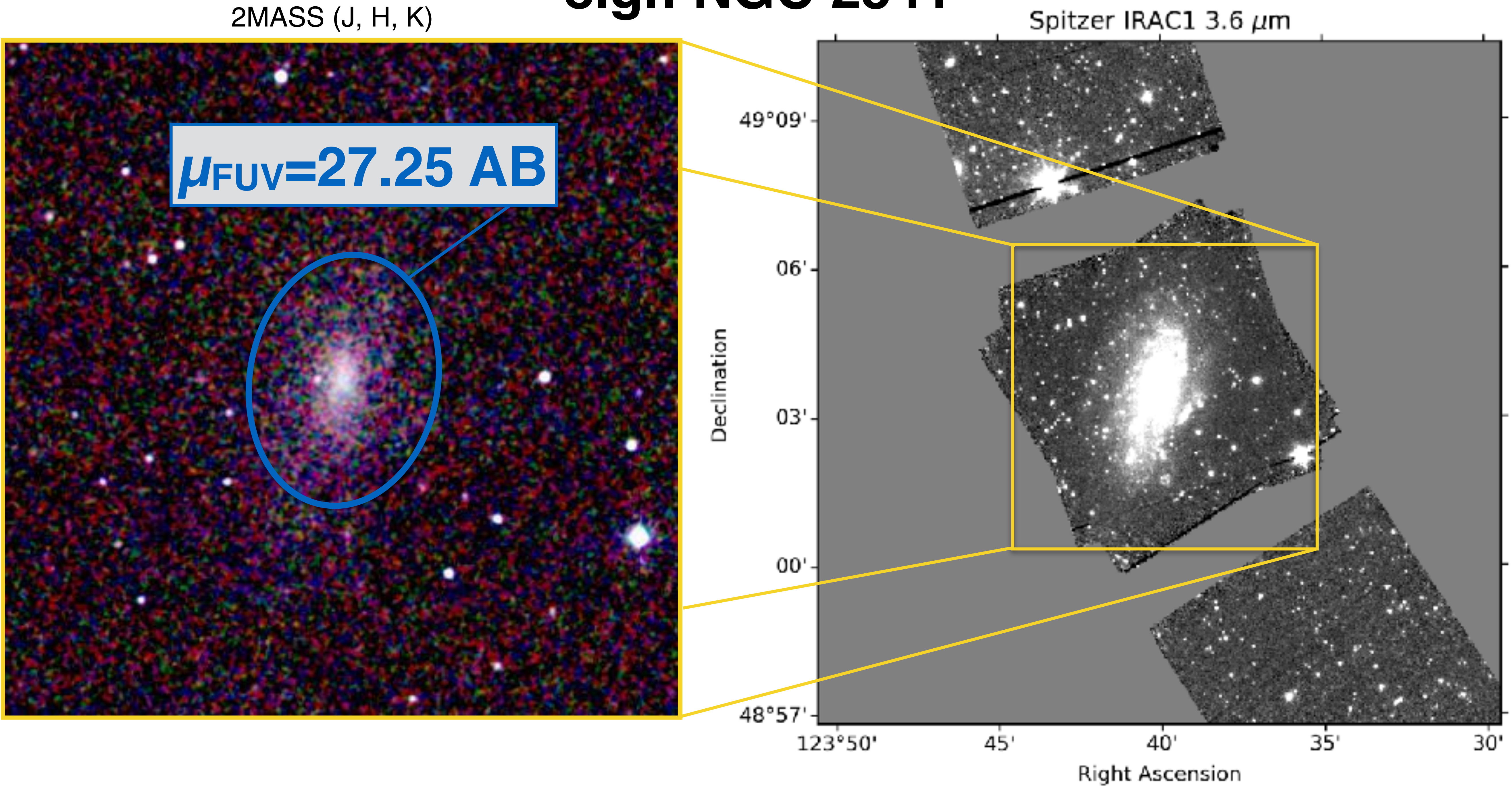

4.4 Results: XUV-disk galaxies classification

Type 2 (Blue Disk) XUVs matching with 17 “classical” Type 2

e.g.: NGC 2541

2MASS (J, H, K)

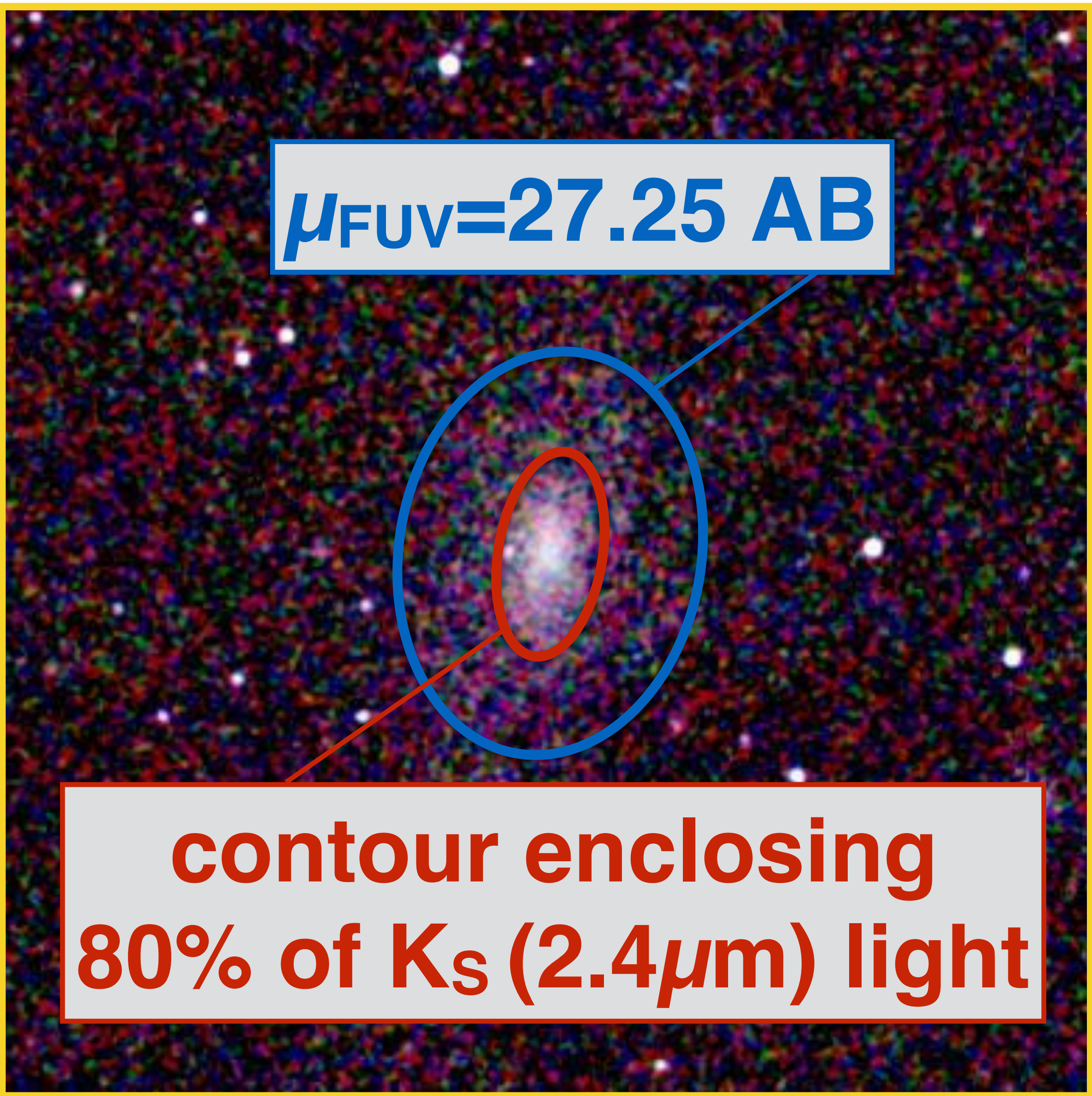

Spitzer IRAC1 3.6 μm

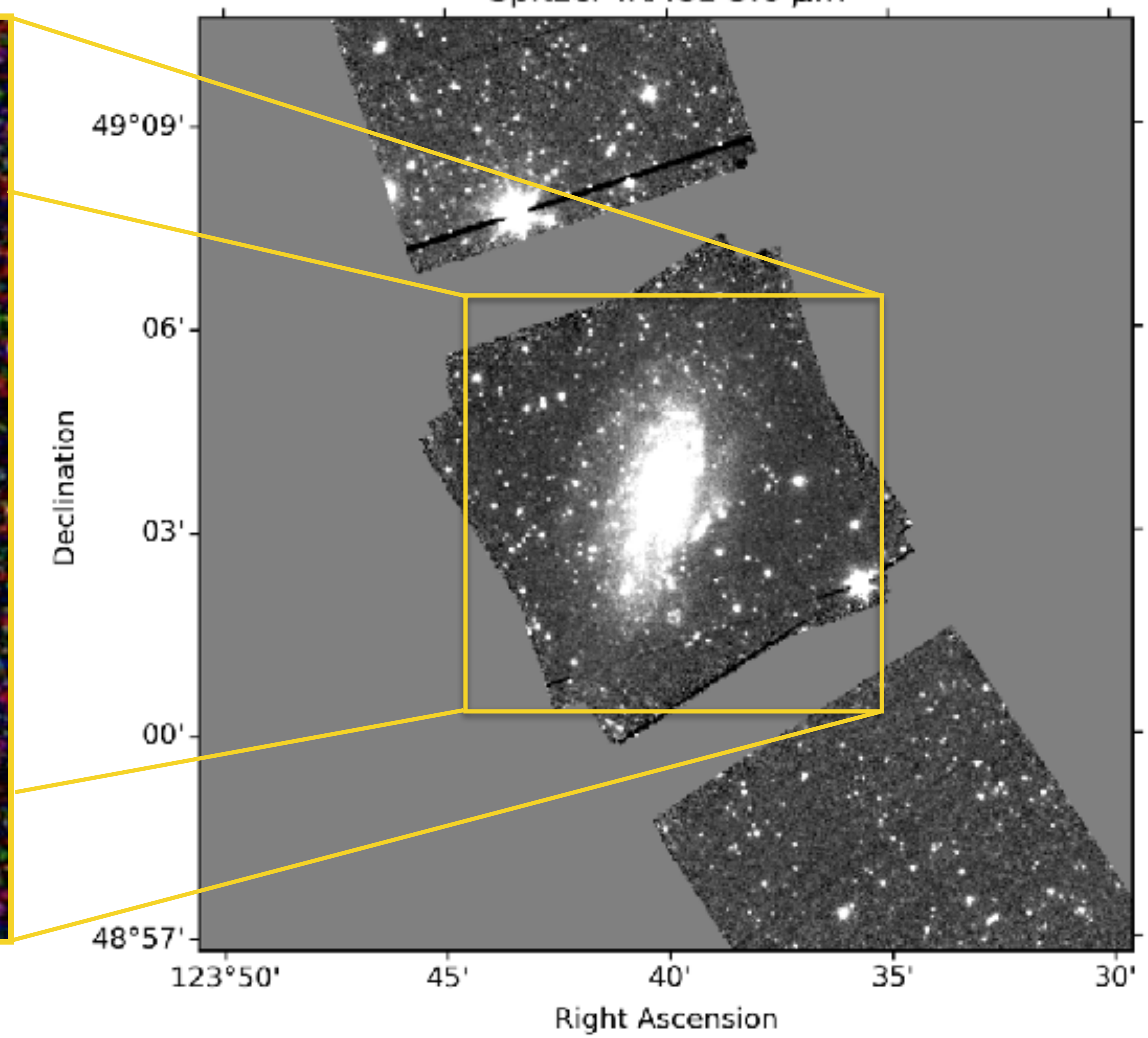

4.4 Results: XUV-disk galaxies classification

Type 2 (Blue Disk) XUVs matching with 17 “classical” Type 2

e.g.: NGC 2541

2MASS (J, H, K)

Spitzer IRAC1 3.6 μm

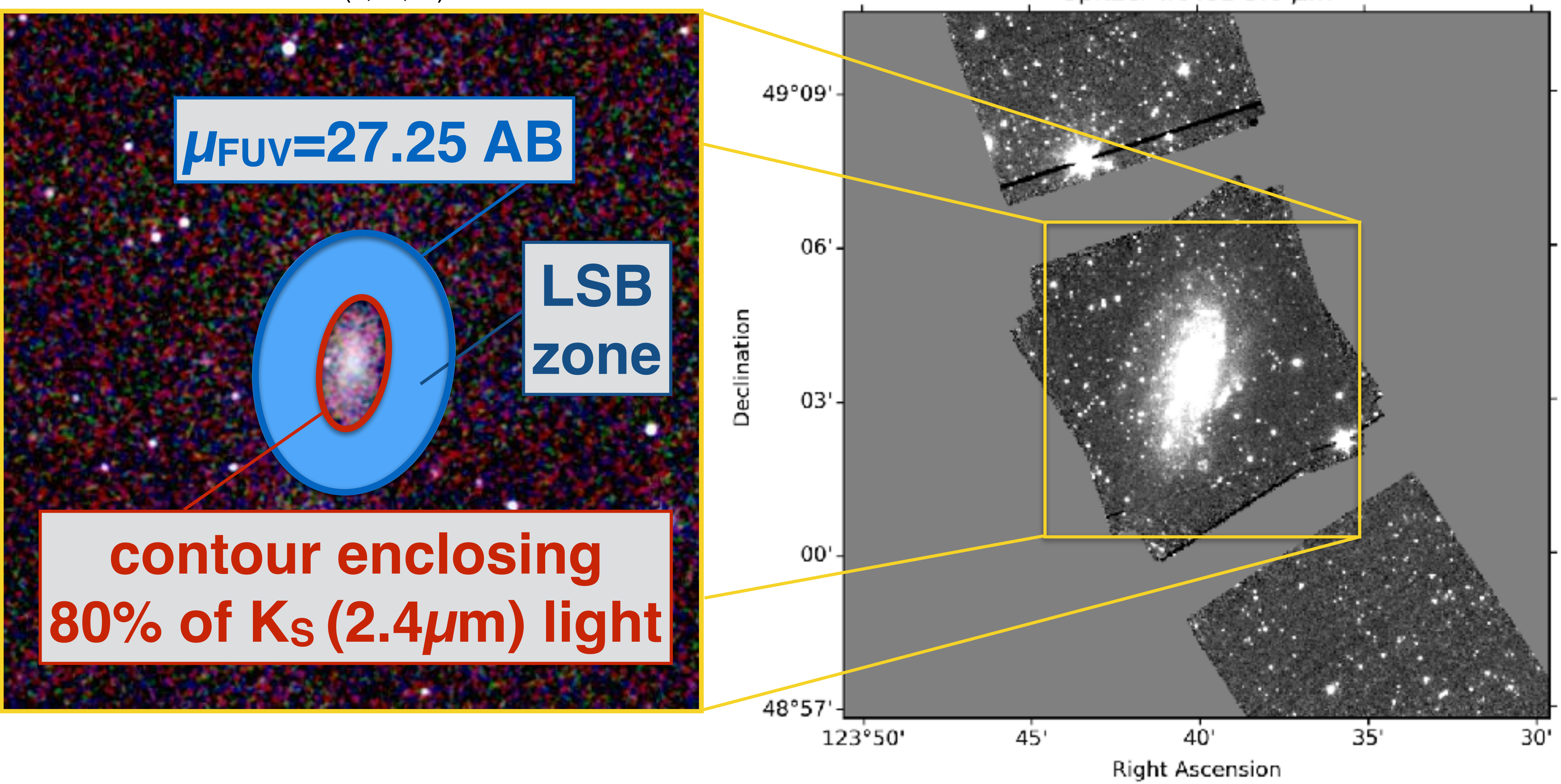

4.4 Results: XUV-disk galaxies classification

Type 2 (Blue Disk) XUVs matching with 17 “classical” Type 2

e.g.: NGC 2541

2MASS (J, H, K)

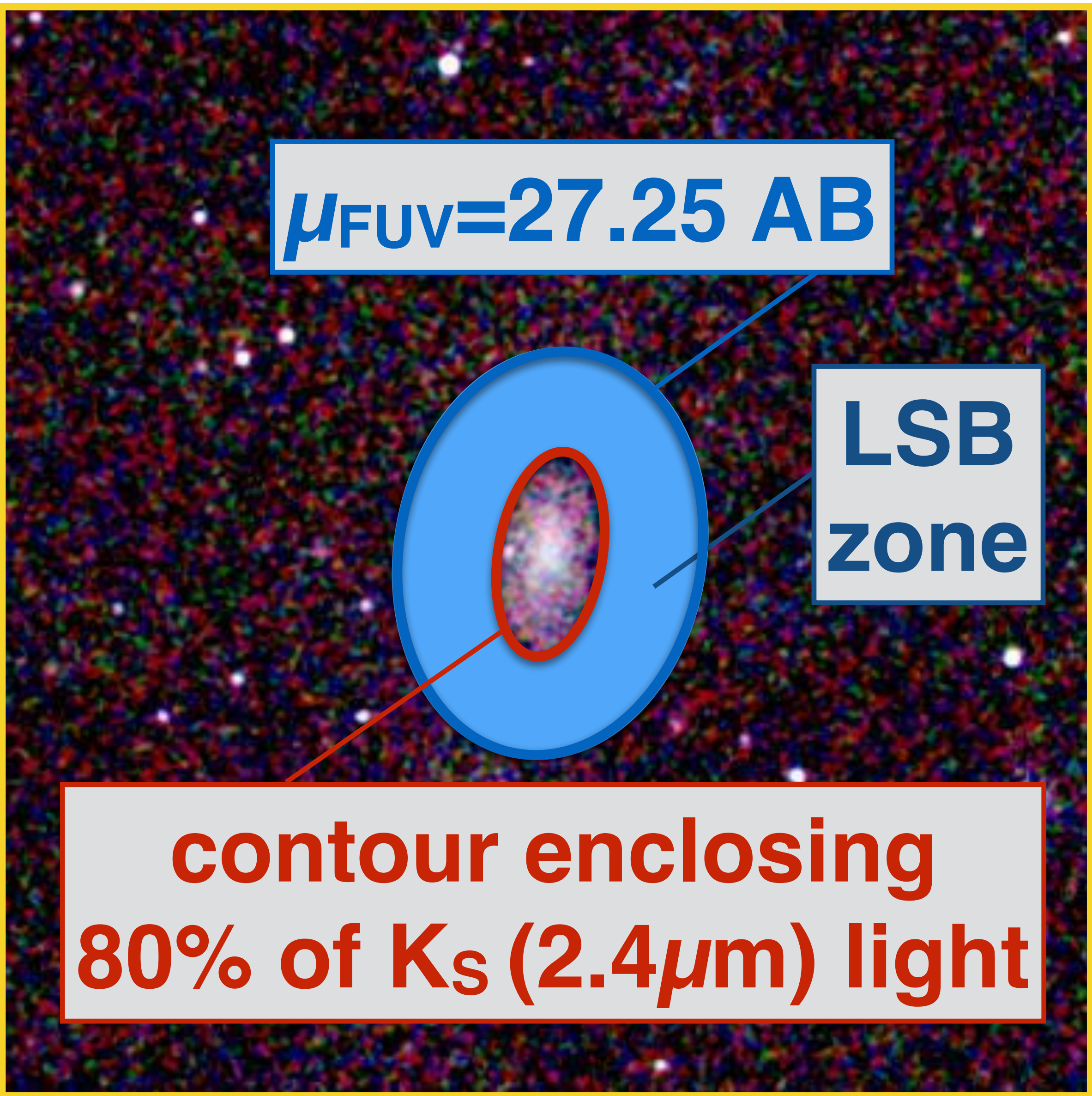

Spitzer IRAC1 3.6 μm

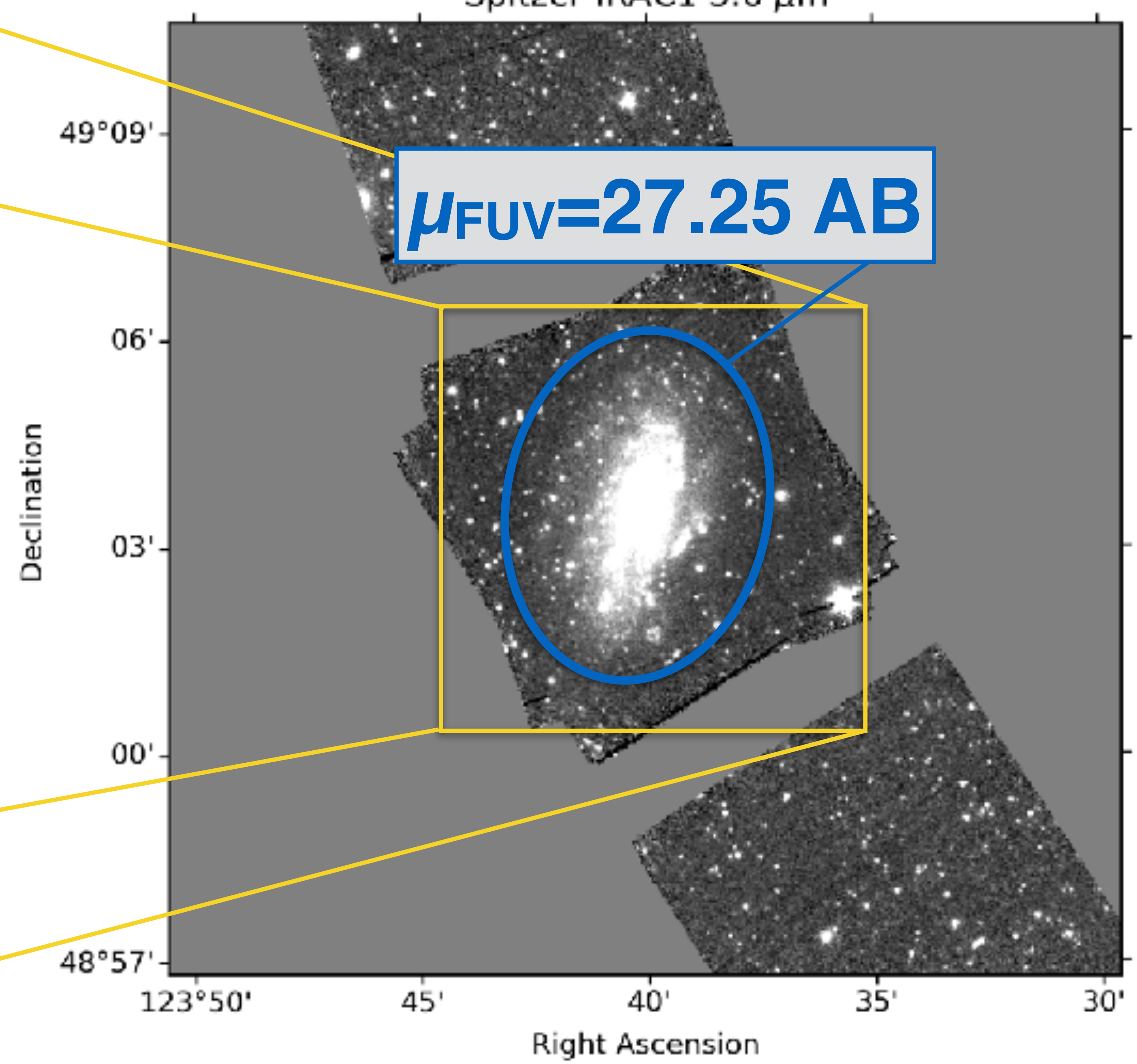

4.4 Results: XUV-disk galaxies classification

Type 2 (Blue Disk) XUVs matching with 17 “classical” Type 2

e.g.: NGC 2541

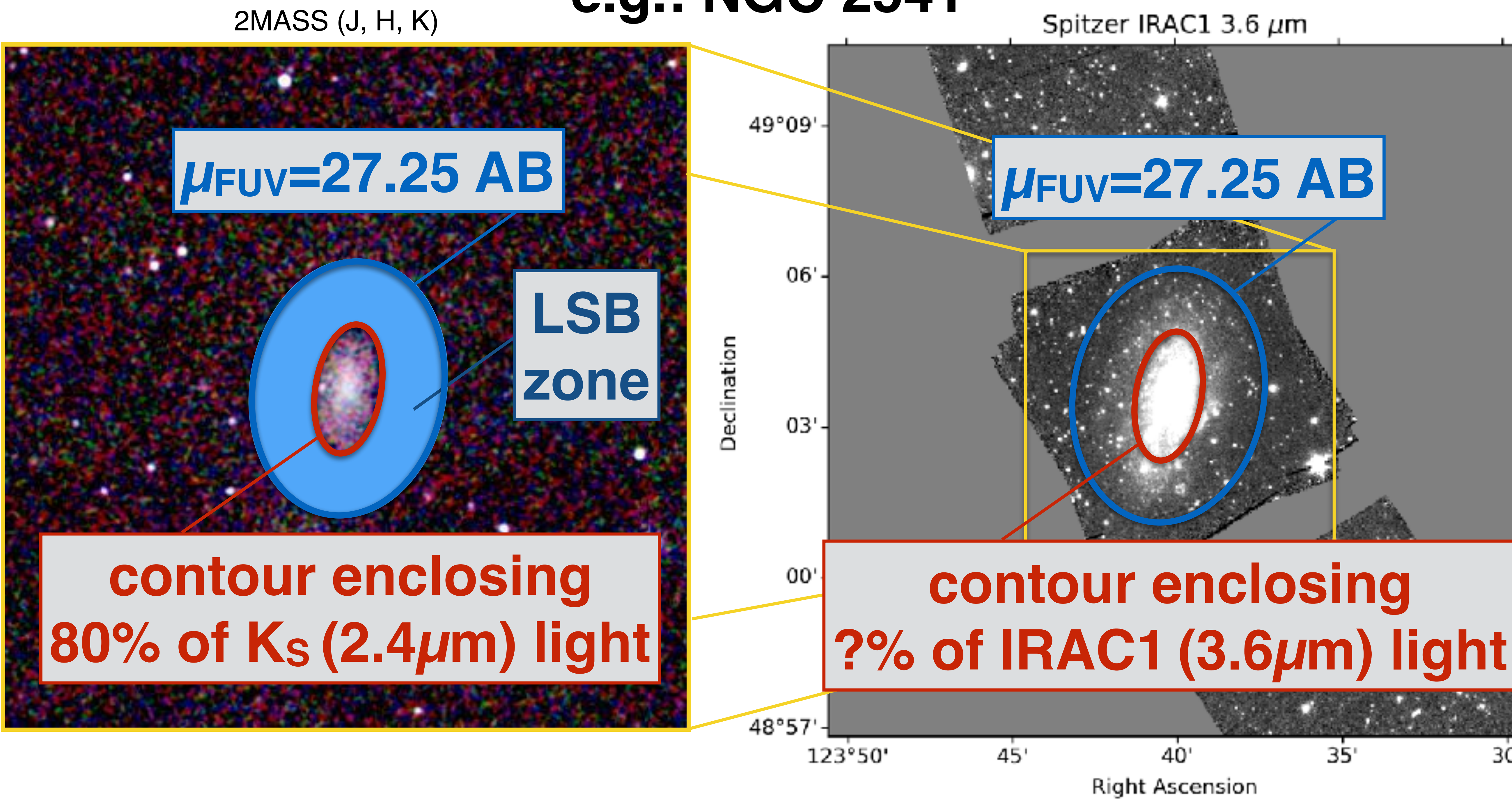

4.4 Results: XUV-disk galaxies classification

Type 2 (Blue Disk) XUVs matching with 17 “classical” Type 2

e.g.: NGC 2541

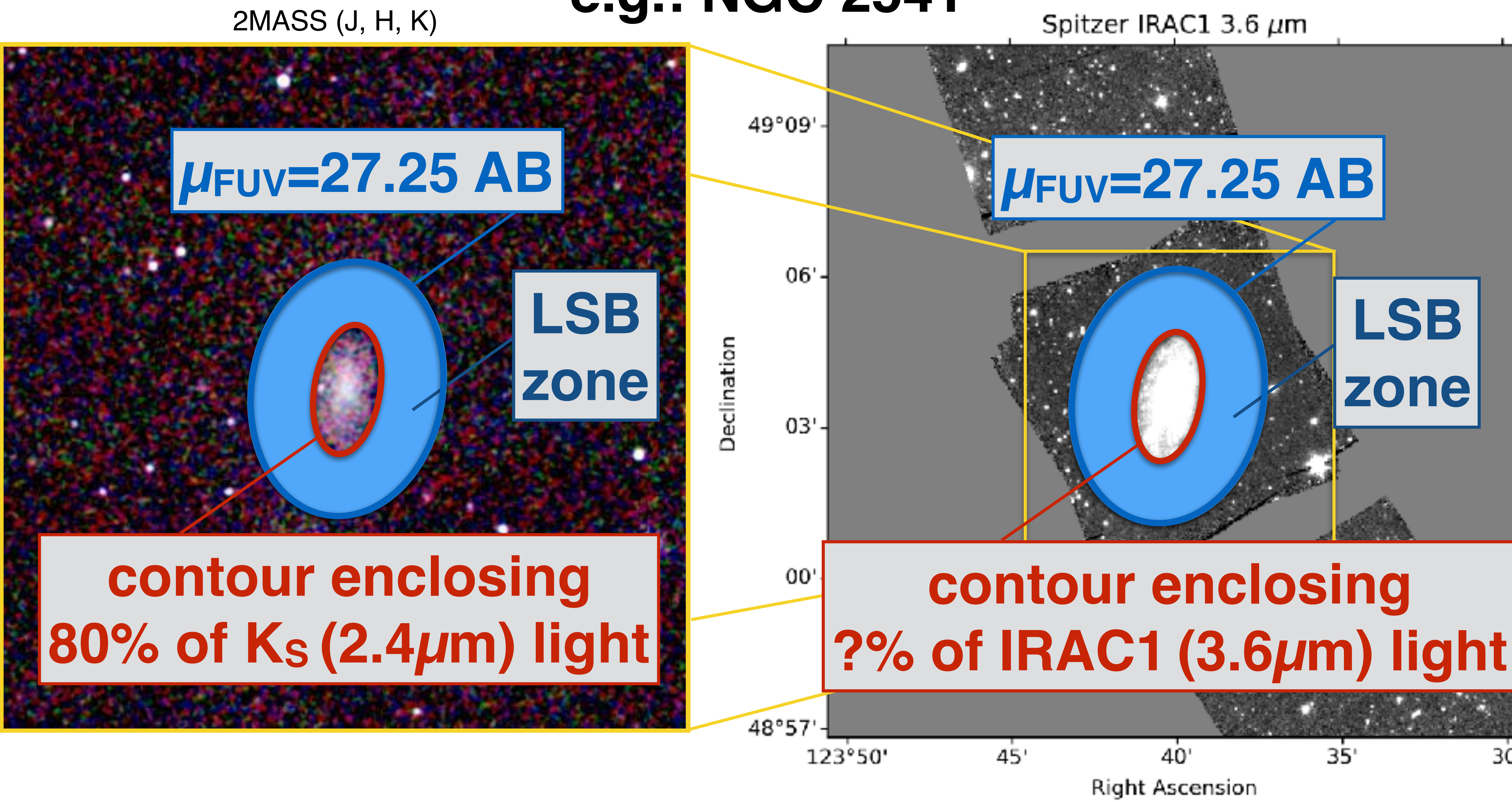

4.4 Results: XUV-disk galaxies classification

We try to match our Type 2 criteria to be used with our 3.6µm images to be able to closely reproduce the selection of the "classical" Type 2 of **Thilker+,2007**, which were defined from 2MASS K_s images.

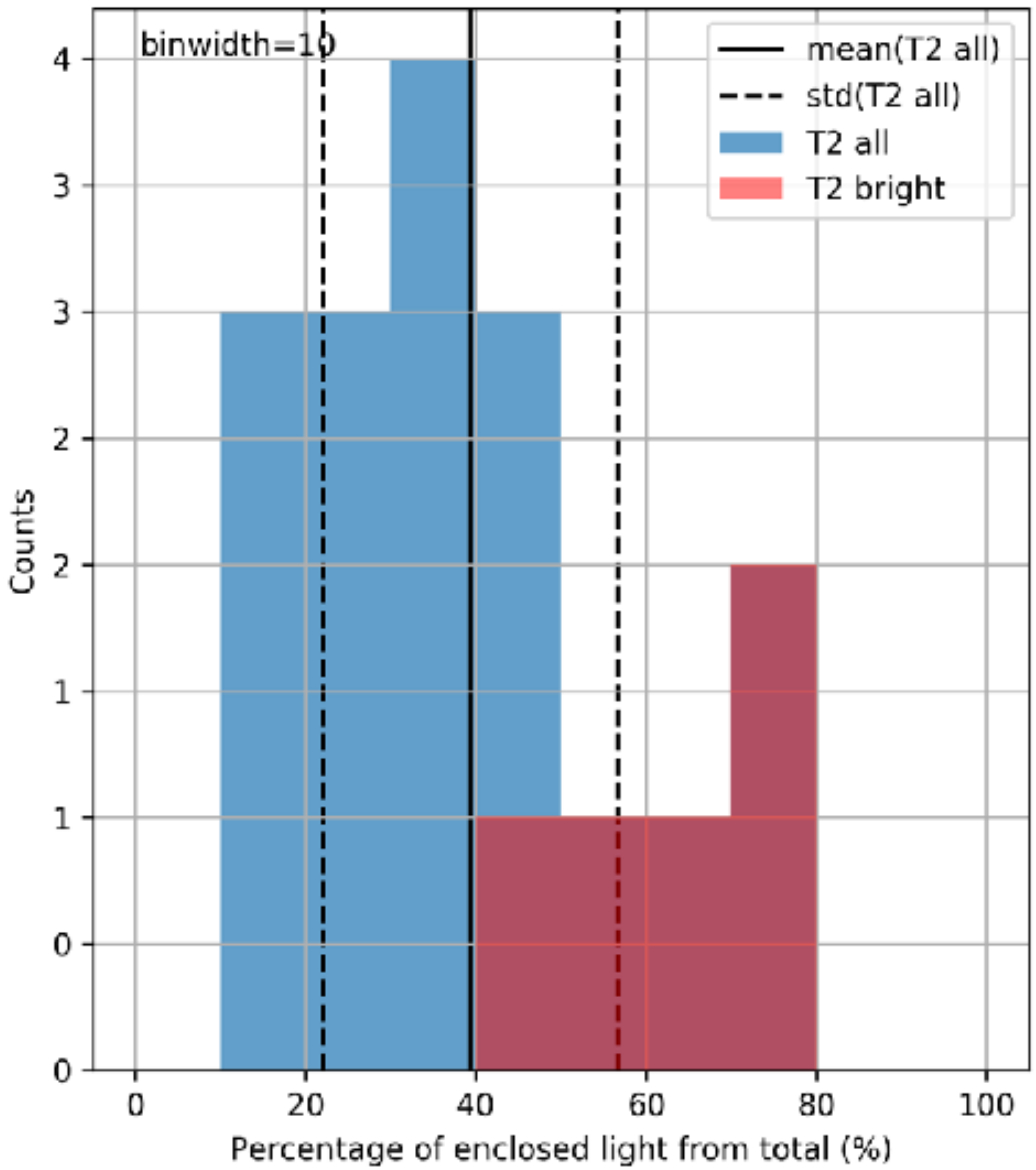

Left: **We opt for 60% of enclosed 3.6 µm light**,to reproduce best the "classical" T2's $S(K_{80})$,area at which 80% of the K_S-band light is enclosed.

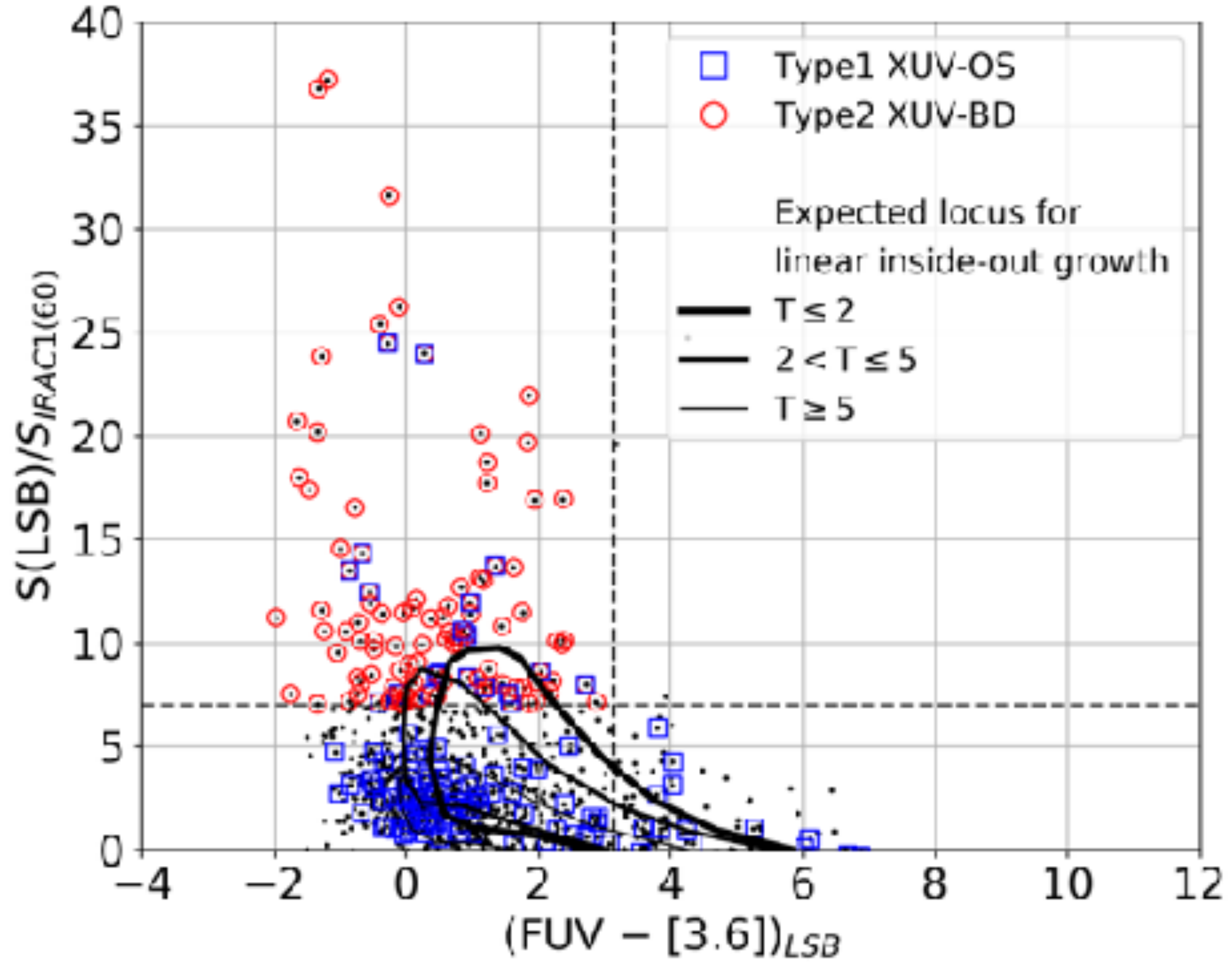

Top: areas are computed using the contour enclosing 60% of the 3.6 µm light

4.4 Results: XUV-disk galaxies classification

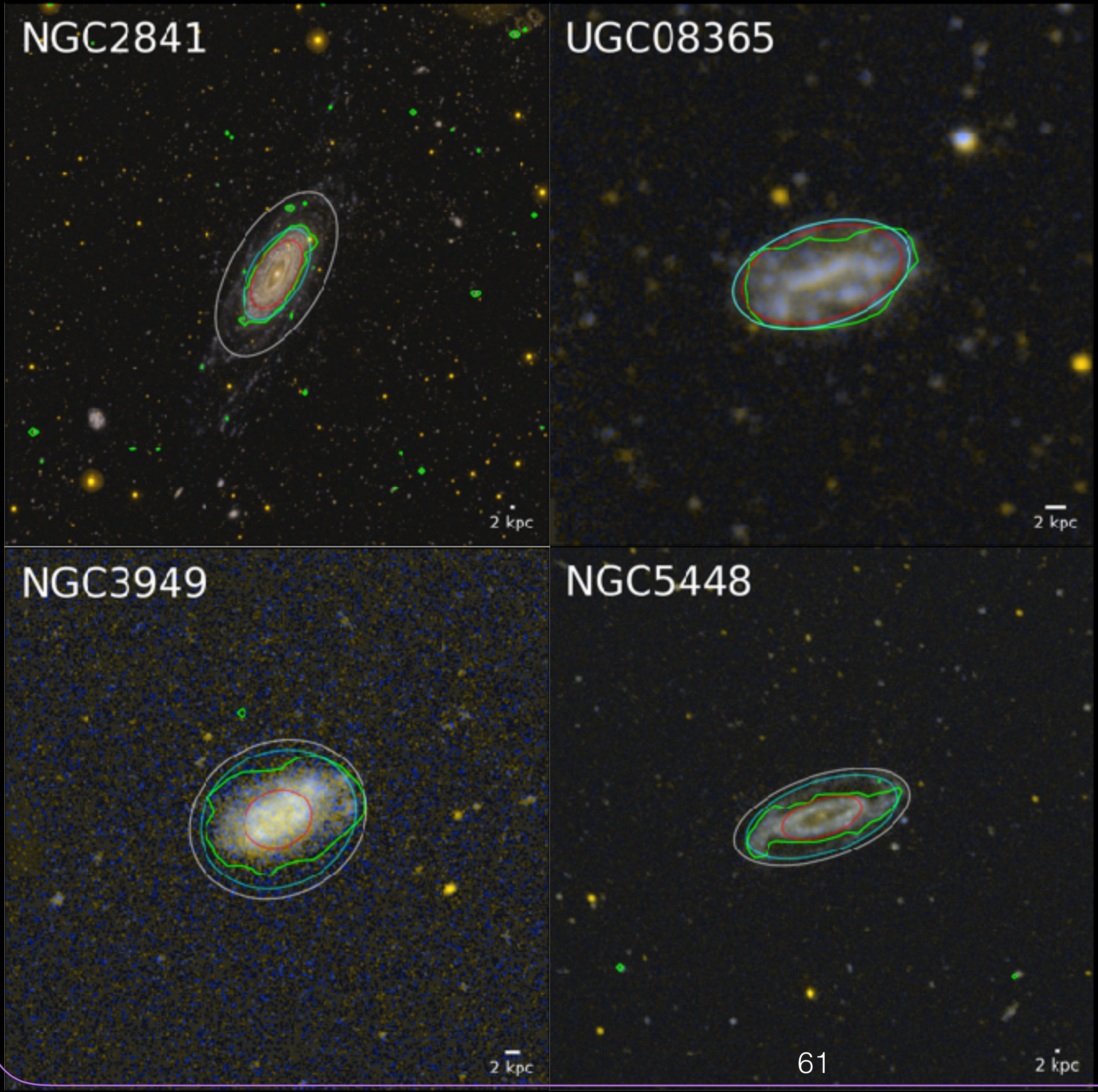

Examples of Type 2 XUV-disk galaxies

TOTAL in the GALEX/S4G sample: 110/1931 (<6%)

NGC2841 is a Type 1+2

4.4 Results: XUV-disk galaxies classification

The (FUV - NUV) color distribution of 217 Type 1, 110 Type 2 (including 21 Type 1+2)

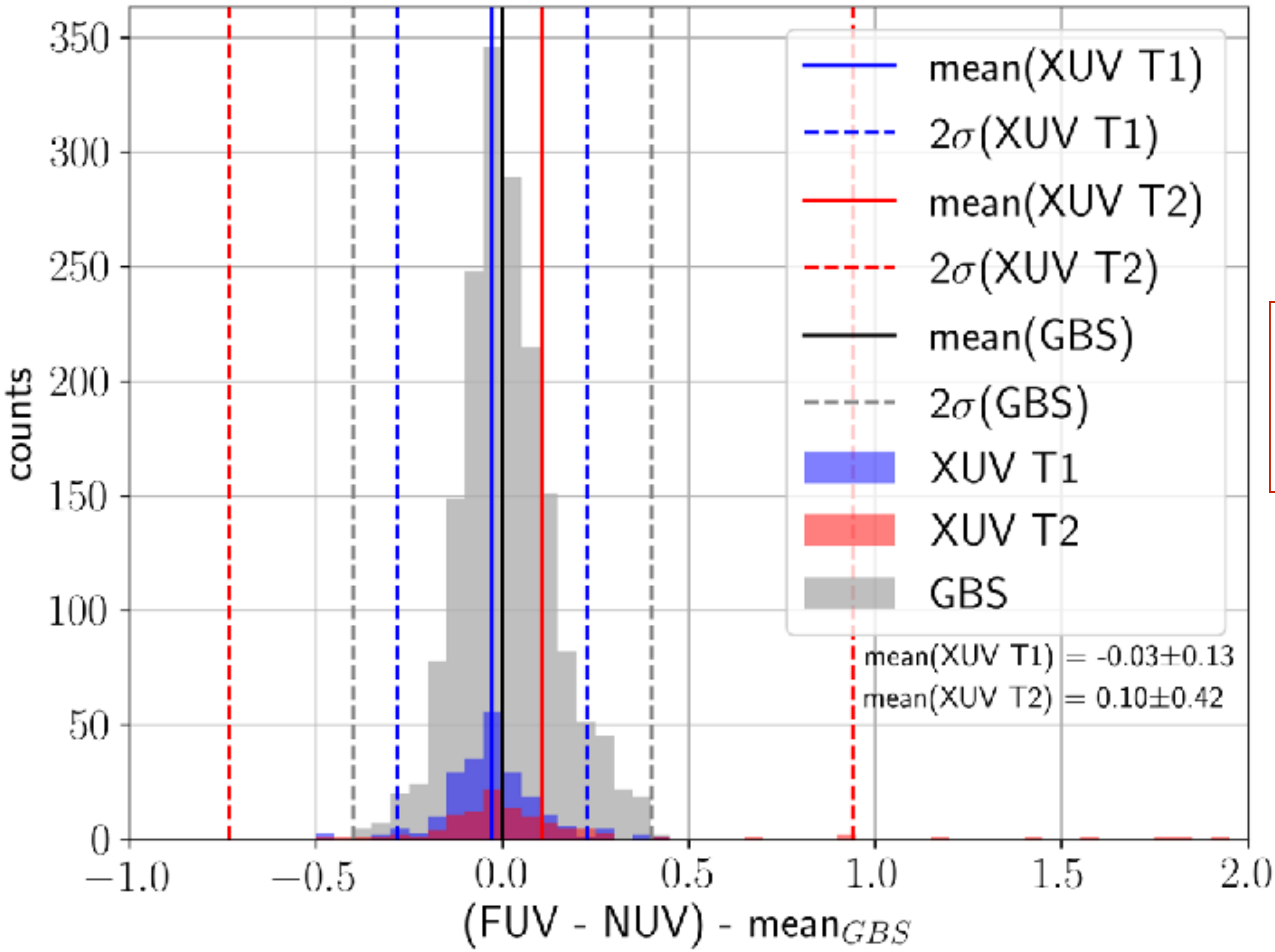

XUV-disk galaxies (both Type 1 and 2) follow the same distribution as the GBS galaxies

4.4 Results: XUV-disk galaxies classification

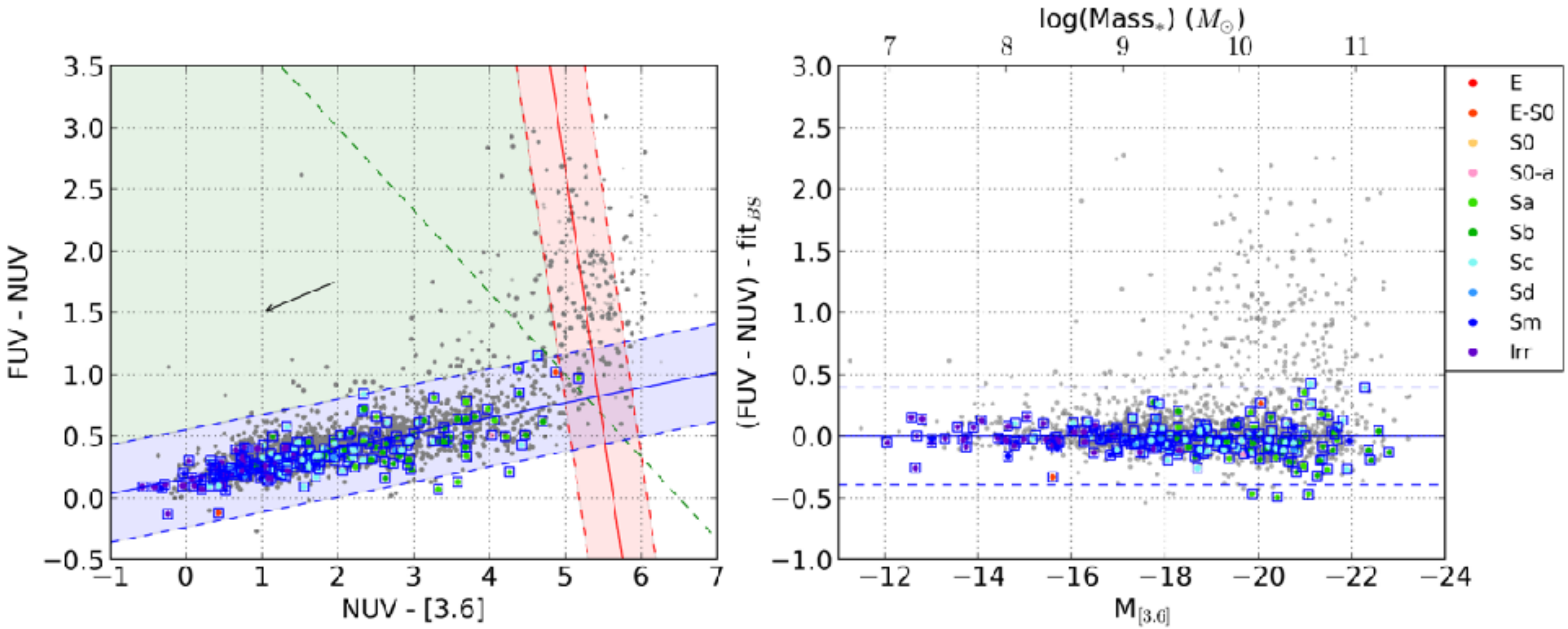

All Type 1 are in the **GBS**

□ = Type 1 (outer-structure)
○ = Type 2 (blue-disk)
⊡ = Type 1+2 (both)

4.4 Results: XUV-disk galaxies classification

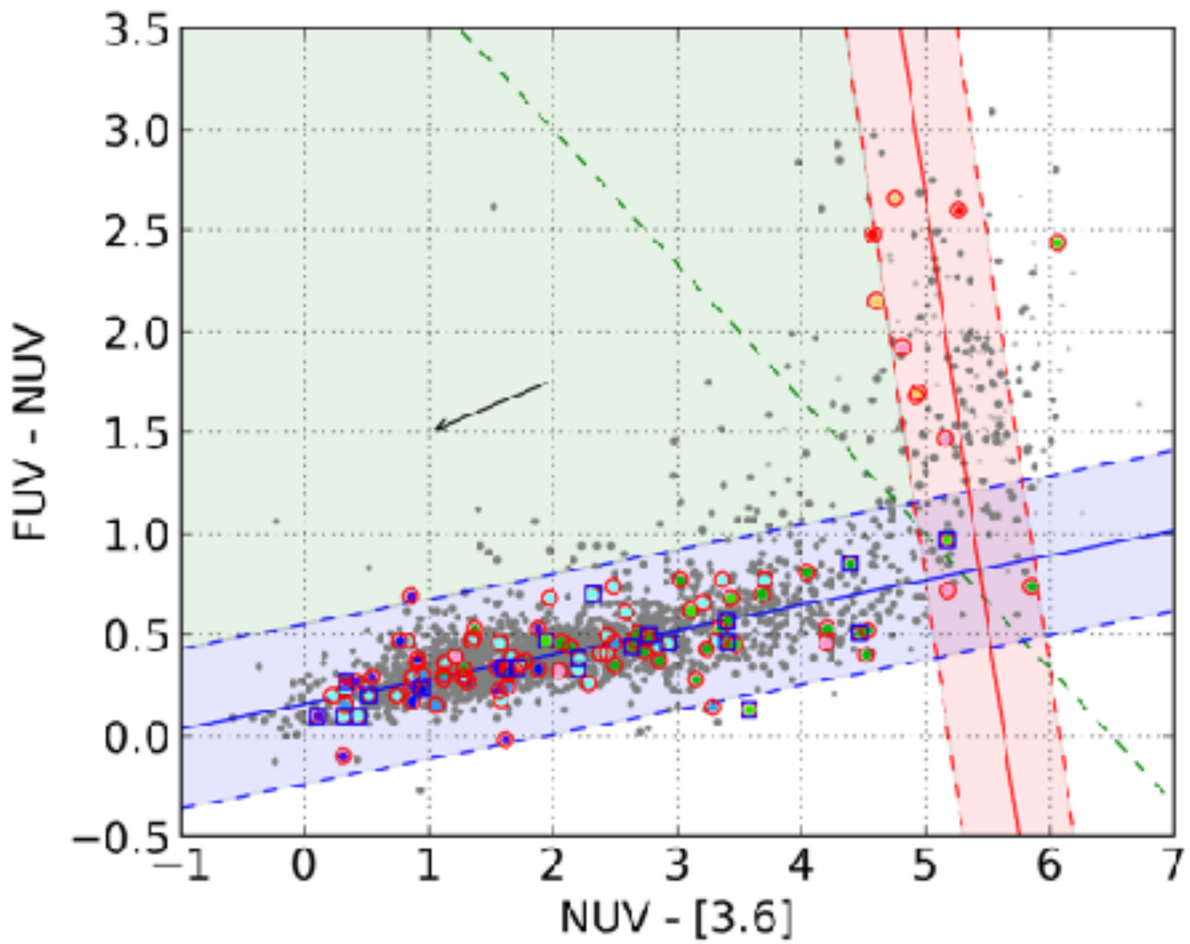

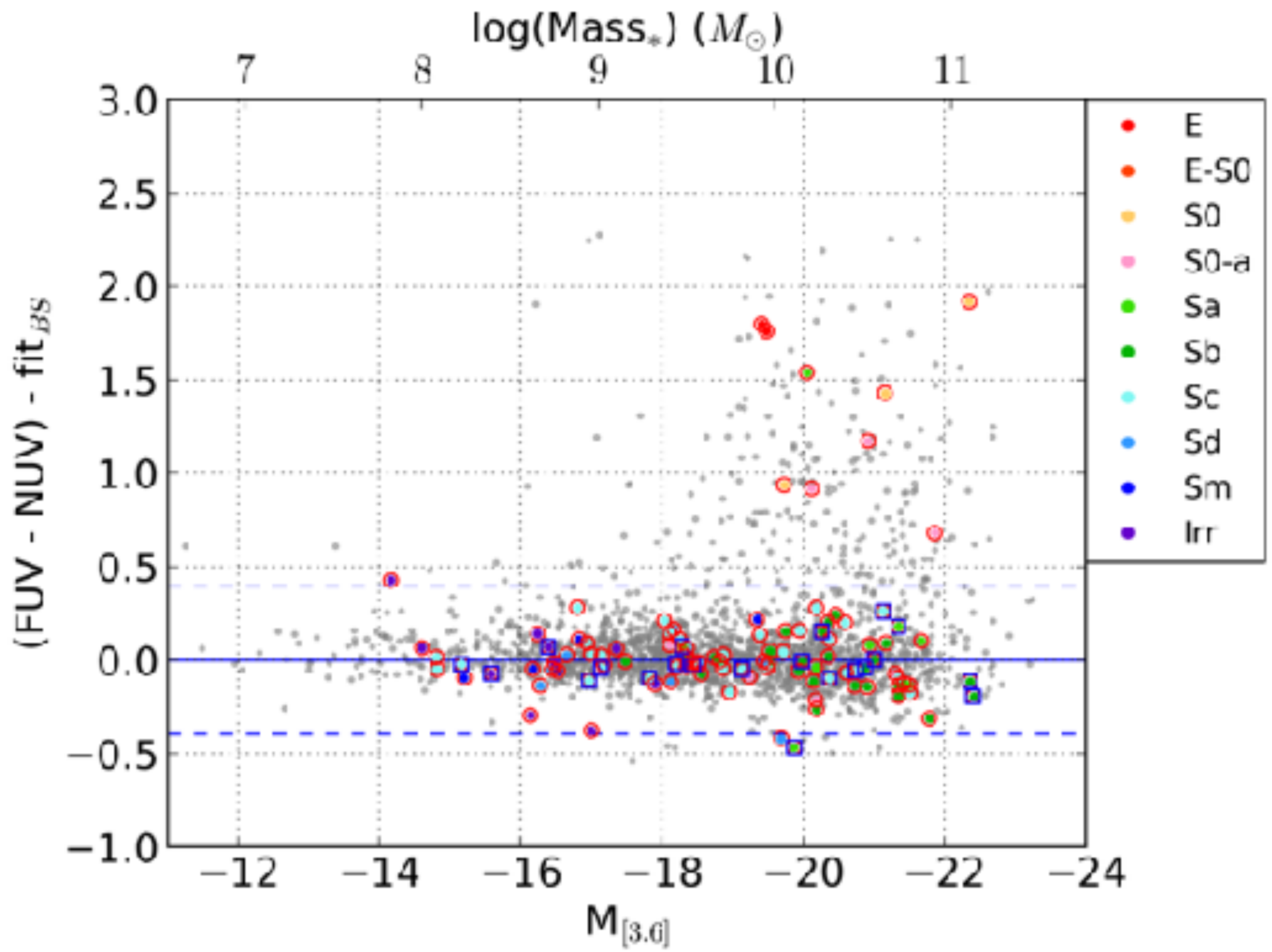

All Type 1 are in the **GBS**

□ = Type 1 (outer-structure)
○ = Type 2 (blue-disk)
▣ = Type 1+2 (both)

Most Type 2 are also in the **GBS**, but a few are found in the **GRS**

4.4 Results: XUV-disk galaxies classification

Conclusions:

- We obtain 217 Type 1 (outer-structure) XUVs (10x previous sample)
- We obtain 110 Type 2 (blue-disk) XUVs (6x previous sample)
- 21 galaxies are Type 1+2 (both)
- All Type 1 and most type 2 are found in the GBS (9 type 2 in the GRS)
- 9% are in Virgo (slightly larger fraction to overall GBS galaxies ~7%)
- 40% of XUVs are of type Sc

4.5 GTC observations of XUV-disk galaxies

The Extended Region Project (TERP)

Telescope: GTC
Instrument: OSIRIS
Mode: MOS
Target: NGC3274
Exposure time: 1 hour

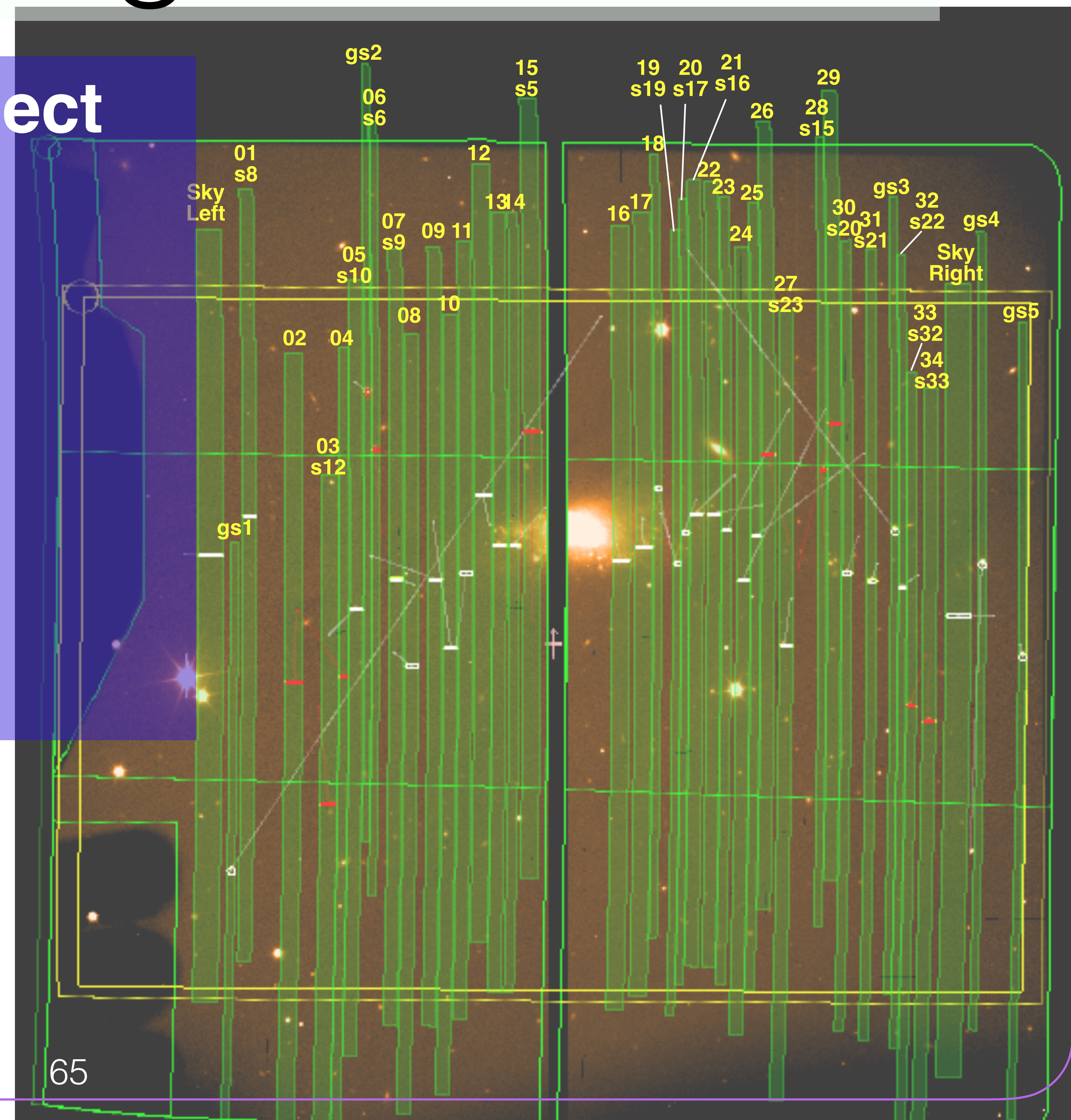

Multi-Object Spectroscopy mask created with OSIRIS Mask Designer v3.25

4.5 GTC observations of XUV-disk galaxies

GTC/OSIRIS (sloan-r)

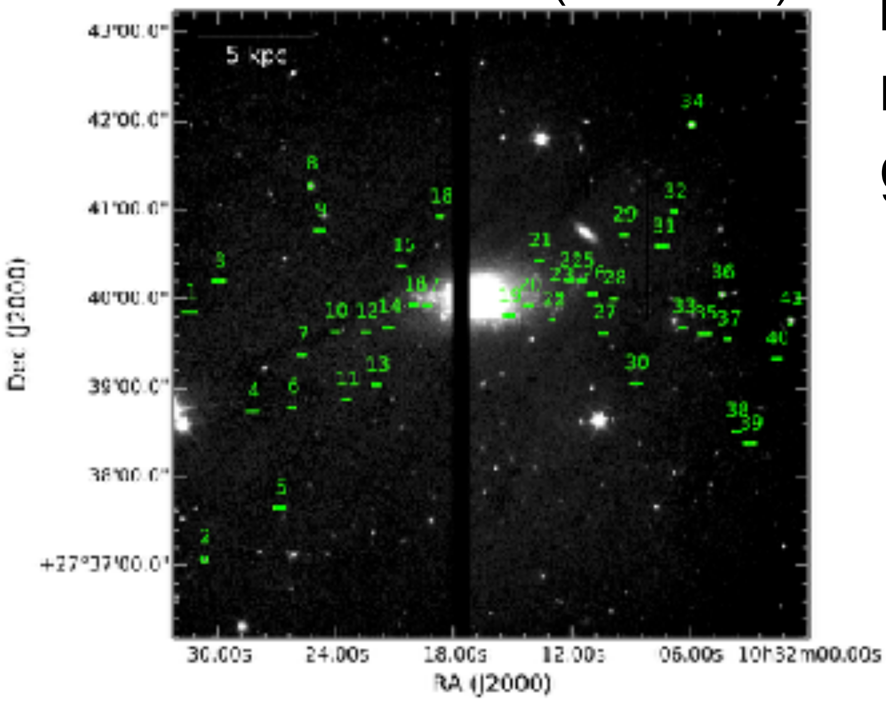

NGC3274

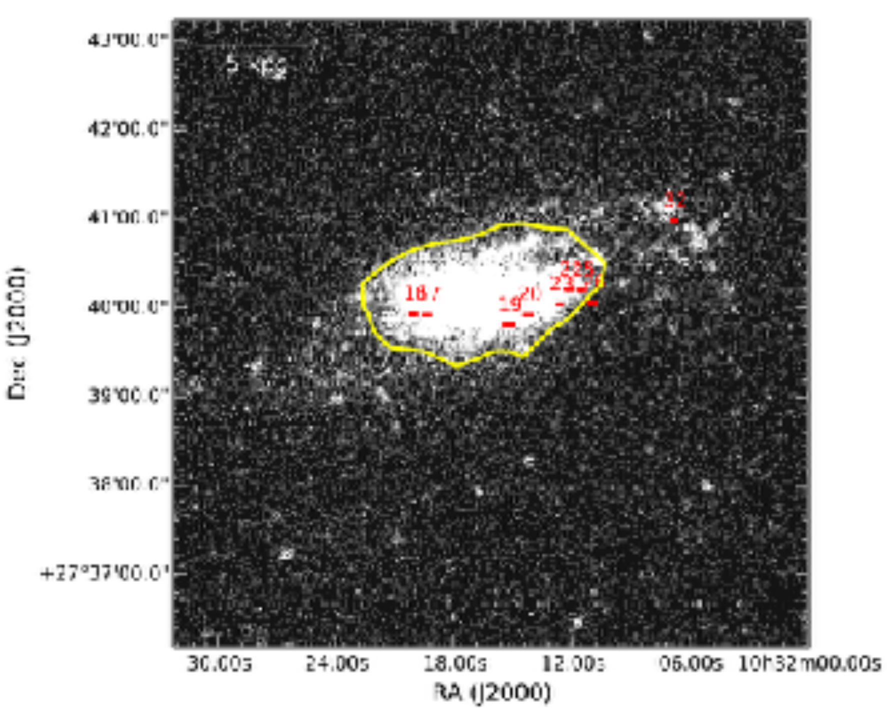

GALEX FUV

We obtained spectra for 5 regions inside μFUV=27.25 mag arcsec^{-2} (yellow contour and green solid line) and 4 regions outside of the low-mass ($M^{*}\sim10^{9}$ M_{Sun}) XUV-disk galaxy **NGC 3274 @ z=0.02**

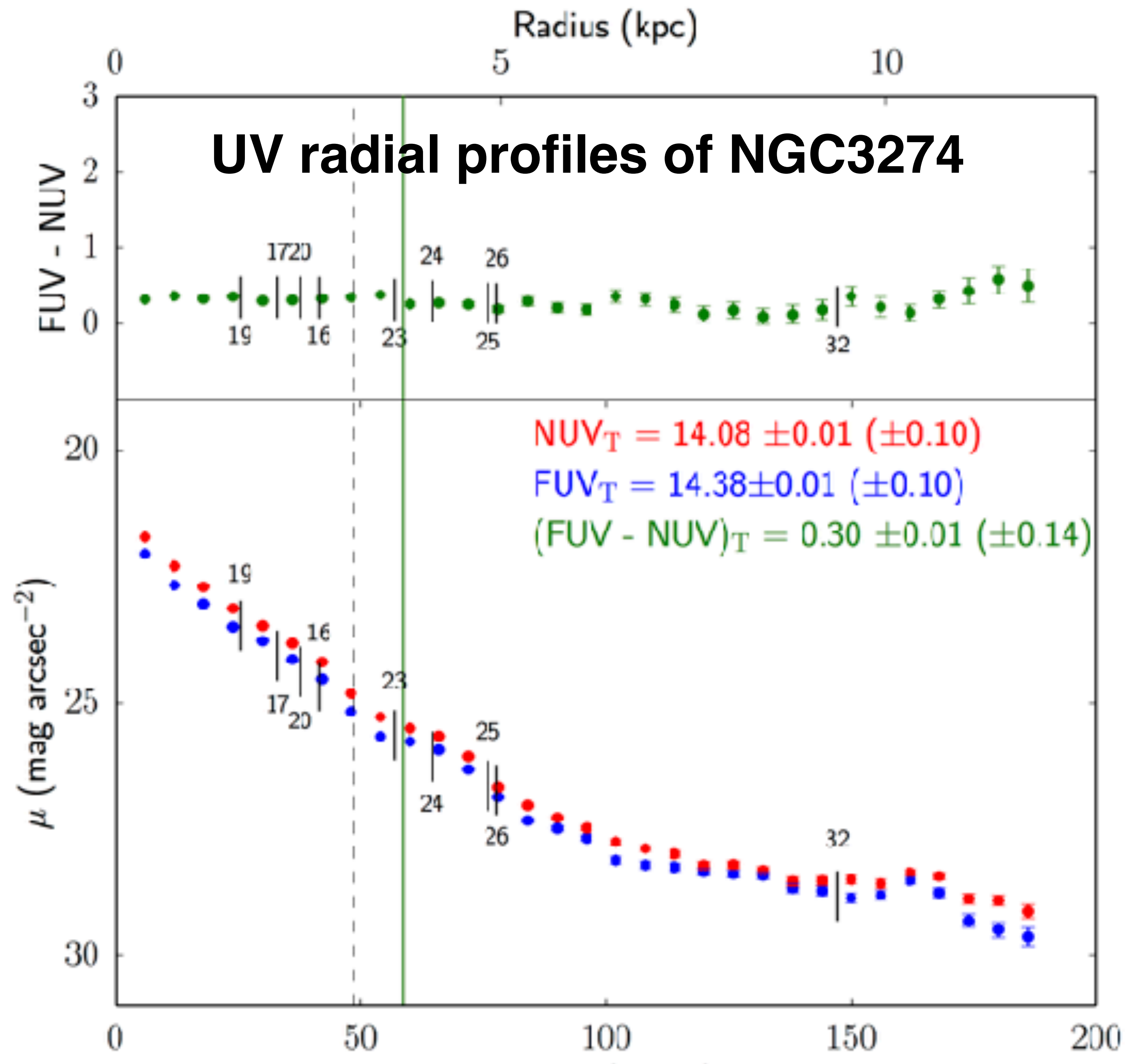

4.5 GTC observations of XUV-disk galaxies

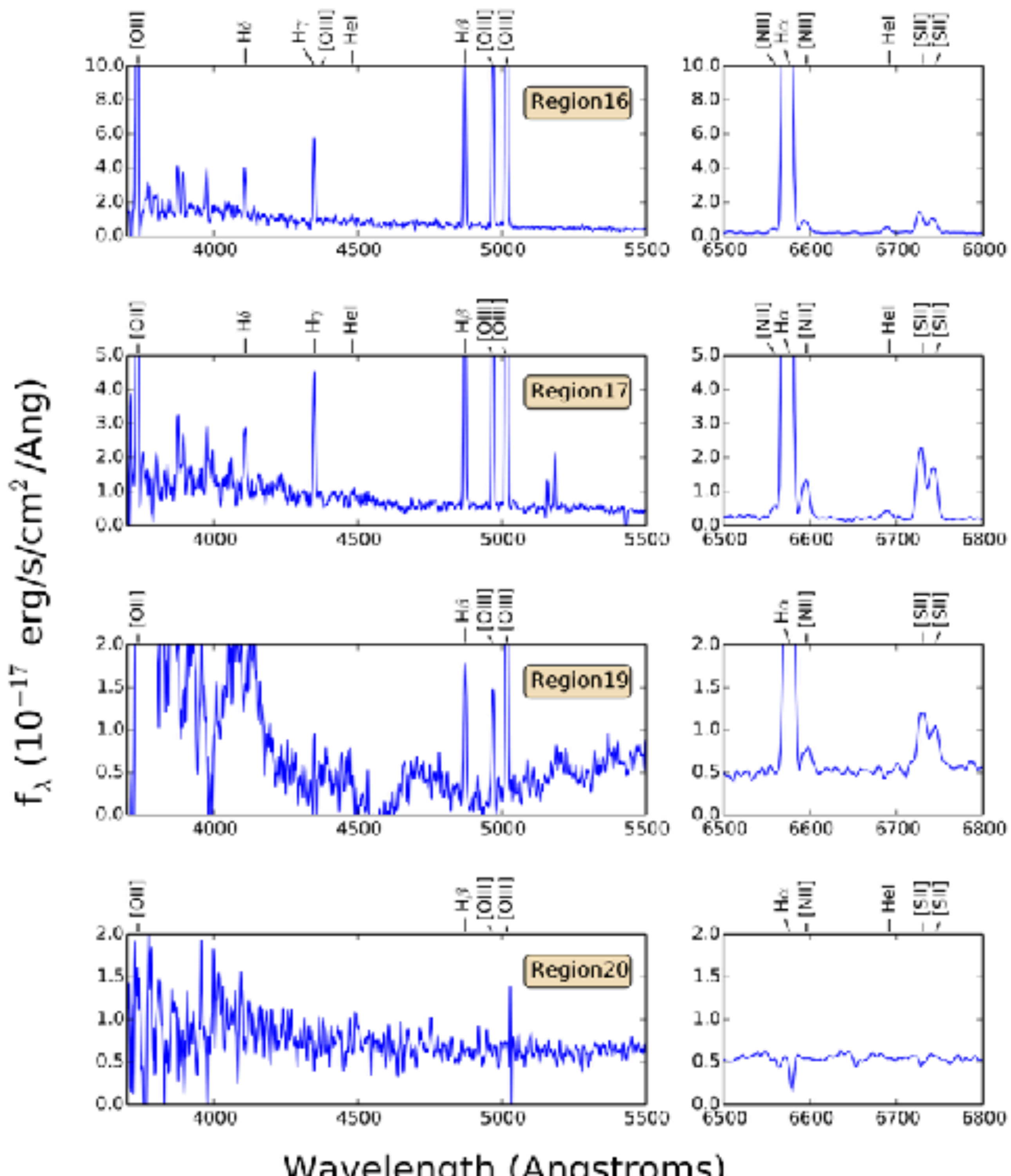

Spectra shown here are not corrected for extinction nor radial velocity, but only for sky emission [continuum fitting by Dr. Catalán-Torrecilla (private communication)]

HII regions

We are able to identify the following emission lines:

Hα 6563Å

Hβ 4861Å

Hγ 4341Å

Hδ 4102Å

[OII] 3726Å + [OIII]3729Å

[OIII]4959Å

[OIII]5007Å

[NII]6548Å

[NII]6583Å

HeI 6678Å

[SII]6716Å

[SII]6731Å

4.5 GTC observations of XUV-disk galaxies

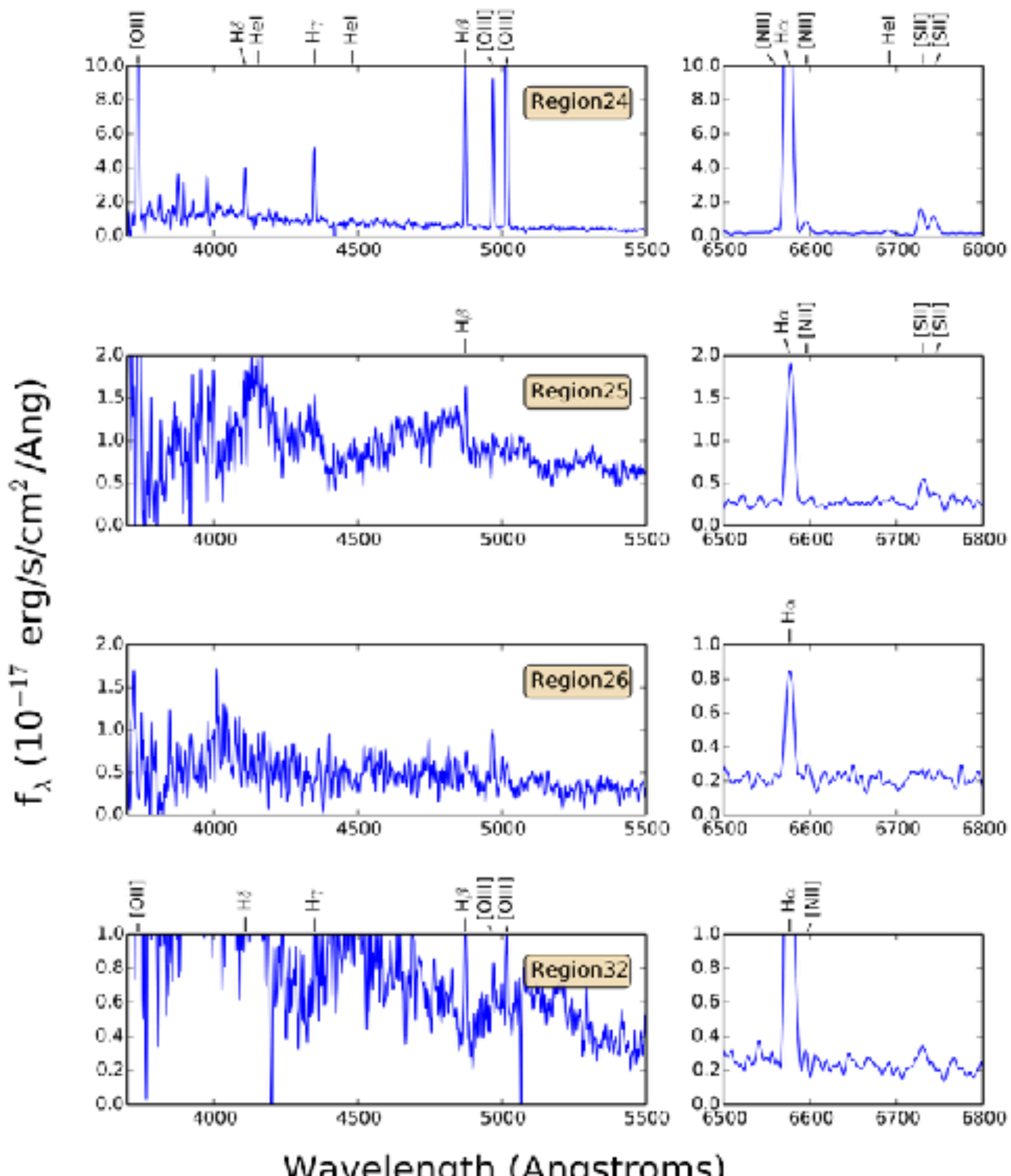

Spectra shown here are not corrected for extinction nor radial velocity, but only for sky emission [continuum fitting by Dr. Catalán-Torrecilla (private communication)]

HII regions

We are able to identify the following emission lines:

Hα 6563Å

Hβ 4861Å

Hγ 4341Å

Hδ 4102Å

[OII] 3726Å + [OIII]3729Å

[OIII]4959Å

[OIII]5007Å

[NII]6548Å

[NII]6583Å

HeI 6678Å

[SII]6716Å

[SII]6731Å

4.5 GTC observations of XUV-disk galaxies

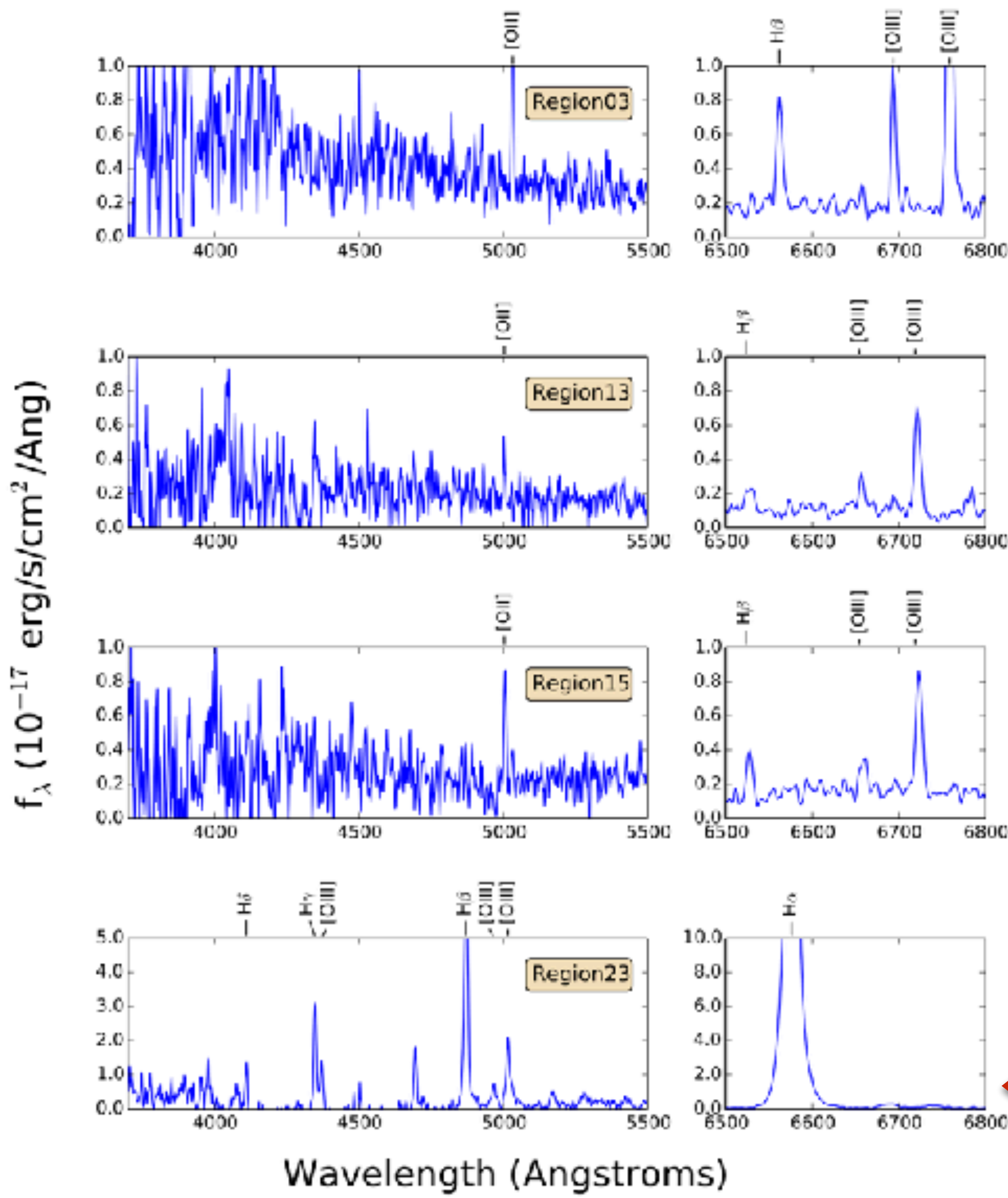

Non-HII regions

z=0.35 (galaxy)

z=0.342 (galaxy)

z=0.342 (galaxy)

z=0.02 (same as target)

Very wide Hα!
Velocity close to 770 km s^{-1}!
Possibly a variable star, a nova, or a Luminous Blue Variable (LBV) star?

4.5 GTC observations of XUV-disk galaxies

Putting the emission-line ratios of our spectra to the test:
the Baldwin-Phillips-Terlevich (BPT) diagrams (**Baldwin et al. 1981**) tell us that the observed spectra are from genuine HII regions

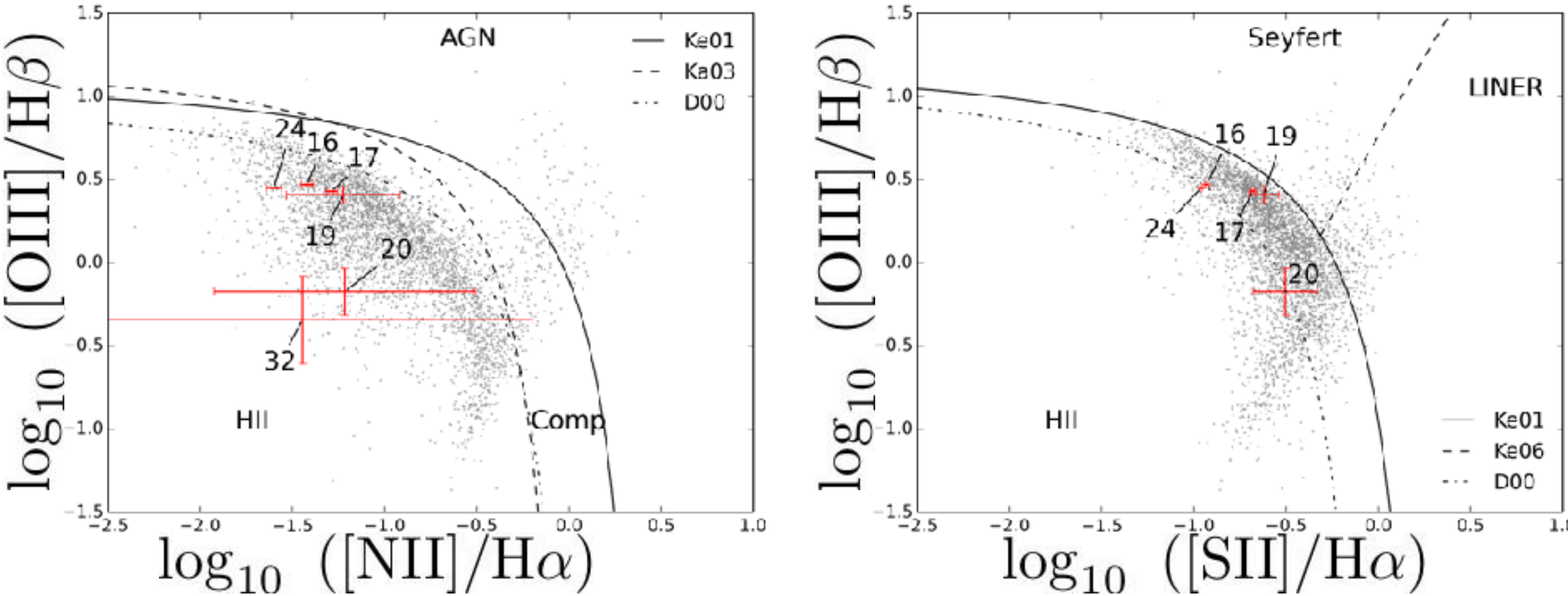

~4000 SDSS (DR12) galaxies with
$0 \leq z \leq 0.01$ are shown in grey

4.5 GTC observations of XUV-disk galaxies

We use two calibrators (N2 and O3N2) and two calibration methods (**Pettini & Pagel, 2004**, and **Marino et al., 2013**) to get the oxygen abundance.

Oxygen abundances are lower than solar (<8.69) for the inner regions, but inconclusive for the outskirts with these data.

However, this method proved to be feasible and we were awarded 19 hours more telescope time

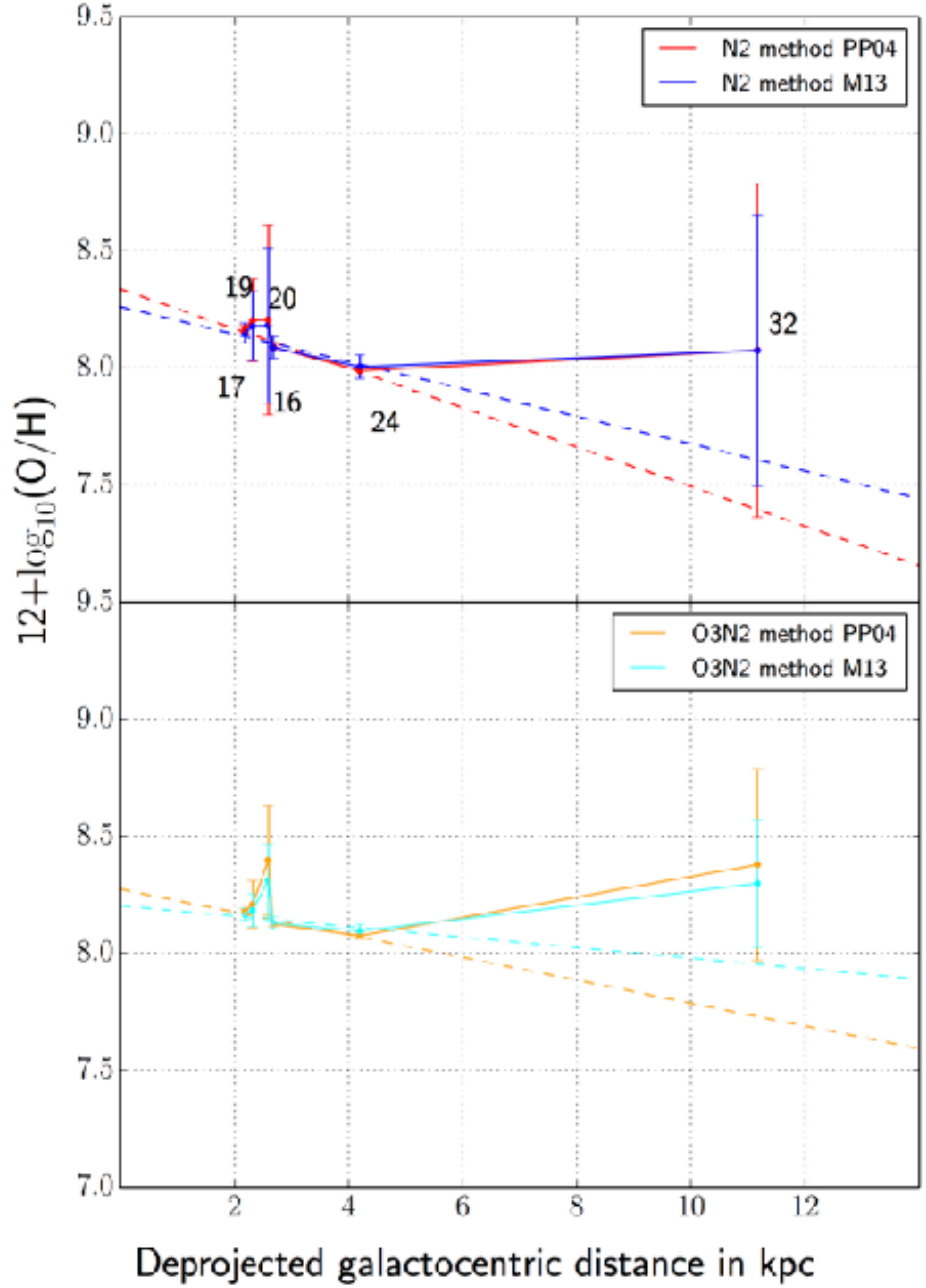

4.5 GTC observations of XUV-disk galaxies

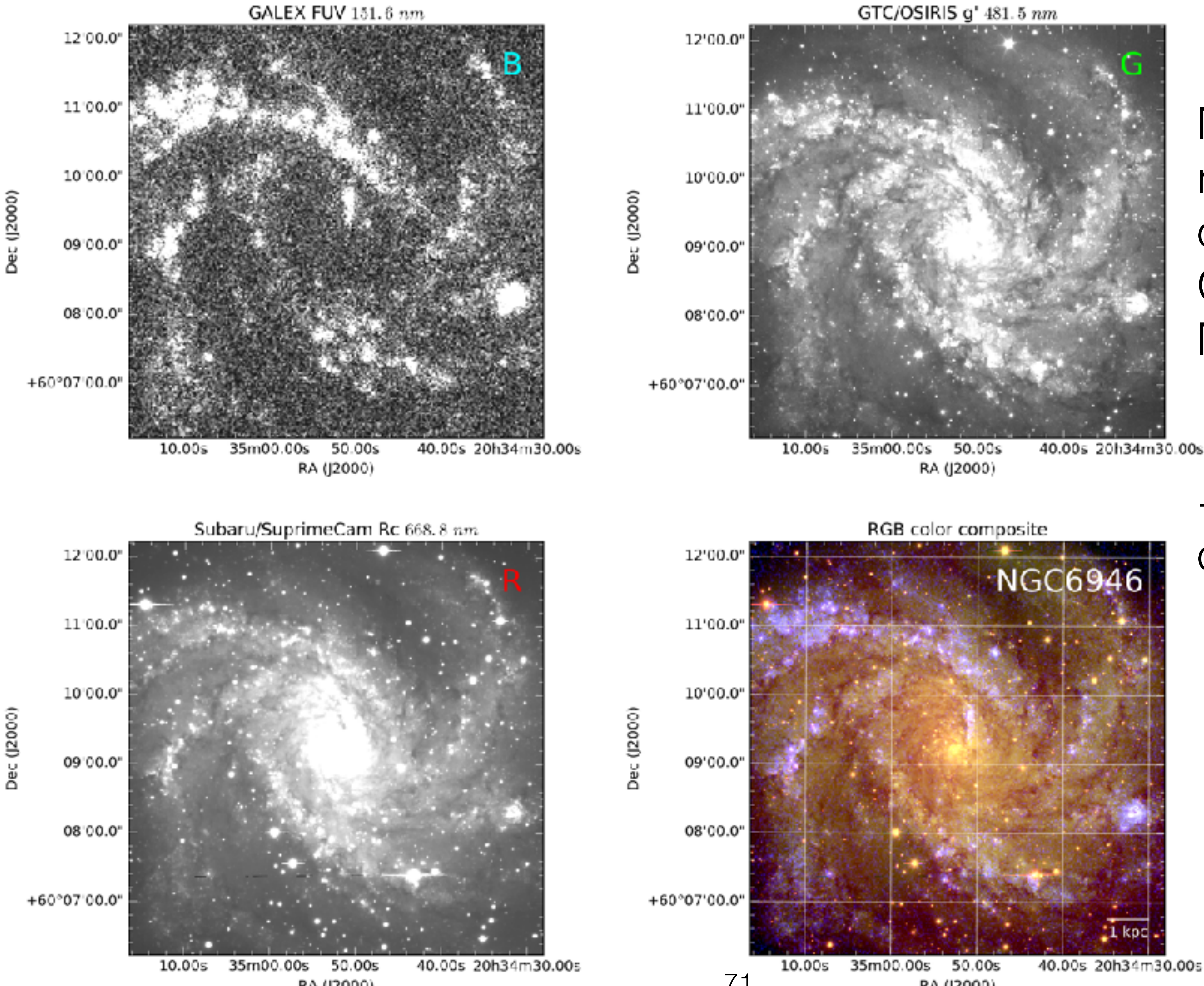

More HII regions observed with GTC/OSIRIS/MOS

+60 spectra obtained!

5. Future work

Using MEGARA@GTC to observe XUVs

5. Future work

Can be prepared with the ETC!

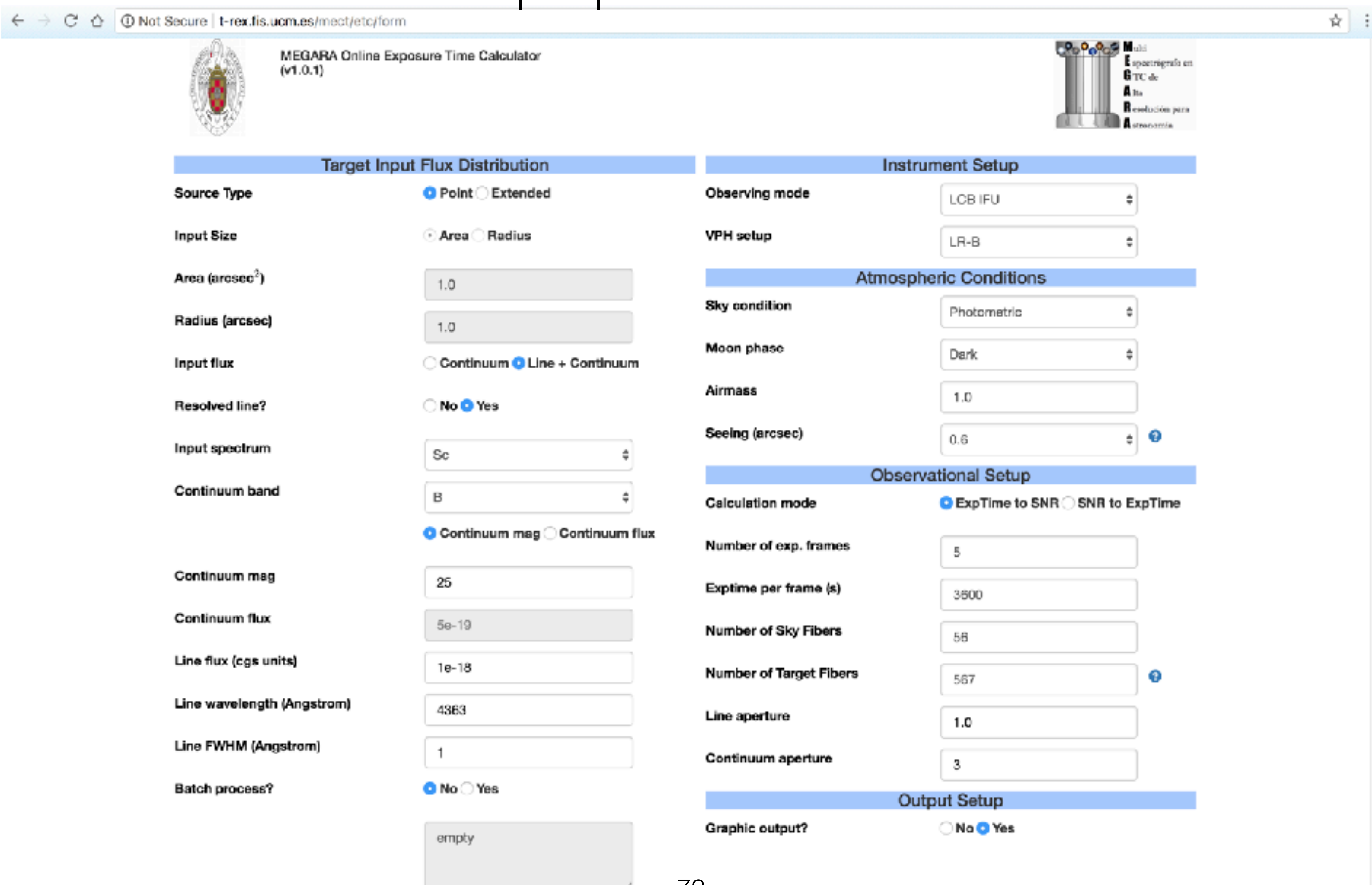

5. Future work

Can be prepared with the ETC!

t-rex.fis.ucm.es/mect/etc/form

Calculation Mode: Exposure time to SNR

Observing Mode: LCB, VPH: LR-B, Source Type: Point

Computation time: 7.1 seconds;

OUTPUT CONTINUUM SNR
(at lambda_c(VPH) = 4800.0 AA)

	* Continuum SNR reached for input exptime (3600.0 seconds per frame, with 5 frames, and Total exptime of 18000.0 seconds) per spaxel zones due to PSF (LCB mode): fiber diameter=0.62 arcsec; Seeing FWHM=0.6 arcsec						
	** per frame			** all frames			
	C (45.8%) 1 fiber	C+R1 (98.20%) 7 fibers	C+R1+R2 (100.00%) 19 fibers	C (45.8%) 1 fiber	C+R1 (98.20%) 7 fibers	C+R1+R2 (100.00%) 19 fibers	percentage of enclosed total flux
	1.02	0.85	0.53	2.28	1.89	1.18	per voxel
1Å	1.14	0.95	0.59	2.55	2.11	1.32	per AA
	26.38	21.71	13.49	58.99	48.54	30.16	integrated spectrum

Input source spectrum
Sky spectrum

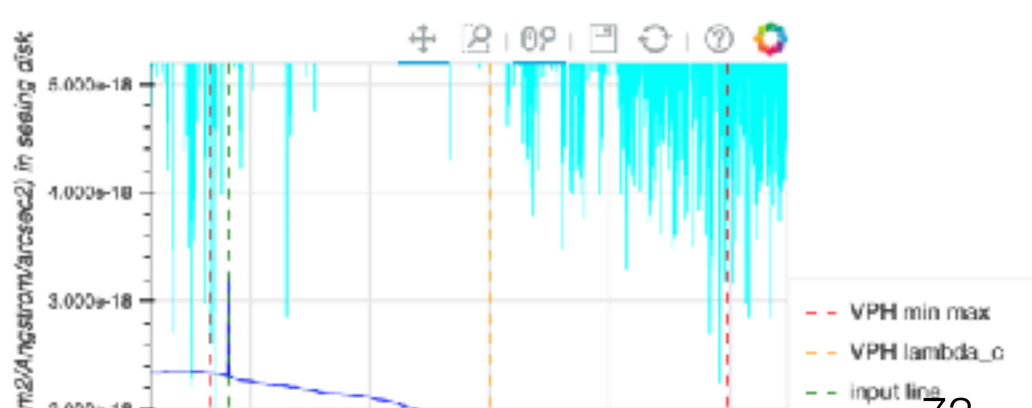

OUTPUT LINE SNR: L
(at lambda_line = 4363.0 AA)

	per frame	all frames	
	0.79	1.77	per fiber per detector pixel
	3.16	7.07	per fiber per voxel
1Å	3.45	7.73	per fiber in aperture per AA
	3.45	7.73	per fiber in aperture
	3.05	6.82	total in aperture

INPUT PARAMETERS:	
Calculation mode:	Exposure time to SNR
Source type:	Point
Area:	0.28 arcsec^2
Observing mode:	LCB
VPH:	LR-B
Input flux type:	Line+Continuum
Source spectrum:	Sc smooth
Input continuum:	B = 25.00mag
Input flux:	6.403e-19 erg/s/cm^2/Å
Continuum flux per arcsec^2 within the seeing disk (@λ_C(VPH)):	1.862e-18 erg/s/cm^2/Å/arcsec^2
Resolved line?:	Y
Line wavelength:	4363.0 AA
Line flux (integrated):	1e-18 erg/s/cm^2
Line FWHM:	1.0 AA
*Sky Condition:	Photometric
Moon:	Dark
Airmass: X=	1.0
Seeing(@X=1):	0.6 arcsec
Sky-flux(R,@X):	8.432e-18 erg/s/cm^2/Å/arcsec^2
Seeing(@X):	0.6 arcsec
*Observation:	

5. Future work

Can be prepared with the ETC!

Not Secure | t-rex.fis.ucm.es/mect/etc/form

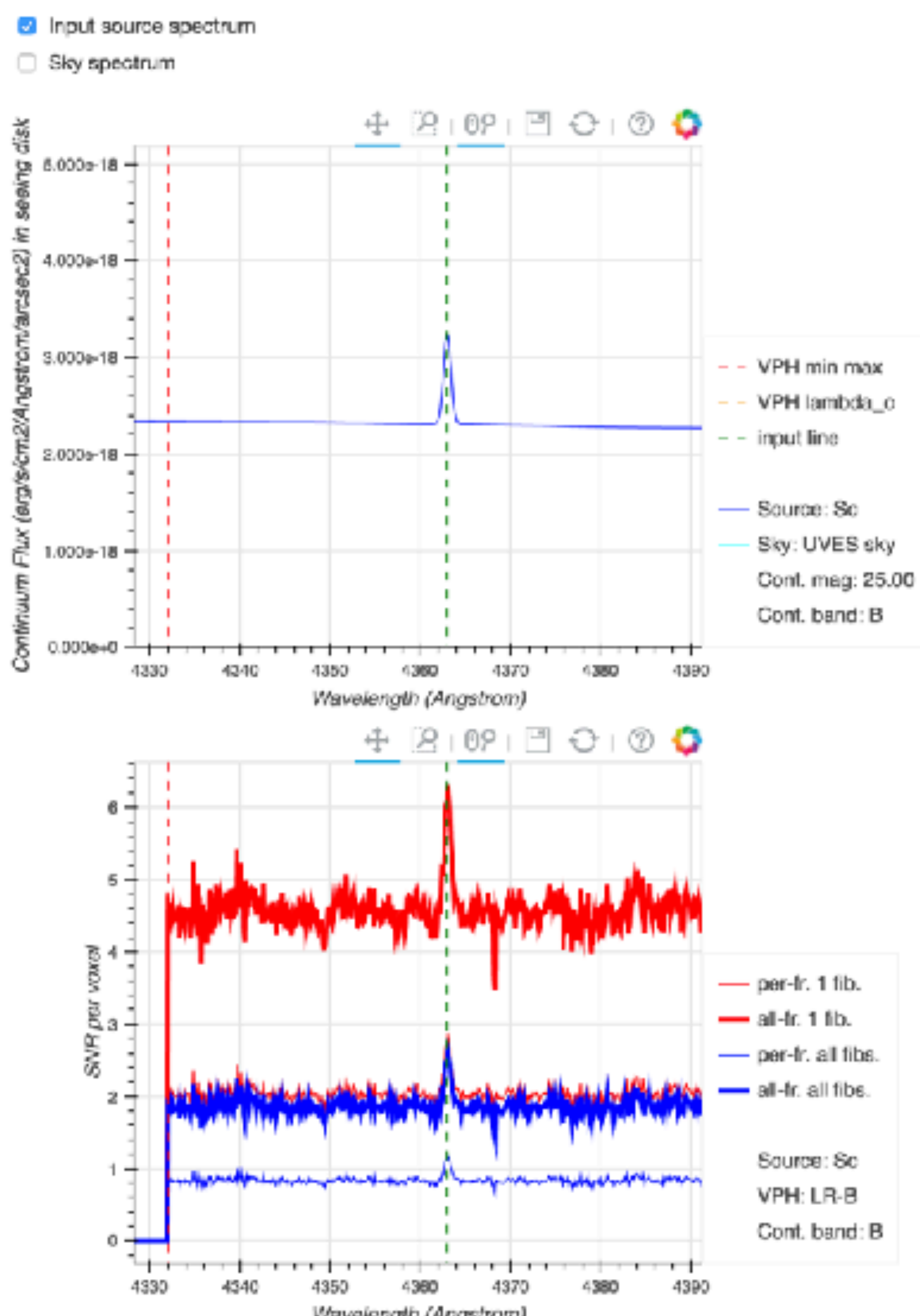

Source spectrum:	Sc smooth
Input continuum:	B = 25.00mag
Input flux:	6.403e-19 erg/s/cm^2/Å
Continuum flux per arcsec^2 within the seeing disk (@λ_C(VPH)):	1.862e-18 erg/s/cm^2/Å/arcsec^2
Resolved line?:	Y
Line wavelength:	4363.0 AA
Line flux (integrated):	1e-18 erg/s/cm^2
Line FWHM:	1.0 AA
*Sky Condition:	Photometric
Moon:	Dark
Airmass: X=	1.0
Seeing(@X=1):	0.6 arcsec
Sky-flux(R,@X):	8.432e-16 erg/s/cm^2/Å/arcsec^2
Seeing(@X):	0.6 arcsec
*Observation:	
Number of frames:	5
Exptime per frame:	3600.0 s
Total exptime:	18000.0 s
NP_Dark:	65500.0
Sky-fibers:	56

5. Future work

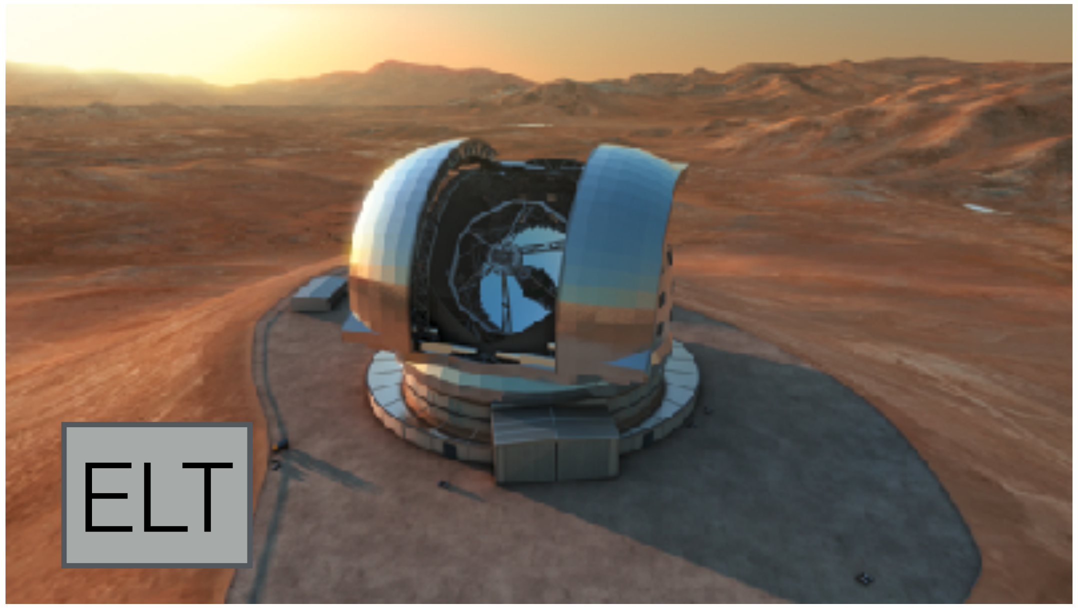

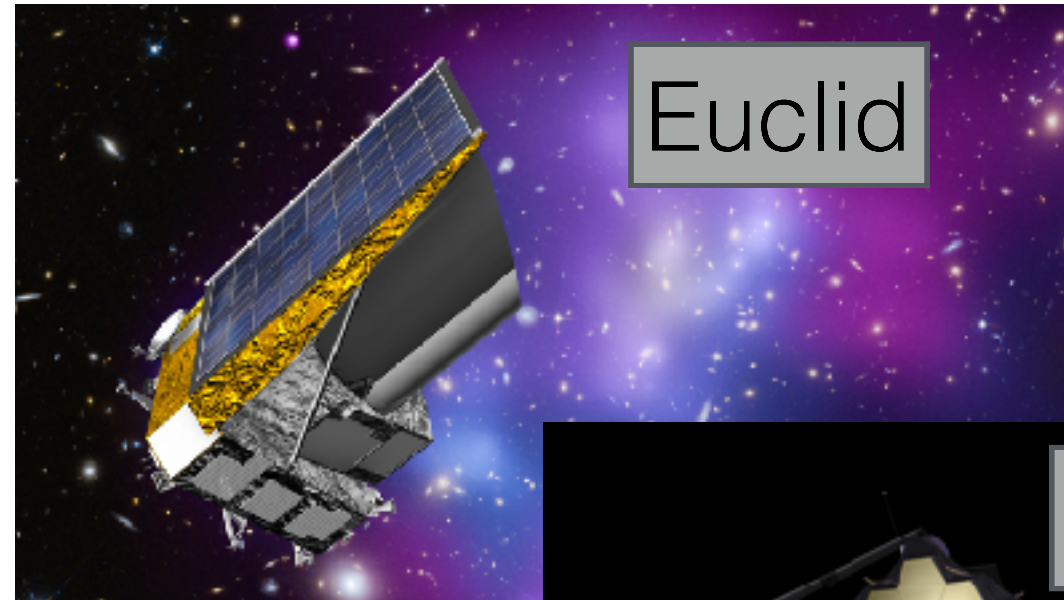

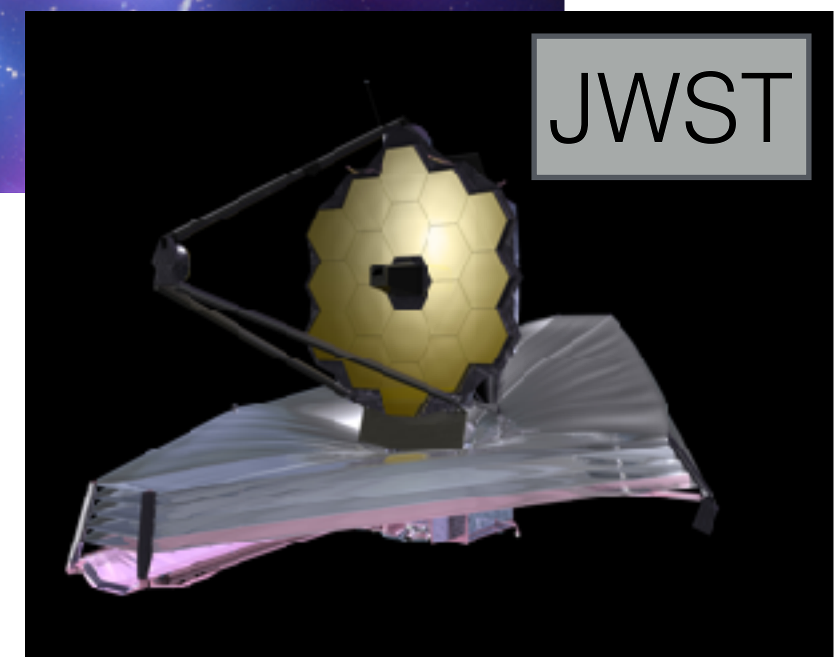

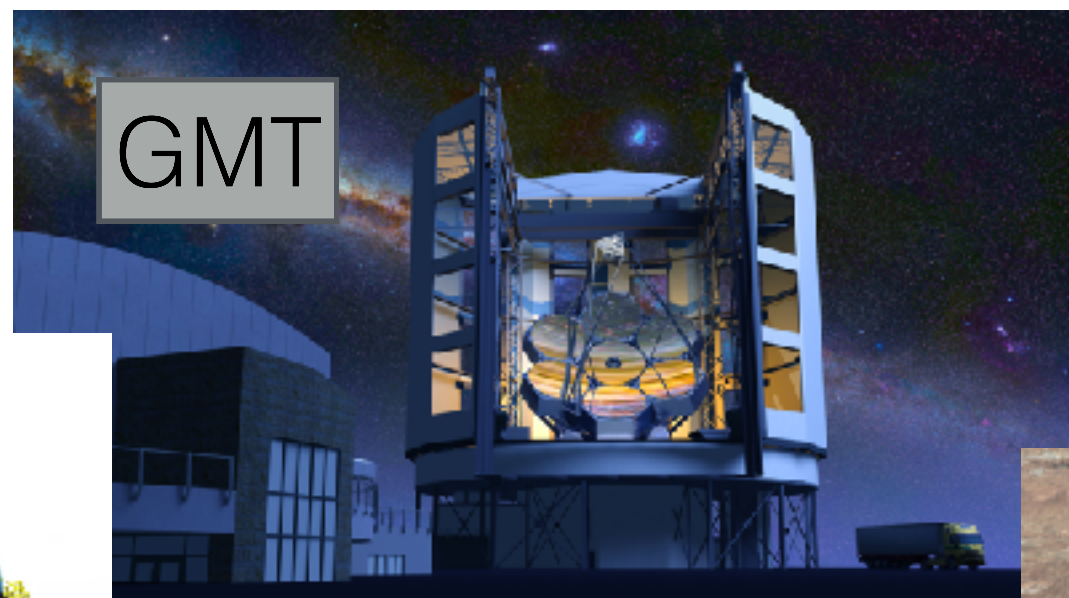

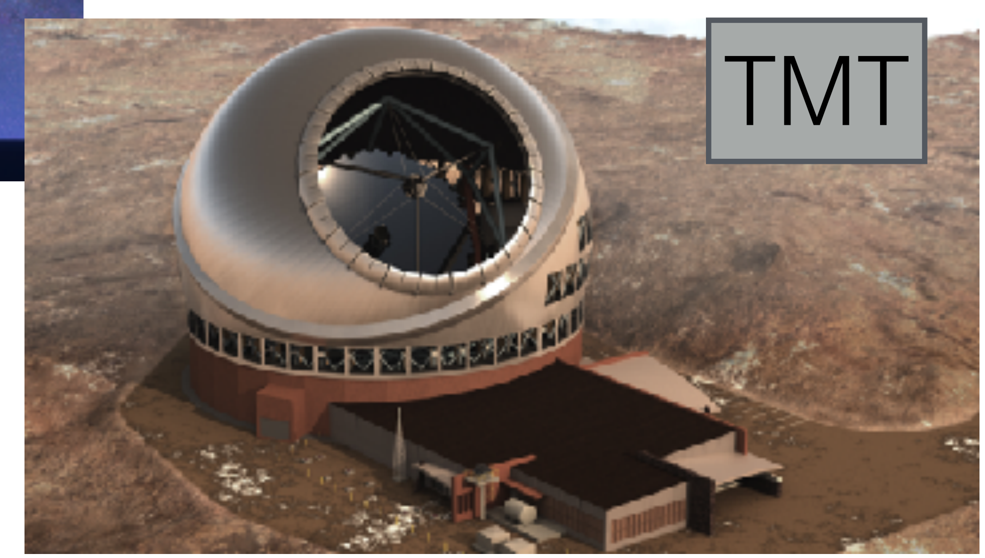

5. Future work

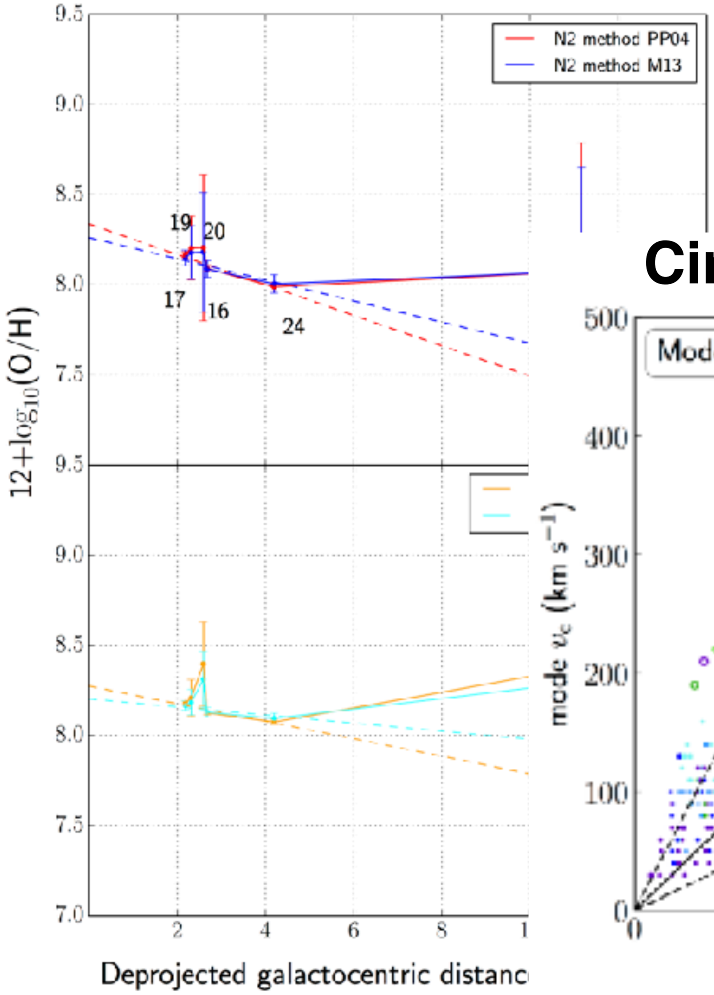

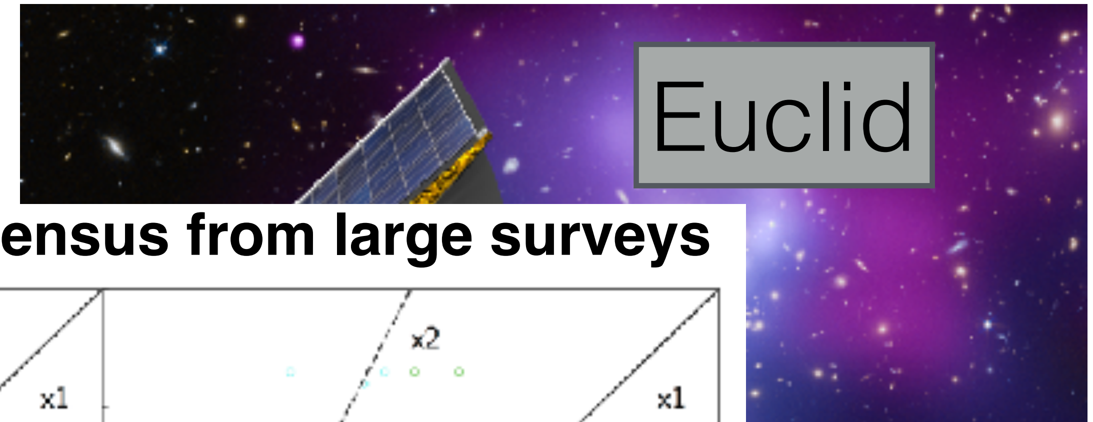

Circular velocity census from large surveys

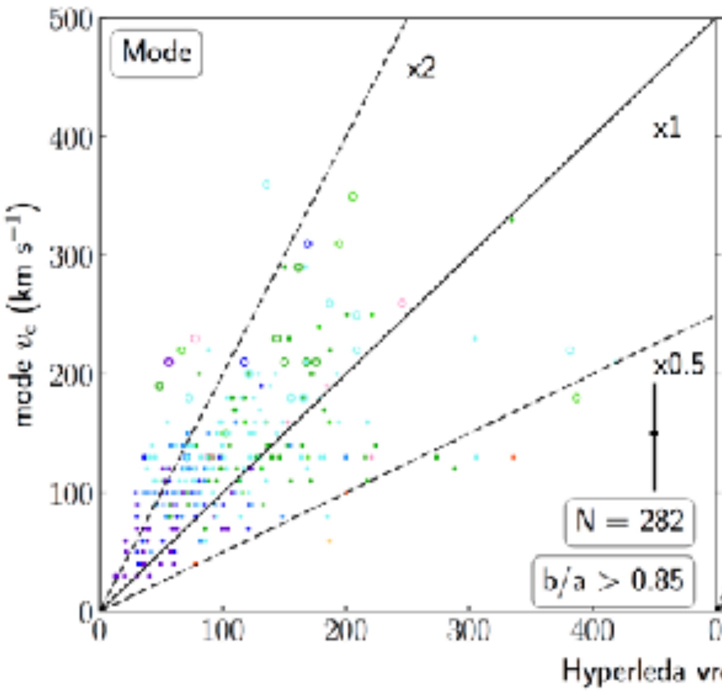

UV+IR color-color diagram at high-z

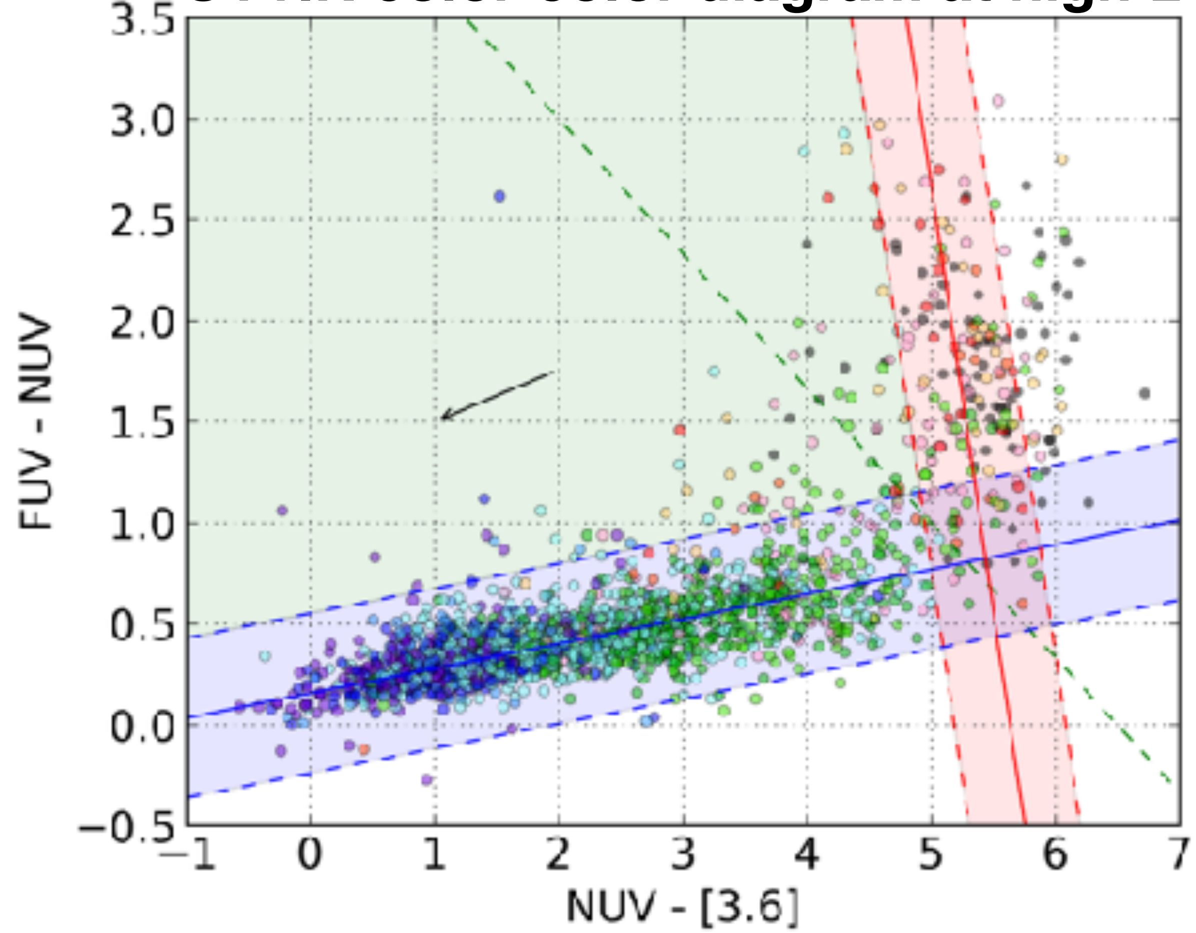

Better metallicity gradient measurement of XUV-disk galaxies

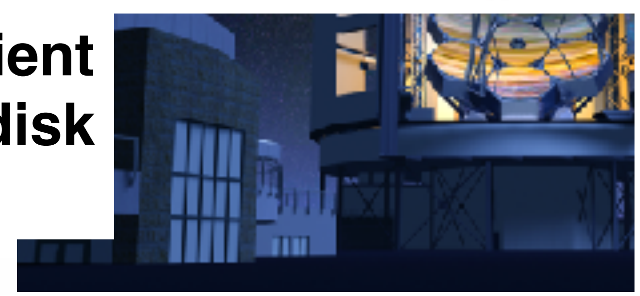

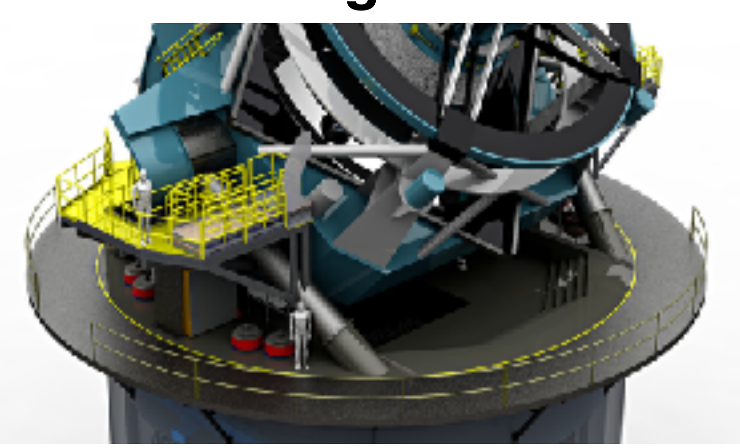

6. Conclusions (1/4)

- We start off from the **S4G sample of 2352 galaxies as our base-sample** for which we gathered GALEX FUV and NUV data.

- Sky subtraction, masking, interpolation, and photometry were performed using the **same aperture for both FUV and NUV as for the 3.6 *μ*m** IRAC1 images.

- Data products are the surface brightnesses and color radial profiles μ_{FUV}, μ_{NUV}, and (FUV - NUV), the asymptotic magnitudes FUV and NUV, false-color RGB images, all complemented by the [3.6] (asymptotic) and $\mu_{3.6}$ data.

- The final sample comprises **1931 galaxies of all morphological types with homogenized photometry**. We call this catalog of nearby galaxies **the GALEX/ S4G sample.** It is one of **the best-to-date**, in terms of (1) size, (2) multi-wavelength coverage (UV to IR), (3) homogenized data with good spatial-resolution (6 arcsec).

6. Conclusions (2/4)

About the global properties (**Bouquin et al. 2015**)

- Galaxies are distributed into **two extremely narrow sequences** that we call the **GALEX Blue Sequence (GBS)** and **GALEX Red Sequence (GRS).** The GBS has a scatter around the mean of roughly ~1 mag (at $\pm 2\sigma$ rms) in (FUV - NUV) color.

- The region with redder (FUV - NUV) than the GBS but bluer in (NUV - [3.6]) than the GRS is the **GALEX Green Valley**. We find a **higher fraction of S0-a and Sa galaxies** than any other regions of this diagram. We also find a **higher fraction of GGV galaxies belonging to the Virgo** cluster **—> nearby galaxies evolution not only driven by mass but also by environment.**

- In **Zaritsky, Gil de Paz, Bouquin, 2014 and 2015**, we found a correlation between the (FUV - NUV) color and the stellar mass-to-light ratio $\Upsilon_\star$. The correlation is: **the bluer the (FUV - NUV) the larger the $\Upsilon_\star$**. Adding more ETGs from other catalogs still yielded the same correlation. The UV emission from ETGs is most likely UV-upturn stars of the EHB. If so, the more UV-upturn stars, the more the UV emission. Since UV-upturn stars are low-mass stars, **we conjectured that the (FUV - NUV) color may be used to probe the low-mass end of the IMF**.

- Future work: color-color diagram with redshift.

6. Conclusions (3/4)

About the spatially-resolved data (**Bouquin et al. 2018**)

- We see **disk-reddening occurring in both GRS and GGV galaxies**, with GGV galaxies slightly bluer than the GRS, but definitively redder than GBS. Average disk-reddening seems to flatten beyond $\mu_{[3.6]}$=20.89 mag arcsec^{-2}.

- Galaxies are well-separated in the μ_{FUV} vs. $\mu_{[3.6]}$ and in the spatially-resolved (FUV - [3.6]) vs. $\mu_{[3.6]}$. They indicate **a clear cut at 10^{-12} yr^{-1} in sSFR**.

- Moreover, GGV and GRS galaxies remain with a constant radial values in sSFR below 10^{-12} yr^{-1}, in regions fainter than $\mu_{[3.6]}$=20.89 mag arcsec^{-2} or $\Sigma_\star<3\times10^8$ $M_\odot$ kpc^{-2}. Results are found to be consistent with **Kauffmann et al. 2006**.

- From the slopes and y-intercepts of the outer disk linear fits and comparing them to the disk models of **Boissier & Prantzos (2000)** **we are able to obtain circular velocity and spin parameters within a factor of 2** to the truly measured ones (HyperLEDA). This could be a powerful technique for much larger surveys.

6. Conclusions (4/4)

About the XUV classification:

- We found **217 Type 1**, **110 Type 2**, and 21 Type 1+2. This is an **increase by ten-fold for T1**, and **six-fold for T2** from previously available samples.
- We have obtained both global and spatially-resolved properties of these galaxies.
- All Type 1 XUVs and most Type 2 XUVs **are GBS galaxies** globally and/or their outskirts is in the GBS when looking at their spatially-resolved data.
- only 9% of XUVs are Virgo galaxies, hinting to XUVs preferring **less-dense environments, and are excellent test-cases for secular evolution.**
- We took spectra of HII regions in XUV-disk galaxy NGC 3274 (M_{*}~$10^9 M_{Sun}$) and measured the most prominent emission lines. We infer the oxygen abundance $8.0 < 12 + \log(O/H) < 8.5$, with a negative gradient in the inner regions (up to 5 kpc) but large uncertainties make the shape of the gradient inconclusive in the outskirts.
- Future work: analysis of spectra of HII regions of NGC6946

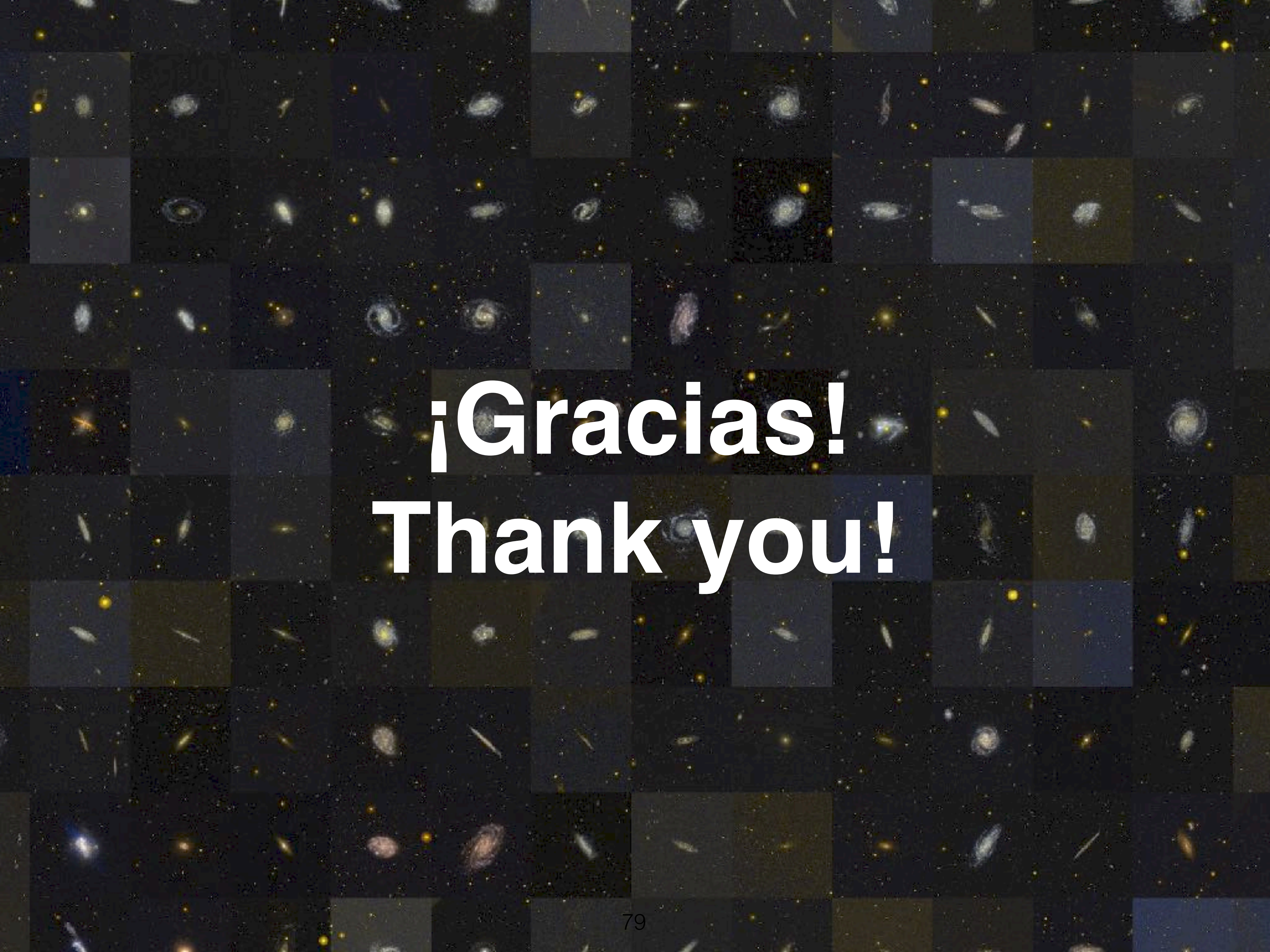

¡Gracias!
Thank you!